New approaches to fluorescence-based diagnostics for human African trypanosomiasis

Federica Giordani

Thesis submitted in fulfilment of the requirements for the degree of Doctor of Philosophy

Institute of Infection, Immunity & Inflammation
College of Medical, Veterinary & Life Sciences
University of Glasgow

November 2010

Abstract

In the absence of any vaccine, prophylactic drug and effective vector control, the fight against human African trypanosomiais (HAT) is based on the the combination of active case-finding and consequent drug treatment of identified positive cases. Unfortunately, low sensitivity and specificity of current diagnostic techniques often result in misdiagnosis, leaving infected patients without cure or exposing them to inappropriate chemotherapy protocols, which use dangerous and expensive drugs. The development of more efficient, simple, cheap and field-robust diagnostic tests is, therefore, urgently needed.

In the field, direct observation by light microscopy of trypanosomes in human fluids (blood, lymph node aspirate, cerebrospinal fluid) is considered the ideal way of confirming HAT infection. However, in practice this approach is problematic, especially for the Gambian form of the disease, where patients may present with very low parasitaemia. Detection limits of parasitological techniques can be improved by adding a preliminary step of sample concentration, although this further increases the laboriousness of HAT diagnostic algorithm.

Recent advances in fluorescence microscopy could be exploited to facilitate trypanosome detection. The introduction and implementation of fluorescence microscopy in HAT endemic countries would offer the advantages of an increased overall sensitivity of microscopical examination and a more rapid screening of the specimen. In contrast to traditional, expensive and fragile fluorescence microscopes, new LED-illuminated instruments are relatively cheap, very efficient and portable, lending themselves to utilisation in poorly equipped rural settings. In order to design a new diagnostic tool that exploits LED technology, however, selective and reliable fluorescent markers to label trypanosomes in human fluids are needed.

The development of new tools to assist in the diagnosis of African trypanosomiasis by use of LED fluorescence microscopy was the overall objective of this project. The work was mainly focused on testing various fluorescent compounds for their ability to selectively stain trypanosomes. Fluorophores were otained from commercial and academic sources, or else directly synthesised during the project. An important requirement evaluated was the compounds' compatibility with the currently available SMR LED Cytoscience fluorescence microscope, developed and kindly provided by our collaborator Prof. D. Jones (Philipps University, Marburg).

The utility of a UV LED-driven microscope in performing the arsenical drug resistance test was also assessed. This assay, developed in our laboratory to detect trypanosome strains resistant to arsenical and diamidine compounds, could represent a useful tool for chemotherapeutic decision making in the field, where resistance to arsenical drugs is a rising problem.

Table of Contents

List of Figures

List of Tables

Acknowledgement

I am particularly grateful to my supervisor Prof. M. P. Barrett, for his trust and his invaluable support throughout these three years of PhD. I am also very thankful to my supervisor Dr. A. Sutherland, for making the period I spent in his chemistry laboratory a very useful and positive experience.

I would like to thank my assessors, Dr. R. Burchmore and Prof. M. Turner, for their advice and support, and all the people who contributed to this project, especially Prof. D. Jones (Philipps University, Marburg, Germany), who developed the LED fluorescence microscopes, and Prof. D. W. Boykin (Georgia State University, Atlanta, USA), who provided the fluorescent diamidine compounds.

This work would have not been possible without the financial support of the “Sir Halley Stewart Trust”, to whom I am very grateful.

I wish to thank all the friends and colleagues I had the privilege to work with at the University of Glasgow. I am very thankful to the Loudon group, for their patience in teaching me some chemistry, and to all the people of Level 5 and 6 of the GBRC, in particular those in M. Barrett’s group and those I shared the office with: Anne, Pius, Isabel, Eduard, Jana, Darren, Gordon, Nicola, Caroline, Paul. A special thanks to Pui Ee for her help with the animal work but, most of all, for being such a good friend of mine. Thanks to Chris, for sharing his wisdom with me and...for all the banjo demonstrations. Many thanks to Dave, for his generous help with the molecular biology work and for the precious gift of his time and understanding.

I owe a very special thanks to my family, whose support gives me the strength to face every new day.

The list of the acknowledgements would not be complete without mentioning this beautiful country that hosted me, Scotland, which “may not be big, but her heart, like her landscapes, is mighty” (C.W.).

Author's Declaration

I declare that the results presented in this thesis are my own work, except when stated otherwise, and that this work has not been submitted for a degree at another institution.

Federica Giordani

November 2010

Abbreviations

ν_{max}/cm^{-1}	infrared absorption frequencies
$[\alpha]_D$	specific rotation
ACT	actin
Amp	ampère
AMP	ampicillin resistance marker (β-lactamase)
AO	acridine orange
Ar	aryl (or argon)
b.f.	bloodstream form
BP	bandpass
bp	base pairs
br	broad
BSA	bovine serum albumin
Bzl	benzyl
c	concentration
calcd	calculated
cat	catalyst
CATT	card agglutination test for trypanosomiasis
Cbz	carbobenzyloxy
CCD	charge coupled device
CD_3OD	deuterated methanol
$CDCl_3$	deuterated chloroform
CI	chemical ionisation
cm	centimetre
CNS	central nervous system
CSF	cerebrospinal fluid
d	doublet
DABCO	1,4-diazabicyclo(2,2,2)-octane
DAPI	4'-6-diamidino-2-phenylindole
DC	double centrifugation
DCM	dichloromethane
dd	doublet of doublets
DFMO	α-difluoromethylornithine (eflornithine)
dH_2O	distilled water
DMAP	4-dimethylaminopyridine
DMF	*N*,*N*-dimethylformamide
DMSO	dimethylsulfoxide
DMSO-d6	deuterated dimethylsulfoxide
DNDi	Drugs for Neglected Diseases Initiative
dNTPs	deoxynucleotide triphosphates
E. coli	*Escherichia coli*
EDCI	1-(3-dimethylaminopropyl)-3-ethyl-carbodiimide hydrochloride
EDTA	ethylenediaminetetraacetic acid disodium salt dihydrate
EI	electron impact (ionization)
ELISA	enzyme-linked immunosorbent assay
eq	equivalent
Et	ethyl
EtOAc	ethyl acetate
EtOH	ethanol
f	forward
FAB	fast atom bombardment

FCS	fetal calf serum
FIND	Foundation for Innovative New Diagnostics
FISH	fluorescence *in situ* hybridization
FITC	fluorescein-5-isothiocyanate
g	gram
gDNA	genomic DNA
GFP	green fluorescent protein
h	hour
HAPT	high affinity pentamidine transporter
HAT	human African trypanosomiasis
HRMS	high resolution mass spectrometry
Hyg	hygromycin
HYG	hygromycin resistance gene (hygromycin phosphotransferase)
Hz	Hertz
IC_{50}	median inhibition concentration
IFAT	immunofluorescent antibody test
IPTG	isopropyl-β-D-1-thiogalactopyranoside
IR	infrared
J	NMR spectra coupling constant
kb	kilobase
kDa	kilodalton
kDNA	kinetoplast DNA
L	litre
LAMP	loop-mediated isothermal amplification
LAPT	low affinity pentamidine transporter
LB	Luria Bertani
LED	light-emitting diode
lit.	literature
LMRS	low resolution mass spectrometry
LP	longpass
Lys	lysine
M	molar
m	multiplet
mAECT	miniature anion-exchange centrifugation technique
MeOH	methanol
mHCT	microhaematocrit centrifugation technique
MHz	mega Hertz
min	minute
ml	millilitre
mm	millimetre
mM	millimolar
mmol	millimole
mp	melting point
ms	millisecond
MW	molecular weight
NA	numerical aperture
NASBA	nucleic acid sequence-based amplification assay
NEO	neomycin resistance gene (neomycin phosphotransferase)
NEt_3	triethylamine
ng	nanogram
nm	nanometre
nM	nanomolar
NMR	nuclear magnetic resonance

NTDs	neglected tropical diseases
o/n	overnight
ºC	degrees Celsius
OC	oligochromatography
OD	optical density
ORF	open reading frame
ORI	origin of replication
PAC	puromycin resistance gene (puromycin *N*-acetyltransferase)
PARP	procyclic acidic repetitive protein
PBS	phosphate-buffered saline
PCR	polymerase chain reaction
ppm	part per million
q	quartet
QBC	quantitative buffy coat
r	reverse
r.t.	room temperature
RFLP	restriction fragment length polymorphism
RFP	red fluorescent protein
RHOD	rhodamine
rpm	revolutions per minute
rRNA	ribosomal RNA
s	singlet
SDS-PAGE	sodium dodecyl sulfate polyacrylamide gel electrophoresis
sec	second
t	triplet
T. b.	*Trypanosoma brucei*
t-Boc	*tert*-butoxycarbonyl
TDR	WHO Programme for Research and Training in Tropical Diseases
Tet	tetracycline
TFA	trifluoroacetic acid
Tyr	tyrosine
U	unit
UV	ultraviolet
V	volt
v	volume
VAT	variable antigen type
VSG	variant surface glycoprotein
w	weight
w.t.	wild type
wb	whole blood
WHO	World Health Organisation
X-Gal	5-bromo-4-chloro-3-indolyl-β-D-galactopyranoside
δ	chemical shift
λ_{EM}	wavelength of maximum emission
λ_{EX}	wavelength of maximum excitation
µg	microgram
µl	microlitre
µm	micrometre
µM	micromolar

1

General introduction

1.1 Human African trypanosomiasis

Human African trypanosomiasis (HAT), also known as sleeping sickness, is a deadly parasitic disease endemic to sub-Saharan Africa (Stich *et al*., 2002). HAT belongs to the so-called "neglected tropical diseases" (NTDs), a group of infections affecting the world's poor that includes, among others, leishmaniasis, Chagas' disease, dengue, leprosy, schistosomiasis and onchocerciasis. The World Health Organisation (WHO) estimates that one billion people (one sixth of the world's population) are affected by at least one of the NTDs (http://www.who.int/neglected_diseases/en/). Unfortunately, since these diseases persist almost exclusively in the most marginalised communities of undeveloped countries, very little resource is spent to lighten their tremendous social and economic burden. HAT represents a major public health threat in Africa and together with nagana, the animal form of African trypanosomiasis, is considered a main obstacle for development of rural regions of the continent (Simarro *et al*., 2008). Since 1997, WHO has been raising awareness of this most neglected disease, favouring the establishment of national control programs and the involvement of public and private partnerships (Stich *et al*., 2003). These efforts have significantly reduced the incidence of HAT in endemic countries by implementation of surveillance and drug availability.

1.1.1 The aetiological agent

The aetiological agent of HAT is a haemoflagellate protozoan belonging to the species *Trypanosoma brucei* (genus *Trypanosoma*, order Kinetoplastida) (Cox, 2004). Of the three subspecies of *T. brucei* only two are infectious to humans (*T. b. gambiense* and *T. b. rhodesiense*), while *T. b. brucei* causes infection in wild and domestic animals (Barrett *et al*., 2003). Sporadic cases of human infection with other trypanosome species have been reported (Truc *et al*., 1998c; Joshi *et al*., 2005), but, at least in one case, infection could be ascribed to a mutated apolipoprotein L1 found in the serum of the patient (Lun *et al*., 2009), which is a component of the trypanolytic factor that normally protects humans from animal trypanosome infection (Pays and Vanhollebeke, 2008). Both *T. b. gambiense* and *T. b. rhodesiense* are transmitted to the human host by the bite of an infected tsetse fly (genus *Glossina*), which acts as vector of the disease.

The two forms of HAT differ greatly (Welburn *et al*., 2001a). *T. b. gambiense* is responsible for more than 90% of reported cases of HAT and causes a chronic form of the illness, which can last for months or years before major symptoms arise. Checchi and

colleagues indirectly estimated the duration of the Gambian form to nearly three years in absence of treatment, equally split between the two stages (see Section 1.1.4) of the disease (Checchi *et al*., 2008a). On the other hand, *T. b. rhodesiense* causes an acute form that usually leads to the patient's death within weeks or few months (Brun *et al*., 2009). However, exceptions to these rules, with acute Gambian disease and chronic Rhodesiense trypanosomiasis cases, are observed (Garcia *et al*., 2006). Moreover, despite most *T. b. gambiense* infections being fatal in absence of treatment, human trypano-tolerance, with self-resolving and asymptomatic chronic infections, has been postulated (Checchi *et al*., 2008b). Other differences between the Rhodesiense and Gambiense forms lie in their clinical features and the chemotherapy protocols used, in their epidemiology and transmission and, therefore, in the control strategies applied (Fèvre *et al*., 2006).

1.1.2 Disease burden

HAT transmission is restricted to the African continent (Figure 1.1), but around 50 cases per year are diagnosed elsewhere in people who had travelled to affected regions (Sinha *et al*., 1999; Ripamonti *et al*., 2002; Lejon *et al*., 2003a). Endemic foci of the disease have a discrete distribution, correlated to the presence of the tsetse flies. There are nearly 300 active foci identified, confined to an area that stretches south of the Sahara and north of the Kalahari desert (Barrett *et al*., 2003). *T. b. gambiense* infection is found in west and central Africa: Angola, Democratic Republic of the Congo and Sudan are the most affected countries by the Gambian form, with more than 1,500 new cases per year reported up to 2004 (WHO, 2006b). *T. b. rhodesiense* is found in the eastern and southern part of the continent. The above mentioned study identified Malawi, Uganda and United Republic of Tanzania as the countries with the highest incidence of this HAT form (50–1,500 cases per year). Uganda is the only country in Africa known to be affected by both *T. brucei* subspecies, but the distribution of these parasites is, at least for the time being, separate (Picozzi *et al*., 2005).

Compared to other parasitic diseases like malaria or worm infections, incidence of HAT is lower, but its potential to give rise to devastating epidemics as soon as active surveillance is abandoned makes this illness a major health priority in endemic countries (Cattand *et al*., 2001). Systematic control programs established by European authorities resulted in efficacious intervention in the big epidemics that occurred between the end of the 19th and the beginning of the 20th century, bringing the disease to a nearly elimination by the 1960s (Pépin and Méda, 2001; Maudlin, 2006). After the colonial era, however, the number of

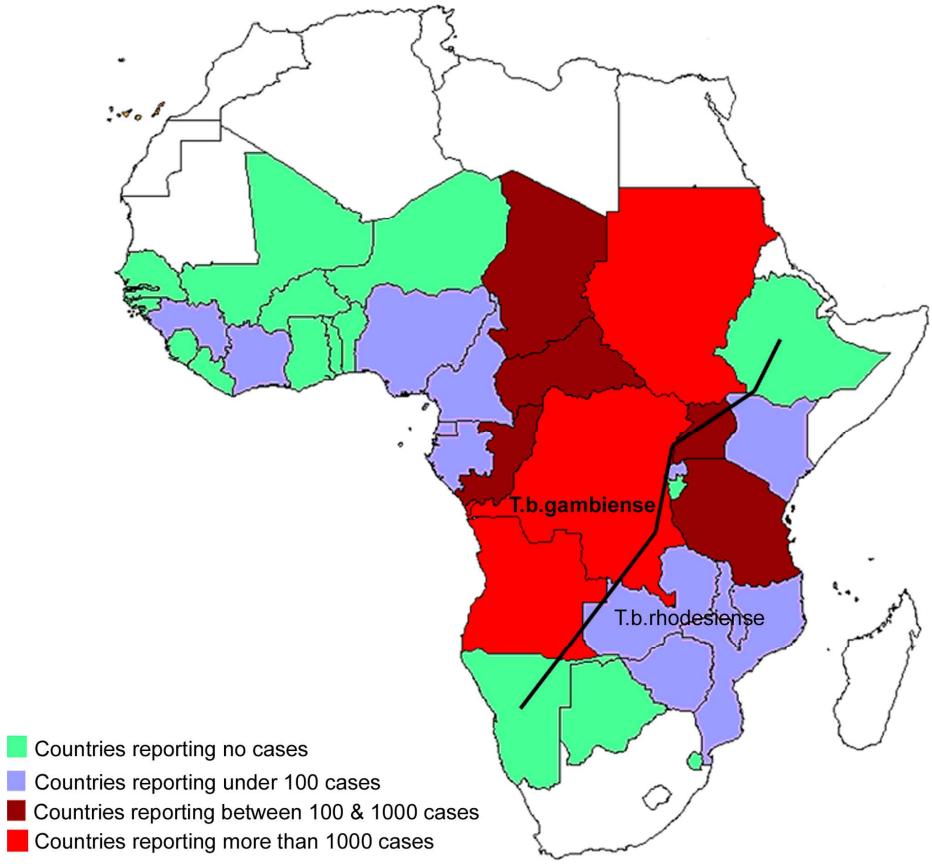

Figure 1.1 – Map of Africa showing the geographical distribution of *T. b. gambiense* and *T. b. rhodesiense*.
The epidemiological status of the endemic countries is indicated with different colours. (Reproduced from Simarro *et al*., 2008; doi:10.1371/journal.pmed.0050055.g003).

cases increased rapidly, due to lack of surveillance and awareness from local government, but also to poverty, political instability, wars and displacement of populations (Smith *et al*., 1998; Cattand, 2001; Brun *et al*., 2009). Today, a total of 60 million people in 36 African countries are continuously exposed to the risk of infection by one of the two forms of HAT, but only 3-4 million are under surveillance (Cattand *et al*., 2001). For this reason, accurate epidemiological data for sleeping sickness are difficult to collect and reported incidence of the illness is often considered an underestimate (Fèvre *et al*., 2008; Welburn *et al*., 2009). Despite this uncertainty, at the end of the 20th century, WHO estimated an annual number of cases of at least 300,000 (40,000 – 50,000 deaths), of which only 13% were identified and treated (WHO, 2001). Fortunately, improvement in control policies and new international initiatives have led, during the last decade, to a steady decline of total cases, currently estimated to be 50,000 – 70,000 (WHO, 2006b; Barrett, 2006).

1.1.3 Vector and transmission

HAT is transmitted to humans through the bite of infected haematophagous arthropods belonging to the *Glossina* species. Gambian trypanosomiasis is typically acquired from

riverine tsetse flies of the *G. papalis* group, but also *G. fuscipes*, *G. tachinoides* and *G. calliginea* can act as vectors of *T. b. gambiense* (Cattand, 2001). The reservoir of this infection is considered exclusively human. Therefore, the cyclic transmission human-fly-human is the main cause of the persistence of the disease. Nevertheless, natural infections with *T. b. gambiense* have been reported in domesticated animals (pigs, dogs and sheep) and may occur in wild fauna as well (Njiokou *et al*., 2006), although the epidemiological impact of this reservoir on humans remains as yet undetermined (Pépin and Méda, 2001; Brun and Balmer, 2006; Fèvre *et al*., 2006). *T. b. rhodesiense*, on the contrary, is a zoonotic parasite found in savannah habitats. Human infection with this species is sporadic, but when it occurs the disease is highly virulent and progresses very rapidly. Rhodesiense trypanosomiasis is transmitted by tsetse flies belonging to the *G. morsitans* group (and, at lesser extent, to *G. pallidipes*, *G. swynnertoni* and *G. fuscipes*) that have fed on infected domestic (cattle in particular) and wild (especially ungulates) animals, which, therefore, serve as the main reservoir of the parasite (Pépin and Méda, 2001; Welburn *et al*., 2001b). Tsetse flies are usually active during the day, but some species can bite at night and both sexes can transmit the infection (Fèvre *et al*., 2006). Interactions between vector and parasite are complex. Only a very small percentage of natural population of tsetse flies are infected by *T. brucei* species and this can explain the absence of correlation between insect concentration and incidence of the human disease (Pépin and Méda, 2001). Other possible routes of infection with trypanosomes are through blood transfusions, infected needles or congenitally (Barrett *et al*., 2003).

1.1.4 Life cycle

Trypanosomes are pleomorphic, single-celled parasites with a two-host life cycle: mammalian and arthropod (Chappuis *et al*., 2005; Brun *et al*., 2009). The cycle (Figure 1.2) starts when an infected tsetse fly takes its blood meal on the mammalian host and it inoculates the metacyclic trypomastigote form of the parasite present in its saliva. Trypanosomes quickly transform into the long slender trypomastigotes and proliferate by binary fission at the site of the bite for a few days, leading to an inflammatory chancre. The parasites, then, spread to the draining lymph nodes and the bloodstream (first or early haemolymphatic stage of infection), through which they reach other organs such as the spleen, liver, heart and endocrine system. After a few weeks (*T. b. rhodesiense*) or several months (*T. b. gambiense*) trypanosomes cross the blood-brain barrier (BBB) to invade the central nervous system (CNS) through mechanisms that are still poorly understood (Enanga *et al*., 2002): the patient is, then, said to be in the meningoencephalitic, second (or

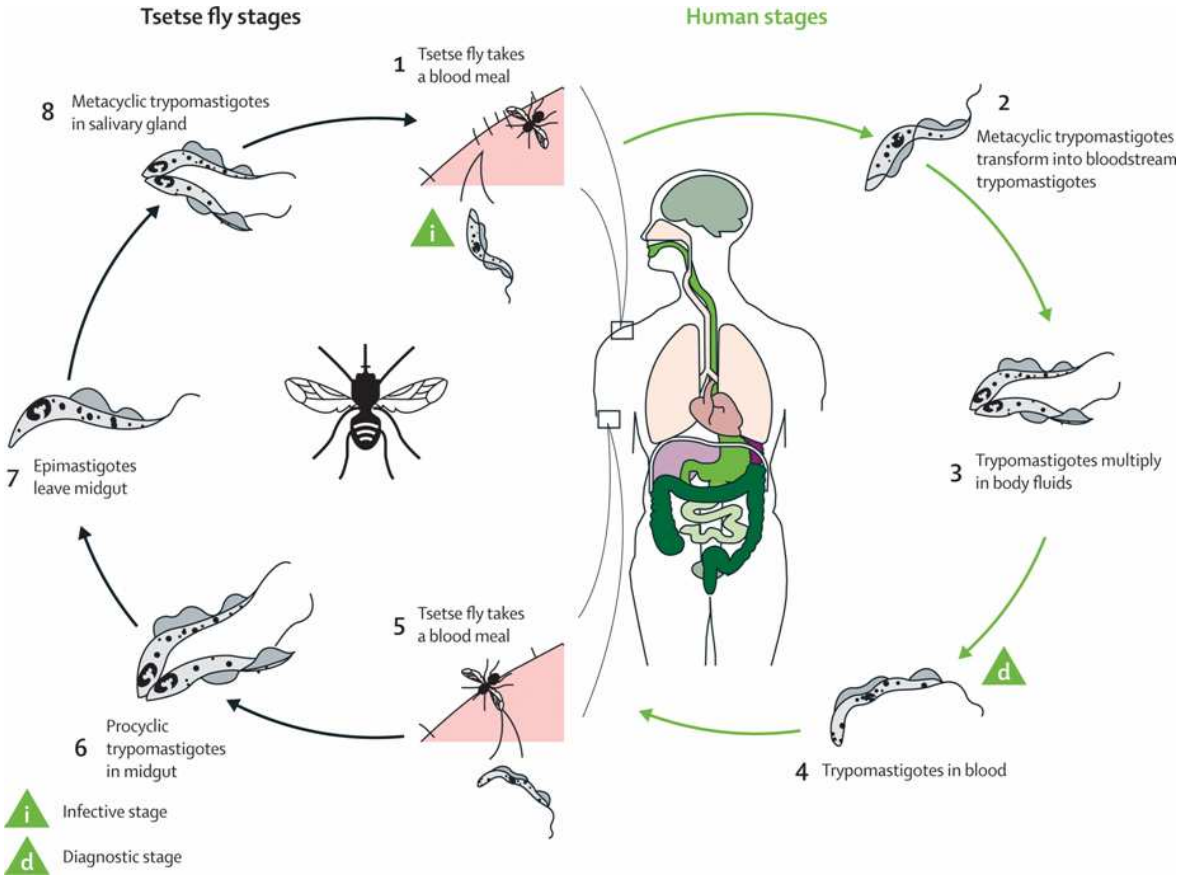

Figure 1.2 – Schematic representation of the digenetic life cycle of *Trypanosoma brucei* in the mammalian host and in the tsetse fly vector.
(Reproduced with permission from Blum *et al*., 2008).

late) stage of infection. When parasitaemia in the host increases, long slender trypomastigotes transform into non-dividing, short-stumpy trypomastigotes, which are taken up by the tsetse fly (which remains infective for its entire life), where they complete their life cycle. In the insect's midgut trypanosomes transform into the procyclic stage and after two or three weeks they migrate to the salivary glands. Here other transformations lead to their development into metacyclic forms, ready to be injected into a susceptible vertebrate host during the next blood meal.

During their whole life cycle African trypanosomes remain exclusively extracellular, thus fully exposed to the host's immune response. To survive complement-mediated lysis and specific immune attack, parasites shield invariant surface molecules with a thick coat made of variant surface glycoproteins (VSGs). Only one VSG is expressed at a time and, once neutralising specific antibodies have been produced from the host, trypanosomes switch to a different VSG, thus allowing the population to survive (Machado *et al*., 2006; Morrison *et al*., 2009). This antigenic variation process explains the intermittent parasitaemia and the long asymptomatic incubation period typical of *T. b. gambiense* infection and it makes the development of a vaccine remote (Cattand, 2001).

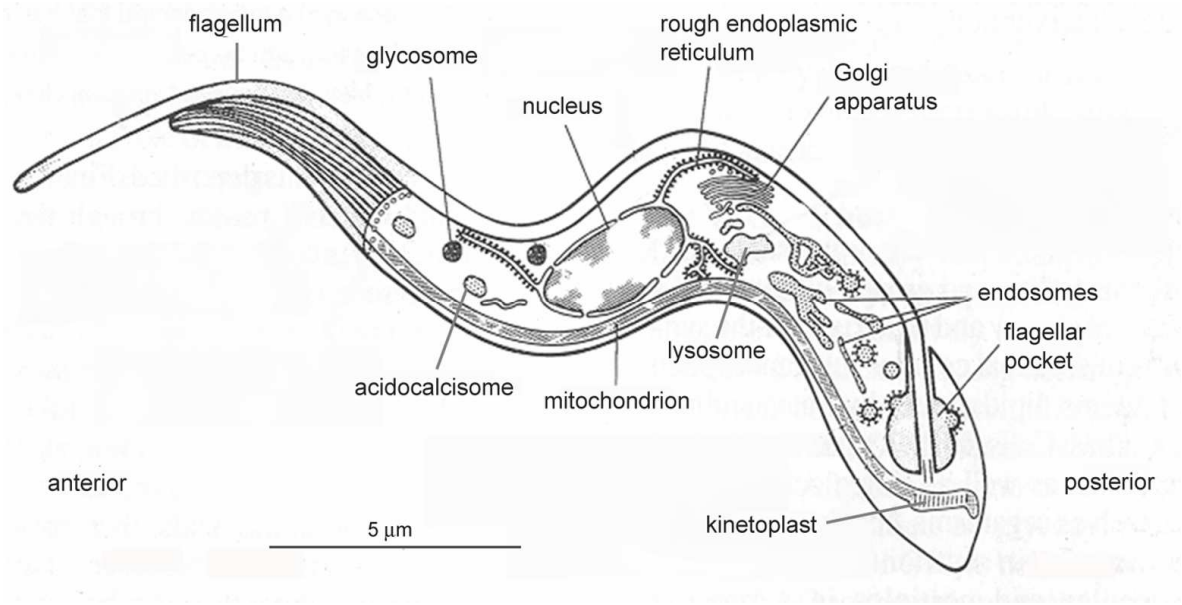

Figure 1.3 – Diagram of a bloodstream *Trypanosoma brucei* cell illustrating the major organelles.
Glycosomes and acidocalcisomes are not drawn to scale.
(Modified from ILRAD Reports vol. 7 (1), Jan. 1989; available online at the website http://www.ilri.org/InfoServ/Webpub/Fulldocs/Ilrad89/Trypano.htm).

1.1.5 Cell morphology and cell compartments

African trypanosomes are eukaryotic, unicellular organisms, with a spindle-shaped cell 18-20 µm long and 3 µm thick (Field *et al*., 2004; Figure 1.3). These parasites move thanks to a single flagellum that, in the trypomastigotes, arises from the posterior end of the cell, runs the whole length of the cell body, to which it is attached by an undulating membrane, and extends beyond it at the anterior end. Tightly connected to the basal body of the flagellum is the kinetoplast, a complex network of mitochondrial DNA composed of 30-50 DNA maxicircles (22 kb) and 5,000-10,000 minicircles (1 kb) interlocked together to form a disk-shaped structure (Chen *et al*., 1995; Liu *et al*., 2005). Minicircles encode for guide RNAs, which control editing specificity of maxicircle transcripts for rRNAs and subunits of respiratory complexes (Simpson and Shaw, 1989; Hong and Simpson, 2003). The kinetoplast is contained in the posterior part of the single trypanosome mitochondrion, an organelle that elongates longitudinally throughout the whole cell body. In slender trypomastigotes the mitochondrion shows only a few short cristae and little metabolic activity, due to the fact that this form of the parasite relies on glycolisis and not on oxidative phosphorylation for energy production (Schnaufer *et al*., 2002). When the cell enters mitosis, the kinetoplast DNA replicates and divides before the nuclear genome (Field *et al*., 2004). The flagellum emerges from an invagination of the plasma membrane called the flagellar pocket (Field and Carrington, 2009). This structure is involved in various cell activities including immune evasion, by continuous clearance of VSG-

immunoglobulin complexes, and cell trafficking, being the only site where endocytic and exocytic processes occur (Morgan *et al*., 2002). The organisation of the cell compartments from the flagellar pocket towards the anterior side is highly polarised. Associated to the pocket is the Golgi complex with its endocytic and secretory vesicles confined between kinetoplast and nucleus. The single lysosome is usually close to the nucleus, which is located at the midpoint of the cell (Field *et al*., 2004). The nuclear genome of *T. brucei* includes 11 diploid, megabase-sized chromosomes and various aneuploid, mini- and intermediate chromosomes (30-700 kb), which harbour VSGs sequences and expression sites similar to those present in the subtelomeres of the megabase chromosomes (Berriman *et al*., 2005). The endoplasmic reticulum is distributed in the whole cytoplasm as well as the acidocalcisomes, acidic electron-dense granules with a diameter of around 0.2 μm, important for the homeostasis of various elements including several cations, dications (Na^+, Ca^{2+}, Mg^{2+}, Zn^{2+}) and phosphate (Docampo and Moreno, 1999; Rodrigues *et al*., 1999). Acidocalcisomes, which have no counterpart in mammalian cells, can be visualised inside different *Trypanosoma* species by their specific staining with acridine orange (Vercesi *et al*., 1994; Mendoza *et al*., 2002). Glycosomes are other membrane-bound organelles, homogeneous in size (0.27 μm diameter), present throughout the whole cell body of *T. brucei*. These structures, which are closely related to peroxisomes, contain glycolytic enzymes and are particularly abundant in bloodstream trypomastigotes (240 per cell) (Opperdoes, 1987).

1.1.6 Control strategies

All countries affected by HAT have national programs dedicated to surveillance of the disease (Simarro *et al*., 2008). Control is based on two approaches: the reduction of the reservoirs (human or animal) of the parasite and the reduction of the chance of contact between vector and human host by means of vector removal (Welburn *et al*., 2001a). For *T. b. gambiense* form, where humans represent the main reservoir, active case-finding (and therefore, correct diagnosis) and treatment of the infected patients are the strategies adopted to interrupt transmission (Simarro *et al*., 2006; Brun *et al*., 2009). For *T. b. rhodesiense,* instead, the control of infection in livestock (and, to a minor extent, in wildlife) through the use of curative or prophylactic trypanocides or application of insecticides to the animals plays a crucial role (Hutchinson *et al*., 2003; Fèvre *et al*., 2006; Simarro *et al*., 2008). For Rhodesian HAT, vector control can also be an efficient approach for containing the transmission of the disease (Welburn *et al*., 2009). The fight against tsetse flies involves the use of insecticides and the installation of traps or screens (Torr *et*

al., 2005; Lindh *et al*., 2009). A new technology available to decrease tsetse population consist in the release of sterilised tsetse males (sterile insect technique, SIT), but its cost-effectiveness is disputed (Vreysen, 2001).

1.1.7 Chemotherapy

Since African trypanosomiasis is considered invariably fatal if untreated, chemotherapy is mandatory. Unfortunately, as for the other neglected tropical diseases, drug research and development for HAT is a minor activity due to lack of profit perspectives for pharmaceutical companies (Trouiller *et al*., 2002). Although today new initiatives, like the Drugs for Neglected Diseases Initiative, DNDi (http://www.dndi.org/index.php), are trying to face this problem, HAT treatment still relies on only four drugs (Figure 1.4), three of them introduced over 50 years ago (Ollivier and Legros, 2001). Recently, nifurtimox (an orally administered 5-nitrofuran licensed for the treatment of Chagas' disease) for use in combination with eflornithine (see later), has been added to the list (Delespaux and de Koning, 2007; Figure 1.4). The production and availability of these drugs is in constant danger and continues only thanks to agreements between WHO and the suppliers (Etchegorry *et al*., 2001; Barrett *et al*., 2003). All of these four drugs are far from ideal, with problems associated to toxicity, route of administration, low efficacy and resistance (Legros *et al*., 2002; Fairlamb, 2003). HAT therapy is even more complicated during the second stage of the disease, since drugs have to reach the brain by crossing the blood-brain barrier, which otherwise protects parasites from compounds active in the haemolymphatic compartment (Enanga *et al*., 2002; Lejon and Büscher, 2005).

Pentamidine and Suramin are the drugs used to treat the early stage of HAT. Pentamidine isethionate (Lomidine®) was introduced in the early 1940s and, since then, it has been used for the treatment of *T. b. gambiense* infection without being associated with any significant resistance outbreak (Delespaux and de Koning, 2007). During the colonial era this compound was also widely used as mass chemoprophylactic agent (Ollivier and Legros, 2001). Pentamidine is administered by intramuscular injection (7-10 doses of 4 mg/kg daily or every two days) and it is relatively well tolerated (Legros *et al*., 2002). Three transmembrane transporters responsible for the selective accumulation of pentamidine inside trypanosomes have been identified (de Koning, 2001a) and two more have recently being discovered (Ortiz *et al*., 2009), but the mechanism of action of this slow-acting diamidine is still unclear. Suramin sodium (Germanin®) is a polyanionic sulfonated naphthylamine used as first line treatment for *T. b. rhodesiense* form of HAT since 1920.

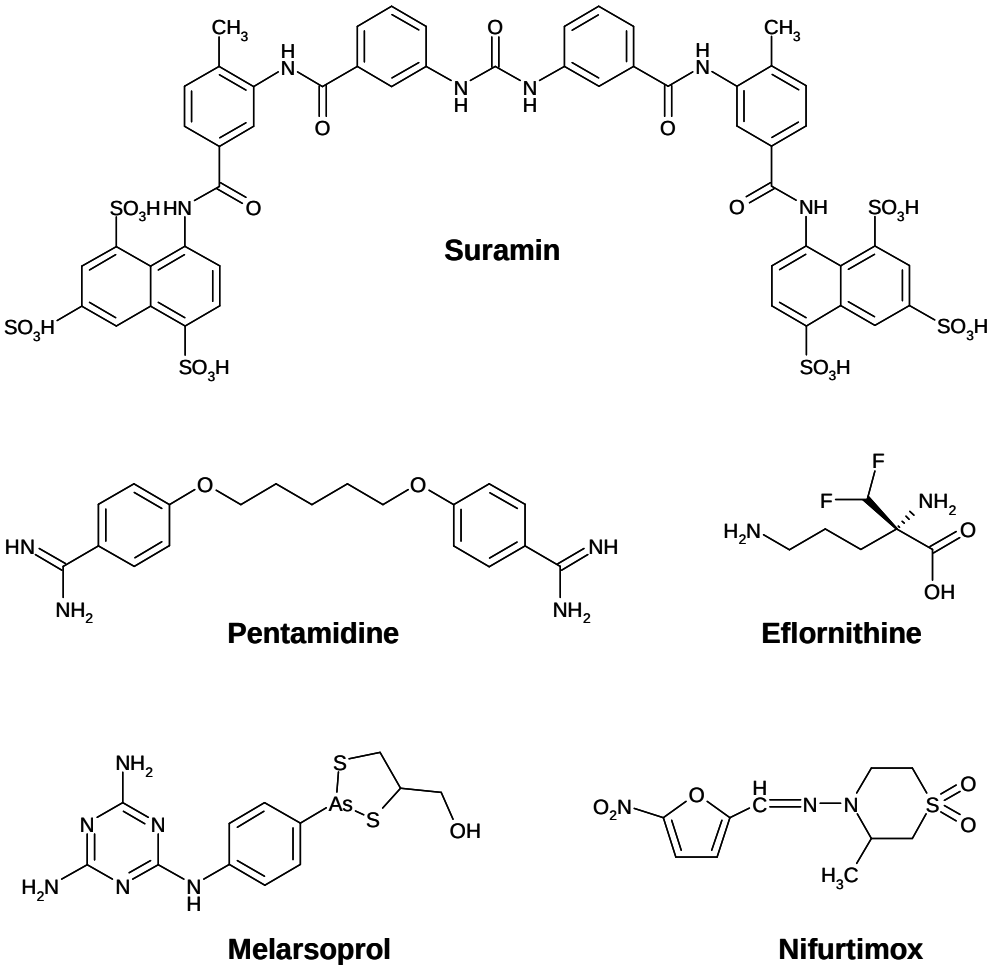

Figure 1.4 – Chemical structure of the drugs used for human African trypanosomiasis treatment.
Nifurtimox, a drug licensed for Chagas' disease, has recently been included in the Essential List of Medicines for HAT chemotherapy in association with eflornithine.

It can also be used as second drug of choice for Gambian first stage trypanosomiasis. Suramin is administered intravenously (typically, five injections every 3-7 days over a four weeks period) and can have severe adverse reactions like anaphylactic shock, neurotoxicity, kidney damage and cutaneous reactions (Legros *et al*., 2002). As for pentamidine, the trypanocidal mechanism of suramin is poorly understood (Barrett *et al*., 2007). This compound is known to inhibit many enzymes and a multiple mode of action is compatible with the absence of resistance cases observed in the field (Fairlamb, 2003), although resistant lines are easily selected in the laboratory (Scott *et al*., 1996).

Melarsoprol and eflornithine are the two drugs used to treat late stage HAT. Melarsoprol (Arsobal®, Mel B) was introduced in 1949 and is active on both forms of sleeping sickness. Treatment protocols with melarsoprol traditionally consists of various intravenous injections of the drug (3.6 mg/kg body weight, dissolved in propylene glycol) separated by periods of 7-10 days (Cattand, 2001). Only hypotheses exist on the mode in which this drug kills trypanosomes, the disruption of the parasite thiol-redox balance being one often

proposed (Fairlamb, 2003). Melarsoprol is an organo-arsenical compound extremely toxic to humans and it is responsible for the death of up to 5% of patients to whom it is administered, due to a post-treatment reactive encephalopathy. Furthermore, over the last decade, an increasing number of clinical failures (up to 30% in some areas), particularly in the treatment of *T. b. gambiense,* have been observed (Brun *et al*., 2001; Ollivier and Legros, 2001). Apart from poor treatment regimens, these failures have been associated, at least partially, to alterations or loss of the parasite's P2 amino-purine transporter (Carter and Fairlamb, 1993; Matovu *et al.*, 2001a), which is involved in the uptake of melarsoprol but also of diamidines like pentamidine and diminazene aceturate (a veterinary trypanocide), leading to worries about possible cross-resistance onset (Barrett and Fairlamb, 1999; de Koning 2008; Section 1.2.8). The alternative drug for treatment of melarsoprol-refractory late sage *T. b. gambiense* is eflornithine (Ornidyl®, DFMO). Introduced in 1990, this drug is not active on *T. b. rhodesiense*, is expensive (five times more than melarsoprol) and requires a high dose treatment: 400 mg/kg daily subdivided into four intravenous infusions for 7 or 14 days (Burri and Brun, 2003). Treatment failures have been observed (Balasegaram *et al*., 2009), but it must be taken into consideration that the compound has a cytostatic effect that requires an active immune system to clear infection (Bitonti *et al*., 1986). Nevertheless, DFMO has a much lower toxicity than melarsoprol: side effects include seizures, gastrointestinal problems and myelosuppression (Priotto *et al*., 2006). Originally developed as a cancer treatment, the intracellular target of eflornithine is well known: the drug acts as a suicide inhibitor of the enzyme ornithine decarboxylase, disrupting the essential polyamine biosynthetic pathway of the parasite and leading to several downstream effects (Barrett *et al*., 2007; Delespaux and de Koning, 2007).

Since DFMO registration, the first new drug candidate for HAT therapy has been an oral diamidine designed for the early stage of the disease, DB289, but, despite its efficacy, the compound's development was recently stopped due to toxicity issues (Thuita *et al*., 2008). Diamidines remain interesting drug leads against HAT and other compounds, more potent than DB289 and including blood-brain barrier permeant derivatives, have already been identified (Wenzler *et al*., 2009). Nitroimidazoles are another class of molecule active against trypanosomiasis (Denise and Barrett, 2001); among them, fexinidazole, developed by DNDi, is currently in Phase I trials (Torreele *at al*., 2009). Thanks to recent advances in the knowledge of parasite biology new drug targets may be validated in the future (Croft *et al*., 2005; Barrett *et al*., 2003 and 2007). Moreover, improved therapeutic protocols and combinations of existing drugs are under evaluation for the advantages they can offer (in

particular the limitation of side effects and delay of drug resistance development, but also the reduction of costs and treatment duration). A new, shorter 10-day protocol with melarsoprol (2.2 mg/kg daily intravenously) has already been introduced with success for Gambian trypanosomiasis: it does not eliminate toxicity, but it reduces hospitalisation period and costs (Schmid *et al*., 2005). Combination therapies of nifurtimox with either melarsoprol or DFMO have been tested for treatment of HAT second stage: the association of nifurtimox with eflornithine, in particular, has given encouraging results during early clinical trials (Bisser *et al*., 2007; Priotto *et al*., 2006 and 2009) and, recently, this drug combination has been included in the Essential List of Medicines for HAT treatment by WHO (http://www.who.int/neglected_diseases/en/).

1.2 Diagnosis of *T. b. gambiense* infection

Accurate diagnosis and staging of sleeping sickness infection is of the utmost importance for disease management and control (Louis *et al*., 2001). Early detection of the disease allows not only to treat the patients with the cheaper, less toxic drugs for the first stage of the disease, but also to reduce the human reservoir of the parasite in the case of *T. b. gambiense* infection (Fèvre *et al*., 2006). Unfortunately, diagnosis of HAT still represents a major problem, due to insensitivity and laboriousness of the techniques available especially in remote locations with limited facilities. Passive case-finding (self-reporting patients) is extremely inefficient, as infected individuals can manifest symptoms only after many months, and usually refer to local health centres when already in the second stage (Ekwanzala *et al*., 1996; Smith *et al*., 1998; Abel *et al*., 2004; Odiit *et al*., 2004). Therefore, more effective active case-finding programs have been established to screen the whole population at risk through the work of specialised mobile teams (Ruiz *et al*., 2002; Robays *et al*., 2004; Simarro *et al*., 2006). HAT is diagnosed using a combination of tests. Every endemic country has adopted a specific algorithm for detection of infected subjects, but all strategies comprise a sequence of screening and confirmation steps (Figure 1.5). Suspected HAT cases are identified using indirect diagnostic tools (clinical features, serological tests and, to a lesser extent, molecular tests) and must always be confirmed by direct microscopy. On infected individuals staging of the disease is carried out to decide on the treatment protocol to use. Stage determination requires an invasive lumbar puncture and is usually performed in local treatment centres. Direct and indirect diagnostic procedures must also be applied during follow-up periods to check for relapses, but also to monitor seropositive individuals not confirmed by parasitological techniques (Chappuis *et al*., 2005).

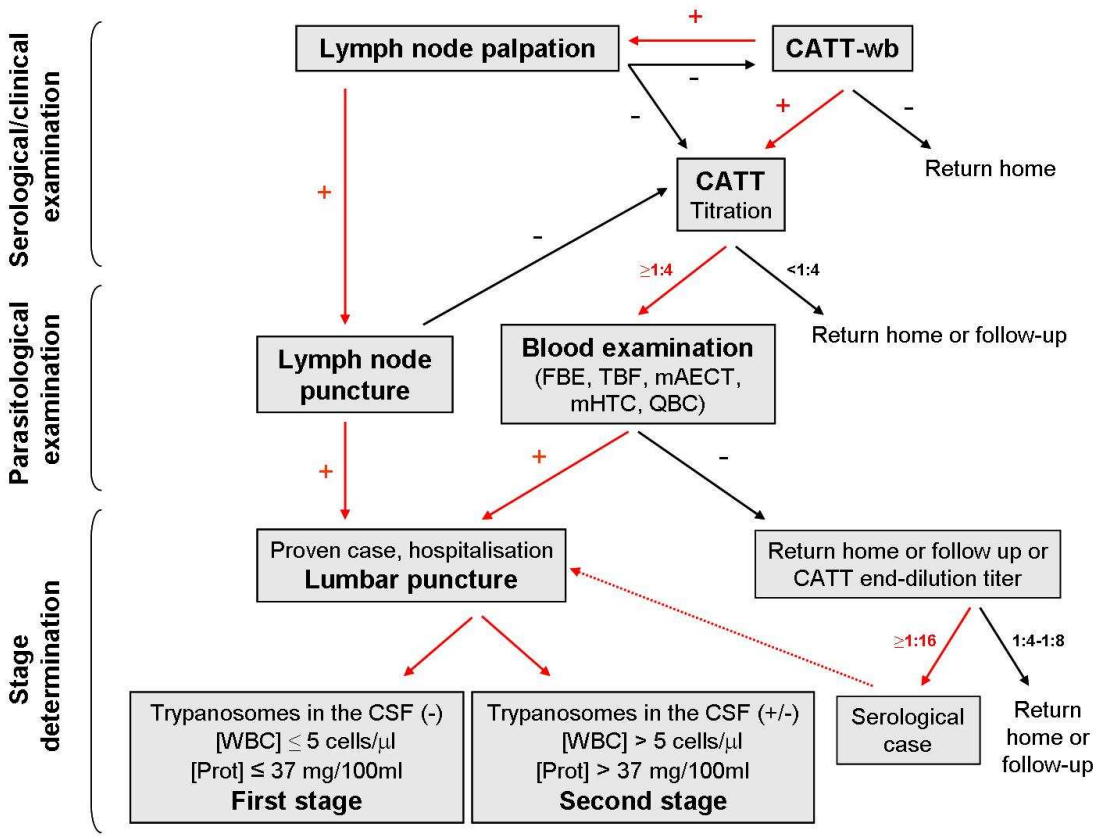

Figure 1.5 – General flow chart for *T. b. gambiense* diagnosis.
Every endemic country utilises a specific algorithm that can slightly differentiate from the one illustrated here. Threshold values indicated for second stage determination are those recommended by the World Health Organisation (WHO, 1998). The diagnostic techniques indicated in the figure are described in Section 1.2.
CATT-wb: card agglutination test for trypanosomiasis on whole blood; FBE: fresh blood examination; TBF: thick blood film; mAECT: miniature anion-exchange centrifugation technique; mHTC: microhaematocrit centrifugation technique; QBC: quantitative buffy coat; CSF: cerebrospinal fluid; WBC: white blood cells; Prot: protein; +: positive test result; -: negative test result.

None of the various assays available today for HAT diagnosis is ideal: practicality, costs and low efficiency are the main drawbacks. A test's diagnostic accuracy is usually quantified by means of its sensitivity and specificity, which are respectively defined as the proportion of true positives (true positives/true positives+false negatives) and of true negatives (true negatives/true negatives+false positives) that are correctly identified by the assay (Altman and Bland, 1994a; Akobeng, 2007). More useful to clinicians to decide about the probability of disease in patients are the positive and negative predictive values, which represent the proportion of people with a positive test result who actually have the disease (true positives/true positives+false positives), and the proportion of people with a negative test result who do not have the disease (true negatives/true negatives+false negatives), respectively (Altman and Bland 1994b; Banoo *et al.*, 2007). Predictive values are dependent on the population and change if the prevalence of the disease changes, while specificity and sensitivity remain unvarying. Since sensitivity and specificity are usually

inversely related, the choice of an assay with a certain precision depends on the case under study: in situations where it is important to detect the highest number of affected patients (like mass screening programs), a highly sensitive test is preferable, while for case confirmation tests a high specificity is needed to avoid the risk of false positives (Empson, 2001; Nendaz and Perrier, 2004).

1.2.1 Clinical features

HAT is difficult to diagnose at an early stage, when symptoms are largely variable and aspecific and the disease can be easily confused with other common tropical infections, especially malaria (Louis *et al*., 2001). Fever, general malaise, headache, facial oedema, anaemia, cutaneous lesions are all manifest during the haemolymphatic stage (Kennedy, 2006a). The only specific features are a local inflammation at the site of the tsetse bite, called the chancre, and an enlarged posterior cervical lymphadenopathy (Winterbottom's sign). The chancre generally occurs 5-15 days after the inoculation of the parasite, but it is seldom observed in Africans (Büscher and Lejon, 2004). Palpation of enlarged neck glands and microscopic examination of the aspirate in positive cases is generally used for HAT diagnosis (Lutumba *et al.*, 2005; Section 1.2.3.2). The diffuse inability of the local primary healthcare facilities to promptly identify the disease results in considerable delays in diagnosis and treatment, with consequent increase of risk of unfavourable prognosis and of human suffering (Bukachi *et al*., 2009). HAT becomes more easily recognizable as the disease progresses. Later clinical features reflect the involvement of specific organs: gastro-intestinal problems, cardiovascular disturbances, endocrine dysfunction and, sometimes, eye involvement can occur (Kennedy, 2006a; Blum *et al*., 2008). When the infection reaches the meningoencephalitic stage, signs of nervous system disruption become evident and extensive in Gambian trypanosomiasis. Sleep-pattern disturbances, with dysregulation of the circadian rhythm, represent the most typical feature at this stage and lend HAT its common name "sleeping sickness". Other neurological changes include painful peripheral sensory disturbances, tone and mobility disorders, mental changes and psychiatric disorders. If untreated, patients stop eating, lapse into a semi-coma and finally die (Kennedy, 2006a and 2006b).

1.2.2 Serological tests

Application of serological assays to obtain indirect indication of infection (by antibody detection) is a widely used approach to rapidly screen the population at risk in endemic

areas but, as for clinical features, these tests are just indicative of the presence of trypanosomes. Since immunological tests lack sensitivity and specificity, subsequent parasitological confirmation has to be performed on the positive cases identified for final diagnosis (Chappuis *et al*., 2005). In the field, however, mobile teams often face complex situations where patients with a positive serology are not confirmed by microscopy (a phenomenon called seropositivity) and the question of whether to provide treatment to these subjects is disputed (Koffi *et al*., 2006). The main cause of seropositivity is probably the low sensitivity of parasitological methods that gives rise to false negatives (Section 1.2.3), but this phenomenon can also be explained by false serological positives generated by cross-reactivity with animal trypanosomes or other co-infecting parasites. Moreover, an efficient immune system response could allow some subjects to control the virulence of the infection and keep it under detection limits of current diagnostics (Garcia *et al*., 2000 and 2006). The serological tests available are very useful, but they are not ideal, because of their use of not defined recombinant proteins against variable antigens. Therefore, new protein markers for HAT serodiagnosis are under study (Hutchinson *et al*., 2004).

1.2.2.1 CATT/*T. b. gambiense*

Since its introduction in 1978, the card agglutination test for trypanosomiasis (CATT/*T. b. gambiense*) has been the most widely used technique for mass population screening in the field (Chappuis *et al*., 2005). The test is a cheap, fast and simple agglutination assay able to detect specific antibodies to the *T. b. gambiense* variable antigen type (VAT) LiTat 1.3, common in the serum of patients infected with this subspecies. Recently, a thermostable format of the test has been developed (Hasker *et al*., 2010). To perform the assay, a drop of reagent, consisting of lyophilised, blue-stained bloodstream trypanosomes expressing the LiTat 1.3 antigen and resuspended in PBS, is mixed with a drop of fresh, heparinized, capillary blood on a white plastic card, which is then shaken for 5 minutes on a 12/220 V card rotator. The result is immediately read by the naked eye: in subjects previously exposed to *T. b. gambiense* the trypanosomes agglutinate and form a blue clot. The test sensitivity on undiluted whole blood (CATT-wb) varies from 87 to 98%, while specificity can reach 90-95% (Penchenier *et al*., 2003; Chappuis *et al*., 2005). Serial dilutions of blood, plasma or serum before applying the test improve its specificity. The use of end-dilution titers have been suggested as a useful tool for therapeutical decision making for CATT-wb positive patients (Simarro *et al*., 1999; Chappuis *et al*., 2004), although this approach can be risky because of the poor positive predictive value of the test where disease prevalence is low (Inojosa *et al*., 2006). Moreover, a study on cost-effectiveness of

different confirmation algorithms showed that the use of parasitologic confirmatory tests by concentration methods without CATT titration had a better efficiency (Lutumba *et al*., 2007). The CATT loses its efficacy on samples from patients infected with strains of trypanosomes that lack, or do not express, the LiTat 1.3 antigen, resulting in false negatives, but the distribution of these strains seems limited (Dukes *et al*., 1992). Similarly, false positives can occur in patients infected with other trypanosome species or parasitic diseases, which cross-react with non-variant epitopes on the surface of trypanosomes present in the reagent (Jamonneau *et al*., 2000; Inojosa *et al*., 2006). Furthermore, the agglutination can be inhibited by complement factors, a phenomenon called prozone, when the test is performed on undiluted, heparinized blood or serum with low dilutions (<1:4). In these cases, addition of EDTA to the dilution buffer eliminates the problem by increasing the sensitivity with only a minor loss of specificity (Pansaerts *et al*., 1998; Magus *et al*., 2002). Other disadvantages of CATT are that it does not work on *T. b. rhodesiense* and it does not differentiate between past and current infections: this is the reason why this test can not be used to assess treatment efficacy during follow-up (Section 1.2.7), since circulating antibodies can persist for several years after cure (Paquet *et al*., 1992).

Variations on the same theme of the CATT have been proposed as, for example, the micro-CATT (micro-card agglutination test for trypanosomiasis). This test allows the collection and storage (at 4 ºC) of dried blood samples on a filter paper (Miézan *et al*., 1991). The micro-CATT showed the same specificity of the CATT-wb but a lower sensitivity in the field (Truc *et al*., 2002). Furthermore, although it requires smaller volumes of reagents, it is a more expensive method than the CATT-wb because more consumables are needed to perform the assay.

1.2.2.2 LATEX/*T. b. gambiense*

The LATEX/*T. b. gambiense* is an agglutination card test developed as a field alternative to the CATT-wb. The reagent is based on the combination of three purified variable surface antigens (LiTat 1.3, 1.5 and 1.6) absorbed on latex particles, in order to avoid non-specific cross reactions frequent in complex antigen preparations (Büscher *et al*., 1991). The test follows a procedure similar to the CATT, but as it is usually performed on diluted blood (≥1:4) it is more laborious to perform (Jamonneau *et al*., 2000). The LATEX/*T. b. gambiense* showed a higher specificity (up to 99%) but a lower, or similar, sensitivity (form 84 to 100%) when compared to the CATT assay (Truc *et al*., 2002; Penchenier *et al*., 2003).

1.2.2.3 Immunofluorescent antibody test (IFAT) and enzyme-linked immunosorbent assay (ELISA)

The enzyme-linked immunosorbent assay (ELISA) and the indirect immunofluorescent antibody test (IFAT) can detect specific host antibodies (IgM, IgG), related to the presence of parasites in blood, plasma, serum or cerebrospinal fluid, after 3-4 weeks of infection. Tests use purified trypanosomal glycoproteins or lysates of whole trypanosomes of selected antigen types (Büscher and Lejon, 2004). The immunofluorescent antibody test has been used with success for HAT control in different countries (Noireau *et al*., 1988; Simarro *et al*., 2006) due to its high sensitivity and specificity (evaluated as superior to the CATT test). The ELISA methods can be performed with serum, filter paper eluates or cerebrospinal fluid (Lejon *et al*., 1998), but they were also shown to be able to detect specific antibodies against *T. b. gambiense* VSGs in the saliva, with sensitivity and specificity above 90%, thus opening new perspectives for the development of a new, non-invasive serological test (Lejon *et al*., 2006). The ELISA assay can also be used for detection of parasite antigens in patients' sera (Liu *et al*., 1989). This approach has the advantage of demonstrating that the parasite is still, or has recently been, present in the host and does not rely on his immune response. Various antigen candidates are currently under evaluation, although their low concentration in circulation could represent a major limitation for the development of a test for African trypanosomiasis (Radwanska, 2010). Moreover, studies on animal infections raised doubts about the sensitivity and specificity of this approach (Rebeski *et al*., 1999). Due to the need of expensive and sophisticated equipment and trained personnel, the use of IFAT and ELISA is restricted to specialised laboratories (Chappuis *et al*., 2005).

1.2.3 Parasitological methods

Direct detection of parasites in human fluids (lymph node aspirate, blood or cerebrospinal fluid) through light microscopy has always represented the "gold standard" of HAT diagnosis (Büscher and Lejon, 2004; Chappuis *et al*., 2005). Due to risks related to available drugs, confirmation of infection by parasitological techniques for clinically or serologically diagnosed suspects should always be done before starting treatment (Louis *et al*., 2001). Microscopy has virtually 100% specificity, but suffers from a very low sensitivity, that significantly affects the overall efficacy of African trypanosomiasis diagnosis in the field, failing to confirm 20-30% of infections (Robays *et al*., 2004; Lutumba *et al*., 2005). The main cause of this limited sensitivity is represented by the low

and fluctuating parasitaemia typical of *T. b. gambiense* infection: parasites seldom exceed 10,000 trypanosomes/ml (a number easily detectable) but can be present at numbers lower than 100 trypanosomes/ml (below the detection limit of the most sensitive parasitological methods in use) (Chappuis *et al*., 2005). To decrease the number of false negatives, it is possible to examine various samples over consecutive days, or to follow-up seropositives at regular intervals, but these strategies are difficult to apply in rural settings. Processing samples with concentration techniques before viewing improves the sensitivity and increases the cost-effectiveness of confirmation algorithms (Lutumba *et al*., 2007), but it also makes parasitological methods more laborious and expensive, limiting their routine use (Lutumba *et al*., 2006). Despite all of these drawbacks, light microscopy is widely used in the field because of its simplicity, its immediate results and the lack of a valid alternative.

1.2.3.1 Chancre aspirate

Trypanosomes can be detected in the chancre several days earlier than in the blood (Chappuis *et al*., 2005), especially in the Rhodesian form (Louis *et al*., 2001), but a blood smear is more sensitive. The chancre aspirate can be viewed directly under the microscope or after fixation and Giemsa-staining. This procedure is seldom used in the field because most infections are detected when the chancre has already disappeared (Büscher and Lejon, 2004).

1.2.3.2 Lymph node aspirate

Due to its simplicity, cervical lymph node palpation is systematically done (often in association with CATT) for population screening in many endemic countries. Even if this test is considered less cost-effective than the agglutination assay (Lutumba *et al*., 2005), in some areas it appears to be the best method for early diagnosis of human African trypanosomiasis (Vanhecke *et al*., 2010). When enlarged lymph nodes (Winterbottom's sign) are identified, they are punctured and the fresh aspirate is spread on a slide and covered with a coverslip. The wet preparation is then quickly examined (to avoid lysis of parasites in the sample) by light microscopy at ×400 total magnification for the presence of motile trypanosomes. The sensitivity of this method varies between 40 and 80%, depending on the parasite strain, the stage of the disease (sensitivity is higher during the first stage) and the prevalence of other infections causing lymphadenopathy (Louis *et al*., 2001; Büscher and Lejon, 2004).

1.2.3.3 Thin and thick blood films

To prepare wet blood films, 5 or 10 µl of finger-prick blood are placed on a slide and examined microscopically under a coverslip at ×400 total magnification (Louis *et al*., 2001). Trypanosomes are revealed by their moving between the erythrocytes. In spite of its very low sensitivity, with a detection limit as high as 10,000 trypanosomes/ml (1 parasite/200 microscope fields) this method is still used in some centres (especially for *T. b. rhodesiense*) because it is very simple, cheap and offers immediate results (Büscher and Lejon, 2004). Fixed thin blood films stained with Giemsa or Field's solutions have a similar low sensitivity (Chappuis *et al*., 2005). The preparation of a thick blood film is, therefore, preferred since it slightly improves the sensitivity to 5,000 trypanosomes/ml (Louis *et al*., 2001). To prepare a thick blood film, 20 µl of finger-prick blood is placed on a small area of the microscope slide and defibrinated by the use of the corner of another slide. The sample is then left to dry without being fixed, protected from direct sunlight, stained with Giemsa or Field's solution and finally observed under the microscope at ×1,000 total magnification (Büscher and Lejon, 2004). This technique is the most widely used in the absence of a centrifuge, even if examination of each slide can take 10 to 20 minutes and must be carried out by an expert microscopist, since parasites are often deformed during sample preparation and are easily missed (Chappuis *et al*., 2005).

1.2.3.4 Microhaematocrit centrifugation technique (mHCT)

The blood concentration technique of microhaematocrit centrifugation (mHCT), also called the capillary tube centrifugation technique (CTC) or Woo test (Woo, 1970), is generally used during mass surveys to test CATT-positive suspects in whom the diagnosis could not be confirmed by classical methods (Chappuis *et al*., 2005). The mHCT is relatively easy to perform: it consists in filling three-quarters full heparinized capillary tubes with 50-60 µl of finger-prick blood. After being sealed at their end, the tubes are centrifuged at high speed for 6-8 minutes in a haematocrit centrifuge, in order to concentrate the trypanosomes present in the blood at the level of the buffy coat. The capillary tubes are then mounted on a special holder and can then be directly viewed at low magnification (×100 or ×200 total magnification) for mobile parasites (Louis *et al*., 2001; Chappuis *et al*., 2005). By examining more than one capillary tube (usually 6 or 8), the sensitivity of mHCT increases, and fewer than 500 trypanosomes/ml can be detected (Büscher and Lejon, 2004). The mHCT is quite time-consuming and the presence of microfilariae in the blood can hamper detection of smaller trypanosomes (Lutumba *et al*., 2006). The need of a

centrifuge represents the major drawback to the implementation of this technique in the field (Jannin and Cattand, 2004).

1.2.3.5 Miniature anion-exchange centrifugation technique (mAECT)

Since its adaptation for field diagnostic use in 1979 (Lumsden *et al*., 1979), the miniature anion-exchange centrifugation technique (mAECT) has been continuously improved (Kimber, 1984; Zillmann *et al*., 1996; Truc *et al*., 1998b; Büscher *et al*., 2009). This method purifies trypanosomes from blood using anion-exchange chromatographical columns containing diethylaminoethyl-cellulose (DEAE-52) and then it concentrates them by centrifugation before viewing (Lumsden *et al*., 1979). The chromatographical separation depends on difference in surface charges of the blood cells and the parasites, which are less negatively charged because their glycoprotein coat keeps the negative phospholipid head groups away from the matrix. When infected blood is mixed with PSG (phosphate saline glucose) buffer at pH 8 and is added to the column, the red and white blood cells adhere to the DEAE gel particles, while trypanosomes, being at their isoelectric point, flow through and are collected at the bottom of a sealed glass tube. After low speed centrifugation, the tip of the tube is mounted on a special holder and examined for the presence of trypanosomes using light microscopy at low magnification. Since a large blood volume (300-350 µl) is used, high sensitivity is achieved (the detection limit is less than 100 trypanosomes/ml) (Louis *et al*., 2001). The efficiency of the technique could be further improved by processing on the column the buffy coat obtained from a larger volume of blood (5 ml) (Camara *et al*., 2010). However, the mAECT also has some drawbacks: the manipulations are quite time-consuming, materials are expensive and an energy source is needed (Chappuis *et al*., 2005). Initial evaluation in experimentally infected animal blood showed that this technique was more sensitive than the mHCT (Sachs, 1984). Both the mAECT and the mHCT need 30 minutes for results, but the microscopy phase for the mAECT is faster (1 minute, compared to 5 minutes for the mHTC) (Lumsden *et al*., 1979). The mAECT is currently considered the most sensitive parasitological technique for detection of trypanosomes in blood, with sensitivity in the field in the range of 75.3-84.5% (Miézan *et al*., 1994; Lutumba *et al*., 2006).

1.2.3.6 Quantitative buffy coat (QBC)

The quantitative buffy coat (QBC, Becton-Dickinson) is a very sensitive technique initially developed for rapid cell count and applied to malaria diagnosis. It is a modification of the

mHCT method that associates concentration of the parasites by centrifugation with their fluorescence staining using acridine orange (Bailey and Smith, 1992; Chappuis *et al*., 2005). For sample preparation, 60 µl of finger-prick blood are loaded into capillary tubes containing EDTA, acridine orange and a small floating cylinder and are centrifuged at high speed for 5 minutes. Fluorescent DNA of motile trypanosomes can be visualised in a darkroom in the expanded buffy coat by using a UV light connected to a special objective (60×) containing the appropriate filter. The need of this fragile equipment prevents the use of this test by mobile teams, limiting its application to referral centres (Chappuis *et al*., 2005). The QBC is a very sensitive technique, with a detection limit estimated lower than 500 trypanosomes/ml (Louis *et al*., 2001). Compared to the mAECT, the QBC was found to have a slightly lower sensitivity both on finger-prick and venepuncture samples, but due to its simplicity and rapidity (only 15 minutes instead of the 30-45 minutes needed for mAECT result) its use was recommended for routine screening (Truc *et al.*, 1998a). Nevertheless, the costs of this technique can represent a major obstacle for its implementation in low-income countries.

1.2.3.7 *In vivo* and *in vitro* isolation of trypanosome strains

Trypanosome strains have always been isolated for research purposes from patients through inoculation of infected blood or cerebrospinal fluid into susceptible laboratory animals. Immunosuppressed African *Mastomys natalensis* rats are considered the best recipient for primary propagation of *T. b. gambiense*, with a success rate of 50% (Büscher *et al*., 2005; Maina *et al*., 2007b), but *Grammomys surdaster* thicket rats were shown to lead to even higher percentages of success (Büscher *et al*., 2005). The process of isolation and propagation in rodents is problematic, especially for the low virulent Gambian strains, and requires long incubation times (Brun *et al*., 2001). A simpler kit for *in vitro* isolation (KIVI) of trypanosome strains under field conditions proved effective both for human and animal samples (Truc *et al*., 1992). The procedure of the kit consists of inoculating, aseptically, several millilitres of blood in culture medium, where bloodstream parasites transform into procyclics and multiply at room temperature during the successive weeks (Büscher and Lejon, 2004). The KIVI kit can have a diagnostic value in detecting infections when other parasitological techniques fail, but it is seldom applied due to delays to obtain the results (Louis *et al*., 2001). The long adaptation periods needed to propagate isolates can have as a consequence the selection of clones or the modification of the original isolate and, for this reasons, the number of passages must be kept at a minimum (Brun *et al*., 2001). Recently, *T. b. gambiense* parasites were successfully amplified from

cerebrospinal fluid of HAT patients by *in vitro* culture on a fibroblast feeder layer (Giroud *et al*., 2009), a new promising technique which was found more efficient than inoculation in BALB/c mice.

1.2.4 DNA technologies

The applications of DNA techniques in diagnostics are quickly expanding. This is due to the many advantages these technologies offer, first of all their high sensitivity and specificity, superior to those of traditional parasitological tools. Moreover, they allow differentiating between trypanosomes of veterinary importance and, especially, between the two human pathogenic subspecies *T. b. rhodesiense* and *T. b. gambiense*, otherwise morphologically indistinguishable. This will become a crucial aspect of disease control in the case of overlap of the two human forms (Picozzi *et al*., 2005). The continuous simplification of molecular diagnostic procedures makes their use in the field, even in relatively simply equipped laboratories, a real option (Mugasa *et al*., 2009).

1.2.4.1 PCR

The polymerase chain reaction (PCR), together with other molecular biology techniques, has been widely used for research purposes to identify infecting trypanosome DNA in animal and human blood (Gibson, 2001 and 2002a; Becker *et al*., 2004; Brun and Balmer, 2006). Different molecular probes have been tested for detection and identification of single trypanosome isolates from patients (Jamonneau *et al*., 2001). Among them, the classical TBR 1-2 primers, which recognise a repeated satellite sequence of the subgenus *Trypanozoon*, showed high sensitivity in human blood samples (up to 100%) with a specificity higher than 92% (Penchenier *et al*., 2000; Solano *et al*., 2002), but these primers can not differentiate between the three *Trypanosoma brucei* subspecies. Other markers are available for detection of *T. b. gambiense* infection, such as the genes encoding for the variant surface glycoproteins LiTat 1.3 and AnTat 11.17 (Bromidge *et al*., 1993), but these antigens are not homogeneously expressed in all isolates (Dukes *et al*., 1992). A specific target for the Gambian form has been identified in the receptor-like flagellar pocket glycoprotein TgsGP (Berberof *et al*., 2001), which has been shown to detect down to 10 trypanosomes/ml of human blood (Radwanska *et al*., 2002b). For *T. b. rhodesiense*, a PCR based on the use of primers targeting the human serum resistance associated gene (*SRA*), which confers resistance to lysis by human serum and is ubiquitous in this species (Gibson *et al*., 2002b), has been successfully applied as a molecular marker (Radwanska *et al*.,

2002a; Njiru *et al*., 2004). Regardless of the primers utilised, PCR is generally more sensitive than other serological and parasitological diagnostic methods currently in use, showing detection limits of 0.1 trypanosome/ml of cattle blood and 1 to 40 trypanosomes/ml of human blood (Jamonneau *et al*., 2004). Experimental work on animals has demonstrated that its application allows detection of active infection or relapse at a very early stage (Clausen *et al*., 1998; Bengaly *et al*., 2001). Moreover, as PCR can be performed on samples from both blood and cerebrospinal fluid, this approach offers a possible tool not only for diagnosis but also staging of HAT (Truc *et al*., 1999; Jamonneau *et al*., 2001; Section 1.2.5). Unfortunately, despite the high potential as a confirmatory assay for infection, the use of this technique is restricted to research laboratories and it is not commonly used for HAT diagnosis because of the need of expensive thermocyclers and of complex DNA purification protocols. Furthermore, PCR can be relatively slow and suffers a significant risk of sample contamination (Mugasa *et al*., 2008). Finally, this technique has not been fully validated yet: it has problems of reproducibility and can provide results at odds with those of both serological and parasitological tests (Koffi *et al*., 2006).

1.2.4.2 Loop-mediated isothermal amplification (LAMP)

Efforts have been made in order to simplify PCR protocols and make this technique more suitable for field requirements. One of the most promising innovations is a new isothermal PCR-like method, called loop-mediated isothermal amplification (LAMP) (Notomi *et al*., 2000). This technique, already commercialised for various infectious diseases, allows accurate and robust amplification of the target sequence in a single heating step (60-65°C), which can be performed in a water bath, and the results can be visualised by a simple colorimetric reaction (Njiru *et al*., 2008a and 2008b; Mori and Notomi, 2009). When applied to *Trypanozoon* isolates using primers targeting the repetitive insertion mobile element (RIME), this methodology showed a very high sensitivity (as low as 0.001 trypanosomes/ml) and reproducibility (Njiru *et al*., 2008b). Other probes have been designed for detection of specific trypanosome species including *T. b. gambiense* (Thekisoe *et al*., 2007) and *T. b. rhodesiense* (Njiru *et al*., 2008a). Moreover, the test is fast (results are available in 35 minutes) and less prone to inhibitory factors than classical PCR, a characteristic that enables the use of unprocessed template, whether buffy coat, heat-treated blood or serum (Njiru *et al*., 2008a and 2008b), although there is some evidence of a loss of sensitivity on crude samples (Thekisoe *et al*., 2009).

1.2.4.3 Molecular dipstick test (HAT-PCR-OC)

The molecular dipstick test is a simple detection tool for PCR products based on oligochromatography (OC). In positive samples, amplicons hybridize with a specific gold-conjugated probe and migrate on a chromatographical membrane where they result in a visible line in only 5 minutes. The test developed for *T. brucei* (HAT-PCR-OC) had 100% specificity and sensitivity on blood samples and was able to detect a single parasite in only 180 µl of blood (Deborggraeve *et al*., 2006).

1.2.4.4 Nucleic acid sequence-based amplification (NASBA) and NASBA-OC

The nucleic acid sequence-based amplification assay (NASBA) consists in a self-sustained real-time PCR based on the amplification of RNA targets under isothermal conditions (41°C) (Deiman *et al*., 2002). The detection of the unstable mRNA has two advantages: it is indicative of active transcription and it avoids possible DNA contamination (Büscher and Lejon, 2004). By amplification of the 18S ribosomal RNA, this assay was able to detect specifically *Trypanosoma brucei* species (without distinction between *T. b. gambiense* and *T. b. rhodesiense*) with a sensitivity of 70% on clinical samples and a detection limit of 10 trypanosomes/ml (Mugasa *et al*., 2008). The association of NASBA with oligochromatography (OC) for amplicon detection makes this assay even easier and cheaper. During a study conducted by Mugasa and collaborators, the NASBA-OC showed higher sensitivity than standard microscopy both on blood (73%) and cerebrospinal fluid (88.2%) (Mugasa *et al*., 2009). Results were available in only 90 minutes (compared to the two or more hours needed for PCR or NASBA alone) and were highly reproducible.

1.2.4.5 Fluorescence *in situ* hybridisation test (PNA FISH)

The peptide nucleic acid fluorescence *in situ* hybridization (PNA FISH) is a new technique designed to facilitate detection of trypanosomes in blood smears by the use of fluorescent molecular probes that hybridise to parasitic RNA sequences. The use of fluorescein-labelled peptide nucleic acid (PNA) probes, targeting the 18S rRNA of the subgenus *Trypanozoon*, showed a detection limit of 500 trypanosomes/ml of blood (Radwanska *et al*., 2002c), but 90 minutes were necessary for hybridisation.

1.2.5 Stage determination

When a HAT case is confirmed, the stage of the disease must be determined in order to guide treatment (Bisser *et al*., 2002; Kennedy, 2006a; Rodgers, 2009). Since specific neurological symptoms occur late and no blood test indicating brain involvement is available, this can only be done by analysis of a cerebrospinal fluid (CSF) sample obtained from the patient by invasive lumbar puncture (Enanga *et al*., 2002; Kennedy, 2008). Direct evidence of central nervous system (CNS) invasion is represented by the finding of trypanosomes in the CSF, but since this approach can be very insensitive, WHO also recommends the use of other indirect parameters related to the host's neuroinflammatory immune response: white blood cell count and protein concentration (WHO, 1998). Positivity of one of these two tests defines the second stage even in absence of parasite detection or clinical symptoms (Bisser *et al*., 2002). Nevertheless, cut-off values for these assays are disputed and the exact definition of second stage is not definitive (Kennedy, 2006a and 2006b). Improved diagnostics for disease staging is urgently needed and evaluation of alternative CSF parameters for indirect stage determination is currently under investigation (Lejon and Büscher, 2005).

1.2.5.1 Trypanosome detection in CSF

Detection of trypanosomes in the CSF is sufficient to classify a subject in the meningo-encephalitic stage of the illness (Lejon and Büscher, 2005). The CSF has to be examined immediately after lumbar puncture, because trypanosomes in this medium seem to be very fragile and they start to lyse within 10 minutes (Büscher and Lejon, 2004). This technique is simple and cheap, but it suffers from insufficient sensitivity since it can detect parasites only when their concentration is >1,000 trypanosomes/ml (Lejon and Büscher, 2002). The sensitivity can be increased by single or, especially, by double centrifugation (DC) of the CSF sample. The first technique consists of viewing the sediment obtained from centrifugation of several millilitres of CSF spread on a glass slide, while in the second method this sediment is further centrifuged in a flame-sealed capillary tube which is, then, directly examined by microscopy (Cattand *et al*., 1988). Due to the number of manipulations and the equipment required, these techniques are not widely applied (Chappuis *et al*., 2005). A simplification of the DC test was developed by Miézan and colleagues, who showed that the direct examination of the CSF sediment at the bottom of a sealed Pasteur pipette obtained after a single centrifugation had the same sensitivity as the DC technique but it was faster (10 minutes) (Miézan *et al*., 2000). The introduction of a

new plastic collector tube, originally developed for the mAECT, could further ameliorate this technique, increasing the sensitivity to <2 trypanosomes/ml of CSF (Büscher *et al*., 2009).

1.2.5.2 White blood cell count in CSF

Despite its lack of specificity, the white blood cell count is the most widely used (and often unique) technique for stage determination and follow-up (Lejon and Büscher, 2001 and 2005). The WHO upper limit for normal white cell concentration is set at 5 cells/µl, but it has been proposed to raise this value to 10 cells/µl (Chappuis *et al*., 2005) or 20 cells/µl (Lejon *et al*., 2003b), since patients found with 6 to 20 cells/µl in their CSF were successfully cured by pentamidine (Doua *et al*., 1996). These subjects, considered to be in the so-called "early second stage" or "intermediate stage" of the illness, often present non-concordant markers that complicate staging (Bisser *et al*., 2002). Once the CSF is collected (at least 5 ml), the leukocyte count must be carried out quickly to prevent cell lysis (Chappuis *et al*., 2005). In African trypanosomiasis, the CSF can present with a special type of enlarged B-cell, known as morular cells of Mott, containing cytoplasmic vacuoles filled with IgM, which can be considered pathognomic, although they are not specific for HAT (Lejon and Büscher, 2005). A recent work showed how the detection and quantification of B lymphocytes may be useful to stage the disease (Bouteille *et al*., 2009).

1.2.5.3 Protein concentration in CSF

In CSF of late stage HAT patients protein concentration is elevated (0.4-2 mg/ml) (Kennedy, 2006b), but it can also be raised during the first stage of the illness, due to the diffusion of the abundant serum immunoglobulins in the CSF (Chappuis *et al*., 2005). Cut-off values set by WHO for sleeping sickness vary according to the quantification method used (WHO, 1998). Recent data suggest that the protein concentration threshold of 370 mg/litre for the colorimetric method is too low and should be raised (Lejon *et al*., 2003b). This technique is seldom applied in African sleeping sickness control centres, because the methods are sophisticated, reagents needed are unstable and the results do not offer much more information than CSF cell count (Lejon and Büscher, 2001 and 2002).

1.2.5.4 Other markers and tests for second stage determination

CSF of second stage *T. b. gambiense* patients contains high levels of immunoglobulins, especially IgM, which are considered a strong early indicator of inflammation in the CNS

due to parasite invasion (Bisser *et al*., 2002), even if other neurological infections could cause the same effect (Lejon *et al*., 2003b). Studies on quotients CSF/serum concentration for IgM, IgG and IgA confirmed that the elevated concentration in the CSF was due to intrathecal synthesis and only partially to blood-derived immunoglobulins and that the predominant IgM presence was the most sensitive (95%) marker for brain involvement (Lejon *et al*., 2003b). Determining the IgM content in the CSF can be very difficult to carry out under field conditions but a semiquantitative latex agglutination test for IgM in CSF (LATEX/IgM) has recently been designed for field use, thanks to its reagent stability at 45ºC for more than 2 years (Lejon and Büscher, 2002). End titres (highest dilution causing an agglutination) ≥1:8 were shown to be 89.4% sensitive and 92.7% specific for presence of intrathecal IgM synthesis (Lejon *et al*., 2002b). The possibility to use the LATEX/IgM agglutination test also for stage determination of *T. b. rhodesiense* infection is under evaluation (Lejon *et al*., 2002b).

Other antibodies with different affinities are being evaluated as possible second stage markers (Lejon and Büscher, 2001). Among them, autoantibodies against brain-specific components such as neurofilaments and galactocerebrosides have been found in CSF of HAT patients (Vincendeau and Bouteille, 2006). Simple test formats to detect these antibodies not only in CSF, but also in other biological fluids like saliva, could represent a great improvement towards a less invasive assay for staging (Jannin and Cattand, 2004).

Cytokines and chemokines mediate the host's neuroinflammatory immune response and high levels of these molecules in CSF have been associated to neurological involvement in *T. b. gambiense* disease (Courtioux *et al*., 2006; Hainard *et al*., 2009). Interleukin-10, in particular, has significantly raised concentrations in plasma (Courtin *et al*., 2006) and CSF of infected patients and it could represent an interesting marker for treatment and follow-up, since its levels lower immediately after treatment (Lejon *et al*., 2002a). A combination of different markers (two chemokines, CXCL8 and CXCL10 and a brain damage marker, H-FABP) was shown to correlate to HAT second stage with 97% sensitivity (Hainard *et al*., 2009). However, the use of these indicators for staging suffers various drawbacks, such as the not direct applicability in the field, the necessity of invasive lumbar puncture and the need to exclude other brain inflammatory diseases.

Finally, the finding of trypanosome DNA in CSF by the use of PCR techniques could represent another possible tool for staging of sleeping sickness (Truc *et al*., 1999).

1.2.5.5 Polysomnography

Polysomnography is a promising non-invasive diagnostic technique that could be used to discriminate between the two stages of African trypanosomiasis (Buguet *et al*., 2005). It combines different tools (electro-encephalogram, electro-oculogram and electro-myogram) which allow the monitoring of sleep structure and phases, both known to be seriously compromised in second stage HAT patients. The detection of abnormal sleep onset rapid eye movement periods (SOREMPs) that occur shortly after CNS involvement, has been proven to be proportional to illness severity and to recede after treatment, showing a possible application also in follow-up studies.

1.2.6 Other diagnostic approaches

Novel diagnostic approaches based on the detection of specific biomarker patterns related to the presence of the disease ("fingerprints") are under study. A proteomic signature analysis technique, for example, has been demonstrated to be much more accurate than any other diagnostic test, being able to distinguish between trypanosome-infected and non-infected serum samples with a sensitivity of 100% and a specificity of 98.6% (Papadopoulos *et al*., 2004). The proteomic analysis is impracticable in the field but it could represent a very sensitive tool for the identification of new biomarker proteins for successive applications in diagnostics or drug discovery (Agranoff *et al*., 2005). Following this principle, Hainard and collaborators evaluated various molecules identified by proteomic analysis as possible indicators for HAT second stage (Hainard *et al*., 2009). Similarly, the comparison of metabolite patterns could offer another approach for discovering "fingerprints" to use for HAT diagnosis or staging. A study carried out by Wang and collaborators demonstrated the utility of the analysis of the metabolome for diagnostics, by showing a correlation between *T. b. brucei* infection in mice and systematic perturbations in the metabolites profile of the animal's urine and plasma (Wang *et al*., 2008).

1.2.7 Follow-up

Ideally, patients should be periodically checked (visits at 3, 6, 12, 18, 24 months) for a total period of two years after treatment to confirm complete cure (WHO, 1998), but in practice this is hardly achieved in the field, where compliance with follow-up is extremely low (Legros *et al.*, 1999). Unfortunately, unsuccesful treatment regimens are far from rare and early detection of these failures would increase the chances of the patients to be cured.

Causes of drug relapses are still unclear. Many phenomena could be involved in this process, such as low drug potency, under-dosing, pharmacokinetic differences between individuals, presence of co-infections (especially HIV), poor health of the patient at the moment of admission to the treatment centre or decreased susceptibility of trypanosomes to the drug. To assess chemotherapy success both direct and indirect diagnostic techniques are used, but standard operational criteria are still lacking. Since no blood markers for cure have been identified so far and the CATT test resulted unreliable during follow-up examinations (Lejon *et al*., 2010), treatment failure is usually identified as a deterioration of the CSF parameters. This phenomenon normally occurs in 3-9% of late stage patients treated with melarsoprol (Maina *et al*., 2007a). Detection of trypanosomes in blood, lymph nodes or CSF indicates treatment failure or relapse, but due to low sensitivity of parasitological techniques, increased leukocyte count and recurrence of neurological symptoms are also often evaluated (Lejon and Büscher, 2001 and 2005; Mumba Ngoyi *et al*., 2009). Patients hospitalised with severe brain inflammation or as previous relapsing cases are at high risk of treatment failure (Legros *et al.*, 1999; Lejon *et al*., 2008). A recent work on *T. b. gambiense* patients identified the association between white cell count ≥ 8 cells/ml and LATEX/IgM end titre ≥ 1:4 as being 97 % and 100% specific for relapse prediction after 12 and 18 month from treatment respectively (Lejon *et al*., 2008). The identification of criteria for treatment outcome would have the great advantage of shortening the follow-up period of patients with low risk of failure (Mumba Ngoyi *et al*., 2010). Since normalisation of CSF values is generally slow, the use of the PCR technique for earlier detection of relapses by mean of trypanosome DNA amplification is strongly advocated (Truc *et al*., 1999).

1.2.8 Diagnosis of drug resistance

HAT treatment is complex for a number of reasons: need for hospitalisation, toxicity, stage-specificity and high costs of the drugs are all major issues in endemic countries. Moreover, the loss of efficacy of melarsoprol (the drug most used to treat the second stage of the Gambian form and the only one available for late stage *T. b. rhodesiense* infection) has become a pressing problem. In recent years the number of melarsoprol treatment failures has increased to alarming levels in some areas, reaching values of 30% in Uganda (Legros *et al.*, 1999). Drug resistance of some trypanosome strains to melarsoprol has been indicated as an important cause for these chemotherapic failures in individuals infected with *T. b. gambiense* (Brun *et al*., 2001; Matovu *et al*., 2001a), but other factors may contribute (Maina *et al*., 2007a), such as differences in drug pharmacokinetics between

individuals (Legros *et al.*, 1999). A major problem for drug resistance study is the difficult isolation and propagation of trypanosomes from relapsing patients, thus limiting the number of samples available for successive *in vitro* and *in vivo* drug sensitivity tests in the laboratory (Brun *et al*., 2001; Section 1.2.3.7).

Various mechanisms, affecting both drug levels inside the parasite and the drug target(s), can contribute to reduced sensitivity to trypanocidal compounds (Barrett and Fairlamb, 1999; Mäser *et al*., 2003). Resistance to melaminophenyl arsenicals and diamidines has been, at least partially, ascribed to altered activity of the *T. brucei* P2 amino-purine transporter involved in their uptake (Carter and Fairlamb, 1993; Barrett and Fairlamb, 1999; Mäser *et al*., 1999; Delespaux and de Koning, 2007). The loss of P2 function was found responsible for diminished internalisation of these classes of compounds and multidrug resistance onset (Barrett and Fairlamb, 1999). Increased drug export through over-expression of a *T. brucei* multidrug-resistance protein, called MRPA, has also been found to cause melarsoprol-resistance *in vitro*, but data were not supported *in vivo* (Alibu *et al*., 2006). Instead, mutations in the *TbAT1* gene, which encodes for the P2 transporter, have been identified in resistant trypanosomes both in laboratory strains and field isolates (Mäser *et al*., 1999; Matovu *et al*., 2001a). The use of a PCR/*Sfa*NI RFLP technique (PCR amplification of the *TbAT1* gene followed by analysis of the restriction fragment length polymorphism for *Sfa*NI) allowed identification of mutated forms of the transporter, but this method was not able to identify all resistant strains, since many of them had a wild type sequence of the *TbAT1* gene (Mäser *et al*., 1999; Matovu *et al*., 2001b). Deletion of the whole *TbAT1* gene is also a rare, but possible, event in field isolates (Matovu *et al*., 2001b). The treatment of patients infected with strains less sensitive to melarsoprol has both the consequences of unnecessarily exposing them to the highly toxic side effects of the arsenical compound and of contributing to the maintenance of the alleles associated with resistance in the trypanosome population (Kazibwe, 2008). In a recent paper, Kazibwe and colleagues showed how the withdrawal of melarsoprol as first-line drug in a focus with high levels of treatment failures correlated with disappearance of mutant alleles in the trypanosome isolates, identified with the PCR/*Sfa*NI RFLP technique (Kazibwe *et al.*, 2009). This study demonstrates the potential benefits of drug resistance tests for treatment decision making and rational management of HAT in resource-poor settings.

In our laboratory, a rapid and easy fluorescent test able to identify resistance to arsenical and diamidine drugs, by exploiting altered activity of the P2 transporter in resistant strains, was developed (Stewart *et al.*, 2005). The test utilises the diamidine DB99 [2,5-bis(4-

amidinophenyl)-3,4-dimethylfuran], which is actively transported by trypanosomes through the P2 permease and accumulates in DNA-containing organelles (nucleus and kinetoplast). DB99 is intrinsically fluorescent and its internalisation inside parasites can be monitored using a standard fluorescence microscope (λ_{EX}=330 nm, λ_{EM}=400 nm). The test was proven able to discriminate between various sensitive (stained) and resistant (unstained) strains in mice blood, both from *in vitro* culture and field isolates, if exposure to the drug was kept inferior to 1 minute.

1.3 Diagnosis of *T. b. rhodesiense* infection

T. b. rhodesiense causes an acute, febrile form of HAT in east Africa and can lead to death of the patient within months (Barrett *et al*., 2003). The parasite is harboured in a wide animal reservoir (Smith *et al*., 1998; Stich *et al*., 2002), infected livestock representing a major cause of maintenance and spread of the disease (Hutchinson *et al*., 2003; Picozzi *et al*., 2005). Before the advent of molecular technologies, the immune trypanolysis test (Rickman and Robson, 1970; Van Meirvenne *et al*., 1995) had been the only tool to discriminate between human infective (mainly *T. b. rhodesiense*) and non-infective trypanosome species isolated from animals and it was widely used for epidemiological purposes.

For diagnosis of *T. b. rhodesiense* an effective serological tool, equivalent to the CATT, is still lacking and is difficult to envisage due to the higher degree of VSG variability than in *T. b. gambiense* (Louis *et al*., 2001). Case-detection for Rhodesiense trypanosomiasis is, therefore, based on passive surveillance (Hutchinson *et al*., 2003) and initial diagnosis relies on clinical symptoms (Garcia *et al*., 2006). For *T. b. rhodesiense* infection biological parameters are generally more abnormal than for *T. b. gambiense* form, including severe anaemia, liver dysfunction, thrombocytopenia and cardiac failure that often causes the death of the patient (Lejon and Büscher, 2005). On the contrary, the neurological symptoms typical of the Gambian disease are not frequent in Rhodesiense trypanosomiasis and a clear distinction between first and second stage is more difficult to determine (Kennedy, 2006a). Parasitological confirmation and staging are based on the same methods used for *T. b. gambiense* disease but, since *T. b. rhodesiense* infection presents a high and persistent parasitaemia, the detection of the parasites is relatively easy (Kennedy, 2008) and direct examination of thin or thick blood smears or lymph node aspirate is usually sufficient (Smith *et al*., 1998). More sophisticated assays like ELISA and PCR are available, but not applicable in the field (Chappuis *et al*., 2005).

1.4 African animal trypanosomiasis

African animal trypanosomiasis (also called nagana) represents a major obstacle to livestock production and, therefore, to the development of the rural areas of the continent, with a loss estimated at more than $ 1,000 million annually (Kristjanson *et al*., 1999). The disease is mainly caused by three tsetse-transmitted trypanosome species, *Trypanosoma congolense*, *Trypanosoma vivax* and, at lesser extent, *Trypanosoma brucei* ssp., which infect or co-infect both domestic and wild mammals. Animal trypanosomes are not infective to humans because they are susceptible to lysis by the trypanolytic factor present in human serum (Pays and Vanhollebeke, 2008). Once injected into the mammalian host, *T. congolense* and *T. vivax* do not usually leave the blood vessels, even if they can cause tissue lesions, while *T. brucei* can cause cerebral infection (Naessens, 2006). Typical clinical features in cattle are fever, anaemia, and immunosuppression, with gradual loss of weight and emaciation that usually leads to death of the animal through heart failure. Some local bovine breeds are able to control anaemia and parasitaemia and remain productive after having contracted trypanosomiasis: a phenomenon defined as trypano-tolerance (Naessens, 2006).

Control of the disease relies on the use of insecticides applied to animals to protect them from tsetse bites and on chemotherapy/chemoprophylaxis. Three compounds are used for treatment of nagana, independently of the infecting species: diminazene aceturate (a diamidine), homidium (the phenanthridine ethidium) and isometamidium (a hybrid molecule from ethidium and diminazene). Isometamidium is also used as a prophylactic agent (Leach and Roberts, 1981; Connor, 1992). All of these drugs have toxic effects on animals and cross-resistance of isometamidium with homidium and, to a lesser extent, with diminazene, limits their efficacy (Codjia *et al*., 1993; Peregrine *et al*., 1997; Afewerk *et al*., 2000; Delespaux and de Koning, 2007). The identification of new molecular markers is currently under study to improve drug resistance diagnosis and substitute conventional field and laboratory tests, which are laborious and expensive (Delespaux *et al*., 2008).

Diagnostic techniques used for detection of animal trypanosomes are essentially the same as those applied to humans (Molyneux, 1975; Leach and Roberts, 1981; Connor, 1992) and the problems encountered are similar (Uilenberg, 1998). The diagnosis is usually carried out on blood samples, while lymph node aspirate is less used and CSF is examined only exceptionally. The “gold standard” in the field to detect and differentiate animal trypanosome species (which can be identified by morphological characteristics) is

represented by the cheap light microscopy examination of wet or dry thin and thick blood smears (Connor, 1992). However, as for human African trypanosomiasis, this approach is highly insensitive and laborious due to the very low levels of parasitaemia in chronic infected animals. For wet preparations, the buffy coat under phase contrast illumination (Murray *et al*., 1977) is the most sensitive technique. Serological techniques like ELISA and IFAT are widely used but only for surveillance purposes (Eisler *et al*., 1998; Reyna-Bello *et al*., 1998; Ezeani *et al*., 2008), as well as new PCR methods, which allow differentiation between clinically important species and subspecies (Cox *et al*., 2005; Picozzi *et al*., 2002 and 2008).

1.5 Need for new diagnostics

The fact that so many diagnostic methodologies have been applied and proposed for sleeping sickness is a demonstration that none of them meets all the requirements of an ideal test with regard to simplicity, efficiency, rapidity and low cost. Despite the crucial importance of correct diagnosis for disease management in developing countries, relatively limited resources are invested in microbial diagnostics, which remains, together with drug research, particularly neglected (Checchi *et al*., 2006; Perkins and Small, 2006; Anonymous, 2007). Several international organisations are trying to address the issue. WHO, with its programme for Research and Training in Tropical Diseases (TDR), has set up a network to facilitate research and introduction of new diagnostic tests (Remme *et al*., 2002). More significantly, a public-private partnership named FIND (Foundation for Innovative New Diagnostics, http://www.finddiagnostics.org/), was launched in 2003 to fill this gap by promoting the introduction of new products for diagnosis of infectious diseases (such as LAMP, the loop-mediated isothermal amplification of DNA) and by implementation of those already existing (Steverding, 2006; WHO, 2006a). The FIND commitment to HAT is aimed at the improvement of both serological and parasitological techniques. Concrete results of these efforts have been the development of a new concentration method by lysis of the red blood cells and a new improved kit for mAECT, now produced in the Democratic Republic of Congo and marketed in the other endemic countries (Büscher *et al*., 2009). However, as already mentioned (Section 1.2.3.5), the mAECT is not ideal and new possibilities have to be explored. For example, since the real bottleneck of HAT diagnosis is represented by the low sensitivity of the confirmatory step by light microscopy, its improvement by the use of fluorescence microscopy could bring concrete benefits in the detection of trypanosomes among a complex matrix such as blood.

1.6 Fluorescence microscopy for diagnosis of infectious diseases

Light microscopy has always represented the cornerstone of laboratory diagnosis of infectious blood and tissue parasites, but, despite the minimal amount of equipment required, the low concentration of organisms and their difficult differentiation hamper this procedure (Rosenblatt, 2009). In recent years, fluorescence microscopy applications have been expanding in many fields of biological research as well as clinical pathology and medical diagnosis, becoming one of the most powerful tools for high contrast imaging (Lichtman and Conchello, 2005; Yuste, 2005). Compared to traditional light microscopy, this technology can offer equal simplicity but higher specificity, sensitivity and rapidity of screening and, for these reasons, it has been increasingly exploited for infectious disease diagnosis and monitoring (Sanborn *et al*., 2005).

The avalability of more affordable instrumentation has allowed the use of fluorescence techniques also in countries with little resources, where it has been successfully utilised to improve diagnosis of various infections, including tuberculosis and malaria, which otherwise still rely on light microscopy of stained films. A systematic review of numerous studies on the subject demonstrated that fluorescence microscopy for tuberculosis diagnosis was on average 10% more sensitive than classical sputum smear light microscopy and equally specific (Steingart *et al*., 2006). The detection of *Mycobacterium tuberculosis* by auramine O or auramine-rhodamine staining, by enabling microscopists to use lower magnifications, also decreased the time needed for smear examination. Moreover, auramine O labelling of the specimens is a simpler procedure than the standard Ziehl-Neelsen technique (Hendry *et al*., 2009; Minion *et al*., 2009). For the diagnosis of malaria the same advantages of rapidity and efficacy of fluorescence techniques over classical tools (Giemsa-stained blood smears) have been observed (Keiser *et al*., 2002). Both the use of acridine orange for direct staining of blood films (Delacollette and Van der Stuyft, 1994; Kong and Chung, 1995; Gay *et al*., 1996) or in association with the quantitative buffy coat (Wongsrichanalai *et al*., 1991) and the combination of DAPI and propidium iodide (Caramello *et al*., 1993) proved useful, especially for the detection of low levels of parasitaemia. A dual staining method for malaria, using a fluorescent dye (SYBR Green I), to rapidly detect parasites within red blood cells, and Giemsa, for speciation, has also been developed (Guy *et al*., 2007). The implementation of fluorescence microscopy for use in endemic low-income countries offers many benefits, but the process also faces

various problems principally related to a lack of resources, inconsistent electricity supplies and the instability of microscopy reagents (Keiser *et al*., 2002; Steingart *et al*., 2006). Moreover, trained microscopists are needed to distinguish non-specific fluorescent staining of debris and the microorganisms for diagnosis (Shapiro and Perlmutter, 2008). The high cost and fragility of fluorescent microscopes and their light sources is also a major issue (Delacollette and Van der Stuyft, 1994; Hänscheid, 2008). To address this problem a more affordable interference filter, specific for acridine orange, to be mounted on normal light microscopes was designed for malaria diagnosis (Kawamoto, 1991; Delacollette and Van der Stuyft, 1994). The current development of new light sources for fluorescence that exploit light-emitting diode (LED) technology (Section 1.6.3), offers considerable promise towards the availability of more affordable and simple fluorescence microscopes suited for field use (Marais *et al*., 2008).

1.6.1 The fluorescence process

Fluorescence is a property of a small number of molecules called fluorophores or fluorochromes, which generally contain polyaromatic hydrocarbons or heterocycles in their chemical structure. Fluorochromes include various organic dyes (like fluorescein or rhodamine) extensively used for labelling of molecules, cells, and tissues (Suzuki *et al*., 2007; Gonçalves, 2009). An increasing number of fluorescent genetically-encoded proteins (such as the green fluorescent protein, GFP) are today available and utilised in protein localisation and gene expression studies in living cells (Chalfie *et al*., 1994; Shaner *et al*., 2004). Fluorophores are able to absorb light with a specific energy and re-emit it at longer wavelengths as fluorescence following a three step process (Lichtman and Conchello, 2005; Figure 1.6). Initially, the fluorophore absorbs a photon of energy $h\nu_{EX}$ emitted by an external source (such as an incandescent lamp or laser) that allows one of its electrons to pass from its ground state S_0 to an excited outer orbital (S_1'). Conjugated double bonds present in these molecules can distribute excited electrons, so that the energy necessary for their excitation is relatively low. During the brief period of time (measured in picoseconds) in which the fluorophore exists in its excited state, it can undergo internal conversions, vibrational relaxation and it can interact with its molecular environment. These events have, as a consequence, a partial dissipation of its energy, yielding a relaxed singlet excited state (S_1). Finally the fluorophore spontaneously returns to its ground state S_0 by emitting a photon $h\nu_{EM}$ with a lower energy (and, therefore, a longer wavelength) than the excitation photon, because of the energy dissipation that occurred during the excited-state lifetime.

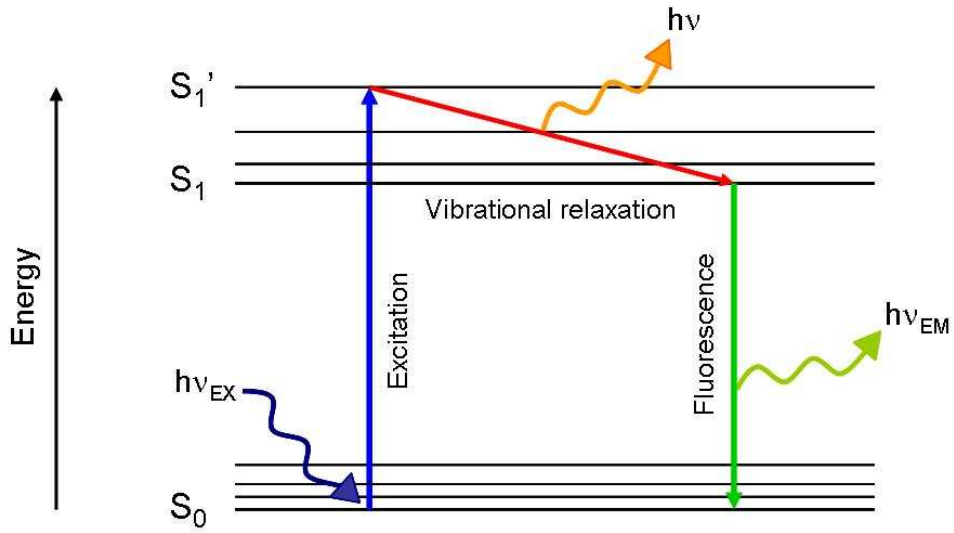

Figure 1.6 – Diagram illustrating the fluorescence process.
After absorption of a light photon ($h\nu_{EX}$), an electron of the fluorophore is excited form the ground state (S_0) to an outer orbital (S_1'). Here, a partial energy dissipation of the excited state occurs and the electron is converted into a lower excited state (S_1). Finally, the fluorophore returns to the ground state by emitting, as fluorescence, a photon $h\nu_{EM}$ with lower energy than the excitation photon (see Section 1.6.1 for more details).

For molecules in solution, the different discrete electronic transitions give rise to energy spectra of excitation and emission, which generally have mirror symmetry (Lichtman and Conchello, 2005). Under the same conditions, the wavelength of the emitted light is not related to the excitation wavelength and its intensity is proportional to the amplitude of the fluorescence excitation spectrum. The difference between the exciting and the emitted wavelength, called the Stokes shift, is fundamental to the sensitivity of fluorescence techniques, allowing the detection of emitted light against a low background, isolated from the excitation one. The high sensitivity is also a consequence of the fact that each fluorophore can generate thousands of photons and that they can be cyclically excited and detected, unless irreversibly damaged in the excited state (photobleaching phenomenon). Photobleaching (Chapter 3) is defined as the chemical destruction of a fluorescent molecule as a result of its excitation (Petty, 2007) and must not be confused with quenching, which is a reversible loss of fluorescence caused by non-covalent interactions between the fluorophore and its environment.

The fluorescent signal of a fluorophore depends on its absorption and emission efficiencies, which are respectively quantified in terms of molar extinction coefficient (ε) and quantum yield (QY). The value of ε is specified for the absorption maximum wavelength and represents the probability that the molecule will absorb a photon. Typical ε values for small fluorophores are comprised between 25,000 to 200,000 M^{-1} cm^{-1}. The quantum yield of a fluorophore is a measure of the total light emission over the entire

fluorescence spectral range and, therefore, of the efficiency with which the absorbed light produces fluorescent emission. High fluorescent intensities are obtained for QY close to 1. Fluorescence intensity for a given fluorophore is proportional to the product of ε and QY (Lichtman and Conchello, 2005).

1.6.2 The fluorescence microscope

The basic parts of a fluorescence microscope include a high intensity light source to excite the fluorophore and a series of filters to select photons of the excitation wavelength and to separate them from the light emitted by the fluorophore (Lichtman and Conchello, 2005). A detector (usually a digital CCD camera) is needed to collect emitted photons and convert them to a recordable output signal (Petty, 2007). The most commonly used light source is a low-pressure mercury (or xenon) arc lamp, where the ionization of the gas is obtained by a high voltage current. Since these lamps emit in a wide range of wavelengths across the visible spectrum (380-750 nm), an excitation filter to preselect the excitation wavelength and block all others is required. In epifluorescent microscopes (the most efficient and widely used) (Figure 1.7) a dichromatic (also called dichroic) beamsplitter mirror, then, reflects the excitation light into the objective while allowing the emitted light, at higher wavelength, to pass through. In this system the objective has not only a function of imaging and magnification of the specimen, but also of condenser for the excitation light. A secondary barrier filter is usually present to prevent any scattered excitation light from reaching the eyepiece (Sanborn *et al*., 2005). In modern fluorescence microscopes barrier filters and dichromatic mirror designed for a particular spectral range are all contained in a holder, called filter cube.

Despite the great improvements in optics and detection devices, the illumination sources used for fluorescence (mercury and xenon arc lamps) have, until recently, not advanced (Cole and Turner, 2008). Apart from their high purchase and operational costs, conventional gas discharge bulbs have other technical drawbacks: their broad-spectrum emission has wide, uncontrolled intensity variations and high quantities of dangerous UV radiation, which can not be completely shielded by blocking filters, is emitted. Moreover, these bulbs require several minutes to reach optimal intensity, they produce high amounts of heat and their lifespan is short (200-300 hours). In the case of mercury bulbs, environmental problems of disposal must also be taken into account (Anthony *et al*., 2006; Cole and Turner, 2008; Robertson *et al*., 2009).

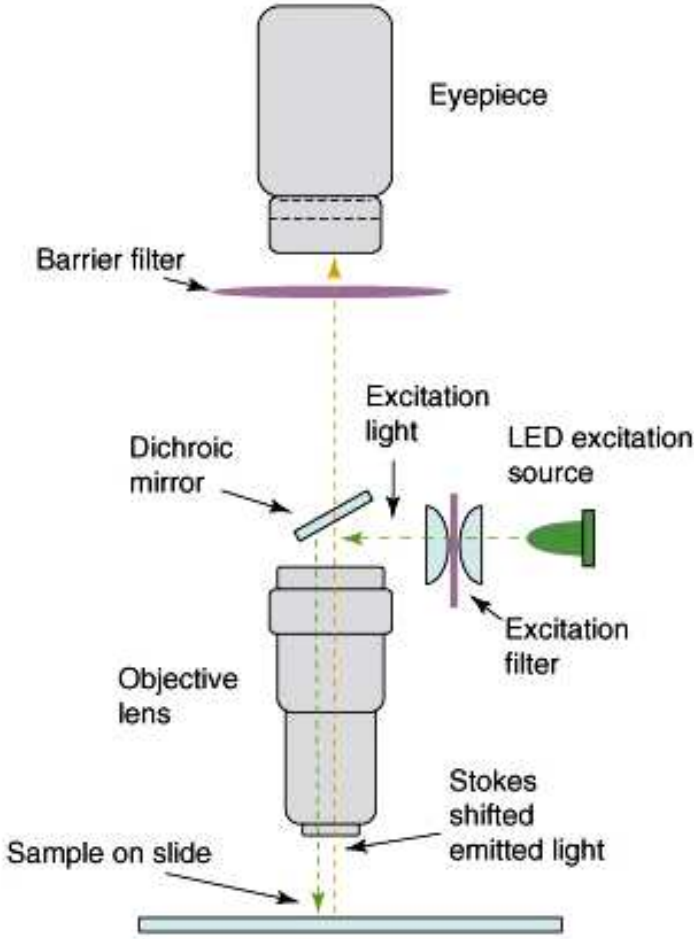

Figure 1.7 – Schematic illustration of the light path of an epifluorescence microscope. Epifluorescence microscopy utilises the objective both to focus the excitation light on the specimen and to collect the emission signal. This technique is preferred to transmitted fluorescence (where the excitation light passes through the specimen) because it produces a better contrast. In this figure, a LED light source is used, but the same principles are valid for traditional mercury or xenon arc lamps.
(Reproduced with permission from Jones *et al*., 2007).

1.6.3 Light-emitting diodes (LEDs) for fluorescence microscopy

Today, a new generation of microscopes or light source modules, based on light-emitting diodes (LEDs), are available both for transmitted light and fluorescence imaging (Jones *et al*., 2005 and 2007; Hänscheid, 2008; Minion *et al*., 2009). LEDs are small semiconductor diodes of different chemical composition, which determine the wavelength of the monochromatic light, usually limited to a narrow (15 nm) band of emission (Petty, 2007). The numerous advantages that these new illumination sources have over conventional fluorescent vapour arc lamps have been pointed out by several authors (Cole and Turner, 2008; Lang *et al*., 2008; Shapiro and Perlmutter, 2008; Robertson *et al*., 2009). LEDs are very efficient in terms of converting electricity at low voltage to light and have a very long lifespan (up to 50,000 hours). By being roughly monochromatic, they do not generate UV emission and work only at the chosen wavelength, although this can also represent a

disadvantage, since it limits the number of fluorophores that can be used (Anthony *et al*., 2006). The diodes produce only minimal heat, are smaller than classical bulbs and they are easier to use: they do not need lamp adjustment, in theory they do not need excitation filters and can be repeatedly turned on and off directly without the need of a shutter. All of these characteristics make LEDs a very cheap and convenient light source for fluorescence applications: their cost is less than 10% of the price of a mercury vapour bulb (Anthony *et al*., 2006). Moreover, since LEDs need only a low voltage power supply, they can be run on batteries, a crucial aspect for their use in resource-poor settings. However, since LEDs emit photons in all directions, capturing enough light for microscopy is problematic and only some of them are sufficiently intense to be exploited for fluorescence applications (Cole and Turner, 2008).

The benefits offered by LED technology have already been tested for diagnostic purposes. The simple substitution of traditional light sources with LEDs has proven successful for detection of malaria parasites (Guy *et al*., 2007) and auramine O-stained *Mycobacterium tuberculosis*, giving sharp, even and highly contrasted images (Anthony *et al*., 2006; Hung *et al*., 2007). LED fluorescence microscopy was shown to be equally sensitive to classical mercury lamp source microscopy on sputum specimens (Marais *et al*., 2008). Shapiro and Perlmutter showed the possible application of this new technology to the development of a simple and robust fluorescence image cytometer for malaria and tuberculosis diagnosis (Shapiro and Perlmutter, 2008). Some studies also reported that the examination of samples with LED-illuminated microscopes was still possible in an environment that was not completely darkened (Hung *et al*., 2007; Marais *et al*., 2008). A recent collaboration between FIND and the Zeiss group for the development of a new, affordable LED-driven microscope for high burden countries is the latest validation of this new technology for diagnosis of infectious diseases (http://www.finddiagnostics.org/).

1.6.4 Fluorescent probes for trypanosomes

One of the main difficulties encountered in HAT diagnosis is the direct observation of parasites in blood when using light microscopy, given the low numbers of parasite generally found in infected individuals. A possible way to raise the sensitivity could be to label trypanosomes with fluorochromes, so that they are more easily detectable among other blood cells by using a fluorescent microscope. Some fluorescent applications designed to improve diagnosis of African trypanosomiasis have already demonstrated to be efficacious. These include the utilisation of acridine orange to help detection of parasites in

the quantitative buffy coat technique (Bailey and Smith, 1992; Section 1.2.3.6), or the more sophisticated fluorescein-labelled peptide nucleic acid probes developed for *in situ* detection in the PNA FISH technique (Radwanska *et al*., 2002c; Section 1.2.4.5). Non-specific staining of dyes like acridine orange can represent a problem since other human cells in the sample (especially white blood cells) can become fluorescent. The very different morphology between trypanosomes and white blood cells, however, allows easy differentiation. Many other studies on trypanosomes have used fluorescence microscopy for research purposes, by taking advantage of the innate fluorescence of various trypanocidal drugs and related compounds, or by adding specific fluorescent groups to non-fluorescent molecules to study their internalisation and localisation inside parasites. Azema and collaborators labelled hexoses with a fluorescent adduct (dansyl group) to track their accumulation inside trypanosomes through the THT1 hexose transporter (Azema *et al*., 2004). They demonstrated that dansylated hexoses cross the membrane of bloodstream form parasites without labelling erythrocytes, despite the fact that their internalisation seemed non-specific. This was probably because fluorescence within red cells was quenched due to the high concentration of haemoglobin in their cytoplasm. A similar approach was followed by other authors to study differential uptake of fluorescent compounds into wild type and melarsoprol- or pentamidine-resistant cells: fluorophores like DAPI and Hoechst 3342 (both diamidines), ethidium bromide (a phenanthridine trypanocidal) and acriflavine (an acridine) were all shown to accumulate at higher rates in sensitive cells than in resistant strains (Frommel and Balber, 1987; Bridges *et al*., 2007). Intrinsic fluorescence of the trypanocides isometamidium, ethidium bromide and the analog propidium was also exploited to identify their intracellular targets by microscopy (Cox *et al*., 1984; Boibessot *et al.*, 2002). Identically, accumulation and localisation of various fluorescent diamidine compounds, including DB75, were extensively studied by microscopy (Sturk *et al*., 2004; Mathis *et al*., 2006; Lanteri *et al*., 2008). A work conducted in our laboratory by Stewart and collaborators exploited the slower accumulation of diamidines in melarsoprol-resistant strains to develop a simple fluorescent arsenical drug resistance test (Stewart *et al*., 2005; Section 1.2.8 and Chapter 3).

1.7 Aim of this thesis

The overall objective of this project was to develop new tools to assist in the diagnosis of African trypanosomiasis and to improve the current test for drug resistance detection by exploiting LED fluorescence microscopy. Starting from the arsenical drug resistance assay designed in our laboratory (Stewart *et al*., 2005), we explored its validity using a

Figure 1.8 – The prototypical SMR portable LED fluorescence microscope (Cytoscience). This compact microscope has a standard epifluorescence design (see Figure 1.7) and utilises a 472 nm excitation LED light source. Technical details are in Section 2.5.4.2. (Reproduced with permission from Jones *et al*., 2007).

microscope equipped with a UV LED light instead of the traditional mercury arc used by Stewart and collaborators. A large part of the work was, then, focused on the evaluation of various chemical fluorescent probes for their ability to selectively enter and label trypanosomes, in order to identify valid compounds to use in the design of a more effective fluorescence field diagnostic test. Prof. D. Jones (Philipps University, Marburg, Germany) collaborated with the project by providing the UV LED prototype and the Cytoscience SMR LED epifluorescence microscope (Jones *et al*., 2005), a very compact, high resolution instrument designed for field use (Figure 1.8). The SMR scope, in addition to having relative low cost (~1,000 €) compared to traditional fluorescence microscopes, is battery-driven and is sealed against dust and water (Jones *et al*., 2007). We deliberately avoided the use of expensive fluorophores present on the market including, for example, fluorescently tagged antibodies, and focused on more affordable chemical dyes that were compatible with the range in which the Cytoscience microscope operates (λ_{EX}=472 nm, λ_{EM}>500 nm). Nevertheless, since LED sources are today available for nearly all wavelengths across the visible spectrum, and appropriate devices could eventually be developed, we also tested some fluorochromes excited outside the range covered by the Cytoscience instrument, utilising a standard epifluorescence microscope. Some of the fluorescent dyes tested were commercially available compounds, while others were new

molecules kindly provided by Prof. D. W. Boykin (Georgia State University, Atlanta, USA), or personally synthesised in collaboration with Dr. A. Sutherland's group (University of Glasgow, Glasgow, UK). Particular attention was paid to the ability of the fluorochromes to yield a bright, specific and stable signal, all important requirements when considering the use of fluorescence for field diagnostics.

2

Materials and methods

2.1 *T. b. brucei in vitro* culture

Non-human infective *T. b. brucei* bloodstream forms (monomorphic Lister 427 strain wild type and derived lines) were cultured in HMI-9 medium (Gibco, Appendix A) including 10% heat-inactivated foetal calf serum at 37°C in a humidified, 5% CO_2 environment (Hirumi and Hirumi, 1994). An aliquot of cells (1-2×10^5 cells/ml) was subpassaged in fresh medium every 48 h, when parasites had reached the mid-log phase concentration of approximately 2×10^6 cells/ml. The bloodstream form 449 line (kind gift of Dr. Christine Clayton, University of Heidelberg), a wild type line stably expressing the tetracycline repressor from the integrated pHD449 plasmid (Biebinger *et al*., 1997), was cultured in HMI-9 plus 10% FCS, including 0.2 μg/ml phleomycin. To maintain the culture as stable as possible, the same cell aliquot was subpassaged for a maximum of 30 times and then substituted with a new one. All cell line stabilates were maintained in liquid nitrogen in a freezing medium (HMI-9) containing 10% glycerol.

2.2 Cell line genotyping

All bloodstream *T. b. brucei* cell lines used during the experiments were regularly checked by PCR. The presence of four genetic markers was assessed: *TbAT1*, the gene encoding the P2 amino-purine transporter present in *T. b. brucei* S427 wild type (Mäser *et al*., 1999); the genes for neomycin resistance (*NEO*) and puromycin resistance (*PAC*), the selective markers used to replace both alleles of the *TbAT1* gene in the *tbat1*$^{-/-}$ line (Matovu *et al*., 2003) and also present in *tbat1*$^{-/-}$-derived lines; actin (*ACT*), as a positive internal control. Primer sequences for the four markers are shown in Table 2.1.

Sequence amplified	Primer pair	Primer sequence
TbAT1	MB183 (f)	5'-GACTGTCGACATGCTCGGGTTTGACTCAGCC-3'
	MB184 (r)	5'-GACTCTGCAGTAGTGCTACTTGGGAAGCCCC-3'
NEO	MB37 (f)	5'-ATGATTGAACAAGATGGATTGC-3'
	MB38 (r)	5'-TCAGAAGAACTCGTCAAGAAG-3'
PAC	MB308 (f)	5'-ATGACCGAGTACAAGCCCACGG-3'
	MB309 (r)	5'-TTGCGGGTCATGCACCAGGT-3'
ACT	MB173 (f)	5'-CCGAGTCACACAACGT-3'
	MB174 (r)	5'-CCACCTGCATAACATTG-3'

Table 2.1 – Oligonucleotides used for cell line genotyping.
***NEO*: neomycin resistance gene; *PAC*: puromycin resistance gene; *ACT*: actin; (f): forward; (r): reverse.**

TbAT1, *NEO* and *ACT* were usually amplified all together in a multiplex PCR reaction containing 2× PCR Master Mix buffer (Thermo Scientific), 0.1 µM of each primer, 1.25 U GoTaq® DNA polymerase (Promega) and template gDNA (0.5-1 ng/µl final concentration) extracted from cells grown *in vitro* using the DNeasy® Blood and Tissue Kit (Qiagen), following manufacturer's instructions. Negative controls (without any DNA) were always included.

Cycling conditions of the multiplex PCR for *TbAT1*, *NEO* and *ACT* were as follow:

1- Polymerase activation	94°C for 5 min
2- Denaturation	94°C for 1 min
3- Annealing	55°C for 1 min
4- Extension	65°C for 4 min
5- Repeat steps 2-4	35 cycles
5- Final extension	65°C for 8 min

PAC was amplified in a single marker PCR reaction. The mastermix was prepared as described above for the multiplex reaction but using 1× PCR Master Mix buffer.

Cycling conditions for *PAC* were the following:

1- Polymerase activation	95°C for 1 min
2- Denaturation	94°C for 30 sec
3- Annealing	60°C for 30 sec
4- Extension	72°C for 1 min
5- Repeat steps 2-4	35 cycles
5- Final extension	72°C for 2 min

PCR products were separated on a 1% agarose gel and visualised with SYBR® Safe DNA gel stain (Invitrogen) under a UV light transilluminator (UVP Inc.).

2.2.1 Retrieval of DNA from FTA® card for PCR analysis

Occasionally, gDNA was extracted from samples absorbed to FTA® cards (Whatman, GE Healthcare). Cards were prepared both for *in vitro* culture genotyping and, especially, for PCR testing of trypanosomes in blood, to check for the presence or absence of the *TbAT1* gene. Each card was spotted with 50-100 µl of the sample (trypanosomes in medium or

blood), air-dried and kept at 4°C until use. Small card disks, cut using a punch tool, were thoroughly washed in 200 µl FTA purification reagent (Whatman, GE Healthcare) 3 times at r.t. (5 min per wash). Disks were then washed twice in 200 µl TE buffer (Appendix B) for 5 min and finally dried for at least 1 h at r.t.. For PCR reaction, the disk was directly immersed in the mastermix solution. *TbAT1* was successfully amplified from blood samples absorbed on FTA® cards using a reaction solution containing 1× PCR buffer (Promega), 0.1 µM of each primer, 1.25 U GoTaq® DNA polymerase (Promega), 2.5 mM $MgCl_2$ and 0.3 mM dNTPs.

For *TbAT1* amplification from FTA® cards cycling conditions were as follow:

1- Polymerase activation	94°C for 2 min
2- Denaturation	94°C for 1 min
3- Annealing	55°C for 1 min
4- Extension	72°C for 90 sec
5- Repeat steps 2-4	30 cycles
5- Final extension	72°C for 2 min

2.3 Trypanosome-infected blood samples

Monomorphic bloodstream form trypanosomes were grown *in vivo* either in adult ICR Swiss and BALB/c female mice or Wistar female rats. Due to the high number of blood samples needed during this project, for routine *ex-vivo* fluorescence microscopy experiments we decided to use the discarded rat blood left after elimination of the buffy coat, which is often used for uptake assays in our laboratory. This had the double advantage of avoiding the sacrifice of too many animals and of obtaining a blood sample with, ideally, a not excessively high parasitaemia. Nevertheless, elimination of the buffy coat containing the trypanosomes also removed the white blood cells from the sample and, therefore, whole blood infected samples (usually from mice) were also used.

For growth in mice, 1×10^6 parasites of the cell line under study were injected intraperitoneally. Parasitaemia was monitored daily by tail-prick blood examination. At peak parasitaemia ($1\text{-}2\times10^8$ parasites/ml, 3-4 days post-infection), infected blood was collected by cardiac puncture in a tube containing CBSS (Appendix B) and heparin and kept ice-cold until use without any other processing. Aliquots of the infected blood were treated with the fluorochrome to test within hours from collection.

Wistar rats were inoculated with 8×10^6 trypanosomes and parasitaemia was checked daily, as for mice. Parasites were harvested at peak parasitaemia by cardiac puncture. The collected blood sample was centrifuged at 1,300×*g* for 15 min at 4°C to separate the buffy coat (used in other experiments in the laboratory). The upper layer of plasma was transferred to a new tube and mixed again with the lower layer containing the red blood cells. Fresh aliquots of this new blood sample, from which most parasites were eliminated, were incubated *ex-vivo* with the appropriate fluorochrome and used for fluorescent microscopy experiments.

The rat blood buffy coat containing concentrated trypanosomes obtained after centrifugation was further purified to prepare protein samples for Western blot (Chapter 6). Parasites were resuspended 1:1 in PSG buffer at pH 8 (Appendix B) and separated from blood cells by anion exchange chromatography, using a DE52 cellulose column. The eluted trypanosomes were collected in a 50 ml polypropylene falcon tube and washed twice (1,300×*g*, 10 min) in CBSS to eliminate every residue of PSG buffer. Parasites were, then, counted on a haemocytometer and resuspended at 1×10^8 cells/ml in CBSS. Protein extraction protocols are described in Section 2.7.7.

2.4 Alamar Blue assay

Trypanotoxicity of target compounds on different *T. b. brucei* cell lines was assessed by the Alamar Blue assay (adapted from Räz *et al.*, 1997). Bloodstream form trypanosomes (100 µl at 4×10^4 cells/ml) were added to each well of a 96-well flat-bottomed white plate, where doubling serial dilutions of the test compounds (100 µM - 0.024 nM) had been previously prepared in a volume of 100 µl HMI-9. After 48 h incubation at 37°C and 5% CO_2, 20 µl of Alamar Blue solution (resazurin sodium salt from Sigma-Aldrich; 0.49 mM in 1× PBS, pH 7.4) were added to each well, and plates were incubated for further 24 h. The reduction of the blue reagent to a colourless form by living parasites was measured with a FLUOstar OPTIMA fluorimeter (BGM Labtech) using a 544 nm excitation wavelength and a 590 nm emission wavelength. Fluorescence data were plotted as a function of drug concentration using the IC_{50} algorithm of Prism 5.0 software (GraphPad) to obtain inhibitory concentrations (50% fluorescence reduction). Untreated cells were used as negative control and known trypanocidal drugs, such as pentamidine, as positive control. All experiments were carried out in duplicate and repeated on at least three independent occasions.

2.5 Microscopy techniques

2.5.1 Fluorophores

Fluorescent compounds were obtained both from academic laboratories and from various commercial sources. DB75 dihydrochloride salt (Chapter 3), the five green fluorescent diamidines DB1464, DB1465, DB1645, DB1680 and DB1692 (Chapter 4) and the dansyl derivative diamidine DB1919 (Chapter 5) were kindly provided by Prof. D. W. Boykin (Georgia State University, Atlanta). DAPI dihydrochloride (Chapter 3), ethidium bromide and acridine orange (Chapter 4) were purchased from Sigma-Aldrich. Propidium iodide was supplied by Molecular Probes (Invitrogen). Pure isometamidium (May and Baker 4180; Chapter 4) was a gift from Mr. Brian Cover (University of Kent, Canterbury). I personally synthesised the amino acid derivatives FG10, FG70 and FG400 in Dr. A. Sutherland's chemistry laboratory (University of Glasgow) (Chapter 5).

Stock solutions of the five green fluorescent diamidines synthesised in Prof. D. W. Boykin's laboratory and of DB75 were prepared at 10 mM in DMSO (2.5 mM for DB1680). DB1919 stock solution was at 20 mM in DMSO. Stocks of ethidium bromide, propidium iodide and isometamidium chloride were at 10 mM in 1× PBS. Acridine orange stock was prepared at 17 mM in dH_2O and DAPI at 50 mM in dH_2O. The three amino acid derivatives were solubilised at 10 mM in DMSO (methanol for FG10). Aliquots of stock solutions were kept at -20°C protected from the light.

2.5.2 In vitro *trypanosome samples for fluorescence microscopy*

2.5.2.1 Fluorescent staining and sample preparation

Live trypanosomes from culture (2×10^7 cells/ml) were treated, at the desired temperature, with the test concentration of fluorochrome, in 1.5 ml Eppendorf tubes (for treatment times up to 4 h) or, for longer times of incubation, in 24-well plates (kept at 37°C in a humidified, 5% CO_2 environment). Wet films of stained live parasites in culture medium, or resuspended in 1× PBS (Appendix B) after washing, were prepared by spreading 50 µl of the sample onto a slide using a coverslip and immediately viewed under a fluorescence microscope. Otherwise, stained cells were immobilised in agarose to facilitate imaging (Section 2.5.2.2). Methanol-fixed trypanosomes from *in vitro* culture (Sections 2.5.2.3) were stained after fixation by directly spreading 50 µl of the dye (or mounting medium)

onto the specimen at the desired concentration and by covering it with a coverslip (this procedure was only used for fading quantification of UV diamidines, Section 2.5.5).

2.5.2.2 Cell immobilisation in agarose

To reduce the motility of cultured live trypanosomes for image acquisition, cells were embedded in agarose (Widener *et al*., 2007; Lanteri *et al*., 2008). After incubation with the fluorophore under study, cells (2×10^7 cells/ml) were collected by centrifugation (1300×*g* for 10 min) and resuspended in a small volume (50 µl or less) of 1× PBS. After an equal volume of 2% w/v low melting point agarose (Sigma-Aldrich) at 37°C was mixed with the cell suspension, an aliquot of the sample was immediately put onto a slide and covered with a coverslip. The agarose was left to solidify at room temperature, or by chilling the slides for 10-15 min at 4°C, before viewing.

2.5.2.3 Cell fixation in methanol

To prepare methanol-fixed parasites to use for photobleaching studies, 50 µl of a 2×10^6 cells/ml culture of *T. b. brucei* w.t. S427 in HMI-9 (10% FCS) were directly spread onto a glass microscope slide using the edge of a coverslip and left to air-dry. Slides were, then, dipped into 100% cold methanol and left overnight at -20°C. Afterwards the methanol was allowed to evaporate from the specimens under a fume-hood and slides were kept in a box at 4°C until use. Before staining, fixed cells were rehydrated by addition of 1-2 ml of PBS for 10 minutes. The excess of PBS was then removed by tilting and the specimen directly soaked with 50 µl of the fluorochrome solution and, eventually, the mounting medium (Section 2.5.2.6) and covered with a coverslip.

2.5.2.4 Cell fixation in glutaraldehyde

Glutaraldehyde was one of the fixatives tested to prepare specimens of transfected trypanosomes produced during the molecular biology work (Chapter 6). 10^7 cells were collected in 1 ml of medium and washed once in 1× PBS at 4°C, before being submerged for 5 min in chilled 2.5% v/v glutaraldehyde (Sigma-Aldrich) solution, prepared in 1× PBS. The fixative was removed from the pelleted parasites by pulse centrifuging at 8,000 rpm in a benchtop centrifuge for several seconds. Parasites were, then, resuspended in 20 µl of 1× PBS, smeared onto a lysine-coated slide (0.1% w/v poly-L-lysine solution from Sigma-Aldrich) and left to settle for 5 min: the negative charges of cells in solution

interacted electrostatically with the positive charges of the polylysine, allowing them to adhere to the slide in a dispersed monolayer (Husain *et al.*, 1980). Mounting medium (40 µl) containing a counterstain for DNA (Section 2.5.2.6) was spread on the specimen by addition of a coverslip, which was successively sealed with nail varnish.

2.5.2.5 Cell fixation in formaldehyde

Fixation in formaldehyde was the method adopted to fix transfected trypanosomes for fluorescence microscopy imaging (Chapter 6). After washing in 1× PBS, transfected and parental lines trypanosomes (1×10^7 cells) were resuspended in 0.5 ml of the buffer and mixed with an equal volume of 6% v/v formaldehyde (Sigma-Aldrich) solution, prepared in 1× PBS. Cells were fixed for 10 min at 4ºC and then separated from the fixative by centrifuging at 8,000 rpm for several seconds. The cell pellet was resuspended in 1× PBS (40 µl) and spread onto lysine-coated slides (20 µl per slide). After the solution had settled, 40 µl of mounting medium containing the DNA counterstain (Section 2.5.2.6) were added and covered with a coverslip, which was sealed in place with nail varnish.

2.5.2.6 Mounting media

The mounting medium for DNA counterstaining was prepared by mixing 0.1% v/v DAPI and 2.5% w/v DABCO (both from Sigma-Adrich) in 9:1 glycerol/1× PBS.

Various mounting media containing antifading agents were tested in attempts to decrease DB75 photobleaching in methanol-fixed cells. Two different solutions containing 5% w/v *n*-propyl gallate (NPG, [3,4,5-trihydroxybenzoic acid propyl ester]) were prepared in 9:1 buffered glycerol (9 parts of glycerol and 1 part of 1× PBS) and 1:1 buffered glycerol. Another antioxidant agent, DABCO, [1,4-diazobicyclo-(2,2,2)-octane], was prepared as a 2.5% w/v solution in 9:1 buffered glycerol (Johnson *et al.*, 1982; Florijn *et al.*, 1995). The third antioxidant agent used was Trolox, [6-hydroxy-2,5,7,8-tetramethylchroman-2-carboxylic acid], a cell-permeable, water soluble derivative of vitamin E, which was prepared at 2 mM in PBS and was used on DB75-stained fixed cells but also in living samples. All three antifading agents were from Sigma-Aldrich. For fading profile measurements, 50 µl of each mounting media containing 3 µM of DB75 were spread onto the slide containing methanol-fixed cells and covered with a coverslip, which was sealed by the use of nail varnish.

2.5.3 Ex-vivo *trypanosome samples for fluorescence microscopy*

2.5.3.1 Thin and thick blood film preparation

Thin blood smears were prepared by spreading a drop of infected blood (5 µl) along the glass slide by using the edge of a coverslip (Houwen, 2000). The smears were covered with a coverslip to produce wet films, which were immediately viewed under the fluorescence microscope. Otherwise, thin films were left to air-dry and, generally, fixed in cold 100% methanol for 2 min. After fixation, blood smears were air-dried again and kept in a slide box until viewing (usually under a 40× objective).

Thick blood films were prepared by putting a drop of blood (20 µl) onto a slide and by spreading it in a circle (1-2 cm in diameter) using the corner of another clean slide. Thick films were thoroughly air-dried but not fixed (since fixation would prevent lysis of erythrocytes by the aqueous stain solution, usually Giemsa, needed to see through the several layers of blood) and viewed under a 100× oil-immersion objective.

2.5.3.2 Staining procedures for blood films

Live *ex-vivo* trypanosomes were stained with various fluorophores by incubating aliquots of fresh infected rat blood with the dye under study inside 1.5 ml Eppendorf tubes, kept at the desired temperature. At the end of the incubation time, aliquots of blood containing stained parasites were used to prepare fresh thin smears. Staining properties of some fluorophores were also assessed after application of a drop of the dye (50 µl) directly to the wet smear, which was, then, covered with a coverslip.

For fluorescent stain of fixed thin films (Section 2.5.3.1), a solution of the fluorochrome (50 µl) was directly applied to the specimen and spread by covering with a coverslip. These samples were viewed under a fluorescence microscope without further processing or washing steps. To stain thick blood films various procedures were followed. These included (1) application of the dye (30 µl) and of a coverslip to the dry smear; (2) dehaemoglobinisation of the dry thick film in dH_2O (5 min), fixation in methanol (2 min) and subsequent staining with 30 µl of the fluorophore solution (Caramello *et al*., 1993); (3) addition of the fluorescent dye directly to the drop of blood before preparing the smear. The efficacy of these protocols is discussed in Chapter 4.

2.5.3.3 Giemsa stain

For trypanosome visualisation under light microscopy, fixed thin blood films and air-dried thick smears were put in a Coplin jar and immersed in a 5% v/v Giemsa stain solution **(**BDH Laboratory Supplies) in phosphate buffer (Appendix B) for 1 h. Excess dye was washed by briefly immerging the slides in dH_2O (5 min). Slides were then allowed to air-dry and kept in a box until viewing.

2.5.4 Image acquisition

2.5.4.1 Zeiss Axioplan fluorescence microscope

Most of the fluorophores studies were performed in a dark room, using a motorized Zeiss Axioplan 2 Imaging epifluorescence microscope (Carl Zeiss) equipped with a HBO 100W short arc mercury lamp (Osram) and 10× eyepieces, and coupled with a Hamamatsu C4742-80-12AG digital CCD camera (Hamamatsu Photonics). Three standard filter sets were generally used (all filter sets were from Carl Zeiss): filter set 49 for DAPI (excitation filter G 365 nm, beamsplitter FT 395 nm and emission filter BP 445/50 nm); filter set 10 for FITC (excitation filter BP 450-490 nm, beamsplitter FT 510 nm and emission filter BP 515-565 nm); filter set 15 for RHOD (excitation filter BP 546/12 nm, beamsplitter FT 580 nm and emission filter LP 590 nm). Other filter cubes were occasionally utilised, such as filter set 43 for DsRed (excitation filter BP 545/25 nm, beamsplitter FT 570 nm and emission filter BP 605/70 nm). Emission was recorded through a PlanNEUFLUAR 40× air, NA 0.75 objective, or a 100× oil-immersion, NA 1.4 objective (both from Carl Zeiss). Typical camera exposure times for imaging were: 33 ms for DAPI, 68 ms (or 100 ms) for FITC and 68 ms for RHOD (the precise values used during each experiment are indicated underneath every figure).

Image acquisition, image processing and quantification studies were performed using the Volocity imaging software (Improvision). Z-stack images, collected at 0.4 μm intervals, were deconvolved using the Volocity Iterative Restoration algorithm, set with a confidence limit of 97.5-98%. Images obtained using different channels were merged using the Adobe Photoshop 7.0 software package.

2.5.4.2 SMR LED microscope and UV LED microscope (Cytoscience)

The portable microscope we used during this project was the prototype for the SMR Cytoscience epifluorescent microscope (Jones *et al*., 2005). This instrument (Figure 1.8) used a 472 nm Golden Dragon LED as excitation light source (Osram) and it had a single, fixed, 40× achromat DIN objective (NA 0.65, 160 mm tube length) (Lambda Praha). The filter set was composed of a 500-510 nm blocking filter (some LED output was in this region), a 580 nm 45° dichromatic mirror and a 515-750 nm emission filter for all wavelengths from green to red. The cost of the microscope was ~1,000 euros.

The UV LED microscope (Figure 3.6) was an adapted Hund bench microscope, equipped with a 365 nm UL LED 500 mA light source (Nichia) and a 40× achromatic objective (NA 0.65) (Hund). The prototype was designed and built by Prof. D. Jones (Cytoscience). Its cost was ~1,200 euros. To acquire images we used a 1.4 MP 160 camera (Lumenera) which had a 2/3 inch Sony Extra HAD (hile accumulation diode) and was connected to a ScopePhoto software (ScopeTek). The cost of the camera was 3,500 euros.

2.5.5 Fluorescence fading measurement

Fading profile of DB75 and DAPI was measured in stained *in vitro T. b. brucei* w.t. S427 cells fixed in methanol. Before the experiment, slides were always freshly stained in the dark with 50 µl of a 3 µM solution in 1× PBS of one of the two fluorophores and covered with a coverslip. Photobleaching of DB75 was quantified either in the absence of antifading agents or after mounting with different mounting media (Section 2.5.2.6). Slides were left to set for 15-30 minutes at room temperature before viewing under the DAPI filter of the Zeiss Axioplan microscope (Carl Zeiss). Images of the continuously illuminated field were captured every 5 seconds for a total period of 5 minutes for DB75 and every 15 seconds for a total period of 12 minutes for DAPI by using the Volocity Imaging software (Improvision). Illumination conditions and acquisition settings were kept identical for experiments with both fluorophores (144 gain, 14 offset, 33 ms exposure time for DAPI filter, 40× air objective NA 0.75). Fluorescence fading was quantified using the quantitation program of the Volocity Imaging software (Improvision). All images were processed by subtracting the background (i.e. the illuminated sample with no cells in the field of view) and then percentage of intensity of fluorescence of the nucleus and kinetoplast of every cell was measured for each time point. Only trypanosomes with a single nucleus and a single kinetoplast were considered. For each dye, and also for each of

the different mounting media used in association with DB75, fluorescence decay of at least 100 stained cells was measured. Since fluorescence intensity of individual cells can vary between samples, several slides were analysed for both fluorophores. All data were plotted using an exponential algorithm of Prism 5.0 software (GraphPad).

2.6 Fluorescence spectra measurement

Excitation and emission spectra of a specific fluorophore were recorded using the LS 55 Luminescence Spectrometer (PerkinElmer), connected to the FL WinLab software (PerkinElmer). Samples were diluted in dH_2O until unsaturated signal strength was achieved. An aliquot of the samples (1 ml) was put in 10 mm quartz cuvettes (Merck) and a pre-scan was performed over the full spectrum range for excitation (200-800 nm) and emission (200-900 nm) with both slits set to 5 nm and the scan speed set to 150 nm/min. The approximate values for the excitation and emission maxima obtained during the pre-scan were, then, used to record the excitation and emission spectra with more accuracy, by running successive scans while keeping either value (excitation or emission maximum) fixed.

2.7 Molecular biology techniques

2.7.1 Genomic DNA extraction

To isolate large quantities of gDNA, 100 ml of a mid-log phase cell culture ($1\text{-}2\times10^6$ cells/ml) were initially washed twice in 1× PBS. The pellet was resuspended in 500 µl of lysis buffer (Appendix C), added with 100 µg of protease K and incubated overnight at 50°C. After mixing with an equal volume of phenol-chloroform-isoamyl alcohol (25:24:1) (Sigma-Aldrich) for 5 min, the DNA was extracted in the aqueous layer by centrifugating at 855×*g* for 10 min. The aqueous phase was transferred to a new tube and washed twice by addition of an equal volume of chloroform. The DNA was precipitated in 0.1 volume of 3 M NaCl and 2 volumes of 100% EtOH and then washed in 70% EtOH, left to air dry and finally resuspended in 100 µl TE buffer (Appendix B).

A DNeasy® Blood and Tissue Kit (Qiagen) was used, following the manufacturer's instructions, to quickly isolate gDNA from transfected clones in order to screen for the presence of the correct *mCherry::TbAT1* or *TbAT1::mCherry* construct (Section 2.7.2.2). In this case, cells from a 5 ml dense culture (2×10^6 cells/ml) were used.

The concentration of extracted gDNA and of purified plasmids was measured using a ND-1000 V31.0 NanoDrop instrument (Thermo Fisher Scientific Inc.).

2.7.2 PCR

2.7.2.1 Amplification of *TbAT1* and *mCherry* ORF

The polymerase chain reaction (PCR) was used to amplify DNA fragments both from genomic material and plasmids. For the project involving the construction of a *Tb*AT1-RFP reporter system (Chapter 6), four sets of primers, containing the required restriction sites, were designed for amplification of *TbAT1* (form gDNA) and *mCherry* (from vector p2664, described in Kelly *et al*., 2007) coding sequences: two sets for the N-t construct (*mCherry::TbAT1*) and two sets for the C-t construct (*TbAT1::mCherry*) (Table 2.2).

Sequence amplified	Primer pair	Primer sequence
mCherry (N-t)	MB405 (f)	5'-ATTAAGCTTATGGCAACTAGCGGCATGGT-3'
	MB406 (r)	5'-ATTGGGCCC*TCCTCC*TGCGGTACCAGAACCTTTGT-3'
TbAT1 (N-t)	MB407 (f)	5'-ATTGGGCCCATGCTCGGGTTTGACTCAGC-3'
	MB408 (r)	5'-ATTGGATCC**CTA**CTTGGGAAGCCCCTCAT-3'
mCherry (C-t)	MB409 (f)	5'-ATTGGGCCCATGGCAACTAGCGGCATGGT-3'
	MB410 (r)	5'-TTAGGATCC**TTA**TGCGGTACCAGAACCTT-3'
TbAT1 (C-t)	MB411 (f)	5'-ATTAAGCTTATGCTCGGGTTTGACTCAGC-3'
	MB412 (r)	5'-ATTGGGCCC*TCCTCC*CTTGGGAAGCCCCTCATTGA-3'

Table 2.2 – Oligonucleotides used for *TbAT1* and *mCherry* ORF amplification. Restriction sites introduced for cloning purposes are underlined; stop codons are in bold; glycine-encoding codons are in italics.
(f): forward; (r): reverse.

All oligonucleotides were synthesised by Eurofins MWG Operon. A high fidelity enzyme (KOD Hot Start DNA polymerase, Novagen) was used to obtain fragments for subsequent cloning (while for routine PCR applications a GoTaq® DNA polymerase, by Promega, was used). PCR mastermix was prepared in a total volume of 25 µl per reaction, containing 1× buffer, 0.3 mM dNTPs, 1.5 mM MgCl, 0.3 µM both of sense (5') and anti-sense (3') primer, 1.25 U of polymerase and the template (~100 ng gDNA, or 0.5 ng plasmidic DNA). The thermal cycler PTC200 DNA Engine Thermal Cycler (MJ Research) was used for DNA amplification. Reaction conditions were optimised for each experiment. In particular, the best annealing temperature for each set of primers was determined by gradient PCR.

For *TbAT1* amplification from gDNA, cycling conditions were as follow:

1- Polymerase activation	95°C for 2 min
2- Denaturation	95°C for 20 sec
3- Annealing	58.4°C for 10 sec
4- Extension	70°C for 35 sec
5- Repeat steps 2-4	30 cycles

For *mCherry* amplification from p2664, cycling conditions were as follow:

1- Polymerase activation	95°C for 2 min
2- Denaturation	95°C for 20 sec
3- Annealing	64.8°C for 10 sec
4- Extension	70°C for 15 sec
5- Repeat steps 2-4	25 cycles

PCR amplicons were isolated and visualised by electrophoresis on a 1% agarose gel stained with SYBR® Safe DNA gel stain (Invitrogen) and then purified from the gel using the QIAquick PCR Purification Kit (Qiagen) following the manufacturer's instructions.

2.7.2.2 PCR screening of transfected trypanosomes

PCR amplification of a fragment spanning *TbAT1* and *mCherry* domains was used to check for the presence of the constructs pMB-G94 (containing *mCherry::TbAT1*) and pMB-G95 (containing *TbAT1::mCherry*) inside transfected trypanosomes. Primers used for screening are shown in Table 2.3. PCR reactions were prepared as previously described (2.7.2.1), using as template ~0.5-1 ng/µl gDNA, extracted with the DNeasy® Blood and Tissue Kit (Qiagen).

Sequence amplified	Primer pair	Primer sequence
mCherry::TbAT1 (fragment)	MB363 (f)	5'-AGCCCTCAATTCATGTATGG-3'
	MB182 (r)	5'-TCATCGCCTCCGTGGGGGTC-3'
TbAT1::mCherry (fragment)	MB181 (f)	5'-CAGAGTTCCGATATGCAGC-3'
	MB410 (r)	5'-TTAGGATCCTTATGCGGTACCAGAACCTT-3'

Table 2.3 – Oligonucleotides used for amplification of a fragment spanning *TbAT1* and *mCherry* domains in transfected trypanosomes.
(f): forward; (r): reverse.

PCR conditions were as follow:

1- Polymerase activation	95°C for 1 min
2- Denaturation	95°C for 1 min
3- Annealing	53.4°C for 1 min
4- Extension	72°C for 90 sec
5- Repeat steps 2-4	30 cycles
5- Final extension	72°C for 1 min

2.7.3 Plasmid and vector construction

In order to ligate PCR amplicons into the plasmid pGEM-T Easy (Promega), which has additional overhanging thymidine at both 3' terminals, they had first to be added with a single 3'-terminal adenosine. This was obtained by incubating the PCR products with 2.5 U of GoTaq® DNA polymerase at 72°C for 15 min before gel extraction. The ligation reactions (10 µl total volume) were prepared by mixing 50 ng of plasmid, 1× T4 ligation buffer, 3 U of T4 DNA ligase polymerase (Promega) and 5 µl of purified PCR product. Reactions were incubated overnight at 4°C.

After bacterial amplification and purification (Section 2.7.4), ligation products were checked for presence of the correct insert size by electrophoretic migration of digested products on a 1% agarose gel. 1 µl of plasmid was digested with 10 U of the specific restriction enzymes in a 10 µl reaction mixture containing 1× of the appropriate restriction enzyme buffer. Digest reactions were always carried out for 2 h at 37°C. Correctness of the ligated sequences was verified by sequence analysis (Eurofins MWG Operon). If the insert proved correct, a higher amount of plasmid containing the PCR amplicon (5 µl) was digested to isolate the inserts for subsequent cloning. When the two enzymes used to isolate the fragments needed different buffers, digest was carried out in two distinct reactions separated by a purification step to eliminate the buffer used for the first reaction (the PCR Purification Kit from Qiagen was used for this purpose). Fragments were then separated from the plasmid backbone by running the digest products on a 1% agarose gel and purified (QiAquick Gel Extraction Kit, Qiagen).

TbAT1 and *mCherry* amplicons were first joined together in pGEM-T Easy and only afterwards cloned into the final expression vector pHD676 (Figure 2.1), kind gift of Dr. Christine Clayton, University of Heidelberg (Biebinger *et al*., 1997), as *Hin*dIII-*Bam*HI

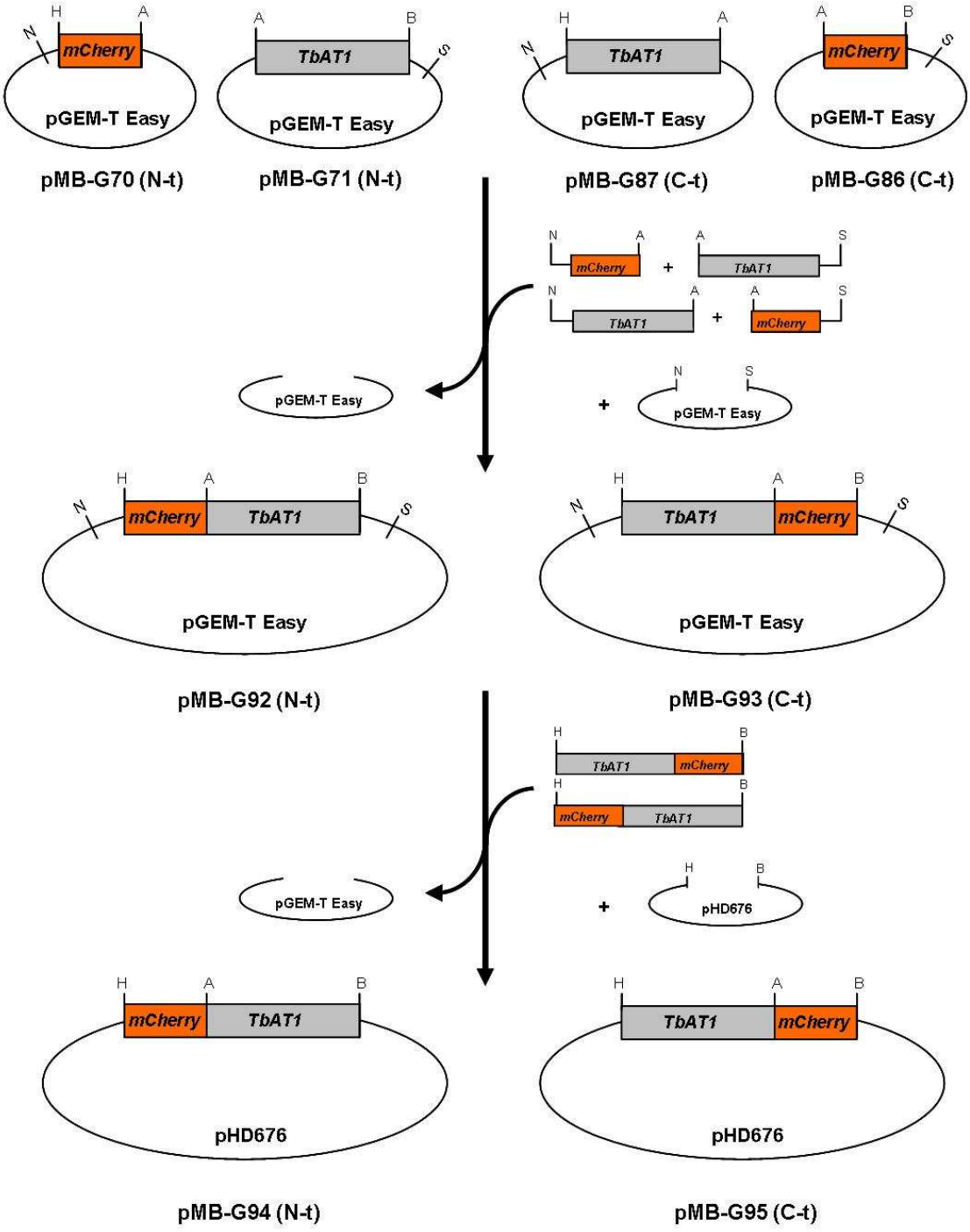

Figure 2.1 – Schematic representation of the steps taken to build pMB-G94 and pMB-G95 vectors.
***TbAT1* and *mCherry* sequences for the N-t construct (*mCherry* ORF upstream the *TbAT1* gene) and C-t construct (*mCherry* ORF downstream the *TbAT1* gene) differed for the restriction sites introduced by PCR for subsequent cloning into the expression vector pHD676. *TbAT1* and *mCherry* genes cloned inside pGEM-T Easy (Promega) were first cleaved and linked together into another pGEM-T Easy plasmid by exploiting the indicated restriction sites contained in its polylinker, in order to generate the fused sequences *mCherry::TbAT1* (N-t) and *TbAT1::mCherry* (C-t). These inserted gene sequences were successively cut as *Hin*dIII-*Bam*HI fragments and cloned into the expression vector pHD676, generating vectors pMB-G94 and pMG-G95. Names of the intermediate constructs are also indicated.**
A: *Apa*I; B: *Bam*HI; H: *Hin*dIII; N: *Not*I; S: *Nsi*I.

fragments. This strategy was chosen since direct insertion of the genes inside the final vector proved unsuccessful. To ligate together *TbAT1* and *mCherry* into pGEM-T Easy various restriction sites contained inside the plasmid polylinker were used (these sites are indicated in Figure 2.1). All ligation reactions were carried out using a 1:1 or 1:2 vector/insert(s) ratio as described above. Final vectors (pMB-G94 and pMB-G95) were sent to Eurofins MWG Operon for sequencing.

2.7.4 E. coli *transformation and plasmid purification*

Large quantities (required for trypanosome transfection) of plasmids containing the gene(s) of interest were obtained by heat shock bacterial transformation and subsequent plasmid purification. The *E. coli* competent cell line DH5α (50 µl) was mixed with the plasmid (10 µl if a ligation product, 1 µl if a miniprep product) for 30 min in ice. Cells were then heat-shocked for 45 sec at 42°C, returned to ice for 1 min, added with 200 µl of LB medium (Appendix B) and left to recover by shaking for 45 min at 37°C. An aliquot of the transformed bacteria was then spread on an LB agar (Appendix B) plate containing 100 µg/ml ampicillin and allowed to grow overnight at 37°C.

When the plasmid pGEM-T Easy (Promega) was used, a preliminary blue-white colony screening was performed to confirm the presence of the target gene(s). Insertion of a fragment into this plasmid disrupts the *LacZ* gene and stops the production of the encoded β-galactosidase. When cells are plated on agarose containing 40 µl of 5-bromo-4-chloro-3-indolyl-β-D-galactopyranoside (X-Gal, 2% w/v, a chromogenic substrate of the enzyme) and 100 µl of 0.1 M isopropyl-β-D-1-thiogalactopyranoside (IPTG, which induces the system by inactivating the *LacZ* repressor), if the insert is present the X-Gal remains unmetabolised and the colony appears white, while in the absence of insert X-Gal is cleaved to a blue product.

Single colonies were cultured in LB plus ampicillin (100 µg/ml) by shaking overnight at 37°C. Bacteria were collected by centrifugation (4,500×*g*, 10 min) and the plasmidic DNA was purified using the QIAprep Spin Miniprep Kit (Qiagen) according to the manufacturer's instructions.

2.7.5 Trypanosome transfection

Before transfection, vectors pMB-G94 and pMB-G95 were linearised, sterilised and concentrated. Linearisation was obtained by digesting at the unique *Not*I site overnight at 37°C. The reaction (300 µl total volume) was prepared by mixing a large amount of purified vector (>50 µg) with 1× buffer D (Promega), 0.1 mg/ml BSA and 2.5 U *Not*I/µg of vector (Promega). After checking for complete digest by 0.8% agarose gel electrophoresis, the restriction enzyme was heat-inactivated at 65°C for 20 min. The whole digest product was then loaded on an agarose gel and purified by gel extraction using the QiAquick Gel Extraction Kit (Qiagen). Vectors were allowed to precipitate in 2 volumes of 100% cold EtOH and 1/10 volume of 3 M sodium acetate (pH 5), for at least 2 h at -80°C. After washing in 1 ml of 70% EtOH, the pelleted constructs were left to air-dry for 30 min under a sterile hood and then resuspended in sterile water (20 µl). Samples were heated 30 min at 37°C and other 20 min at 65°C to help solubilisation. After concentration, the linearised vectors were checked again by 0.8% agarose gel electrophoresis.

For transfection, 1×10^7 cells from a mid-log phase culture ($1\text{-}2\times10^6$ cells/ml) were pelleted and resuspended in 100 µl Amaxa Human T-cell buffer (Lonza Group Ltd.) at 4°C, mixed with 10 µg of linearised vector and immediately put into a cuvette for nucleofection. Program X-001 of the Amaxa Nucleofector® II Device (Lonza Group Ltd.) was used. Transfected parasites were then put into 20 ml of pre-warmed, complete HMI-9 and left to recover overnight at 37°C. The day after, cells were cloned by limiting dilution in 96-well plates in the presence of the selective drug (hygromycin, 5 µg/ml). All clones obtained were then maintained in culture flasks with 10 µg/ml of hygromycin (Clayton *et al*., 2005).

2.7.6 Southern blot

2.7.6.1 gDNA preparation and capillary transfer to membrane

Southern blot analysis was performed to study the integration of linearised pMB-G94 and pMB-G95 vectors into the non-transcribed rRNA spacers (Chapter 6). Genomic DNA (6 µg) obtained by phenol-chloroform extraction (Section 2.7.1) from 449 cell line and two derived clones was digested with seven different restriction enzymes (*Pst*I, *Hin*dIII, *Stu*I, *Bgl*II, *Nco*I, *Xho*I, *Spe*I, all from Promega). Each reaction was performed in a total volume of 60 µl containing the gDNA, 0.1 mg/ml BSA (Promega), 1× specific enzyme buffer

(Promega) and 5 U of each enzyme/µg of gDNA (a second aliquot of enzyme was added 2 h after the set up of the restriction digest). The reactions were carried out overnight at 37°C and the day after another aliquot of enzyme was eventually added if digests had proven incomplete (as visualised by running 2 µl of each sample on a 1% agarose gel). Digested gDNA was then loaded on a 0.7% agarose gel and run at low voltage (40 V) for more than 12 h in 1× TAE buffer (Appendix B) to allow improved separation of DNA fragments.

To prepare the gel for blotting, it was first soaked in 500 ml of depurination solution, to depurinate DNA (twice for 7 min), then in a denaturation solution, to denature the nucleic acids (twice for 15 min) and finally in a neutralisation solution (twice for 15 min) to re-equilibrate the pH to 7.4 (Appendix C). The gDNA fragments were transferred overnight to a neutral nylon Hybond^{TM}-N membrane (GE Healthcare) through upward capillary transfer in 20× SSC (Appendix C) as described by Sambrook and Russell (Sambrook and Russell, 2001). After a brief wash in 6× SSC, the membrane was exposed to UV irradiation to immobilise the DNA onto it by cross-linking, and stored at 4°C until hybridization with radiolabeled probes.

2.7.6.2 Preparation of radiolabeled probes

The whole ORFs of *TbAT1* and *mCherry* were used as probes. The two genes were cleaved from vector pMB-G94 by restriction digest, separated on a 1% agarose gel and purified. Radioactive labelling was carried out using the Prime-It II Random Labeling Kit (Stratagene) following the manufacturer's instructions. Briefly, 25 ng of probe DNA were mixed with 10 µl of random oligo primers in a final volume of 37 µl in water. The solution was heated for 5 min at 95°C before addition of 10 µl of 5× buffer, 2 µl deoxyadenosine 5'-triphosphate [α-^{32}P] (PerkinElmer) and 1µl Exo(-)Klenow (5 U/µl). The radionucleotide incorporation reaction was incubated for 10 min at 38°C and then stopped by addition of 2 µl of Stop mix. Radiolabelled probes were successively purified by eluting through an illustra MicroSpin^{TM} S-200 HR Columns (GE Healthcare). Before addition to the bottle containing the membrane soaked in prehybridisation solution (Section 2.7.6.3), probes were denatured for 5 min at 95°C.

2.7.6.3 Blot hybridisation and autoradiography

Before probing, the membrane was prehybridised in a roller bottle with 15 ml prehybridisation solution (Appendix C) for at least 2 h at 42°C. Herring Sperm DNA

(200 µg/ml) (Promega) was added to the solution after denaturation for 5 min at 95°C. Boiled radiolabeled probe was added to the hybridisation solution and incubated with the membrane for at least 16 h at 42°C. The blot was then washed with a low stringency washing solution (0.3× SSC, 0.1% SDS) twice at r. t. and a further twice at 50°C (for 20 and 45 min respectively). Finally, the filter was covered with an X-ray film (Kodak) and left at -80°C. The film was exposed for the appropriate length of time in order to obtain clear bands and finally developed using the X-OMAT SRX-101A film processor (Konica Minolta).

2.7.6.4 Removal of hybridised probe from membrane

To remove the probe from the membrane in order to reprobe it with another oligonucleotide, the blot was first soaked for 30 min at 42°C in a stripping solution (0.4 M NaOH) and then washed for another 30 min at 42°C with a washing solution at pH 7.6 (Appendix C). To check for complete removal of bound probe the membrane was exposed to an X-ray film as described before (Section 2.7.6.3).

2.7.7 Protein extraction from trypanosomes

2.7.7.1 Total cell lysates

For total protein extraction from trypanosomes, cells (5×10^7 cells/ml) were first washed in STEN buffer (Appendix D) by spinning at 2,500×*g* for 10 min at 4°C. The pellet was then resuspended in PBS containing 1× complete protease inhibitor cocktail (Roche), in order to have 1×10^7 cells/ml per 10 µl of solution. The suspension was added with an equal volume of 2× Laemmli buffer (Appendix D) and thoroughly mixed by pipetting. If samples resulted too viscous, they were passed thorough a syringe several times using a 0.45 × 16 mm needle. Samples were then heated at 65°C for 5 min before spinning at full speed for 1 min to separate supernatant from cell debris and finally stored at -20°C until use.

2.7.7.2 Preparation of protein-enriched fractions

To prepare protein-enriched fractions, 5×10^8 cells were harvested by centrifugation at 1300×*g* for 10 min at 4ºC and washed once in ice-cold PBS. The resulting pellet was resuspended in 2 ml of ice-cold 1% Triton X-114 in 1× PBS, containing 1× complete protease inhibitor cocktail (Roche). The solution was stirred vigorously on ice for 90 min,

after which a 200 µl aliquot was collected and immediately frozen at -20ºC (total lysis sample). The remainder was centrifuged twice at 40,000×*g* for 30 min at 4ºC to precipitate the detergent insoluble fraction. The obtained supernatant was incubated for 10 min at 30ºC and then spun at 5,000×*g* for 20 min at 30ºC, without using the brake during deceleration, to separate the upper aqueous from the detergent-organic phase. Both fractions were put in ice and returned to a volume of 2 ml by adding ice-cold 1× PBS to the detergent phase and ice-cold 10% Triton X-114 in 1× PBS to the aqueous phase for washing. Samples were first vigorously stirred on ice for 60 min and then incubated 10 min at 30ºC. After centrifugation at 5,000×*g* for 20 min at 30ºC, the aqueous wash was separated from the original detergent phase and the detergent phase from the original aqueous phase and discarded. Samples were stored frozen at -20ºC until analysis by SDS-PAGE.

2.7.8 Protein quantification

Protein concentration was determined by the Bradford method using the Bio-Rad Protein Assay (Bio-Rad Laboratories). A small amount of sample (usually 1 µl) was mixed with 200 µl of Bio-Rad dye reagent and 1× PBS (to a total volume of 1 ml) in a 1 cm disposable cuvette. The solution was incubated at room temperature for 30 min to allow colour change of the dye in response to the concentration of protein in the sample. Absorbance (OD) was then determined using a Spectronic Helios-Gamma spectrophotometer (Thermo Fisher Scientific) set at 595 nm and corrected for "blank" (reagent plus buffer). Experimental OD_{595} were finally plotted versus concentration of standards, measured for bovine serum albumin (Sigma-Aldrich), and unknowns were extrapolated.

2.7.9 SDS-PAGE

Protein samples (usually 25 µg) were separated by sodium dodecyl sulfate polyacrylamide gel electrophoresis. Gels (0.75 mm thick) were prepared using 10% polyacrylamide for the running gel and 3% for the stacking gel (Appendix D). Before loading, protein-enriched fractions were added of Laemmli buffer (5 µl of buffer added to 20 µl of sample) and then boiled at 65°C for 5 min. Total protein extracts and prestained protein marker (New England Biolabs Inc.) were also denatured at the same temperature just before loading. Gels were run at 50-70 V for a few hours in 1× running buffer (Appendix D) and then immediately used for Western analysis. After electrophoretic blotting, gels were eventually

stained with a Coomassie Brilliant Blue solution (Appendix D) to check for transfer efficiency.

2.7.10 Western blot

Samples separated by SDS-PAGE were transferred onto an Amersham Hybond™-ECL nitrocellulose membrane (GE Healthcare) by electrophoretic transfer. Once the electrophoretic block was assembled (membrane placed on the side of the gel facing the anode), immunoblotting was performed at a constant voltage (0.1 Amp, for 4 h at 4°C) in 1× transfer buffer (Appendix D). To optimise protein transfer, a Tris-glycine buffer without MeOH was used (Small *et al*., 1988). The membrane was then blocked for at least 1 h at r.t. in 40 ml 1× PBS containing 0.05% Tween-20 (PBS-T) and 5% powdered milk (Marvel). After three washes with 0.05% PBS-T (15 min each, at r.t.), the blot was incubated overnight at 4ºC with the Living Colors® DsRed monoclonal primary antibody (Clontech Laboratories) prepared at a 1:250 dilution in 0.01% PBS-T containing 5% milk. Membrane was then washed thoroughly in 0.05% PBS-T to remove unbound or excess antibodies, and successively incubated (for 3 h at 4°C) with a goat anti-mouse IgG peroxidase conjugate secondary antibody (Calbiochem) at 1:2,000 dilution in blocking solution (0.05% PBS-T containing 5% milk). After 3 further washes in 0.05% PBS-T (15 min per wash) to remove excess antibodies, protein detection was carried out using the chemiluminescent SuperSignal® HPR Substrate kit (Novagen). After the blot was coated with an appropriate quantity of reagent and put into a cassette, a film (Amersham Hyperfilm ECL, GE Healthcare) was exposed to the chemiluminescent signal for the time needed to obtain clear bands. Films were developed using the X-OMAT SRX-101A film processor (Konica Minolta).

2.8 Chemical synthesis: general experimental details

All reactions described in Chapter 5 were carried out in oven-dried glassware and under an inert atmosphere, unless otherwise stated. Starting materials and reagents were obtained from commercial sources (Sigma-Aldrich, Alfa Aesar) and used as received without further purification. All solvents were of reagent grade and distilled or dried, if needed, before use. Purification by flash column chromatography was carried out using Matrex Silica 60Å silica gel, mesh size 35-70 μm (Thermo Fisher Scientific Inc.) as the stationary phase. Thin layer chromatography was performed using aluminium backed plates pre-coated with silica gel 60 (UV_{254}) (Macherey-Nagel) and visualised by staining with

$KMnO_4$. ^1H NMR and ^{13}C NMR spectra were recorded on a DPX 400 spectrometer (Bruker). Chemical shifts (δ) are given in ppm relative to tetramethylsilane, used as internal standard. All NMR *J* values are given in Hz. IR spectra were recorded using sodium chloride plates on a FT/IR 410 spectrometer (JASCO). Samples for IR analysis were used neat or prepared as KBr disks. Mass spectra were recorded on a JMS-700 spectrometer (JEOL). Optical rotations were determined as solutions irradiating with the sodium D line (λ=589 nm) using an AA series Automatic Polarimeter. $[\alpha]_D$ values are given in units 10^{-1} degcm^2 g^{-1}. Melting point of compound FG10 was measured using a Gallenkamp apparatus.

3

Fluorescence-based diagnostic tests involving the UV fluorescent diamidine DB75

3.1 Introduction

3.1.1 DB75

DB75 (furamidine, [2,5-bis(4-amidinophenyl)furan], Figure 3.1) is a diphenyl-diamidine compound extremely active against human African trypanosomes (Boykin, 2002; Mathis *et al*., 2006; Thuita *et al*., 2008) and *Plasmodium* species (Yeramian *et al*., 2005) both *in vitro* and *in vivo*. Its oral prodrug DB289 [2,5-bis(4-amidinophenyl)furan-bis-*O*-methylamidoxime] had reached phase III clinical trials for treatment of HAT early stage, before being dismissed for excessive toxicity in volunteers during a retrospective phase I trial, dosing for 14 days at 100 mg twice daily (Thuita *et al*., 2008; Wenzler *et al*., 2009). DB75, like several other compounds of the DB-series of heterocyclic diamidines, is fluorescent (Wilson *et al*., 2005; Mathis *et al*., 2006 and 2007), with λ_{EX}=356 nm and λ_{EM}=458 nm (Mathis *et al*., 2007). It quickly accumulates at millimolar levels inside trypanosomes, where it concentrates in the DNA-containing organelles: within minutes of incubation with the fluorophore the nucleus shows a bright blue fluorescence, while the kinetoplast can appear with a white-yellow colour when 330-380 nm excitation and ≥420 nm emission wavelengths are used (Mathis *et al*., 2006). With same filter set, Mathis and collaborators found that at later time points (after 2 h) trypanosomes from mice treated with DB75 (7.5 μmol/kg) also demonstrated a yellow fluorescence in other cytoplasmic organelles, believed to be acidocalcisomes (Mathis *et al*., 2006). Like other diamidines, DB75 uptake is mostly dependent on the P2 amino-purine transporter, but a secondary, slow route of internalisation must exist, since trypanosomes lacking this transporter retain some sensitivity to the drug (Lanteri *et al*., 2006). Molecules belonging to this class of compounds bind to the DNA minor groove at AT-rich sites, which are abundant in the minicircles of the kinetoplast DNA, where AT sequences reach 70-75% of the total (Wilson *et al*., 2005; Liu *et al*., 2007; Mathis *et al*., 2007). The high affinity for DNA has been suggested as a possible cause for the biological activity of dications as DB75, which can induce DNA structure instability or interfere with DNA-targeted proteins, such as the mitochondrial topoisomerase II (Shapiro and Englund, 1990; Wilson *et al*., 2005). The finding of other organelles (identified as acidocalcisomes) targeted by the drug, though, may indicate different additional mechanisms of action for DB75 (Mathis *et al*., 2007). Moreover, the fact that akinetoplastic (i.e. without kDNA) *Trypanosoma evansi* (an animal pathogenic species) are also susceptible to diamidines might render the kinetoplast an unlikely target (Gillingwater *et al*., 2009).

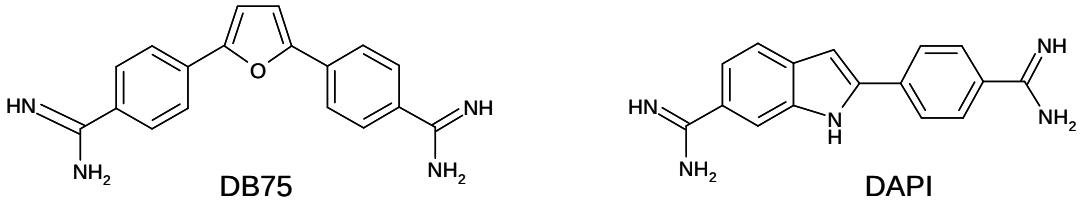

Figure 3.1 – Chemical structure of DB75 and DAPI.

Despite its disappointing failure as a trypanocidal drug, DB75 could still have other applications as a fluorescent marker. Since this compound enters predominantly via the P2 transporter it can, for example, be used to discriminate wild type trypanosomes from drug-resistant parasites, which have lost the P2 transporter, in the arsenical drug resistance test (Stewart *et al*., 2005; Lanteri *et al*., 2006). Another option would be to use DB75 as a more general fluorescent DNA marker for trypanosomes or any cell type, both for research and diagnostic purposes. Thanks to its cost-efficient synthesis (Gillingwater *et al*., 2009), this compound could represent a valid alternative to the widely used, but expensive (~£10 for 1 mg from Sigma-Aldrich) DAPI, another diamidine with very similar fluorescent properties (Kapuscinski, 1995). Both these aspects were investigated.

3.1.2 DAPI

DAPI, [4',6-diamidino-2-phenylindole] (Figure 3.1), is a widely used, DNA-specific, fluorescent stain, initially synthesised during the search for new trypanocidal agents (Kapuscinski, 1995). As DB75, this fluorophore is a UV-excited dication which binds to DNA in a sequence-dependent way, even though the interactions between this compound and the double helix of DNA seem to be more complex than for DB75. DAPI attaches strongly to the minor groove at AT sites, but it also seems to intercalate between the GC base pairs of DNA (Banerjee and Pal, 2008) and at AU sites of RNA (Tanious *et al*., 1992). DAPI-DNA complexes involving GC sequences inside the major groove have also been suggested (Kim *et al*., 1993). Upon binding to DNA, the maximum excitation wavelength of DAPI is red-shifted from 347 nm to 363 nm (bathochromic effect), while the emission has a hypsochromic shift (from 453 nm to 448 nm) and its quantum yield increases more than 20-fold compared to the unbound dye (Kapuscinski, 1990 and 1995). DB75 fluorescence intensity, instead, was found to decrease by 17% in the presence of DNA (Mathis *et al*., 2007). DAPI is known to have good trypanocidal activity (Borowy *et al*., 1985; Lanteri *et al*., 2006). A study carried out by Bridges and collaborators showed that this compound has high affinity for all of the three pentamidine transporters of *T. b.*

brucei (*Tb*AT1/P2, HAPT1 -high affinity pentamidine transporter- and LAPT1 -low affinity pentamidine transporter-) (Bridges *et al*., 2007). These authors showed that fluorescence in S427 wild type cells treated with 10 μM of the compound was already visible after 5 minutes of incubation. Loss of P2 had no significant effects on DAPI internalisation, while additional absence of HAPT increased significantly the time of fluorescence development inside the cells.

3.1.3 Fluorophore photobleaching

Photostability of a fluorochrome is a major issue in fluorescence microscopy. A specific dye must have a relatively long half-life in order to allow acquisition of well-defined images over an extended period of time of exposure under the excitation source. Unfortunately, the most commonly used dyes suffer from photobleaching, a process that causes the photochemical decomposition of the fluorophore especially when exposed under optimal conditions (Petty, 2007). This phenomenon depends on many factors such as the environment, the concentration of the fluorophore and the excitation conditions (Widengren *et al*., 2007). The mechanisms of this complex process are still poorly understood, but it seems that loss of signal is due to a process of photo-oxidation and photoionisation, involved in the formation of reactive radical species of the excited state of the fluorophore (Widengren *et al*., 2007; Vogelsang *et al*., 2008). Apart from reducing illumination levels and time of exposure, three methods are routinely used, often in combination, to retard dye photobleaching: (1) removal of oxygen from the mounting medium, (2) increasing the viscosity of the mounting medium to retard oxygen diffusion or (3) the use of an antifading reagent (Johnson *et al*., 1982; Ono *et al*., 2001; Vogelsang *et al*., 2008). There are several mounting media that can be added to retard bleaching (Valnes and Brandtzaeg, 1985; Longin *et al*., 1993; Florijn *et al*., 1995; Ono *et al*., 2001). They include antioxidant and triplet state quenchers that act as radical scavengers (Widengren *et al*., 2007). Most of them, despite retarding fading, have the drawback of reducing fluorescence intensity, especially when used at high concentrations (Valnes and Brandtzaeg, 1985; Longin *et al*., 1993; Widengren *et al*., 2007).

During our experiments, the use of DB75 for fluorescent staining of trypanosomes showed a fast photobleaching, especially under certain conditions. Therefore, efforts were made to decrease this effect by the use of homemade mounting media. Since different antifading agents vary in efficacy in increasing photostability in a dye-specific manner, three different antioxidant compounds were tested: *n*-propyl gallate [3,4,5-trihydroxybenzoic acid propyl

ester], DABCO [1,4-diazobicyclo-(2,2,2)-octane] and Trolox [6-hydroxy-2,5,7,8-tetramethylchroman-2-carboxylic acid]. *n*-Propyl gallate is a well known antioxidant that acts as an electron donor to reduce a damaged fluorophore back to its fluorescent state (Widengren *et al*., 2007). DABCO is another cheap antifading agent, usually used to retard bleaching of FITC or DAPI (Johnson *et al*., 1982; Florijn *et al*., 1995). Both are widely utilised for mounting of fixed specimens. Trolox, finally, is a cell-permeable, water soluble derivative of vitamin E that has been used to recover photoionized fluorophores and to remove singlet oxygen (Rasnik *et al*., 2006; Vogelsang *et al*., 2008). This strong antioxidant is easily applicable also to living specimens.

3.1.4 Arsenical drug resistance test

Arsenical drug resistance has always represented a major issue in the history of African trypanosomiasis (Ollivier and Legros, 2001; Delespaux and de Koning, 2007). Recently, this phenomenon has been indicated as an important cause for the increasing number of relapses following melarsoprol treatment in patients infected with *T. b. gambiense* (Matovu *et al*., 2001a; Kazibwe *et al.*, 2009). Causes of decreased sensitivity of parasites to trypanocidal compounds are still unclear. They could involve various mechanisms including decreased drug import or increased drug export, compound sequestration or inactivation inside parasites, or decreased affinity for the target (Borst and Ouellette, 1995; Barrett and Fairlamb, 1999). Melarsoprol can enter the cells through passive diffusion, but high levels of uptake into trypanosomes involve internalisation of melarsoprol's *in vivo* metabolite, melarsen oxide, through one of trypanosome's adenosine transporters called P2 (Mäser *et al*., 1999). Low resistance to the drug was obtained *in vitro* by knocking down the *TbAT1* gene that encodes for this transporter (Matovu *et al*., 2003). Higher resistance levels were achieved when the HAPT1 (high affinity pentamidine transporter) activity was also eliminated (Bridges *et al*., 2007). Loss of *TbAT1* gene function can also arise as a consequence of mutations in its sequence, rather than complete loss of the whole ORF, and also when stable expression of the gene is lost (Stewart *et al*., 2010). These findings have been partially confirmed in field isolates, which presented with a similar pattern of mutations in the *TbAT1* ORF (Mäser *et al*., 1999; Matovu *et al*., 2001a). Molecular biology methods such as the PCR/*Sfa*NI RFLP have been described for identification of melarsoprol-resistant strains in field isolates (Mäser *et al*., 1999; Matovu *et al*., 2001b; Kazibwe *et al.*, 2009), but this approach is not able to identify all resistant strains, since some present with a wild type sequence of the *TbAT1* gene (Stewart *et al*., 2010). The design and introduction of similar tests, able to identify melarsoprol-resistant parasites,

would be extremely useful in chemotherapeutic decision making and for disease management.

The rapid and easy arsenical resistance assay developed in our laboratory (Stewart *et al*., 2005) could represent a useful option. This assay is able to identify the altered activity of the P2 transporter in resistant strains, regardless of the genetic changes to *TbAT1,* by the diminished uptake of a fluorescent substrate. The original compound used in the test was the diamidine DB99 [2,5-bis(4-amidinophenyl)-3,4-dimethylfuran], which, like other diamidines, is mainly internalised by P2. Being intrinsically fluorescent, DB99 accumulation in DNA-containing organelles can be monitored under a standard fluorescent microscope (λ_{EX}=330 nm, λ_{EM}=400 nm) and its signal used to discriminate between sensitive and resistant strains, since only wild type cells develop fluorescence within 1 minute of incubation. For longer treatment times other routes of entry for diamidines may contribute to the internalisation of the fluorophore inside resistant parasites, thus making distinction between resistant and sensitive strains less certain (Lanteri *et al*., 2006).

The fluorescent test could prove useful for arsenical drug resistance identification in reference laboratories of endemic countries and the use of a simple and robust LED-illuminated microscope could make it readily applicable. The Cytoscience LED microscope currently available (Jones *et al*., 2007) does not work in the UV spectrum (it being fitted with a higher wavelength emitting LED and filter set, Section 1.7) and can not excite fluorophores in the range needed for DB99. Therefore, Prof. D. Jones (Philipps University, Marburg) developed a new microscope prototype, comprising a simple white light bench microscope, equipped with a UV LED light source (λ_{EX}=365 nm) with a suitable filter set and a digital camera, fitted directly inside one of the eyepieces for image acquisition (Figure 3.6). The efficiency of this new microscope was evaluated on trypanosomes from culture and in infected rat blood after treatment with two different diamidines: DB75 and DAPI (both having similar fluorescent characteristics as DB99). The feasibility of the arsenical drug resistance test using this LED light source to excite DB75-stained *T. b. brucei* cells was also tested, as previously done by other authors with a conventional fluorescence microscope (Stewart *et al*., 2005; Lanteri *et al*., 2006).

3.2 Results

3.2.1 DB75 fluorescence in in vitro *trypanosomes*

DB75 is excited under a UV light source (λ_{EX} and λ_{EM} for this compound are, respectively, 356 and 458 nm) and it stains the DNA-containing organelles (nucleus and kinetoplast) in a very similar way to another nucleic acid-targeting dye, DAPI. For DB75, though, the kinetoplast always appeared as the brightest and most easily detectable organelle under the DAPI filter of our Zeiss Axioplan epifluorescence microscope. When live, wild type, *in vitro*-cultured trypanosomes (S427) were treated with 10 μM DB75, 15-30 minutes were needed to obtain a good signal inside the nucleus and the kinetoplast. Incubation at 37°C, instead of room temperature, accelerated uptake, consistent with the transport-mediated model for internalisation of the compound (Lanteri *et al*., 2006). This fluorescence pattern (nucleus plus kinetoplast) was maintained for long incubation times: treatment of wild type cells with 500 nM DB75 showed no changes in cell distribution up to 24 hours, when, in a high number of trypanosomes, the kinetoplast was no longer visible (Figure 3.2). This is in agreement with previous observations that ascribed this effect to the toxic mechanism of action of diamidines (i.e. disintegration of the kinetoplast, possibly due to an inability to replicate) (Mathis *et al.*, 2006). At this time point (24 h) also in many trypanosomes treated with the same concentration of DAPI the kinetoplast was no more detectable (Figure 3.2).

3.2.2 DB75 fluorescence in ex-vivo *trypanosomes*

DB75 UV fluorescence development in *ex-vivo* trypanosomes (i.e. trypanosomes in rodent blood) was always much faster than in cells from culture: 1-5 minutes exposure to 10 μM of the dye were sufficient for staining *ex-vivo* samples, the shortest times needed when cells were incubated at 37°C instead of room temperature. This difference can be explained by the significant *in vitro* downregulation of the activity of the P2 amino-purine transporter (the permease mainly responsible for DB75 uptake) compared to cells grown *in vivo* (Pui Ee Wong, unpublished; Chapter 6).

For air-dried fixed blood films a lower concentration of the dye (3 μM) was sufficient to obtain a bright fluorescence. In these preparations white blood cells were also highly fluorescent and, for red blood cells, “halos” appear on the background (Figure 3.3). On the other hand, fluorescence of white blood cells was low in wet blood preparations (up to 2 h

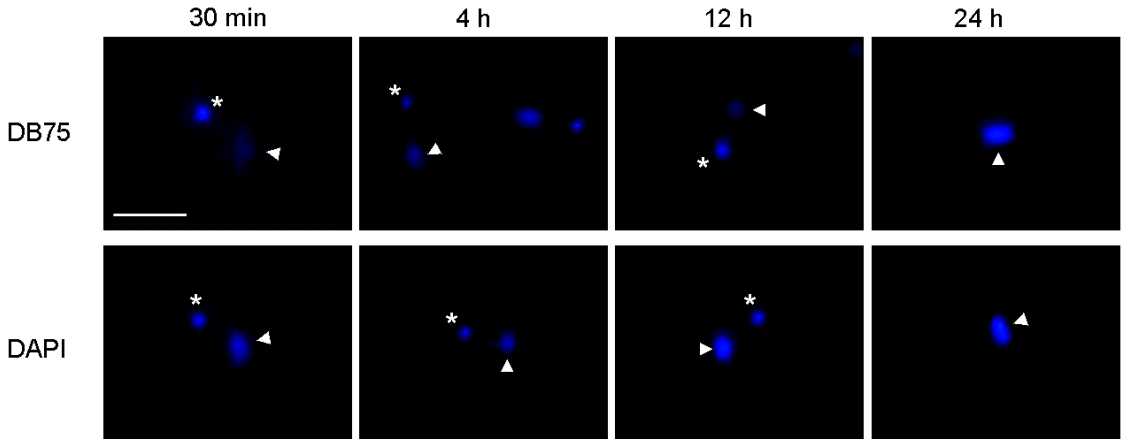

Figure 3.2 – DB75 and DAPI fluorescence acquisition in live, *in vitro* trypanosomes.
***T. b. brucei* S427 w.t. parasites were treated with 0.5 µM of either fluorophore at 37℃. At the indicated time points an aliquot of culture containing live cells was washed, spread on a slide with a coverslip and directly viewed under the Zeiss fluorescence microscope (DAPI filter).**
DAPI 33 ms exposure; 40× objective. *: kinetoplast; ►: nucleus. Bar: 10 µm.

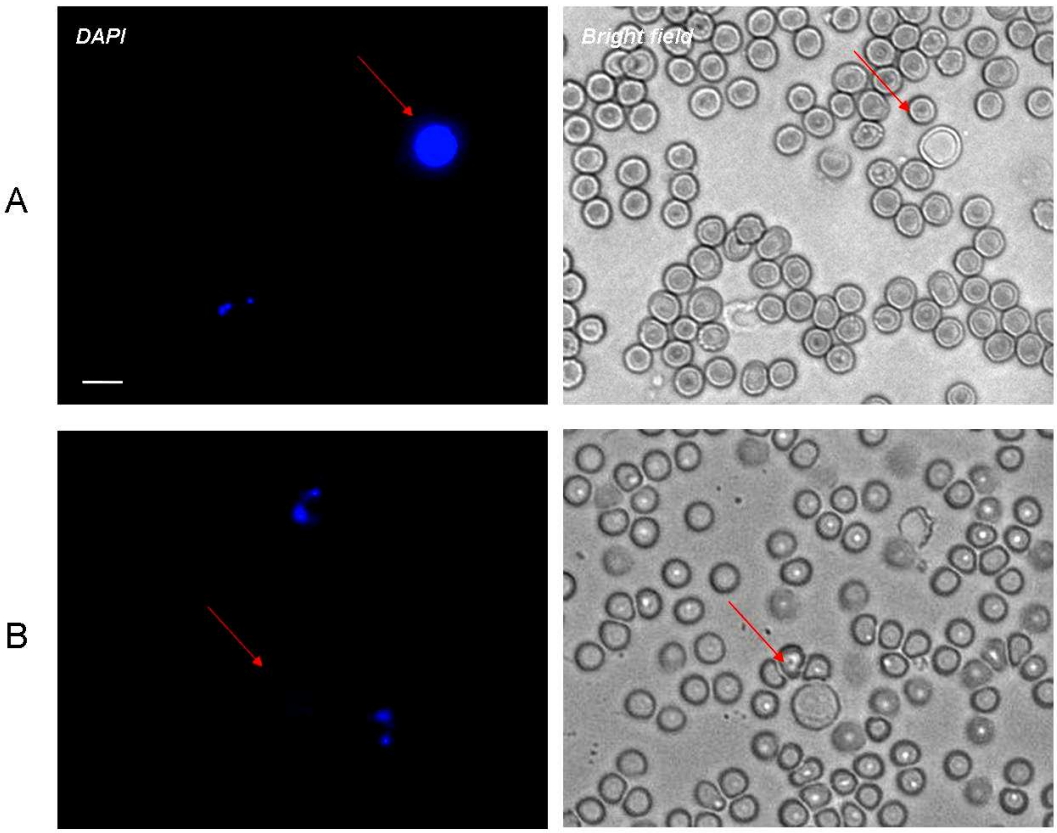

Figure 3.3 – DB75 fluorescence in fixed and fresh infected murine blood samples.
(A) DB75 staining (3 µM, r.t.) of air-dried, fixed thin blood films was nearly immediate. In these preparations the kinetoplast and nucleus of trypanosomes (*T. b. brucei* S427 w.t.) were clearly visible on a blue background of red blood cells, but also the white blood cells DNA was highly fluorescent under DAPI filter set.
(B) In wet blood films the cell membrane integrity ensured specific staining of DB75 (10 µM, r.t., 30 min), with wild type parasites accumulating the fluorophore at higher rates than white blood cells. Note that live trypanosomes in the wet specimen (B) moved during acquisition of the fluorescence and bright field images.
DAPI 33 ms exposure; 40× objective. →: white blood cell. Bar: 10 µm.

incubation), consistent with the selective high level of DB75 uptake by the trypanosome P2 transporter. Studies carried out in our laboratory, nevertheless, have shown that DB75 can be internalised into various living human cell lines, with time needed for visible fluorescence to develop depending on the cell line and varying from 15 minutes to several hours (Chris Ward, personal communication).

3.2.3 DB75 photobleaching

The bright UV fluorescence of DB75 made this diamidine a very interesting DNA probe for trypanosomes (both in fixed and live specimens) and, eventually, also for other cell lines (at least in fixed samples, where the cell membrane integrity is lost and the DNA is freely accessible to the dye). Nevertheless, a key drawback was observed during testing of this fluorophore: the dye suffered a fast photobleaching, especially under certain conditions. In wet preparations of living cells from culture and also in methanol-fixed and successively stained specimens, DB75 UV fluorescence was very unstable, hampering cell viewing and image acquisition, in particular at high magnification. Fading of the compound in live trypanosomes in blood samples, instead, was less marked compared to wet or fixed slides prepared from culture (as already observed by Mathis *et al*., 2007). Air-dried blood films stained with the fluorochrome also showed a more stable signal when observed upon low magnification (40× objective).

3.2.3.1 DB75 and DAPI photobleaching quantification

To quantitatively compare DB75 fluorescence stability to that of the widely used DNA marker DAPI, fading of both fluorophores bound to DNA was measured on methanol-fixed cells stained with 3 μM of either compound and exposed to UV light (Section 2.5.5). Results showed a clear difference between the photobleaching of the two fluorochromes (Figure 3.4). Under our experimental conditions DAPI lost 50% of its fluorescence within 90.8 seconds of continuous illumination, following a single phase decay pattern. The curve did not reach values close to zero because of a small percentage of cells (around 10%) that appeared to be over-stained (due to variation in staining intensities of individual cells) and faded in a lower, more linear way. Previous work had found faster times for DAPI fading (Gallardo-Escárate *et al*., 2007), with loss of half of its fluorescence intensity after only 20 seconds of continuous illumination, but differences in sample preparation and illumination and cell type do not allow direct comparison with this previous study. Under the same

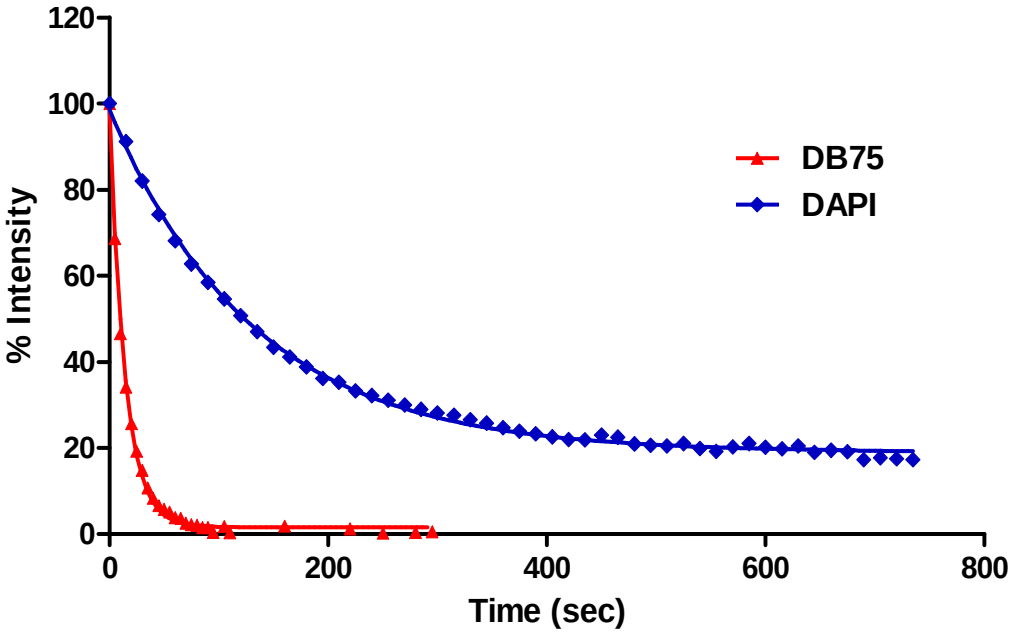

Figure 3.4 – Fading profile of DB75 and DAPI.
***T. b. brucei* S427 w.t. cells fixed in methanol were stained with 3 µM of either compound and exposed to continuous UV light (λ_{EX}=365 nm). Fluorescence bleaching was measured using the Volocity software quantitation package (Improvision) (see Section 2.5.5 for detailed protocol). For each time point data represent the mean of the % of initial intensity of 100 cells, considering the fluorescence of the nucleus and the kinetoplast DNA as a single mean value.**

exposure conditions, DB75 fading also showed a single phase decay, but for this dye fluorescence loss was much faster: within 9.8 seconds 50% of all its fluorescence was lost.

3.2.4 DB75 photobleaching in the presence of antifading agents

In attempts to diminish DB75 photo-instability various mounting media were used in association with the fluorochrome. A new reference curve of DB75 fading (in absence of any mounting medium) was measured for this set of experiments (Figure 3.5) and this time the profile appeared closer to a two phase decay curve, with a fast half-life (i.e. loss of 50% fluorescence intensity) of 5.3 seconds and a slow half-life of 60.3 seconds. The rate of fluorescence intensity fall was slower than that measured previously (Figure 3.4). This difference with the former DB75 fading profile could be mainly ascribed to the different illumination conditions used during this series of experiments (an older bulb with a different alignment, while all others parameters remained unchanged), known to have important effects on bleaching processes (Petty, 2007; Widengren *et al*., 2007). DB75 fading rate, after addition of different antioxidant agents, was then compared to this new curve of the fluorochrome alone under the same experimental conditions.

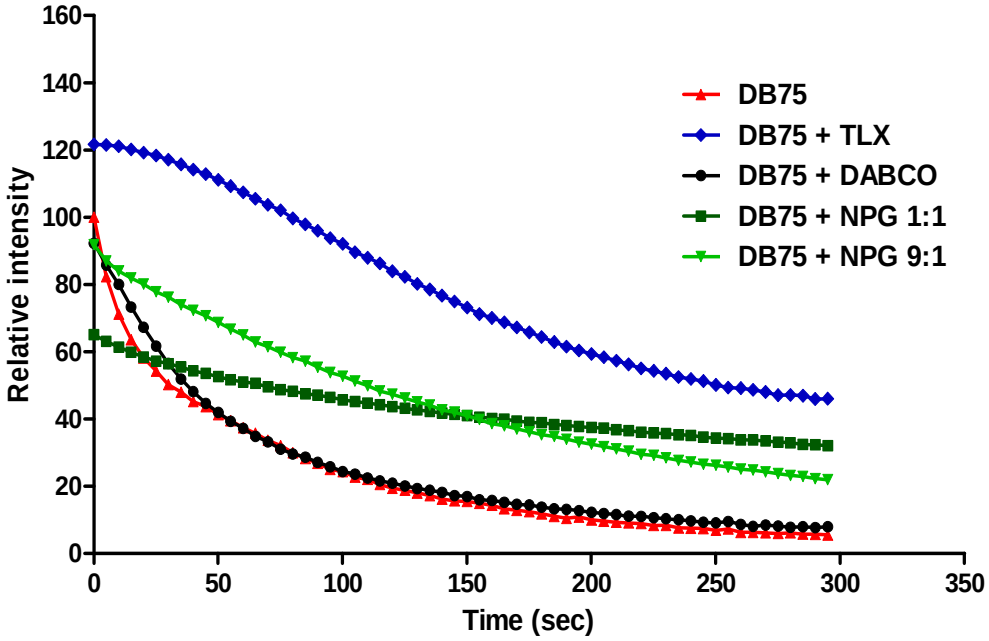

Figure 3.5 – Fading profile of DB75 in the presence of different mounting media.
Fixed *T. b. brucei* w.t. cells were stained with 3 µM DB75 and added with each mounting medium (see Section 2.5.2.6 for sample preparation) before exposure under UV excitation light (λ_{EX}=365 nm). Fluorescence bleaching was measured using the Volocity software quantitation package (Improvision). Fluorescence decay of DB75-stained trypanosomes in the presence of antifading agents is expressed as relative % of intensity to DB75 alone (arbitrarily considered as 100%). Fading of DB75 alone was measured for 300 cells (6 different slides), while fading of DB75 in the presence of antioxidant agents was measured for 200 cells on 4 different slides (150 cells on 3 slides for TLX).
TLX: Trolox (2mM in PBS); DABCO: 1,4-diazabicyclo(2,2,2)-octane (2.5% in 9:1 buffered glycerol); NPG: *n*-propyl gallate (5% in 1:1 or 9:1 buffered glycerol).

3.2.4.1 DABCO

The addition of DABCO (an antifading agent often used in association with DAPI) at 2.5% in buffered glycerol had no significant effects on DB75 fading (Figure 3.5).

3.2.4.2 *n*-propyl gallate

The use of 5% *n*-propyl gallate did decrease the photobleaching of DB75 to a more linear pattern, but it also had a detrimental effect on the initial fluorescence intensity of the dye (Figure 3.5). The use of *n*-propyl gallate in 1:1 buffered glycerol decreased DB75 initial fluorescence of 35%, while the quenching of this agent in 9:1 buffered glycerol was less marked (9% decrease of initial intensity). Moreover, the antioxidant in 1:1 glycerol/PBS solution tended to precipitate and needed to be warmed up to solubilise before use. The fluorescence quenching of *n*-propyl gallate, when used at high concentrations, is a phenomenon previously observed with other fluorochromes (Valnes and Brandtzaeg, 1985; Widengren *et al*., 2007).

3.2.4.3 Trolox

Unlike *n*-propyl gallate, addition of 2 mM Trolox in PBS enhanced the overall intensity of DB75 (22% increase in initial intensity) and consequently retarded the photobleaching yielding a sigmoidal curve (Figure 3.5). This fading profile was only obtained using a Trolox solution that had already turned to a yellowish colour (due, possibly, to partial oxidation). When a freshly made solution of Trolox was used, it still enhanced initial DB75 fluorescence intensity, but this initial emission increase was followed by a fast, single phase decay similar to that measured for DB75 alone (data not shown). The positive effect of Trolox on DB75 fading was confirmed during experiments using living cells, although in these conditions it was not possible to determine the effect of this antioxidant quantitatively, due to fast cell movement.

3.2.5 Assessment of a new UV LED microscope for DB75 and DAPI excitation

When this project started, the use of DB75 and other UV-excited diamidines for fluorescence-based field diagnostics of trypanosomiasis was mainly hampered by the absence on the market of suitable UV LED-driven fluorescence microscopes. Our collaborator Prof. D. Jones (Philipps University, Marburg), therefore, developed a new LED microscope prototype working in this region of the spectrum (Figure 3.6).

The new UV microscope proved easy to use and extremely efficient in exciting DB75 and DAPI, both of which absorb in the UV spectrum range. The fluorescence of live *T. b. brucei* parasites from cell culture, treated with 10 μM of either compound, was particularly sharp. Nucleus and kinetoplast were clearly visible. In particular, the kinetoplast appeared very brilliant following DB75 treatment. After long incubation times (2 h, 37°C) with 10 μM of each compound, a fluorescent tubular structure connected to the kinetoplast and elongating towards the anterior part of the cell body became evident in many trypanosomes (Figure 3.7). This organelle, identified as the mitochondrion based on its peculiar shape, was never observed using the same fluorophores, following the same treatment conditions, under the standard Zeiss fluorescence microscope. However, it was not possible to perform colocalisation studies with the mitochondrion-specific red fluorescent marker Mito Tracker (Field *et al*., 2004) because of the monochromatic UV light source fitted in the LED instrument.

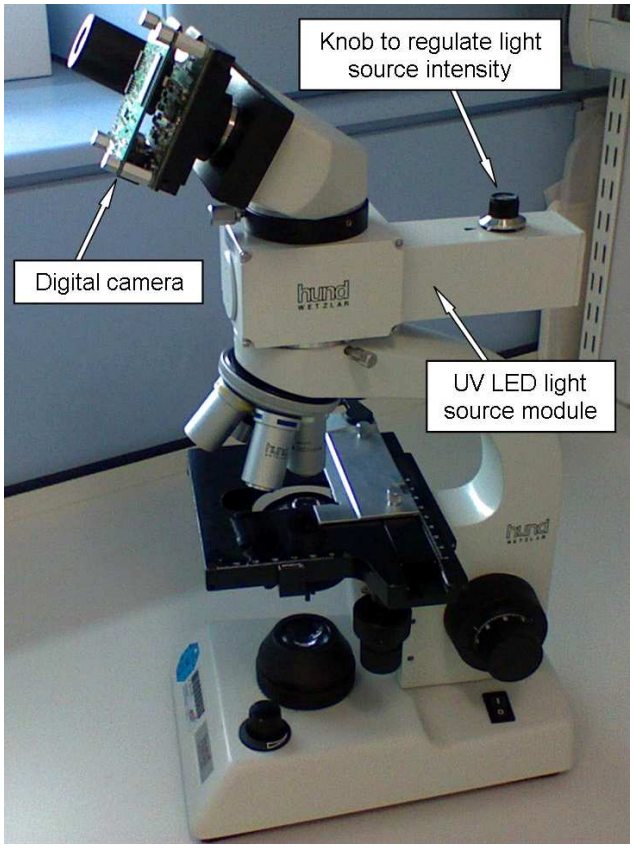

Figure 3.6 – The UV LED microscope built by Prof. D. Jones (Philipps University, Marburg). This adapted microscope was equipped with a 365 nm LED fluorescent light source (Nichia), whose intensity could be simply regulated by changing the voltage using the knob at the top of the module. A digital camera (Lumenera), fitted into one the two ocular lenses, was used for image acquisition. Technical details are in Section 2.5.4.2.

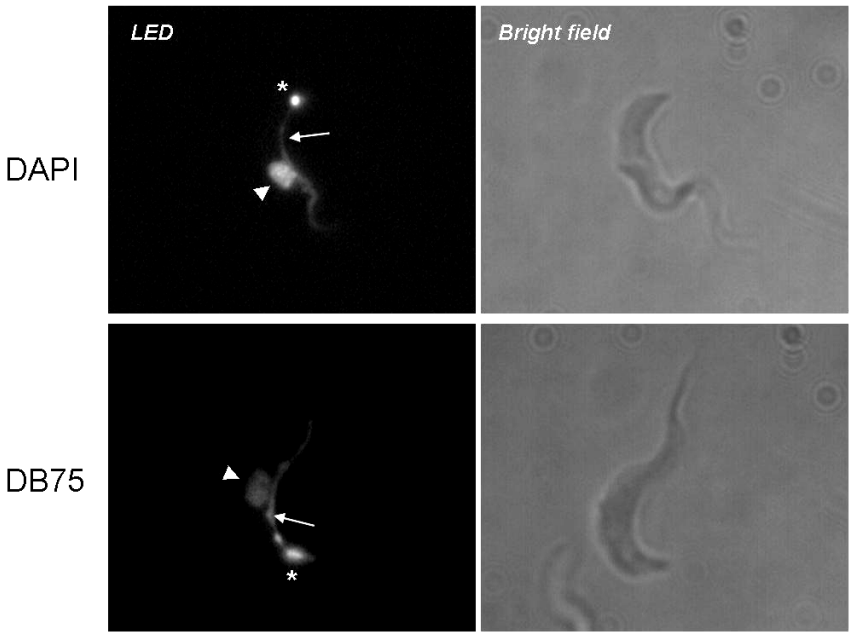

Figure 3.7 – Fluorescence images of trypanosomes stained with DAPI or DB75 acquired using the UV LED microscope.
Wild type *T. b. brucei* parasites from *in vitro* culture were incubated with 10 µM of either compound for 2 h at 37℃ and immobilised in 1% agar ose before viewing using the UV LED prototype (λ_{EX}=365 nm). Bright field images are shown on the right of the corresponding fluorescence micrograph.
LED 65 ms exposure; 60× objective. *: kinetoplast; ►: nucleus; →: mitochondrion.

3.2.5.1 DB75 photobleaching upon excitation with the UV LED light source

DB75 UV fluorescence suffered a fast fading upon excitation with a conventional mercury arc, especially for samples from culture (Section 3.2.3). The use of the LED-driven microscope was expected to have a less detrimental effect on the fluorophore stability, since these light sources do not produce any heat that can damage the sample. Nevertheless, the fading of DB75 did not appear to be diminished under LED excitation. Loss of fluorescence of this compound when exposed to the UV LED light was very fast in *in vitro* live and fixed samples. DB75 appeared less photostable than DAPI also using this new instrument, although a direct comparison with the decay rate measured for the fluorophores under the mercury bulb was not possible. Decreasing the LED power to half the maximum intensity reduced fading, facilitating viewing and imaging during some experiments. In blood samples, photobleaching of DB75 was decreased, as already observed using the mercury arc-driven microscope.

3.2.6 Assessing the suitability of the new Cytoscience UV LED microscope for use with the arsenical drug resistance test

The test developed to report on the presence or absence of the P2 amino-purine transporter associated with drug resistance depends on using UV fluorescent diamidines such as DB99 (Stewart *et al*., 2005) or DB75 (Lanteri *et al*., 2006). Unfortunately, typical field microscopes (i.e. the Cytoscience SMR instrument, Section 1.7) work at longer wavelengths and are not compatible with these fluorophores. The UV LED source microscope developed by Prof. D. Jones at Cytoscience, instead, proved very efficient in exciting DB75 (Section 3.2.5); hence, the possibility to perform the arsenical drug resistance test using this instrument in association with the fluorophore was explored.

For the test, *T. b. brucei* S427 wild type (w.t.) and *tbat1*$^{-/-}$ (lacking the P2 transporter) were grown in mice (female BALB/c) and collected in heparinized blood. The test was repeated only twice because we only had the prototypical microscope at our disposal for a limited period of time. On both occasions the test was carried out on different days for the two lines, since the *tbat1*$^{-/-}$ reached a similar parasitaemia as the w.t. (6×10^7 cells/ml) only after 24 hours longer growth. Aliquots of whole infected blood were directly incubated with 10 μM DB75 and wet thin films were prepared at different time points as previously reported (Lanteri *et al*., 2006). When viewed under the UV light the w.t. line appeared highly fluorescent already after 30 seconds of incubation (Figure 3.8). The kinetoplast and

the nucleus were brightly stained, but DB75 was also visible in the cytoplasm of the w.t. parasites making the whole cell body distinguishable. For this cell line, the fluorescence pattern remained the same over the 5 minutes of observation, with an increase of intensity over time. The *tbat1*$^{-/-}$ line accumulated the diamidine at a much slower rate than w.t., as expected. Nevertheless, DB75 fluorescence in cells incubated for only 30 seconds could still be detected under the LED light source. In particular, the kinetoplast could be seen as a moving spot in the specimen, as a function of the whole cell moving. After a few more minutes the nucleus could also be identified. By contrast, Stewart *et al*. observed a complete lack of fluorescence in *T. b. brucei tbat1*$^{-/-}$ line up to 10 minutes of incubation using a standard fluorescence microscope (Stewart *et al*., 2005). One difference between the test conditions we utilised and those adopted in the published assay was the use of wet smears instead of dried blood films. DB75 uptake in wet samples is not blocked and accumulation of the fluorophore continues during sample preparation and viewing, a factor that could slightly increase fluorescence of the *tbat1*$^{-/-}$ line at earlier time points. Nevertheless, the same arsenical resistance test was performed using wet blood smears stained with DB75 by Lanteri and collaborators, who also could not detect any fluorescence in the *tbat1*$^{-/-}$ line up to 10 minutes incubation using a traditional fluorescence microscope (Lanteri *et al*., 2006). During our experiments, on the other hand, P2-deficient trypanosomes could always be detected, by fluorescence staining, at the earliest time point (30 seconds) in the various blood smears prepared. When these same specimens containing the *tbat1*$^{-/-}$ line were observed under the mercury bulb of the Zeiss microscope, no trypanosomes could be detected by 5 min incubation with 10 μM DB75. Only a very faint autofluorescence emitted by the moving cells could be visualised. After this incubation time, UV emission of P2-deficient parasites could be detected using both microscopes (mercury arc and LED-driven) even when a lower dye concentration (5 μM) was used. PCR amplification technique on aliquots of the blood samples used during these experiments and collected on FTA® cards (Whatman, GE Healthcare; Section 2.2.1) confirmed the absence of the *TbAT1* gene in the P2-knockout line utilised (data not shown).

DB75 excitation in *tbat1*$^{-/-}$ cells using the UV LED-driven microscope seemed, therefore, to be more sensitive than with mercury arc-lamps. This prototypical instrument was able to provide very bright and sharp images of trypanosomes stained with diamidines like DB75 and DAPI, showing up particulars that could be lost by excitation with a traditional broad spectrum mercury bulb.

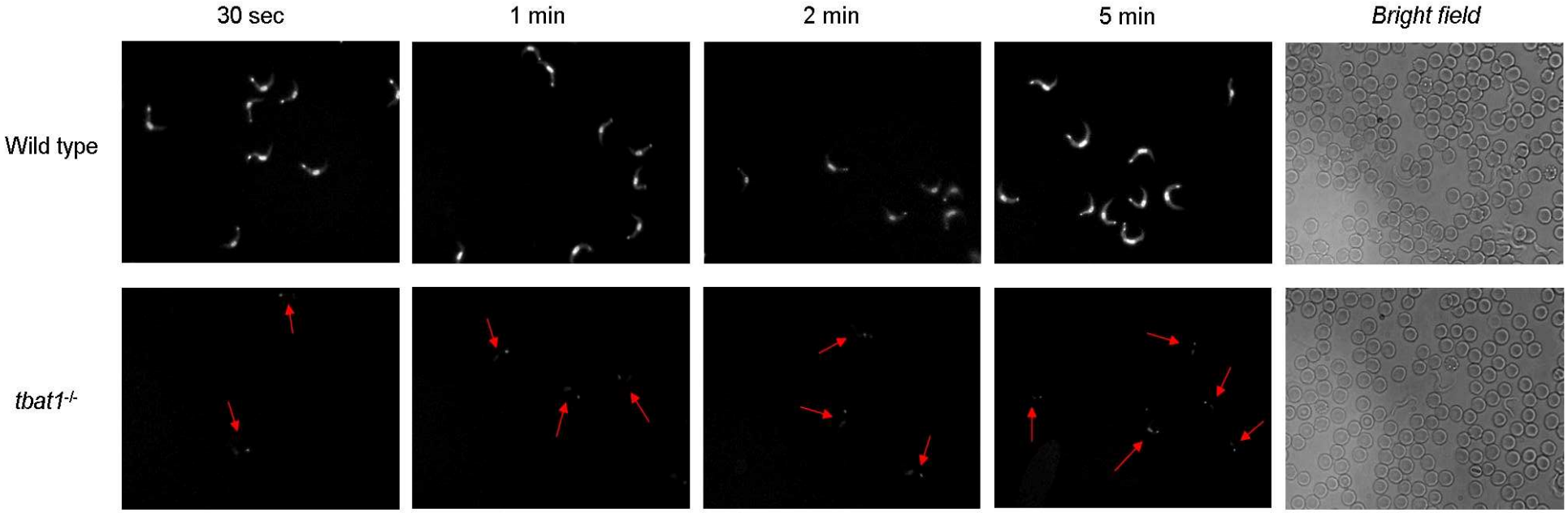

Figure 3.8 – Time course of DB75 internalisation in wild type and *tbat1*$^{-/-}$ cells as observed under the UV LED fluorescence microscope.
***T. b. brucei* S427 w.t. and *tbat1*$^{-/-}$ line (Matovu *et al.*, 2003) were collected from mice in heparinized blood and treated with 10 µM of DB75 at 37℃. At different time points (0.5, 1, 2, 5 min) wet blood smears were prepared and immediately observed under the LED light (λ_{EX}=365 nm) of the prototypical UV LED instrument (developed by Prof. D. Jones at Cytoscience) using its maximum intensity. Representative bright field images are shown on the right (a probable imperfect alignment of the white light source caused the unevenness at the left side of the field).**
LED 70 ms exposure; 40× objective. Arrows indicate *tbat1*$^{-/-}$ trypanosomes.

3.2.7 DB75 fluorescence under FITC filter

In addition to its blue emission following UV excitation, DB75 had also been shown to fluoresce at longer wavelengths once inside various trypanosome cytoplasmic organelles, some of them identified as acidocalcisomes (Mathis *et al.*, 2006). Using the FITC filter of the Zeiss Axioplan microscope (λ_{EX}=470 nm, λ_{EM}=519 nm) we could detect various fluorescent dots generated by the fluorochrome (given at 10 μM) in *ex-vivo* cells, as soon as 5-10 minutes of exposure to DB75 at 37°C (Figure 3.9). The kinetoplast was also always visible and brilliant under this filter set, but the nucleus was never observed. Some of these dots could also be identified under the DAPI filter using the 100× objective. Under our experimental conditions, we could observe around a dozen green fluorescent spots distributed across the whole length of the cell, forming a "pearl necklace" pattern, also visible as electron-dense corpuscles under phase contrast. The number of detectable spots was quite stable up to 2 hours of exposure, after which they seemed to decrease in fluorescence. In order to visualise this green emission, the UV filter had to be avoided, since photons emitted in this region of the spectrum also caused the bleaching of the fluorescence emitted at longer wavelengths. If UV light was not utilised, the fluorescence observed using the FITC filter block appeared more photostable than the emission upon DAPI excitation and it could still be visualised after drying the blood smears and viewing them 24 hours later.

This specific fluorescent pattern of DB75 inside trypanosomes was the product of an active accumulation of the compound inside the cells. After staining the kinetoplast and the nuclear DNA (the first two organelles that could be visualised using UV light), DB75 started to be detectable inside these other cytoplasmic corpuscles, where its concentration increased with time (visualised as an increase of fluorescence intensity). DB75 fluorescence upon FITC excitation needed living cells to develop and it could not be seen when the fluorochrome was used to stain air-dried blood smears, where it only produced the DAPI-like blue emission.

The identity of these cytoplasmic fluorescent corpuscles visualised under FITC filter, following DB75 treatment, is still uncertain and under investigation. Considering their dimension and distribution, they partially seemed to correspond to those viewed by Mathis and collaborators (Mathis *et al*., 2006) in trypanosomes treated up to 2 hours incubation with the dye (Figure 3.10). These authors observed that DB75 fluorescence initially developed inside various (unidentified) punctate cytoplasmic vesicles, before concentrating

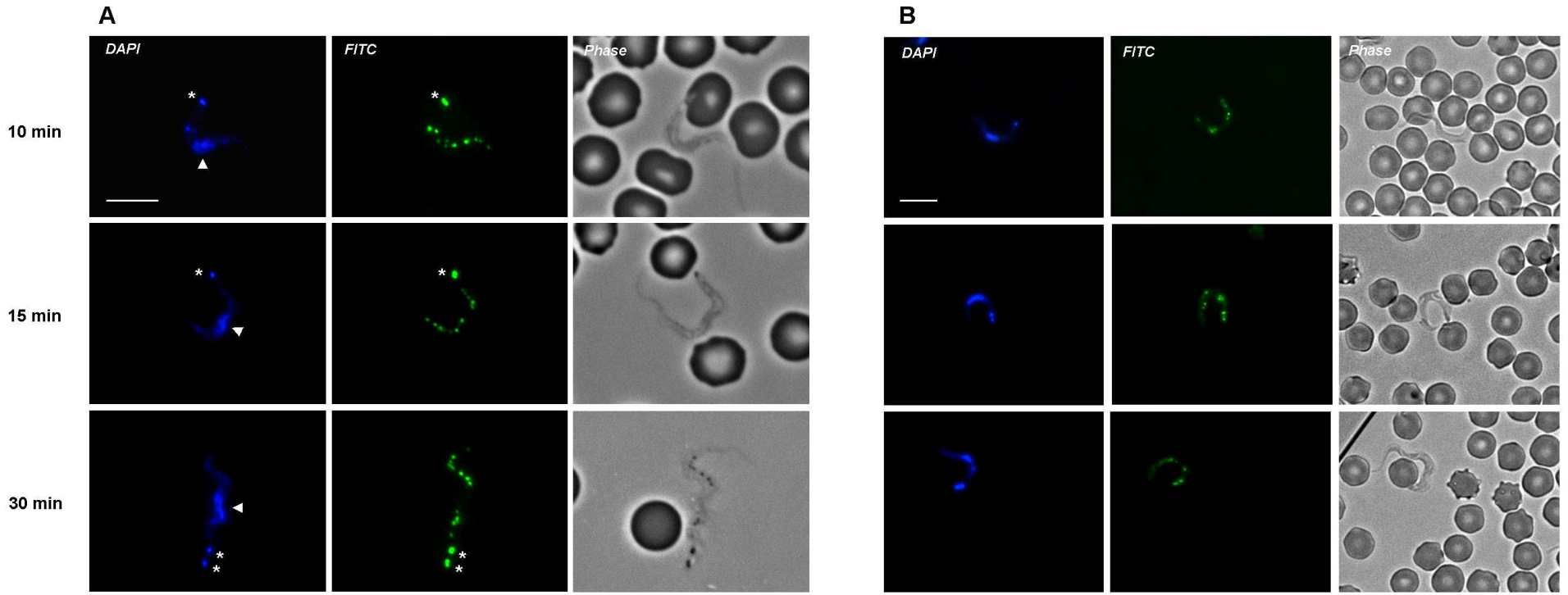

Figure 3.9 – Fluorescence of *ex-vivo* DB75-stained trypanosomes viewed under DAPI and FITC filters.
Trypanosomes (*T. b. brucei* S427 w.t. grown in murine blood) were treated *ex-vivo* with 10 μM DB75 at 37℃. Wet thin blood smears were prepared at different time points and viewed under the Zeiss Axioplan microscope using a 100× objective (A) or a 40× objective (B). The blue fluorescence inside nucleus and kinetoplast developed immediately, within 1 min incubation with the drug. The green fluorescence needed at least 5 min of incubation to develop and its intensity increased with time. The kinetoplast was visible under both filters, while the nucleus did not appear using the FITC channel. Instead, a series of other cytoplasmic organelles, distributed throughout the whole cell body with a "pearl necklace" pattern, were fluorescent under this filter. DB75 green fluorescence was also excited by the LED light source of the Cytoscience SMR epifluorescent microscope (trypanosome fluorescence under this instrument appeared very similar to that visualised under the Zeiss microscope using the 40× objective – panel B, FITC filter). Note that trypanosomes in wet smears were highly motile and their position in the images acquired under different filters can change.
Time of exposure of the camera for DAPI was always maintained at 33 ms, while for FITC filter at ×1,000 total magnification it was decreased at latest time points to avoid saturation of the green fluorescence (100 ms at 10 and 15 min, 40 ms at 30 min). *: kinetoplast; ►: nucleus. Bar: 10 μm.

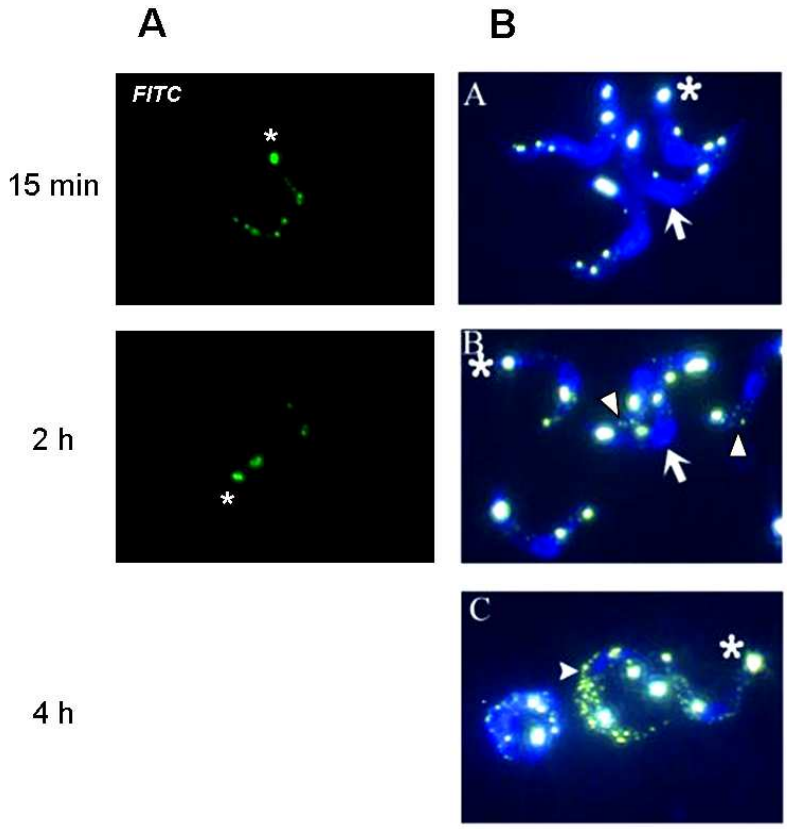

Figure 3.10 – DB75 fluorescence development within bloodstream trypanosomes as visualised during our experiments and in the published work by Mathis *et al*., 2006.
(A) For our experiments, *T. b. brucei* w.t. cells grown in rats were treated *ex-vivo* with 10 μM DB75 at 37℃ for different lengths of time, and the wet smears were viewed under a standard FITC filter (λ_{EX}=470 nm, λ_{EM}=519 nm).
(B) Mathis and collaborators (Mathis *et al*., 2006) administered an intravenous dose of the dye (7.5 μmol/kg) to mice infected with the same trypanosome strain and viewed the blood films using a DAPI filter set (λ_{EX}=330-80 nm, λ_{EM}>420 nm).
(Image reproduced from Mathis *et al*., 2006, with permission from American Society for Microbiology; doi:10.1128/AAC.00192-06).
***: kinetoplast; →: nucleus; ►: acidocalcisomes.**

inside a myriad of smaller organelles (which started to appear by 1 hour incubation dosing 7.5 μmol/kg), indicated as acidocalcisomes (that we could not visualise under our experimental conditions).

The peculiar linear pattern, throughout the whole cell length, of the green dots observed suggested a possible compartmentalisation inside the tubular elongated structure of the mitochondrion, a known target of DB75 (Lanteri *et al*., 2004 and 2008). Colocalization studies of the dye with the mitochondrial marker Mito Tracker Red (Invitrogen) seemed to confirm this hypothesis, showing a close association of the green spots and the mitochondrion structure (Figure 3.11). Cells from culture were used for these colocalization experiments and, in this case, the green fluorescent emission of DB75 had much lower intensity and became detectable at longer times of incubation than in *ex-vivo* trypanosomes (Figure 3.9).

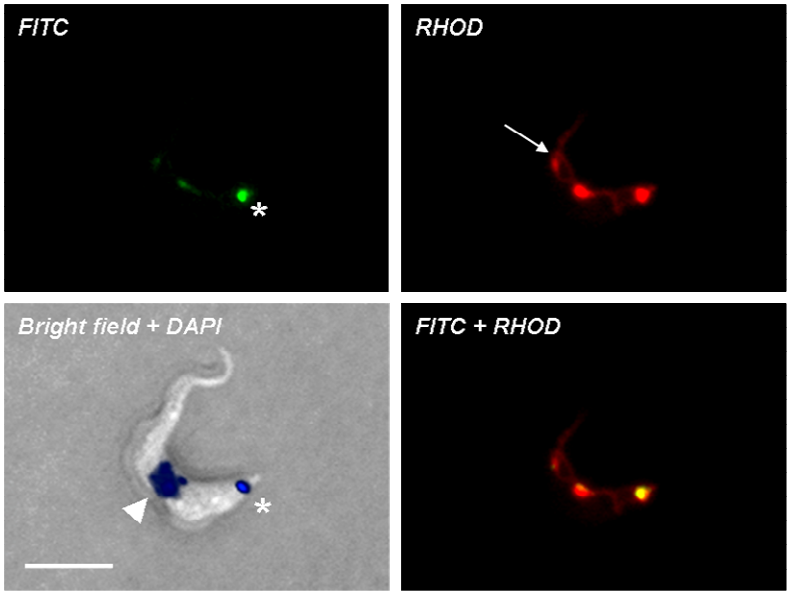

Figure 3.11 – Cellular localization of DB75 and the mitochondrial marker Mito Tracker Red. *In vitro*-cultured *T. b. brucei* w.t. parasites (2×10^7 cells/ml) were treated with 10 µM DB75 for 2 hours at 37℃, to allow the development of a dete ctable fluorescence under FITC filter. Cells were then added with 100 nM Mito Tracker Red CMXRos (Invitrogen) and incubated for further 10 min at 37℃. After washing in PBS, aliqu ots of cells were added with an equal volume of agarose (1% final concentration) and mounted on slides. The green fluorescence of DB75 was viewed under FITC filter, and its blue emission (DAPI channel) was used to localise the nucleus and the kinetoplast. The emission of the mitochondrial marker Mito Tracker Red was visualised using the RHOD filter of the Zeiss Axioplan microscope. Images were merged using the Adobe Photoshop 7.0 software.
FITC and RHOD 68 ms exposure; DAPI 33 ms exposure; 100× objective. *: kinetoplast; ►: nucleus; →: mitochondrion. Bar: 10 µm.

3.2.7.1 Use of DB75 as fluorescent probe for HAT in association with the LED Cytoscience SMR microscope

The green fluorescent emission of DB75 presented various advantages for its eventual use in diagnostic tests for live trypanosomes. The characteristic “pearl necklace” staining pattern viewed under FITC filter could allow an easy detection of parasites among other blood components. Moreover, the signal of the dye observed under this filter was more stable than that generated by exposure to highly energetic UV light. Another important aspect to take into consideration is that it is easier to obtain LED microscopes that work in this region of the spectrum, rather than at low wavelengths.

Interestingly, the green fluorescence of DB75 could be viewed under the LED Cytoscience SMR epifluorescent microscope (λ_{EX}=472 nm) (Section 1.7). No images can be shown for this microscope (as a suitable camera was not available), but under this instrument trypanosomes appeared very similar to those visualised under the Zeiss Axioplan FITC filter using the 40× objective (Figure 3.9 B), the only difference being the more yellowish colour of DB75 under the LED light of the field microscope.

3.3 Discussion

3.3.1 DB75 fluorescence in live and fixed specimens

DB75 is a fluorescent diamidine that is actively concentrated into wild type trypanosomes, where it binds to DNA of the nucleus and kinetoplast yielding a bright emission upon UV excitation. Its fast uptake through the parasite amino-purine transporter termed P2 (Mäser *et al.*, 1999) enables this compound's utilization as a specific fluorescent marker for *T. brucei* when living specimens are used. In wet preparations of infected murine blood, staining of trypanosomes was practically instantaneous after exposure at 37°C, while leukocytes present in the sample showed only a low fluorescence (Figure 3.3 B). When air-dried thin blood smears were stained with DB75 after fixing, this specificity was lost due to cell membrane disruption in these preparations, meaning that white blood cell nuclei were also exposed and were easily labelled by the fluorochrome (Figure 3.3 A). The rapid accumulation of DB75 into live trypanosomes is an important property when considering a possible application of the dye for diagnostic staining of trypanosomes derived from infected human fluids (whether blood or lymph node aspirate or CSF). Parasites in fresh human samples can be very fragile and lyse quickly (Chappuis *et al*., 2005); therefore, fast processing of the specimen becomes essential.

3.3.2 DB75 photobleaching

The photochemical instability of DB75 when excited under UV light represents another important aspect to consider when assessing the suitability of this dye as a reagent to assist diagnosis of trypanosome infections in fluids other than blood. During our experiments, the compound bleached rapidly in wet and fixed specimens prepared from cell culture, while fading appeared less marked in blood samples (whether fixed or fresh).

A range of antifading agents was tested for their impact on DB75 fluorescence. Among them, Trolox acted as a reasonable antifading compound for this fluorophore (Figure 3.5) and it could be easily used in wet as well as fixed samples. Although specimen preparation using mounting media adds to the overall cost and laboriousness of fluorescence microscopy, it could also prove useful for sample storage (Valnes and Brandtzaeg, 1985), by preserving the fluorescent signal for longer periods of time (this aspect was no further investigated).

The use of LED light sources has been suggested to have a retarding effect on photobleaching, since these semiconductor diodes produce very little heat. However, when we excited DB75 under our UV LED microscope, we did observe a fast decrease in its fluorescence intensity even under this light source. Stability of fluorochromes also depends on optimal storage and handling. Stock DB75 solutions used for the experiments were always kept at -20°C, protected from light by wrapping storage bottles in silver foil. Further work would be needed to find optimal conditions for field use.

3.3.3 Assessment of the UV LED microscope for the arsenical drug resistance test

The high dependence of DB75 uptake on the P2 transporter represents a very useful property for its application in the arsenical drug resistance tests, an assay developed to detect resistant trypanosome strains in which this transporter is no more active (Stewart *et al*., 2005). As for other diagnostic fluorescent approaches, the use of this kind of tests is of difficult implementation in poor income endemic countries due to the high costs of purchase and maintenance of fluorescence microscopes. A new generation of LED light sources can overcome these drawbacks and facilitate the introduction of this technology in the field. Since typical LED field microscopes (such as the Cytoscience SMR) work in the FITC range of the spectrum (i.e. green emission), Prof. D. Jones (Philipps University, Marburg) developed and kindly provided us a new UV LED microscope that we tested for its efficacy in exciting UV fluorochromes and in performing the arsenical drug resistance test.

The prototypical microscope proved very efficient in exciting DB75 and DAPI, giving brilliant and sharp images of stained trypanosomes (Figure 3.7). When performing the drug resistance test using this instrument (Figure 3.8), although the difference in DB75 accumulation of *T. b. brucei* sensitive (wild type) and resistant (*tbat1*$^{-/-}$) lines was evident, a low fluorescent signal could always be detected in the P2-deficient line at the earliest time point (30 seconds). This observation was in disagreement with pervious work using the same diamidine (Lanteri *et al*., 2006) or a different one (Stewart *et al*., 2005) as fluorescent probes, excited under traditional mercury arc-driven microscopes. When considering a field application of the test, this result of fluorescence versus low fluorescence is not ideal, since a subjective judgement of the technician would be necessary to decide on the positivity or negativity of the assay (i.e. if the signal, at a certain time point, is bright enough to state that the isolate under examination is drug-sensitive).

Determination of a fluorescent threshold could be even more difficult to assess for human pathogenic strains, where the differences in diamidines internalisation time between resistant and wild type lines could be less evident, as already observed for DB99 (Stewart *et al*., 2005). Therefore, a re-optimisation of the test in association with the UV LED microscope will be needed, in order to go back to the situation of fluorescence versus non-fluorescence of the originally designed assay. This could be done by adjusting the microscope settings (such as the LED intensity) or by modifying the preparation of the sample (different dye doses and times of incubation, use of dried blood films, assessment of other fluorescent substrates).

The reasons for the images' definition obtained using the UV LED instrument are still unclear and under investigation. Sharpness and resolution of microscopy micrographs mainly depend on the objectives used and their numerical aperture (Petty, 2007). In our case, this factor did not seem to have any discriminatory effect, since the objectives fitted in the LED microscope belonged to a standard light bench microscope. The different focus of the mercury gas discharge bulb compared to the LED light source could have more significant consequences on the final specimen image (Jones *et al*., 2005) and this aspect should be further evaluated.

3.3.4 DB75 fluorescence under a FITC filter

Whereas accumulation of DB75 in the nucleus and kinetoplast formed the basis of the original proposed test for P2-deficiency related drug resistance (Stewart *et al*., 2005; Lanteri *et al*., 2006), this compound also accumulates to concentrations allowing detection in other cell compartments that can be visualised under a standard FITC filter (Figure 3.9). In live wild type trypanosomes various fluorescent inclusions became highly stained after only 10 minutes incubation with 10 μM DB75. The kinetoplast was also always visible using the FITC filter set. DB75 emission at this longer wavelength was more photostable than the signal emitted upon UV excitation, but it needed living cells to develop and could not be seen in fixed specimens directly stained with the compound.

The "pearl necklace" staining pattern of the fluorochrome could also be visualised under the LED Cytoscience SMR microscope already available. This very peculiar fluorescent pattern (kinetoplast plus cytoplasmic dots) could be useful to identify trypanosomes in a complex blood sample, where many other components are often stained and hamper the identification of parasites. These blood components do render the detection of the punctate

nucleus and kinetoplast after DB75 treatment, upon UV excitation, problematic for diagnosis. This is due to the fact that these organelles may be difficult to distinguish from the contaminants of the specimen, appearing merely as small dots among many other fluorescent components, especially in fixed samples at low parasitaemia (the use of the Cytoscience UV LED instrument, instead of a classical fluorescence microscope, however, also allowed evidencing the low cytoplasmic emission of DB75-stained cells). When considering this aspect, a fluorochrome able to stain the whole trypanosome cell body, thus providing a clear trypanosomal form, or, as in this case, a dye that produces a very characteristic fluorescent pattern, would enable an easier discrimination from debris as well as other co-infecting parasites. Future work will study the development of DB75 green emission in *tbat1*$^{-/-}$ line, for its eventual use in the arsenical drug resistance test.

The exact identity of the green fluorescent dots visualised under FITC filter following DB75 treatment is unknown. They do not seem to correspond to the vesicles proposed to be acidocalcisomes (Mathis *et al*., 2006), since these only appeared at longer time of incubation with DB75 (after 1 hour), they were smaller in size and higher in number. The organelles we observed using the FITC filter, instead, started to appear already after 5 min of treatment with 10 μM DB75 in *ex-vivo* samples and were never more than a dozen. Also Mathis and collaborators visualised similar punctate corpuscles (Figure 3.10), but their number and distribution was not identical to that we were able to detect. This discrepancy could be ascribed to the different filter set used (FITC filter set with λ_{EX}=470 nm and λ_{EM}=519 nm for us, UV excitation at 330-80 nm with detection of emission at ≥420 nm for Mathis *et al*.), but a different accumulation and compartmentalisation of DB75 in trypanosomes treated *in vivo* (Mathis and colleagues) and *ex-vivo* (our experiments) can not be excluded. The fluorescence compartmentalisation pattern of DB75 had also been demonstrated to be dose-dependent (Wilson *et al.*, 2005) and our use of 10 μm DB75 instead of the 7.5 μmol/kg to treat mice in Mathis *et al*. work could be another reason for the differences we found.

The organelles visualised under FITC filter during our experiments were distributed throughout the whole cell body and this observation exclude possible identification with endocytic and secretory vesicles, which are confined in the posterior part of the cell (Morgan *et al*., 2002). The green fluorescent dots evidenced in trypanosomes after treatment with DB75, instead, appeared to localise within the mitochondrion (Figure 3.11), a known target of this diamidine (Lanteri *et al*., 2008). The compartmentalisation of the fluorescent corpuscles inside the elongated mitochondrial tubular structure would explain

their linear “pearl-necklace” pattern extending from the kinetoplast towards the anterior part of the cell. The cause of DB75 fluorescent emission shift from blue to longer wavelengths once inside this organelle, though, is still poorly understood. Spectral properties of a fuorochrome are often strictly dependent on the pH of the environment, but previous work did not find any correlation between acidification of the medium and a DB75 fluorescent shift (Mathis *et al*., 2006). Another important factor affecting the emission maximum of a fluorophore is its condensation with various cellular components. This phenomenon has already been observed for the closely related diamidine DAPI, which presents with a large bathochromic emission shift (yellow fluorescence) upon binding with polyanions such as RNA, mucopolysaccharides and polyphosphates (Kapuscinski, 1995). We hypothesize that DB75 is actively accumulated by living cells inside the mitochondrion where it condensates with polyanions until a critical concentration, which causes precipitation of the complexes and fluorescence shift to longer wavelengths. Discrete distribution of these negatively charged cellular components inside the mitochondrion could cause the punctate fluorescence pattern visualised. The identity of these components is unknown: although crystalline masses have been found in the mitochondrion of *Trypanosoma evansi*, no similar dense incusions were observed in other salivarian trypanosomes (Vickerman, 1977). The compartmentalisation of the green corpuscles inside the mitochondrial organelle would also explain why DB75 green emission is evidenced in association with the kinetoplast but not with the nucleus (both stained by the fluorophore upon DAPI excitation). Understanding the cause for the fluorescence shift of DB75 emission from blue to longer wavelengths will give important information regarding the identity of the corpuscles visualised under FITC filter and, possibly, on the mechanism of action of this trypanocidal compound.

4

Green fluorescent diamidines and phenanthridines as diagnostic probes for trypanosomes

4.1 Introduction

The diamidine DB75 proved to be an interesting fluorophore for diagnosis of trypanosomiasis. This compound is cost-efficient to synthesise, it is quickly and specifically internalised into parasites and it emits bright fluorescence when excited using standard DAPI and FITC filters (Chapter 3). Moreover, LED-driven microscopes (Cytoscience), compatible with the emission maxima of the compound, are available. Nevertheless, the use of DB75 as a fluorescent marker also presents some issues: for example, the drug resistance test using this diamidine in association with the prototypical UV LED microscope still needs to be optimised, while the photoinstability of this fluorophore and its inability to stain the whole parasite cell body with bright emission are not ideal properties for an ultimate use as a general diagnostic dye.

A variety of other fluorophores was, therefore, screened in order to find compounds with more advantageous properties than DB75. A series of green fluorescent diamidines, with higher wavelength absorbance and emission spectra, was also studied for their use as fluorescent substrates for the arsenical drug resistance test.

4.1.1 Green fluorescent pentamidine analogues

When the arsenical drug resistance test was initially developed (Stewart *et al*., 2005), no UV LED microscopes were available, thus hampering its development into a format more suited for field use. To tackle this problem, two solutions were considered: the development of a new instrument compatible with the UV-excited diamidines (DB75 and DB99) originally used in the test (this aspect is discussed in Chapter 3), or the search for other P2-specific substrates compatible with the Cytoscience SMR LED microscope already available (λ_{EX}=472 nm, λ_{EM}>500 nm) (Jones *et al*., 2005).

A series of pentamidine analogues was specifically synthesised by Prof. D. W. Boykin's group (Georgia State University, Atlanta) with the intention of generating other fluorescent substrates for the arsenical drug resistance test. These compounds (Figure 4.1) maintained the basic dicationic backbone of others diamidines (containing the recognition motif for the P2/*Tb*AT1 transporter), but were added with a series of ultra-conjugated ring structures in the linker, which provided them with emission wavelengths higher than DB75 (and, therefore, more likely to be compatible with the already available Cytoscience SMR microscope) (Table 4.1).

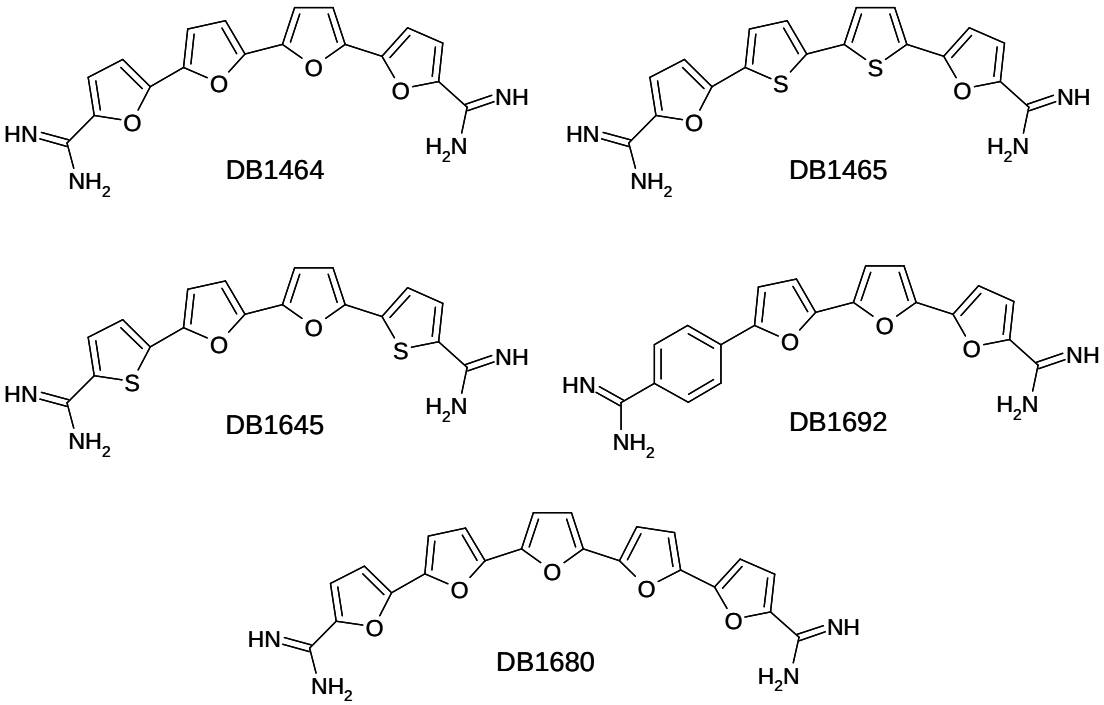

Figure 4.1 – Chemical structure of the five green fluorescent pentamidine analogues. These compounds shared the same diamidine backbone (for P2 recognition) with DB75 and pentamidine and had various combinations of furan, thiophene and phenyl rings in the linker between the two amidine groups, which gave them fluorescent properties.

Compound	λ_{EX} (nm)	λ_{EM} (nm)
DB1464	413	540
DB1465	405	525
DB1645	426	575
DB1692	400	545
DB1680*	397	515

Table 4.1 – Excitation and emission wavelengths of the five green fluorescent diamidines. The spectrum of DB1680 (*) was measured in our laboratory using a 1 µM solution in dH_2O (see also Figure 4.6 A). The excitation and emission maxima of the other four diamidines were determined in Prof. D. W. Boykin's laboratory (Georgia State University, Atlanta). λ_{EX}: wavelength of maximum excitation; λ_{EM}: wavelength of maximum emission.

The ability of these promising compounds to selectively stain trypanosomes was studied both *in vitro* (on cultured bloodstream parasites) and in *ex-vivo* infected rat blood samples. Their potential use as substrates for the arsenical drug resistance test was also evaluated both by studying their uptake-dependence on the P2 amino-purine transporter (using a drug sensitivity assay) and by fluorescence microscopy on strains either expressing, or not expressing, this permease.

4.1.2 Phenanthridines

Phenanthridines are a group of molecules containing a nitrogen heterocyclic core that makes them fluoresce in the red region of the visible spectrum. Phenanthridines were

considered of interest for our project since some of them also possess trypanocidal activity, implying selective internalisation inside these parasites. Ethidium bromide (homidium bromide, Ethidium®, [3,8-diamino-5-ethyl-6-phenylphenanthridinium bromide]) is a fluorophore widely applied in molecular biology as nucleic acid stain. Both ethidium and isometamidium chloride (Samorin®, [8-[(*m*-amidinophenylazo)amino]-3-amino-5ethyl-6-phenylphenanthridinium chloride hydrochloride]) (Figure 4.2) are phenanthridines used for the treatment of animal African trypanosomiasis (Leach and Roberts, 1981). Isometamidium is also applied to livestock as a prophylactic agent (Kinabo and Bogan, 1988). The chemical structure of isometamidium is a hybrid from homidium and the *p*-aminobenzamide moiety of diminazene aceturate (an aromatic diamidine also used in veterinary trypanosomiasis). Despite possessing the recognition motif for the P2/*Tb*AT1 transporter, however, the internalisation of isometamidium inside parasites only partly occurs through this route (Delespaux and de Koning, 2007). Instead, it has been proposed that this compound freely crosses the plasma membrane and is, then, actively concentrated inside the mitochondrion, a main target of the drug (de Koning, 2001b). The high cross-resistance of isometamidium with ethidium (Peregrine *et al*., 1997) suggests the involvement of a common route of uptake for the two compounds. Propidium iodide [3,8-diamino-5-[3-(diethylmethylammonio)propyl]-6-phenylphenanthridinium diiodide] is a phenanthridinium analogue of ethidium, but it is characterised by a more hydrophilic nature, due to the presence of a bulky ionic substituent on the phenanthridine ring (Figure 4.2). Propidium is widely used as nucleic acid stain in fluorescence techniques and to identify dead cells in a population, since it is a membrane-impermeant molecule and it is normally excluded from live cells (Suzuki *et al*., 1997; Riccardi and Nicoletti, 2006). Propidium has also been shown to have trypanocidal activity *in vivo* (Cox *et al*., 1984) and *in vitro* (Gould *et al*., 2008).

Phenanthridines bind to DNA by intercalating between the bases (one molecule of dye for every four or five nucleotides), apparently with no significant sequence preference (Waring, 1965). All of the three phenanthridines considered in this study also stain cytoplasmic RNA (Waring, 1965; Suzuki *et al*., 1997). As occurs with DAPI (Chapter 3), DNA binding changes the spectral properties of these phenanthridine molecules, inducing a shift of both the excitation and emission maxima (Table 4.2) and enhancing the overall fluorescence emission intensity 20- to 30-fold for ethidium and propidium (Waring, 1965) and more than 4-fold for isometamidium (Zilberstein *et al*., 1993; Wilkes *et al*., 1995). The high affinity of phenanthridines for nucleic acids is also responsible for their mutagenicity and it appears to be related to the trypanocidal activity of these compounds, which involves

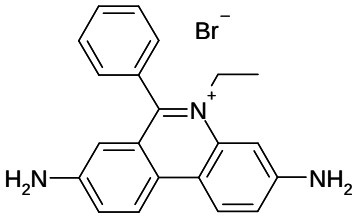

Ethidium bromide

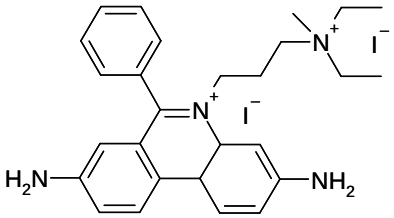

Propidium iodide

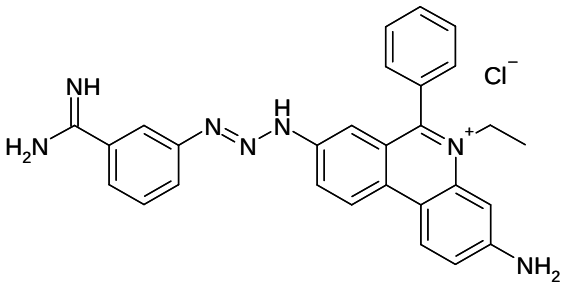

Isometamidium chloride

Figure 4.2 – Chemical structure of the three phenanthridines used in the present study.

Compound	λ_{EX} (nm)		λ_{EM} (nm)	
	free dye	+ds DNA	free dye	+ds DNA
Ethidium bromide	480	518	620	605
Propidium iodide	482	540	608	608
Isometamidium chloride	374	-	600	584

Table 4.2 – Excitation and emission maxima of the three phenanthridines tested. Peak values in the absence (free dye) or presence of DNA (+ds DNA) are indicated. Wavelengths for ethidium bromide and propidium iodide are from the Sigma-Aldrich website (http://www.sigmaaldrich.com/life-science/cell-biology/detection/learning-center/wavelength-index.html). The emission and excitation spectra data for isometamidium chloride are from Zilberstein *et al*., 1993. These authors used lysates of *T. congolense* (IL 1180) for the spectra measurements in the presence of DNA. Free isometamidium has a second emission peak at 645 nm, which is not affected upon DNA binding.
dsDNA: double-stranded DNA; λ_{EX}: wavelength of maximum excitation; λ_{EM}: wavelength of maximum emission.

inhibition of DNA synthesis (Leach and Roberts, 1981; Kinabo and Bogan, 1988). Isometamidium chloride, in particular, was shown to cause linearization of kinetoplast DNA minicircles in *T. equiperdum* by interacting with the complexes formed by topoisomerases and the kinetoplast DNA (Shapiro and Englund, 1990). Another study showed that dyskinetoplastic trypanosomes were not responsive to ethidium bromide treatment in an *in vivo* model, suggesting that the kinetoplast was an important target for the action of the phenanthridine (Agbe and Yielding, 1995).

The intrinsic fluorescence of ethidium, propidium and isometamidium has been used to study their distribution in trypanosomes, in order to identify their intracellular targets. Microscopic examination of *T. brucei* parasites treated *in vivo* with ethidium bromide

showed that this compound localised inside the kinetoplast and the nucleus of the cells, with a fluorescent intensity proportional to the drug concentration (Cox *et al*., 1984). The same authors showed a more diffuse cytoplasmic fluorescence for propidium iodide, which appeared to stain the kinetoplast with a less intense emission than the nucleus (Cox *et al*., 1984). Isometamidium revealed a greater affinity for the kinetoplast than ethidium (Boibessot *et al*., 2002). Boibessot and collaborators also observed that the absorption of ethidium into trypanosomes was slower than that of isometamidium, confirming data published previously (Hawking and Sen, 1960).

4.1.3 Acridine orange

Acridine orange [3,6-bis(dimethylamino)acridine] is a basic nucleic acid dye, isomer of phenanthridine (Figure 4.3). The fluorescence characteristics of this molecule are complex. In diluted aqueous solutions (10^{-7} M) the fluorophore is present as a monomer, while the dimeric form prevails in more concentrated solutions ($>10^{-2}$ M). These two forms have different spectral properties (Table 4.3) and give rise to specific complexes with nucleic acids (Tomita, 1967; MacInnes and McClintock, 1970; Zelenin, 1999). Complex I is formed when the monomer of acridine orange intercalates within bases of double-stranded DNA (with a ratio of one molecule of dye per four bases of DNA). This interaction increases the green fluorescence yield 2- to 2.5-fold as compared to the free dye. Complex II has a red emission and arises from binding of the dimer to single-stranded nucleic acids and RNA, apparently by ionic interactions with the sugar-phosphate backbone (Gardner and Mason, 1967). This interaction induces a 10-fold decrease in the fluorescence yield (Zelenin, 1999) (spectral characteristics of these complexes are indicated in Table 4.3). Acridine orange can also form salt-like complexes with polysaccharides and, at pH>7, it binds to proteins, yielding red fluorescence (Zelenin, 1999).

The fluorescent properties of acridine orange have been intensively exploited for a wide range of purposes. Its double green and red emission can allow discrimination between double-stranded DNA and single-stranded nucleic acids (Watson and Chambers, 1977). By being a membrane-permeant compound, acridine is also used in association with other exclusion dyes (such as propidium iodide) to distinguish living from apoptotic cells (Bank, 1988; Foglieni *et al*., 2001). Another use of this fluorophore is as an *in vivo* marker for acidic cell compartments, such as lysosomes (Zelenin, 1966; Brunk *et al*., 2001) or the trypanosome's acidocalcisomes (Docampo and Moreno, 1999), inside which acridine is actively accumulated, protonated and sequestered.

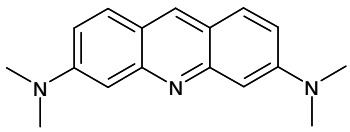

Acridine orange

Figure 4.3 – Chemical structure of acridine orange.

	λ_{EX} (nm)		λ_{EM} (nm)	
	free dye	+ NA	free dye	+ NA
AO monomer/Complex I	494	502-504	530	530
AO dimer/Complex II	465	475	640	640

Table 4.3 – Excitation and emission maxima of acridine orange.
Peak values in the absence (free dye) or presence of nucleic acids (+ NA) are indicated. In aqueous solutions (free dye) the fluorophore exists in two forms, depending on its concentration. At low molarities acridine orange is present as a monomer, which binds to double-stranded DNA by intercalation, yielding green fluorescence (Complex I). The dimer is formed at high concentrations and it binds to single-stranded DNA or RNA yielding red fluorescence (Complex II).
AO: acridine orange; NA: nucleic acids; λ_{EX}: wavelength of maximum excitation; λ_{EM}: wavelength of maximum emission.

Acridine orange is used as fluorescent probe for the diagnosis of malaria: protocols include direct application of the dye to the specimen on microscopy slides (Kawamoto, 1991; Delacollette and Van der Stuyft, 1994; Keiser *et al*., 2002) or coating the interior of the capillary tubes used in the quantitative buffy coat system (Baird *et al*., 1992). This last technique has also been applied to detect trypanosomes in human blood (Bailey and Smith, 1992; Chappuis *et al*., 2005), but its high cost makes it difficult to implement in field settings (Section 1.2.3.6).

The fluorescence spectra of this fluorophore match the wavelength range of the standard FITC filter, which is the spectral region also covered by the LED Cytoscience SMR microscope (Jones *et al*., 2007).

4.2 Results

4.2.1 Fluorescence properties of the five pentamidine analogues

To evaluate if the five green fluorescent pentamidine analogues could represent useful diagnostic probes for trypanosomiasis, their staining properties were studied in parasites both in culture medium (*in vitro*) and in murine blood (*ex-vivo*). Compatibility with the LED-driven Cytoscience fluorescence microscope was also assessed.

4.2.1.1 Fluorescence in *in vitro* trypanosomes

Fluorescence experiments on *in vitro*-grown *T. b. brucei* wild type cells showed that the five pentamidine analogues were actively internalised and accumulated into parasites (Figure 4.4). When given at 50 μM, the fluorophores stained the kinetoplast and cytoplasm of live trypanosomes with a green fluorescence, clearly visible upon FITC excitation (λ_{EX}=470 nm, λ_{EM}=519 nm) at low magnification (40× objective), after 10-15 minutes of treatment. Uptake was highly dependent on the temperature of incubation: the fluorescent signal inside the cells was nearly completely inhibited when treatment was carried out at 4°C and it developed only when cells were treated at room temperature or 37°C, consistent with a mediated uptake of the five diamidines into trypanosomes (Figure 4.5).

Fluorescence intensity of parasites stained with the green fluorescent diamidines increased with time of incubation, but the overall yields were never very high, despite the fact that the excitation wavelengths of the fluorophores matched the 405 nm emission peak of the mercury lamp. The use of higher dye concentrations did not improve their signal, nor did it significantly increase their rate of uptake into parasites (another result consistent with carrier-mediated uptake). The low emission intensity of this series of compounds could be due to their intrinsic low fluorescent yields. A comparison between the spectrum of DB1680 and that of the related diamidine DB75, for example, showed a 6-fold lower emission intensity for DB1680 than DB75, although the green fluorescent dye was used at a higher concentration (20-fold) (Figure 4.6). Another factor which could have lead to suboptimal fluorescence intensity emission of the five compounds could have been the discrepancy between their excitation maxima, all close to 400 nm (Table 4.1), and the standard FITC filter wavelength (λ_{EX}=470 nm) utilised for microscopy experiments. The use of another filter set, which better matches the spectral excitation characteristics of the green fluorescent diamidines, may allow obtaining of higher fluorescence emission yields.

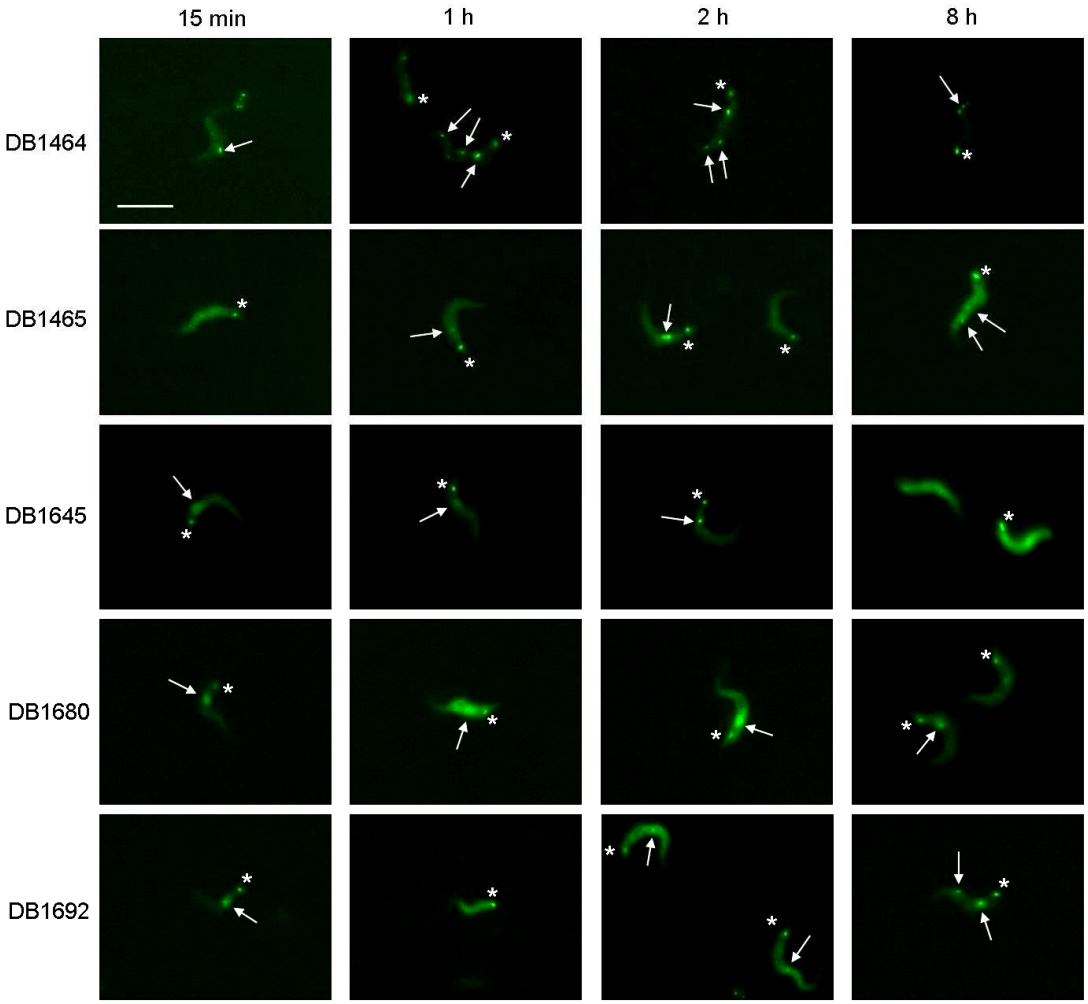

Figure 4.4 – Fluorescence development within *in vitro* trypanosomes treated with the five green fluorescent pentamidine analogues.
***T. b. brucei* w.t. cells from culture were incubated with 50 μM of each compound at r.t.. At the indicated time points, wet films were prepared and directly viewed under the FITC filter (λ_{EX}=470 nm, λ_{EM}=519 nm) of the Zeiss Axioplan microscope. Parasites incubated for 8 h, were treated with 500 nM of each compound at 37℃.**
FITC 33 ms exposure; 40× objective. *: kinetoplast; →: unidentified cytoplasmic corpuscles. Bar: 10 μM.

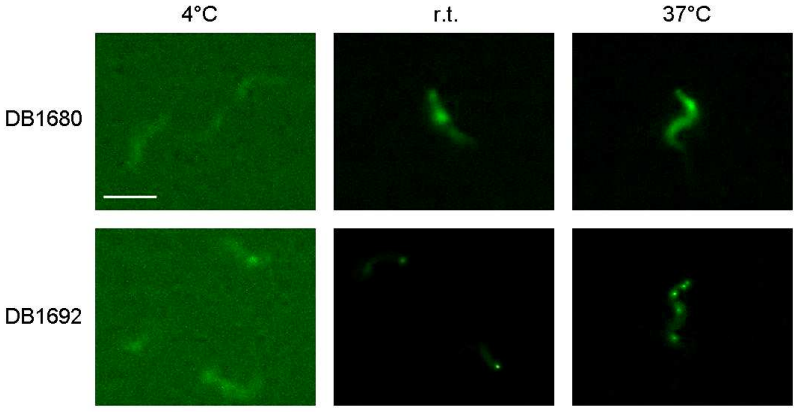

Figure 4.5 – Effect of temperature on the internalisation of DB1680 and DB1692 into *T. b. brucei*.
***In vitro* w.t. parasites were incubated with 50 μM of either compound for 1 h at 4℃, room temperature (r.t.) or 37℃. Wet films were prepared and directly viewed under the FITC filter of the Zeiss microscope. The effects of temperature on the uptake of the other three diamidines of the series (not shown here) were similar to those illustrated in the figure.**
FITC 33 ms exposure; 40× objective. Bar: 10 μM.

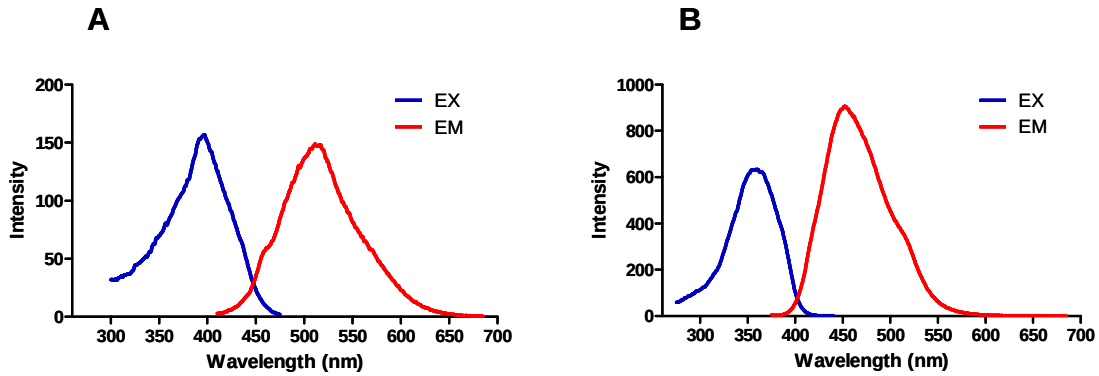

Figure 4.6 – Fluorescence spectra of DB1680 and DB75.
(A) The spectrum of DB1680, measured using a 1 µM solution of the compound in dH_2O.
(B) The spectrum of DB75, measured using a 50 nM solution of the compound in dH_2O.
Note the different scale of the axis of ordinates.
EX: excitation spectrum; EM: emission spectrum.

4.2.1.2 Uptake and intracellular distribution

When wild type trypanosomes, stained with 50 µM of each diamidine, were viewed using the FITC channel (Figure 4.4 and 4.9), two common features, shared by all of the five green fluorescent compounds, could be identified: (1) all of them rapidly concentrated inside the kinetoplast, which remained the brightest organelle beyond 8 hours incubation time; (2) the nucleus could never be visualised. With the exception of DB1464, where this characteristic was less marked, the fluorophores accumulated inside the cytoplasm, making the whole cell shape distinguishable even at low magnification. Punctate fluorescent granules, spread throughout the whole cell length and similar to those observed for DB75 upon FITC excitation (Section 3.2.7), could be detected among the diffuse cytoplasmic signal.

A more pronounced fluorescent spot present in an area between the kinetoplast and the nucleus of the cells was consistently detected by 15 minutes treatment with DB1645, DB1692 and DB1680 (Figure 4.4). Since this region of the trypanosome cell is occupied by the endomembrane compartments (Golgi complex and endosomes, Figure 1.3) and it is in this area that all membrane trafficking takes place (Field *et al*., 2007; Field and Carrington, 2009) we speculated a possible involvement of endocytosis (a highly active process in bloodstream form) in the internalisation of these compounds. This hypothesis was strengthened by the Alamar Blue results, which suggested alternative routes of entry, other than P2, for the fluorophores (Section 4.2.2.1), and by the loss of diamidine internalisation when incubating at 4°C (Figure 4.5), a temperature known to inhibit endocytosis (Brickman *et al*., 1995; Coppens *et al*., 1995; Liu *et al*., 2000), as well as other

active mechanisms of uptake. To further test this idea, the fluorescence patterns were assessed in *in vitro* wild type trypanosomes pre-treated with endocytic inhibitors before staining with the diamidines DB1680 and DB1692. For these experiments we used cytochalasin D (10 μM for 1 h at 37°C), a cell-permeable potent inhibitor of actin polymerisation, which in bloodstream trypanosomes is required for the formation of coated vesicles from the flagellar pocket membrane (García-Salcedo *et al*., 2004). The use of this toxin, together with other membrane stabilizing drugs, was shown to reversibly inhibit human serum lysis, a process that involves endocytosis (Rifkin, 1983; Ortiz-Ordóñez *et al*., 1994). However, fluorescent micrographs did not evidence any significant change in dye distribution following cytochalasin pre-treatment (Figure 4.7), the fluorophores continuing to accumulate as posteriorly localised spots (although their number and size appeared slightly increased following incubation with the toxin). Similarly, no evident effects were observed after pre-treating with chloroquine (up to 200 μM for 1 h at 37°C), a lysomotropic amine which had previously been used as a receptor-mediated endocytosis inhibitor in both procyclic form (Liu *et al*., 2000) and bloodstream *T. brucei* (Coppens *et al*., 1993 and 1995) (data not shown). These experiments did not, therefore, demonstrate an endosomal localisation of the green fluorescent diamidines.

To study in more depth these fluorescent inclusions, trypanosomes had to be immobilised. Methanol fixation of stained trypanosomes, however, proved inadequate, since it washed away most of the incorporated fluorophore. A better system was to immobilise labelled living parasites by embedding them in agarose (Section 2.5.2.2). This system allowed the study of the fluorophores' intracellular distribution in live parasites, avoiding artefacts often produced by common fixation protocols.

When cells were immobilised in agarose and viewed at high magnification the cytoplasmic fluorescent inclusions, already visible under 40× objective, became more obvious (Figure 4.8). Following DB1680 treatment, the vesicular structures tended to be localised to the posterior of the cell, while after incubation with DB1692 other inclusions, present in the anterior part of the cell, were clear, again inconsistent with endocytic vesicles. Interestingly, fluorescent emission from cytoplasmic corpuscles could also be detected at longer wavelengths, using the RHOD filter set (λ_{EX}=546 nm, λ_{EM}=590 nm), a phenomenon already noticed for the diamidine DB75 (for which we observed fluorescence in the blue and green regions of the spectrum; Chapter 3). The red fluorescent signal mostly colocalised with the green emission, but intensity of each fluorescent corpuscle was variable under the different filter sets. For DB1692, a prominent red fluorescent spot

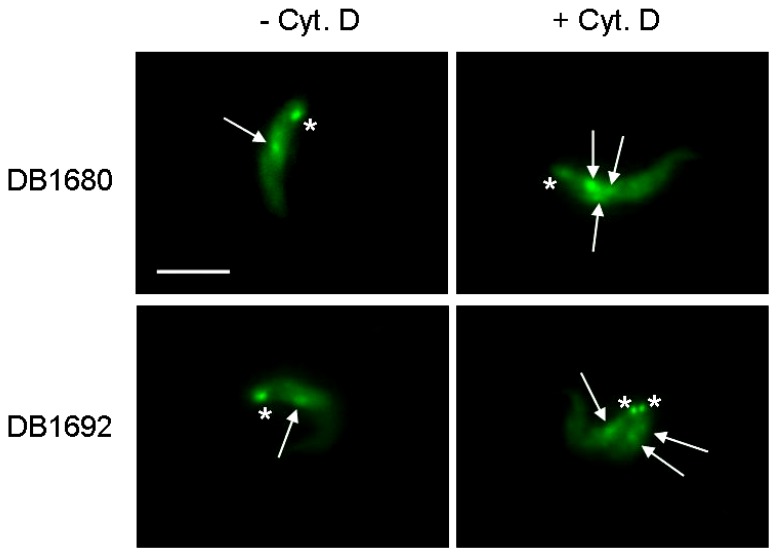

Figure 4.7 – Effect of cytochalasin D on the uptake of DB1680 and DB1692.
***In vitro T. b. brucei* w.t. cells (2×10^7 cells/ml) were pre-incubated with 10 µM cytochalasin D (Cyt. D, Sigma-Aldrich) for 1 h at 37℃ and then tr eated with 50 µM of either diamidine for 1 h at 37℃. Aliquots of live parasites were put on a m icroscope slide, covered with a coverslip and directly viewed under the FITC filter of the Zeiss Axioplan microscope. Trypanosomes not pre-treated with cytochalasin and used as control are shown on the left panels.**
FITC 33 ms exposure; 100× objective. *: kinetoplast; →: hypothetical endosomal vesicles. Bar: 10 µM.

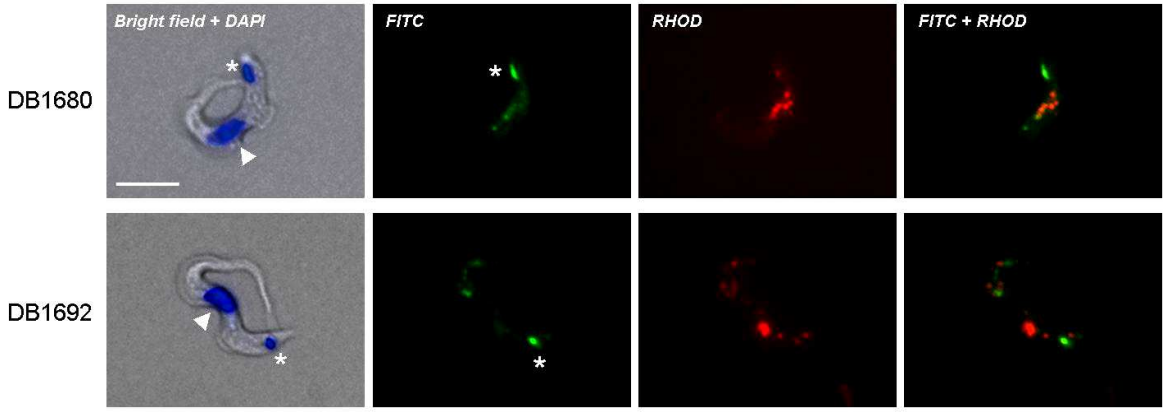

Figure 4.8 – Fluorescence images at high magnification of trypanosomes treated with DB1680 and DB1692.
***T. b. brucei* w.t. cells from culture were incubated with 50 µM of either compound for 1 h at 37℃ and successively put into ice to stop dye upta ke. DAPI (20 µM) was added to the cells as DNA counterstain and left for 30 min before mounting in 1% agarose. Trypanosomes were also viewed without addition of counterstain to exclude possible interference of DAPI in the emission of the green fluorescent diamidines. Cells were viewed using various filters of the Zeiss Axioplan fluorescence microscope, as indicated in the images. Micrographs were merged using Adobe Photoshop 7.0 software.**
Time of exposure of the camera for the three filters (DAPI, FITC, RHOD) was not kept constant; 100× objective. *: kinetoplast; ►: nucleus. Bar: 10 µM.

appeared in a region between nucleus and kinetoplast after 1 hour treatment with the fluorophore, but it was not visible at shorter time of incubation. The other three compounds of the series yielded similar punctate emission upon RHOD excitation (data not shown). These fluorescent corpuscles could be the same as those observed using the FITC channel following DB75 treatment (Figure 3.9), although, following incubation with DB1692, they appeared less homogeneous in size and some were localised at the posterior of the kinetoplast (Figure 4.8). Further studies will be needed in order to understand the origin of these spots. The general low intensity yield and the punctate fluorescent pattern meant that this red emission will be of limited use as a fluorescent diagnostic marker for trypanosomes.

4.2.1.3 Fluorescence in viable *ex-vivo* trypanosomes

To be useful for fluorescence-based trypanosomiasis diagnostics, it is important that fluorophores are able to specifically label parasites among a complex blood matrix, the fluid most widely used for parasitological examination in the field. The five green fluorescent diamidines fulfilled this criterion, since they provided a specific staining of trypanosomes without labelling erythrocytes in infected rat blood films, when given at 50 μM (Figure 4.9). As for *in vitro* samples, in *ex-vivo*-treated specimens the kinetoplast appeared the brightest organelle. The other cytoplasmic fluorescent corpuscles were also visible in these samples. Green fluorescent trypanosomes were readily detectable among blood cells based on their movement and fluorescent dots (especially the bright kinetoplast), which allowed them to be easily distinguished from crystals or debris that fluoresced in the background using a low magnification objective (40×). As already noticed for DB75, however, also these diamidines suffered a relatively fast photobleaching, although the fading appeared less marked in blood samples compared to culture samples.

4.2.1.4 Fluorescence in fixed thin blood smears

When they were applied to fixed thin blood smears, fluorescence of the five pentamidine analogues proved generally quite poor and suffered photobleaching. DB1692 appeared to be the best of the series, labelling trypanosomes in methanol-fixed films with discrete yields (Figure 4.10 A). When a dry thin smear, not fixed in methanol, was stained with the same amount of the compound (10 μM), the quality of fluorescence was highly affected (Figure 4.10 B). DB1692 could also be used to stain methanol-fixed trypanosomes from culture, but in these samples fluorescence yields were low (Figure 4.10 C).

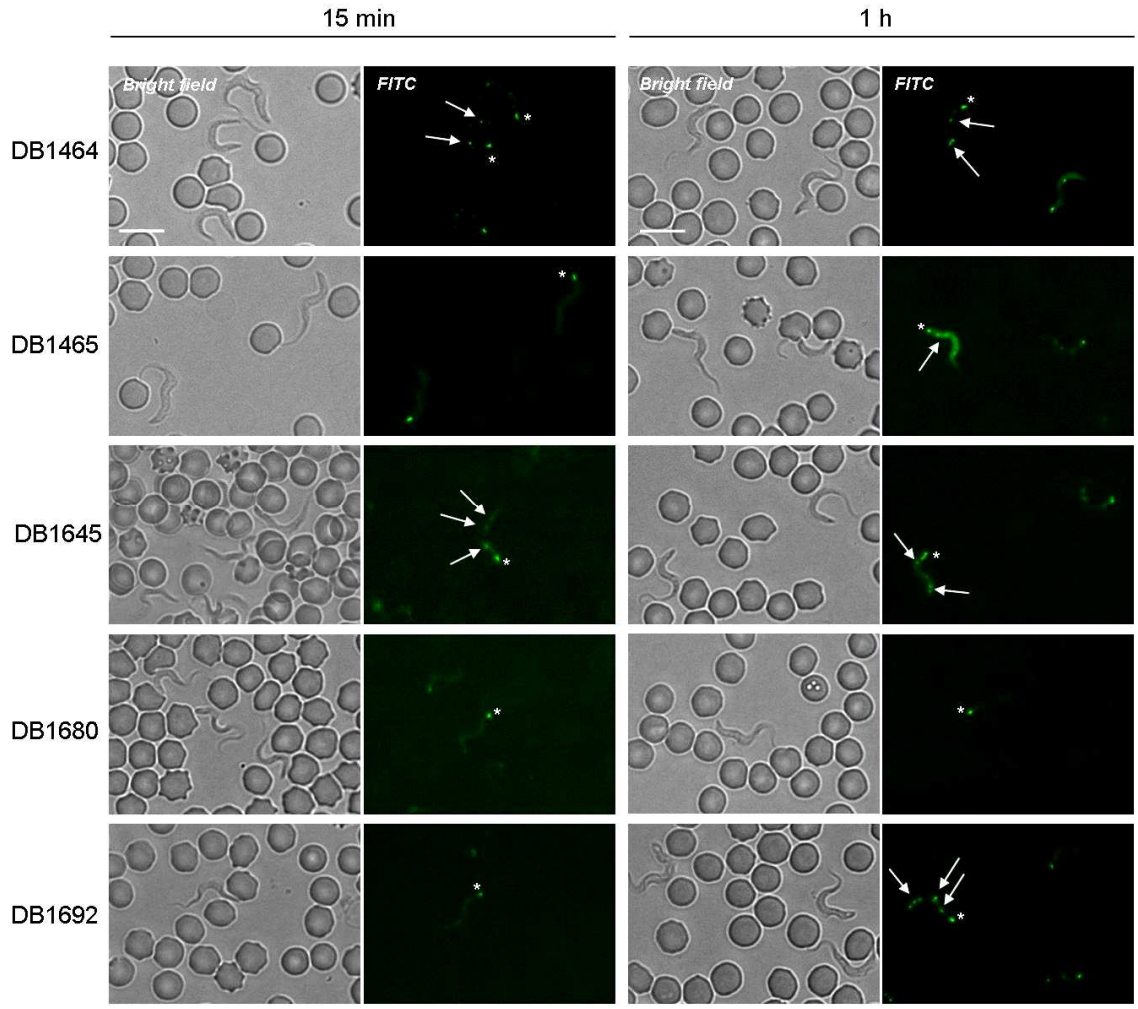

Figure 4.9 – Fluorescence images of live trypanosomes treated *ex-vivo* with each of the five green fluorescent pentamidine analogues.
Aliquots of rat blood infected with *T. b. brucei* w.t. parasites were incubated with 50 μM of each compound at 37℃ and at the indicated time poi nts wet blood smears were prepared and viewed under the FITC filter of the Zeiss Axioplan microscope. Bright field images are shown on the left of the corresponding fluorescent micrograph (note that position of motile trypanosomes can change in the two images).
FITC 100 ms exposure; 40× objective. *: kinetoplast; →: cytoplasmic corpuscles. Bar: 10 μM.

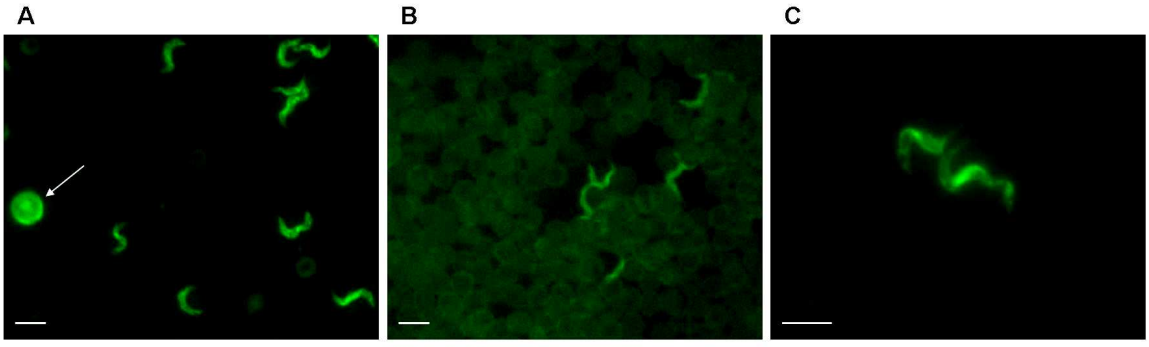

Figure 4.10 – Fixed *T. b. brucei* w.t. trypanosomes stained with DB1692.
(A) Thin blood smear fixed in methanol and labelled with 10 μM DB1692. (B) Thin blood smear, air-dried but not fixed in methanol, and labelled with 10 μM DB1692. (C) Trypanosomes from culture, fixed in methanol and stained with 10 μM DB1692. For all of the three samples, 50 μl of dye solution were applied and spread with a coverslip. Specimens were viewed under the FITC filter of the Zeiss Axioplan microscope.
FITC 68 ms (A and B) or 450 ms (C) exposure; 40× objective (A and B); 100× objective (C). →: white blood cell. Bar: 10 μM.

4.2.1.5 Compatibility with the LED Cytoscience SMR microscope

The green fluorescent series of pentamidine analogues was specifically designed to create P2 substrates with longer wavelengths than the UV diamidine DB75, in order to generate new substrates to use in the arsenical drug resistance test (Stewart *et al*., 2005), in association with the already available LED Cytoscience SMR field fluorescence microscope (Jones *et al*., 2005 and 2007). Unfortunately, although of longer excitation wavelength than DB75 (Table 4.1), the excitation maxima of the compounds of this series were still too short to be compatible with the narrow band-emitting LED source of the Cytoscience instrument (λ_{EX}=472 nm). DB1680 and DB1692 were the only two compounds out of the five that yielded an extremely faint emission when observed under this microscope (no images are available because no suitable camera could be connected with the instrument). As previously discussed (Section 4.2.1.1), the standard FITC filter of the Zeiss fluorescence microscope was not ideally matched with the spectral characteristics of these diamidines, and the use of a more appropriate filter set (also for the LED instrument) might allow a better exploitation of their fluorescent properties.

4.2.2 Use of the green fluorescent pentamidine analogues as substrates for the arsenical drug resistance test

The five green fluorescent diamidines appeared to be accumulated into wild type trypanosomes by a carrier-mediated process, although low fluorescence emission allowed detection of the intracellular dyes only after 10-15 minutes. As with other diamidine molecules, these compounds were expected to be internalised mainly by the P2/*Tb*AT1 amino-purine transporter and, therefore, to enter only marginally into arsenical- and diamidine-resistant parasites lacking this transporter's activity. Tight dependence on the P2 carrier for their uptake would have made these compounds alternative probes to the UV diamidines DB99 and DB75 for the arsenical drug resistance test.

4.2.2.1 Trypanocidal effect on wild type and P2-deficient *T. b. brucei* strains

To investigate the involvement of the P2 transporter in the molecules' uptake, the Alamar Blue assay was first performed. For the test, three different *T. b. brucei* strains were used: wild type S427 line, *tbat1*$^{-/-}$ line, which lacks the gene that encodes for the P2 transporter (Matovu *et al*., 2003) and B48 line, a pentamidine-adapted clone derived from *tbat1*$^{-/-}$ and in which the HAPT (high affinity pentamidine transporter) activity is lost (Bridges *et al*., 2007).

Compound	IC_{50} (nM)			Resistance factor	
	w.t.	*tbat1*$^{-/-}$	B48	*tbat1*$^{-/-}$	B48
DB1464	0.87 ± 0.57	6.92 ± 4.12	7.25 ± 1.51	8.0	8.3
DB1465	6.85 ± 3.72	71.40 ± 8.80	333.90 ± 24.52	10.4	48.7
DB1645	14.50 ± 6.32	232.93 ± 86.19	610.44 ± 133.21	16.1	42.1
DB1692	17.64 ± 9.79	436.10 ±82.39	344.20 ± 31.29	24.7	19.5
DB1680	266.20 ± 45.93	590.95 ± 84.94	340.48 ± 23.51	2.2	1.3
Pentamidine	0.61 ± 0.65	0.91 ± 0.41	166.95 ± 20.04	1.5	273.7

Table 4.4 – Trypanocidal activity of the five pentamidine analogues against *T. b. brucei* S427 w.t., *tbat1*$^{-/-}$ and B48 cell lines.
IC_{50} values (drug concentration required to inhibit trypanosome proliferation by 50%) were measured using the Alamar Blue assay (Section 2.4). Trypanotoxicity of pentamidine was used as positive control. Resistance factors were calculated by dividing the IC_{50} value obtained for each compound on the *tbat1*$^{-/-}$ and B48 lines by the value obtained on the w.t. line. All data are reported ± the standard deviation and represent the mean of at least three independent experiments.

The Alamar Blue results on the wild type strain showed a potent trypanotoxicity for all of the five diamidines, with IC_{50} in the nanomolar range (Table 4.4). DB1464 was the most active trypanocide, having an IC_{50} close to the value of pentamidine. For this molecule, loss of P2 (*tbat1*$^{-/-}$ line) corresponded to 8-fold decrease of toxic activity, indicating an involvement of this permease in its uptake into the parasite. Similar loss of activity against the *tbat1*$^{-/-}$ line, but more marked, was also observed for DB1465 and DB1645 (10- and 16-fold resistance factor respectively), which had a very similar molecular structure to DB1464 (Figure 4.1). Unlike DB1464, however, these last two compounds showed a high dependence on HAPT for internalisation, their IC_{50} further increasing 38- and 26-fold, respectively, when also activity of this transporter was lost (B48 line). DB1692 appeared to be the diamidine most dependent on P2 activity, showing an IC_{50} nearly 25-fold higher on the *tbat1*$^{-/-}$ line as compared to the wild type strain, with no further loss of toxicity in the B48 line. The resistance factors measured for these four green fluorescent diamidines were in the same order of magnitude (10- to 20-fold higher for *tbat1*$^{-/-}$ line compared to wild type) of those reported for DB75 and diminazene, two trypanocidal drugs highly dependent on P2 transport (Lanteri *et al*., 2006; Bridges *et al*., 2007). The addition of a single furan ring in the linker of DB1680 drastically affected its trypanocidal activity (the molecule was the less toxic of the series). The IC_{50} of this compound on *tbat1*$^{-/-}$ line was only 2-fold that measured on the wild type strain, a value similar to that of pentamidine, a drug that only partially relies on the P2 permease for uptake. However, if pentamidine internalisation was highly disrupted by loss of HAPT (B48 line), the same effect was not observed for DB1680, indicating that other routes of internalisation must play a role for its uptake.

In conclusion, the Alamar Blue results suggested that the pentamidine analogues synthesised in Prof. D. W. Boykin's laboratory were substrates for the P2 amino-purine

transporter, although other carriers (such as HAPT for DB1465 and DB1645), or other routes of uptake (for DB1680), may play a role for their internalisation into trypanosomes. Endocytosis could represent an alternative mechanism of entrance, but our experiments failed to support this hypothesis (Section 4.2.1.2).

4.2.2.2 Fluorescence in wild type and P2-deficient *T. b. brucei* strains

The Alamar Blue results proved the presence of a link between the compounds' cytotoxicity and active expression of the P2 amino-purine transporter, as expected for diamidine compounds. Fluorescence microscopy was then used to assess if this correlation also resulted in a differential fluorescence development in parasites lacking or expressing the P2 permease, the crucial aspect for their use in the arsenical drug resistance test. For microscopy, the same parasites lines used to perform the Alamar Blue assay (Section 4.2.2.1) were treated with each compound of the series (50 μM) for 15 min and viewed under the FITC filter of the Zeiss fluorescence microscope (Figure 4.11). Unfortunately, fluorescence micrographs did not reveal any significant difference in the diamidines' speed of uptake when comparing wild type, *tbat1*$^{-/-}$ and B48 lines. No differences were noticed even after longer times of incubation (up to 2 hours).

The fact that we could not observe differential uptake in wild type and *tbat1*$^{-/-}$cells after 15 minutes of incubation was not completely surprising: differences in intracellular fluorescence development linked to the presence or absence of the P2 transporter are more evident within the first minutes of incubation (Stewart *et al*., 2005), after which other lower affinity transporters, or differential routes of uptake, can compensate for the absence of this permease's activity. Unfortunately, the low fluorescence yields observed for the green diamidine series, under our experimental conditions, did not allow detectable signal inside trypanosomes at shorter times of treatment (up to 10 minutes). For this reason we do not consider these fluorescent diamidines to be suitable probes for the arsenical resistance test, unless higher yields are obtained with a more compatible filter set.

4.2.3 Ethidium bromide and isometamidium chloride

The compounds belonging to the green fluorescent diamidine series did not possess all of the necessary requisites to become fluorescent diagnostic markers for trypanosomiasis. The main problems associated with their use were a low fluorescent yield upon FITC excitation and a relatively fast photobleaching. Therefore, the staining properties of other

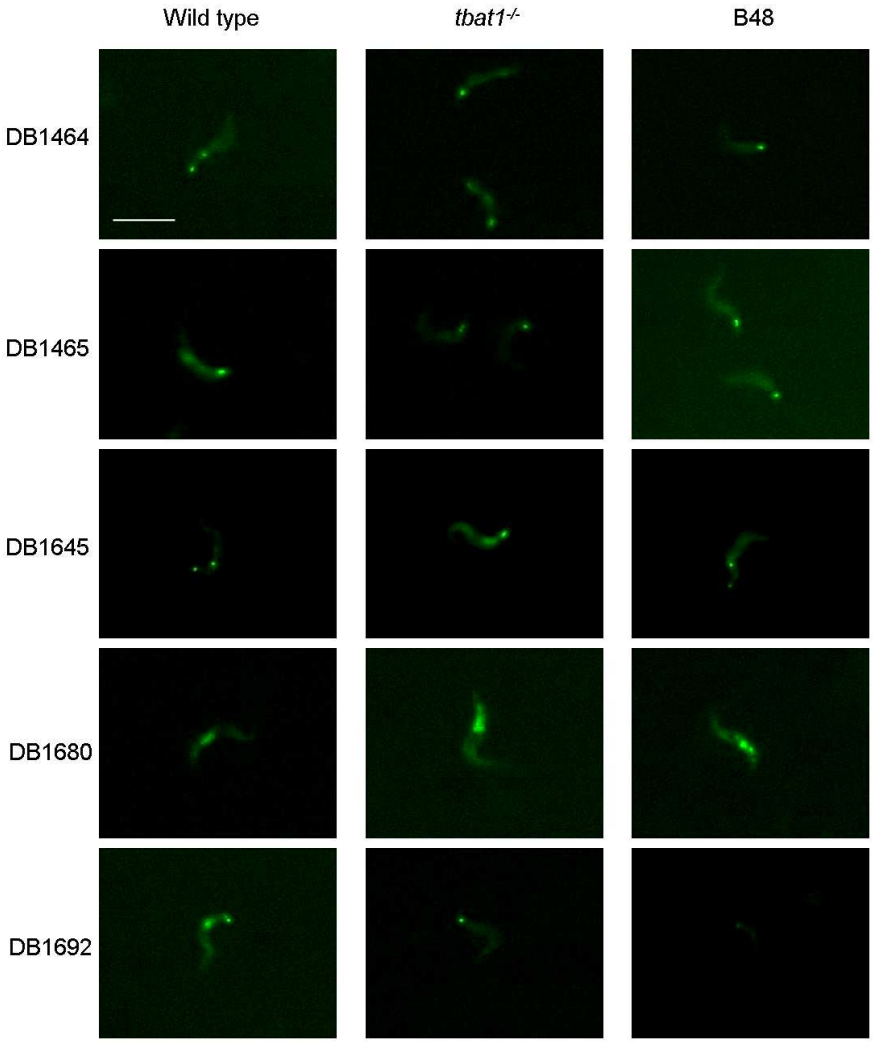

Figure 4.11 – Fluorescence images of *T. b. brucei* w.t., *tbat1*$^{-/-}$ and B48 line treated with each of the five green fluorescent pentamidine analogues.
Cells from culture were incubated with 50 μM of each compound for 15 min at r.t. and directly viewed under the FITC filter of the Zeiss Axioplan microscope.
FITC 33 ms exposure; 40× objective. Bar: 10 μM.

commercially available fluorophores were assessed, in order to find better probes to label trypanosomes. The phenanthridines ethidium bromide and isometamidium chloride were considered of interest for our project, being both fluorescent and specifically absorbed by trypanosomes (Cox *et al.*, 1984; Boibessot *et al.*, 2002). Fluorescence of propidium iodide (an analogue of ethidium) and of acridine orange (an isomer of phenanthridine) were also assessed (Sections 4.2.4 and 4.2.5 respectively).

4.2.3.1 Fluorescence in *ex-vivo* viable trypanosomes

Ethidium bromide quickly permeated live *ex-vivo* trypanosomes, yielding a bright fluorescence of the kinetoplast after only 5-10 minutes incubation with low doses of the compound (0.5, 1 μM) (Figure 4.12). However, we noticed that not all of the cells in the sample were equally stained by the fluorochrome. At these concentrations, fluorescence

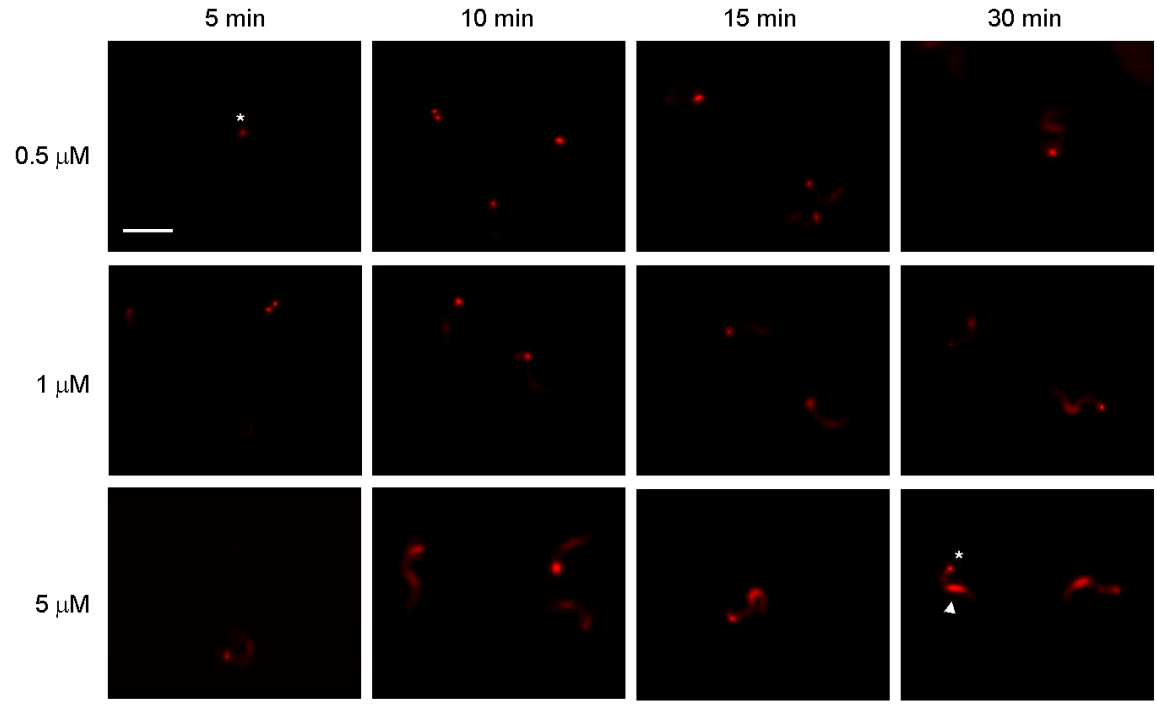

Figure 4.12 – Ethidium bromide fluorescence development within live *ex-vivo* trypanosomes.
Rat blood samples infected with *T. b. brucei* w.t. line were incubated *ex-vivo* with different concentrations of ethidium bromide at 37℃. At the indicated time points thin wet smears were prepared and viewed under the RHOD filter (λ_{EX}=546 nm, λ_{EM}=590 nm) of the Zeiss Axioplan microscope.
RHOD 68 ms exposure; 40× objective. *: kinetoplast; ►: nucleus. Bar: 10 μM.

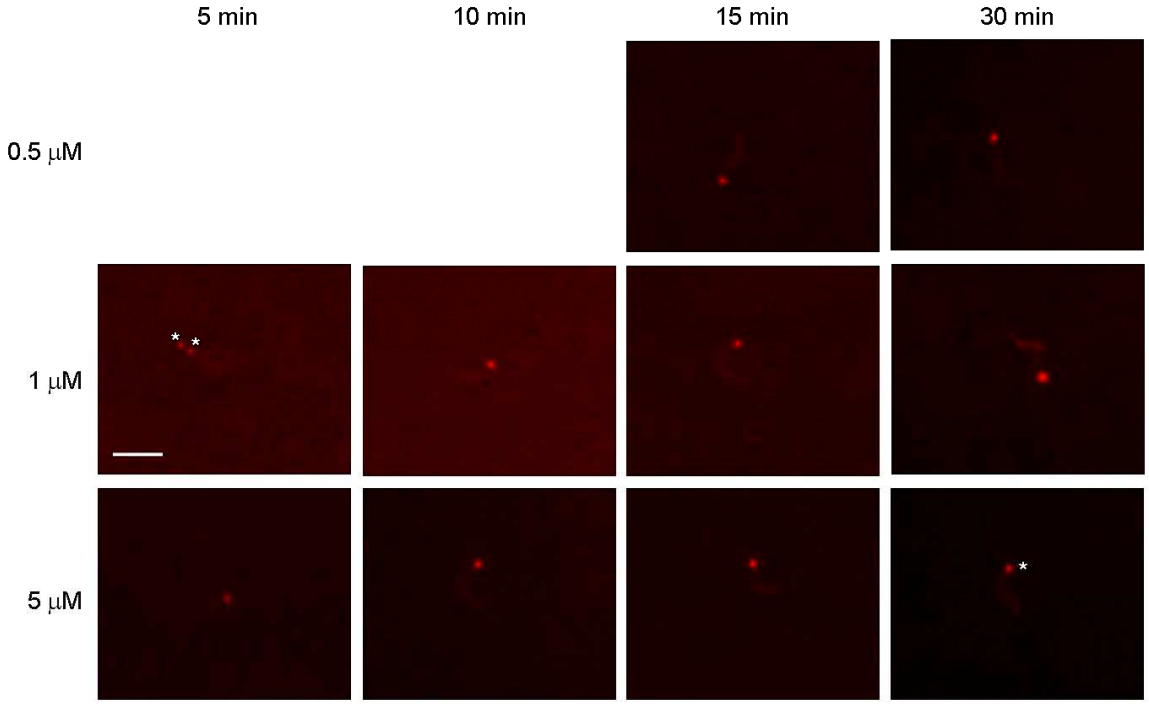

Figure 4.13 – Isometamidium chloride fluorescence development within live *ex-vivo* trypanosomes.
Rat blood samples infected with *T. b. brucei* w.t. line were incubated with different concentrations of isometamidium chloride at 37℃. A t the indicated time points thin wet smears were prepared and viewed under the RHOD filter of the Zeiss Axioplan microscope. No fluorescence could be detected for treatment with 0.5 μM up to 10 min of incubation.
RHOD 68 ms exposure; 40× objective. *: kinetoplast. Bar: 10 μM.

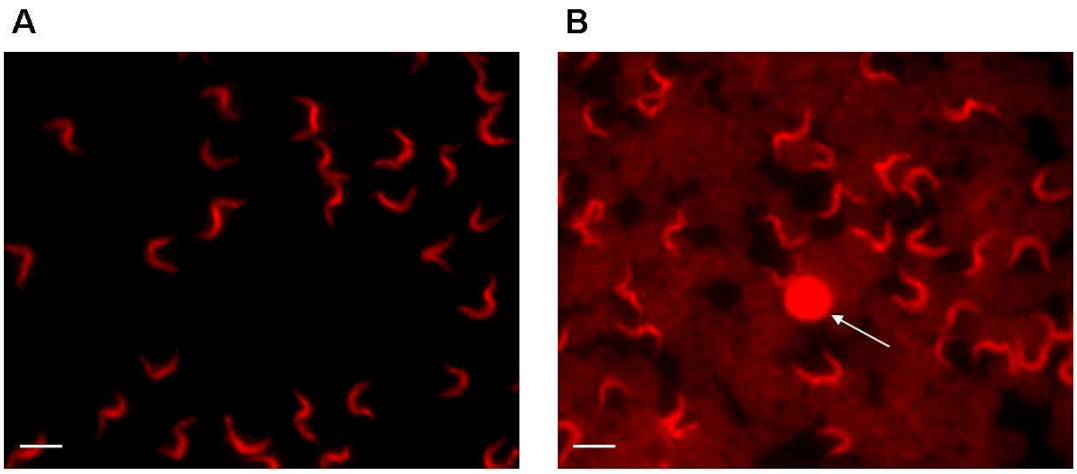

Figure 4.14 – Fixed thin blood smears stained with ethidium bromide and isometamidium. Specimens were stained with 50 µl of 5 µM ethidium bromide (A) or isometamidium (B) and immediately viewed under the RHOD filter of the Zeiss Axioplan microscope. The fixed smears had been prepared a fortnight before the experiments, using murine blood infected with *T. b. brucei* w.t. trypanosomes. Slides were kept in a box until use.
RHOD 68 ms exposure; 40× objective. →: white blood cell. Bar: 10 µM.

development inside the nucleus was slightly delayed compared to that of the kinetoplast. At 5 µM the nucleus was, however, already visible after 5 minutes of treatment, although its emission was comparable to that of the kinetoplast only after further 10 minutes. Nucleus and kinetoplast were the main detectable organelles, but ethidium also produced a low fluorescence from the cell cytoplasm. Red blood cells remained unstained. After longer times of incubation (1 hour when given at 5 µM and 2 hours when given at 1 µM) treatment with ethidium caused bursting of parasites present in the samples.

Treatment of *ex-vivo* trypanosomes with isometamidium chloride, using the same concentrations utilised during the experiments with ethidium bromide, showed a much lower fluorescence (Figure 4.13). The only bright signal easily detectable while examining these samples under RHOD filter was a spot corresponding to the kinetoplast of the parasites. No other organelles could be detected up to 30 minutes incubation using these doses and only a very faint fluorescence in the cell's cytoplasm was evident.

4.2.3.2 Fluorescence in fixed thin blood smears

Ethidium bromide proved a good probe for trypanosome staining in thin fixed blood smears. A low concentration of the dye (5 µM) was sufficient to give a bright red fluorescence to the parasites, while leaving the erythrocytes unlabelled (Figure 4.14 A). Application of an isometamidium solution (5 µM) to the smear, instead, stained the red blood cells (Figure 4.14 B), which yielded a low background emission, only slightly lower

than that emitted by trypanosomes. For these experiments, films that were several weeks old were used. Storage could have determined a slight deterioration of the specimens, causing the homogeneous staining of the parasites' cytosol and hampering the distinction of the nucleus and the kinetoplast.

4.2.4 Propidium iodide

4.2.4.1 Fluorescence in *in vitro* viable trypanosomes

Despite being considered a membrane-impermeant dye, propidium iodide was shown to stain viable *T. brucei* parasites with a bright red fluorescence, more intense than that of its analogue ethidium bromide (Cox *et al*., 1984). Our microscopy experiments confirmed these findings. When *in vitro*-cultured wild type trypanosomes were incubated at 37°C with micromolar concentrations of this phenanthridine (10-50 μM), the fluorophore was absorbed by the cells, staining with a stable fluorescence the nucleus and, to a lesser extent, the kinetoplast (Figure 4.15, left panels). Propidium also dispersed inside the cytoplasm, revealing the shape of the whole cell. For *in vitro* parasites, long times of incubation (greater than 1 hour) were needed to obtain the internalisation of sufficient dye in order to give a relatively good signal-to-noise ratio, indicating a slow mechanism of uptake for this fluorophore.

4.2.4.2 Fluorescence in *ex-vivo* viable trypanosomes

Using prolonged incubation times (1-2 hours), in *ex-vivo* specimens, propidium iodide brightly stained trypanosomes, leaving the erythrocytes non-fluorescent. Interestingly, when parasites grown in rodents were treated *ex-vivo* following the same protocol used for *in vitro* cells, their corresponding fluorescence intensity appeared much higher (Figure 4.15, right panels), even though their general fluorescent pattern was identical. A significant fraction of wild type trypanosomes in infected rat blood samples was killed by this phenanthridine after 2 hours of incubation, the cells appearing to be lysed by the dye (given at 10 or 50 μM). At this time point, the same concentration of the fluorophore did not kill *in vitro* cells. The high trypanocidal activity of propidium on wild type cells was confirmed by our Alamar Blue data: for this compound we measured an IC_{50} of 30.26 ± 7.66 nM (mean of three experiments ± standard deviation).

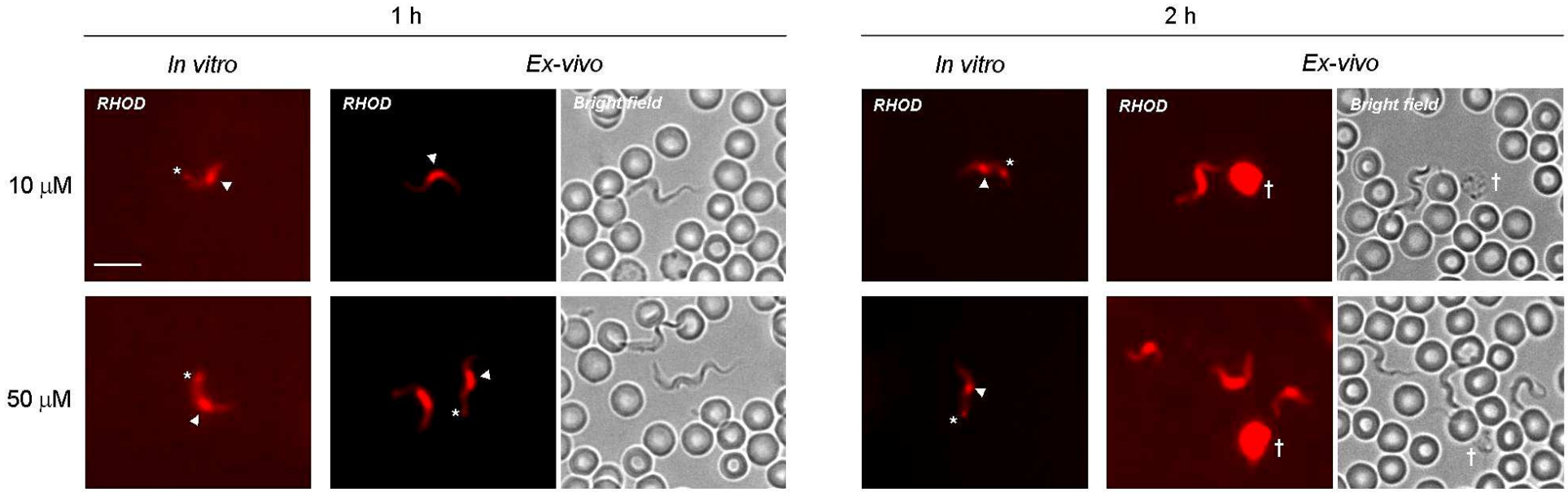

Figure 4.15 – Fluorescence images of *in vitro* and *ex-vivo* trypanosomes stained with propidium iodide.
***In vitro T. b. brucei* w.t. parasites (2×10^7 cells/ml, left panels) and aliquots of rat blood infected with the same cell line (*ex-vivo*, right panels) were incubated with 10 or 50 μM of propidium for 1 or 2 hours at 37℃. Wet films of culture medium and wet thin blood smears containing stained parasites were viewed under the RHOD filter of the Zeiss Axioplan microscope. Bright field images for the *ex-vivo* samples are shown on the right of the corresponding fluorescence micrograph (note that the position of motile trypanosomes can change in the two images).**
RHOD 68 ms exposure; 40× objective. *: kinetoplast; ►: nucleus; †: dead cell. Bar: 10 μM.

The different levels of propidium absorption by *in vitro* and *ex-vivo* trypanosomes could be due to the fact that cells from rodents might be more fragile than those grown in culture, resulting in their being more permeable to the fluorophore. However, *ex-vivo* parasites incubated up to 1 hour with propidium iodide appeared normal and actively motile in the sample. We may also hypothesize a mechanism of transport of this compound into trypanosomes, subject to down-regulation in *in vitro*-grown cells compared to *in vivo*-grown parasites, as occurs with uptake of DB75 by the P2/*Tb*AT1 transporter (Chapter 6). Uptake experiments carried out in our laboratory showed that pentamidine can partially inhibit ehidium bromide internalisation (Chris Ward, personal communication), suggesting a competition for the same surface binding sites. It is possible that propidium, being an analogue of ethidium, is transported by similar permeases into trypanosomes. Co-treatment of *ex-vivo* wild type trypanosomes with propidium (1 μM) and P2-substrates DB75 (10 μM) or adenosine (25 mM), however, did not reveal significant differences in fluorescence development as compared to cells treated with propidium alone (data not shown). This result excluded a primary role of the P2 transporter in the uptake of the phenanthridine. Future fluorescence experiments on mutant strains lacking specific pentamidine transporters could reveal if they are involved in the uptake of propidium iodide and give some indications regarding how it crosses the parasite's membrane.

When viewed at low magnification, the trypanosome's cytosol appeared homogeneously stained by propidium iodide (Figure 4.15). However, when cells were examined at high magnification (100× objective) the cytoplasmic emission showed a punctate distribution (Figure 4.16). These fluorescent granules could correspond to the inclusion bodies already observed in trypanosomes treated with other phenanthridines (Ormerod, 1951; Taylor, 1960). The inclusion bodies were described as cytoplasmic granules mainly composed of ribonulceic acids and proteins, hence a target for propidium iodide, which is a known strong RNA-binding compound.

Since propidium was capable of labelling viable parasites in blood samples, its staining properties were assessed for lower dye concentration and shorter times of incubation. These experiments were carried out in order to identify a protocol more suitable for field diagnostic purposes, for which reagent availability and sample processing time are of fundamental importance. Microscopy showed that in *ex-vivo* samples treated at 37°C, concentrations of the fluorophore as low as 5 μM could stain live trypanosomes in 10-15 minutes, although the emission was not bright (Figure 4.17). Propidum internalisation was dose- and time- dependent: when 0.5 μM of the fluorophore were used, at least 30 minutes

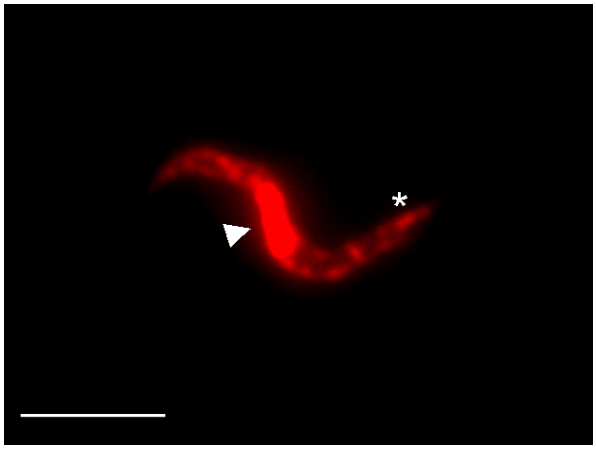

Figure 4.16 – Propidium iodide-stained trypanosome viewed at high magnification. Aliquots of rat blood infected with *T. b. brucei* w.t. parasites were incubated *ex-vivo* with 10 µM propidium iodide for 1 h at 37℃. The wet thin sm ear was viewed under the RHOD filter of the Zeiss Axioplan microscope.
RHOD 68 ms exposure; 100× objective. *: kinetoplast; ►: nucleus. Bar: 10 µM.

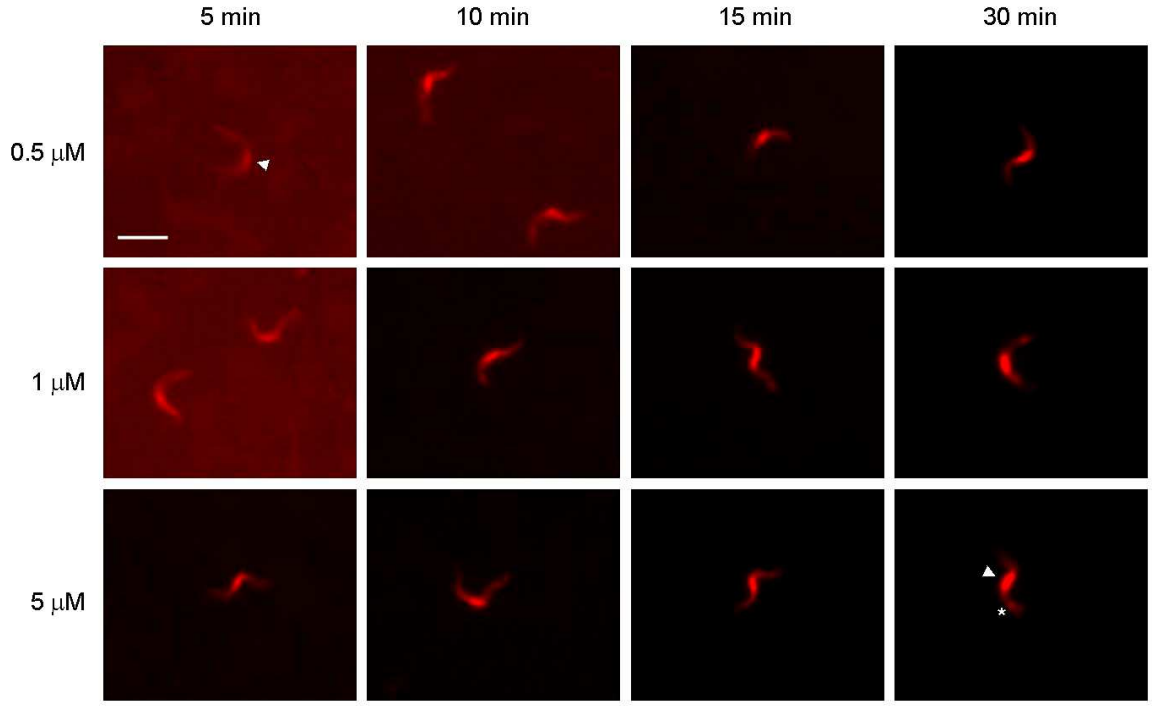

Figure 4.17 – Propidium iodide fluorescence development within *ex-vivo* trypanosomes. Rat blood samples infected with *T. b. brucei* w.t. parasites were incubated with different concentrations of propidium iodide at 37℃. At the indicated time points thin wet smears were prepared and viewed under the RHOD filter of the Zeiss Axioplan microscope.
RHOD 68 ms exposure; 40× objective. *: kinetoplast; ►: nucleus. Bar: 10 µM.

were needed to obtain a discrete staining of trypanosomes, while this time decreased to 15-20 minutes when 1 µM was applied. If incubation was carried out at room temperature, fluorescence development was significantly reduced, possibly due to a lower fluidity of the plasma membrane. During these experiments using wet films, white blood cells labelled by the dye were never observed. This suggested the hypothesis that propidum entered trypanosomes using specific transporters that were not present on leukocytes' surface.

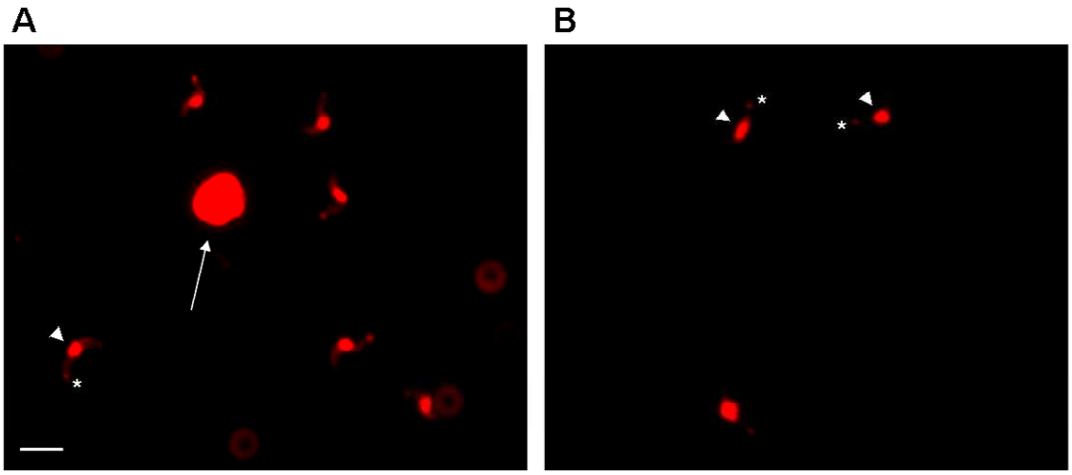

Figure 4.18 – Fixed thin blood smears stained with propidium iodide.
(A) Blood smear air-dried and fixed in methanol before staining with 5 μM of propidium.
(B) Blood smear air-dried and stained with 5 μM of propidium without methanol fixation.
Both specimens were covered with a coverslip and immediately viewed under the RHOD filter of the Zeiss Axioplan microscope. Specimen examination was carried out within few hours from their preparation using murine blood infected with *T. b. brucei* w.t.. Note that the nuclei of trypanosomes on the top right and at the bottom of panel B appear swollen.
RHOD 68 ms exposure; 40× objective. →: white blood cell; *: kinetoplast; ►: nucleus.
Bar: 10 μM.

4.2.4.3 Fluorescence in fixed thin blood smears

Propidium iodide yielded very bright fluorescence in fixed infected thin blood films. In these specimens, where the barrier represented by intact membranes was eliminated, application of 5 μM of the fluorophore gave an immediate red fluorescence inside trypanosomes and nucleated blood cells (Figure 4.18 A). The nucleus and kinetoplast of parasites were brightly labelled as well as other nucleic acids present in the sample. A faster and simpler preparation of the specimens was assessed: air-dried smears were immediately stained with the fluorophore without previous fixation in methanol. In these specimens trypanosomes were brightly fluorescent, but the shape of the cells could appear deformed and damaged, often showing an enlarged nucleus (Figure 4.18 B). When used to stain old, fixed specimens (kept in a box for several weeks) propidium iodide homogeneously stained the whole cell body of parasites (Figure 4.25 A).

4.2.4.4 Compatibility with the LED Cytoscience SMR microscope

Another interesting feature of propidium iodide was its compatibility with the LED Cytoscience SMR fluorescent microscope. Using this instrument, parasites in thin smears and stained with 5 μM of the fluorophore appeared orange-red, easily distinguishable from the red blood cells, green on the background (as already mentioned previously, no images were produced since a suitable camera was not available).

4.2.5 Acridine orange

None of the novel and known fluorescent dyes described above possessed all of the characteristics an ideal probe for trypanosome detection must have (fast labelling, high yield, specificity, photochemical stability, affordability). The widely used fluorophore acridine orange, instead, appeared to have most of these qualities, as confirmed by our experiments.

4.2.5.1 Fluorescence in *in vitro* viable trypanosomes

Acridine orange quickly permeated the parasite's membrane, yielding a bright green fluorescence upon FITC excitation (Figure 4.19). A concentration as low as 1 μM of this compound was sufficient for obtaining a bright signal within 1 minute of incubation. The temperature of treatment did not affect dye penetration inside the cells, indicating passive diffusion (Figure 4.19). Treatment with the fluorophore revealed the nucleus and the kinetoplast of trypanosomes, but it also produced a cytoplasmic diffuse green fluorescence, which greatly facilitated detection of parasites in the specimen. These characteristics made acridine the best fluorescent probe for trypanosomes tested during the project. Nevertheless, its use in the arsenical drug resistance test (Stewart *et al*., 2005) was not possible, since this fluorophore crosses the plasma membrane non-specifically and our experiments showed that its internalisation was completely unaffected by the presence (wild type line) or absence (*tbat1*$^{-/-}$ line) of the P2/*Tb*AT1 transporter on the parasites' surface (Figure 4.19). After only 15 minutes of incubation with the dye (1 μM, 37°C), a few cells from *in vitro* culture started to show some aberrations (i.e. fragmentation of the nucleus, abnormal shape), a probable consequence of the genotoxicity of acridine orange.

In attempt to detect the acidocalcisomes, a known intracellular target of acridine orange, stained parasites were examined at high magnification. Due to the high fluorescent emission of the dye upon FITC filter excitation, however, visualization of these organelles proved difficult and only some of them emerged from the diffuse cytoplasmic green fluorescence (Figure 4.20). A brighter vacuole, situated at the posterior of the cell, and believed to be the lysosome, based on its intracellular position (Shimamura *et al*., 2001), was evidenced using both FITC and RHOD filter set. This vesicular structure, distinguishable from the others by its more intense emission, did not appear in previously published epifluorescence micrographs of *T. evansi* (Mendoza *et al*., 2002) and procyclic trypomastigotes of *T. brucei* (Docampo and Moreno, 1999) treated with acridine orange,

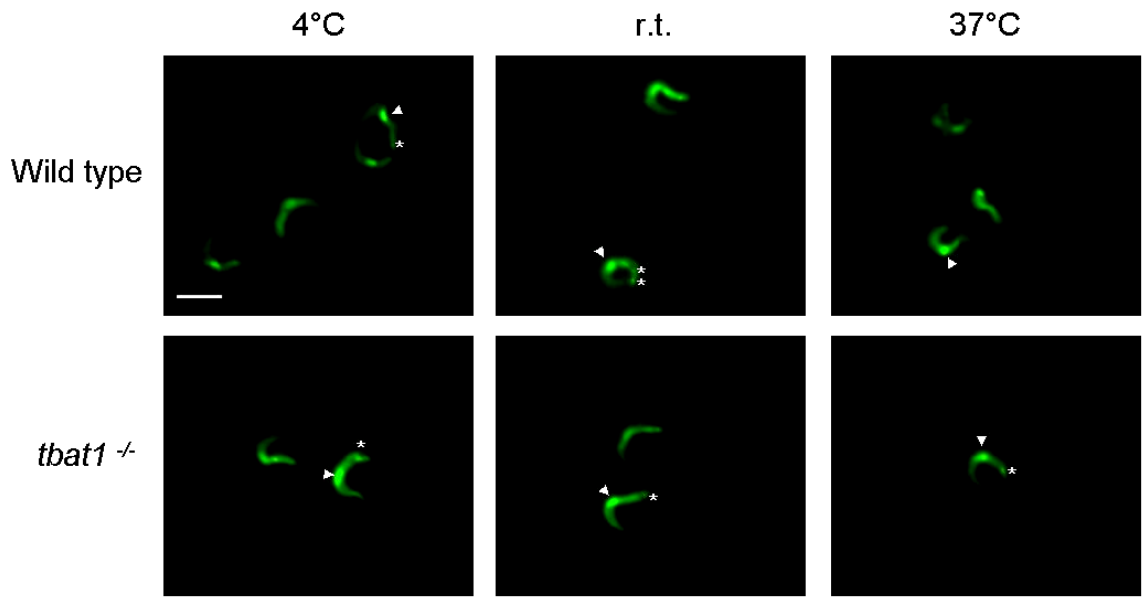

Figure 4.19 – *In vitro* wild type and *tbat1*$^{-/-}$ trypanosomes treated with acridine orange at different temperatures.
Aliquots of *T. b. brucei* w.t. cells from culture were incubated with 1 μM acridine orange at 4℃, room temperature or 37℃ for 1 minute. Wet fil ms were viewed under the FITC filter of the Zeiss Axioplan microscope. Fluorescence intensity of labelled parasites was not affected by different incubation temperatures or by the absence of the P2 amino-purine transporter (*tbat1*$^{-/-}$ line) on the cell surface.
FITC 68 ms exposure; 40× objective. *: kinetoplast; ►: nucleus. Bar: 10 μM.

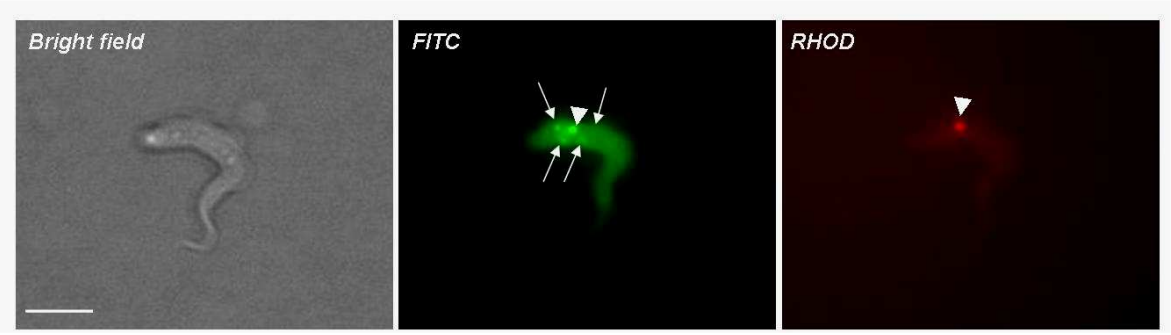

Figure 4.20 – Acridine orange-stained trypanosome viewed at high magnification.
***T. b. brucei* w.t. trypanosomes from culture were incubated with 5 μM acridine orange at 37℃ for 15 minutes and embedded in 1% agarose befo re viewing at ×1,000 total magnification. For fluorescence the FITC and RHOD filters of the Zeiss Axioplan microscope were used.**
FITC 5 ms exposure, RHOD 68 ms exposure; 100× objective. →: acidocalcisomes; ►: lysosome. Bar: 10 μM.

although differences in sample preparation and cell line used do not allow direct comparison with our work.

4.2.5.2 Fluorescence in *ex-vivo* trypanosomes

Acridine orange has already been successfully used to selectively stain parasites, including trypanosomes, among blood cells (Kawamoto, 1991; Bailey and Smith, 1992; Delacollette

and Van der Stuyft, 1994; Adeoye and Nga, 2007). During our fluorescence experiments on infected rat blood, we were able to label viable *T. b. brucei* with a bright green fluorescence, using a very low concentration of the dye (5 μM) (Figure 4.21). Vital staining of parasites was extremely fast (1 minute was sufficient to obtain a bright signal) and red blood cells remained largely unlabelled (although some appeared to fluoresce faintly). Labelling of live trypanosomes in a blood samples could be easily carried out by directly adding few microliters of acridine orange solution directly to the drop of blood before the preparation of the wet film. This procedure, already illustrated for malaria parasites (Metzger and Nkeyi, 1995), had many advantages, being extremely fast (there was no need to air-dry or fix the specimen) and allowing easy discrimination of parasites due to their motility among blood cells.

Direct application of acridine orange (5 μM) to dried, fixed blood smears, was equally effective (Figure 4.22 A). In these specimens trypanosomes were instantaneously stained by the dye. The kinetoplast and the nucleus of parasites appeared very bright, but the entire cell shape of the parasites was also revealed upon FITC excitation. Other nucleated cells in the specimen showed high emission. In an attempt to simplify sample preparation, we also stained a thin air-dried smear with the same dose of acridine orange, eliminating the methanol fixation step (as previously shown for propidium iodide). In this case the trypanosomes' nucleus and kinetoplast also appeared brightly fluorescent, but the cytoplasm remained unstained (Figure 4.22 B). The samples used during these experiments were prepared on the same day as the test. When acridine orange was used to label few weeks old thin blood films, the fluorescence inside trypanosomes appeared more evenly distributed, and no organelles could be distinguished (as already observed for blood smears stained with propidium iodide, Section 4.2.4.3).

4.2.5.3 Compatibility with the LED Cytoscience SMR microscope

The LED Cytoscience SMR microscope was designed to excite green fluorescent compounds such as acridine orange (Jones *et al*., 2007) and the efficacy of the instrument in visualising malaria parasites labelled with this fluorophore has already been proven (Jones *et al*., 2005 and 2007). Similarly, acridine orange-stained *T. b. brucei* could be readily identified under the LED source of the Cytoscience microscope, appearing highly fluorescent over a black background (no images are available).

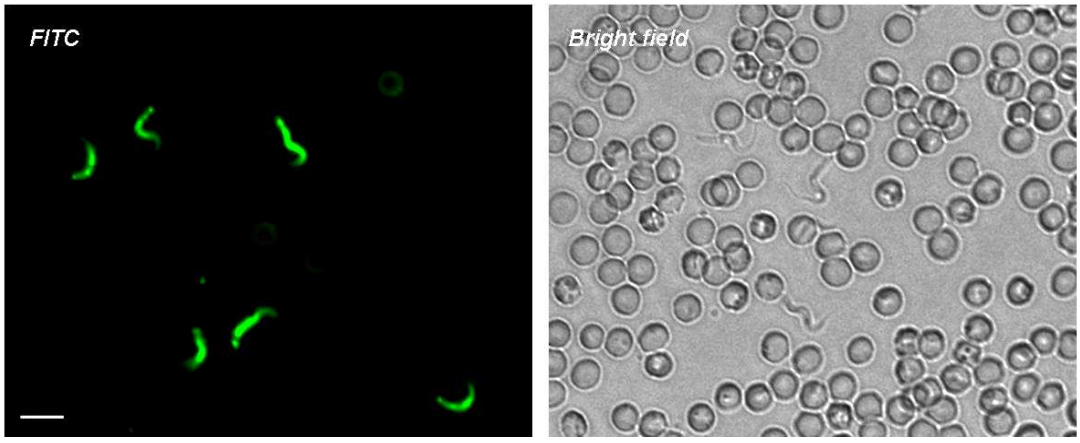

Figure 4.21 – Wet thin blood smear stained with acridine orange.
Murine blood infected with *T. b. brucei* w.t. was incubated with 5 μM acridine orange at r.t. for 1 minute. An aliquot of the sample was then used to prepare the wet smear which was viewed under the FITC filter of the Zeiss Axioplan microscope. Note that the position of motile trypanosomes changed during acquisition of fluorescence and bright field images. FITC 60 ms exposure; 40× objective. Bar: 10 μM.

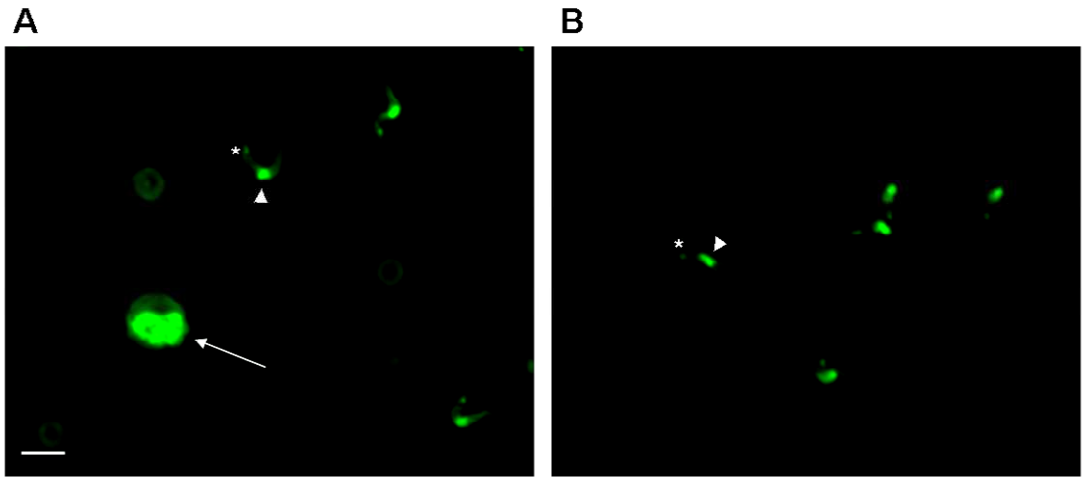

Figure 4.22 – Fixed thin blood smears stained with acridine orange.
(A) Blood smear air-dried and methanol-fixed before staining with 5 μM of acridine orange. (B) Blood smear air-dried and stained with 5 μM of acridine orange without methanol fixation. Both specimens were prepared using murine blood infected with *T. b. brucei* w.t. parasites. After staining, slides were covered with a coverslip and immediately viewed under the FITC filter of the Zeiss Axioplan microscope. Specimens examination was carried out within few hours from their preparation.
FITC 68 ms exposure; 40× objective. →: white blood cell. *: kinetoplast; ►: nucleus. Bar: 10 μM.

4.2.6 Fluorescent staining of thick blood smears

The fluorescent properties of the dyes tested during this project were mainly studied using thin blood films (whether wet or fixed). However, although thin specimens are still used in the field due to their straightforward preparation, their examination suffers a very low sensitivity (Chappuis *et al*., 2005). Preparation of Giemsa-stained thick films is usually preferred for diagnosis, decreasing the detection limit from 10,000 to 5,000 cells/ml (Louis *et al*., 2001; Chappuis *et al*., 2005). Hence, in order to be a useful tool for the diagnosis of

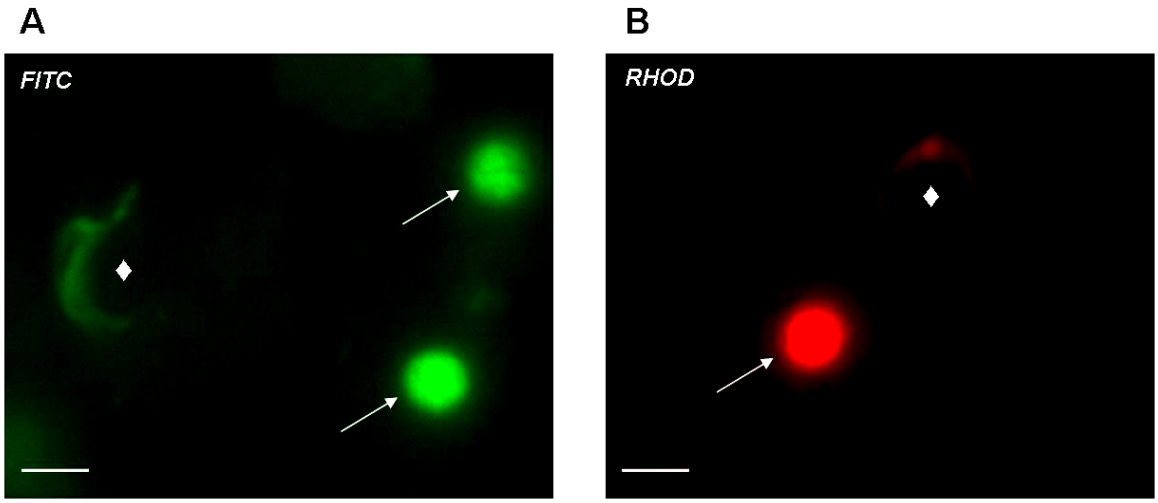

Figure 4.23 – Air-dried thick blood smears stained with acridine orange or propidium iodide. The thick smears infected with *T. b. brucei* were left to air-dry and kept unfixed until staining with 5 μM of acridine orange (A) or propidium iodide (B): 30 μl of either dye solutions were applied to the smear and covered with a coverslip. Acridine orange was excited using the FITC filter of the Zeiss Axioplan microscope, while propidium iodide was excited using the RHOD filter set.
FITC and RHOD 68 ms exposure; 100× objective. →: white blood cell; ♦: trypanosome. Bar: 10 μM.

trypanosomiasis, fluorescence microscopy has to be easily applied to thick blood preparations as well as thin films. Since acridine orange and propidium iodide had proven very efficacious in staining trypanosomes, these two fluorophores were used to assess the feasibility of different staining protocols for fluorescent labelling of infected thick blood films (see Section 2.5.3 for preparation of these specimens).

The first protocol evaluated involved direct staining of air-dried thick smears. To prepare the samples, a drop of either dye (30 μl of a 5 μM solution) was put onto a dry, unfixed thick film, and covered with a coverslip. This resulted in a partial solubilisation and haemolysis of the sample, which was unevenly spread on the microscope slide surface. Fluorescence from these samples was relatively unfocused, with a high background probably being due to the unbound dye (Figure 4.23). White blood cells showed bright fluorescence, while trypanosomes had only low emission. If the fluorophores were applied to the thick smear and allowed to air-dry without applying a coverslip, examination of the specimen revealed the presence of crystals, high background and no specific fluorescence.

A different protocol included a dehaemoglobinisation step to eliminate the red blood cells from the film before staining, as is performed for the preparation of malaria specimens for fluorescence microscopy (Sodeman, 1970; Caramello *et al*., 1993). Air-dried thick smears were soaked in distilled water for 5 minutes, left to dry and then fixed in cold methanol for 2 minutes. After evaporation of the fixative, samples were stained, as previously described,

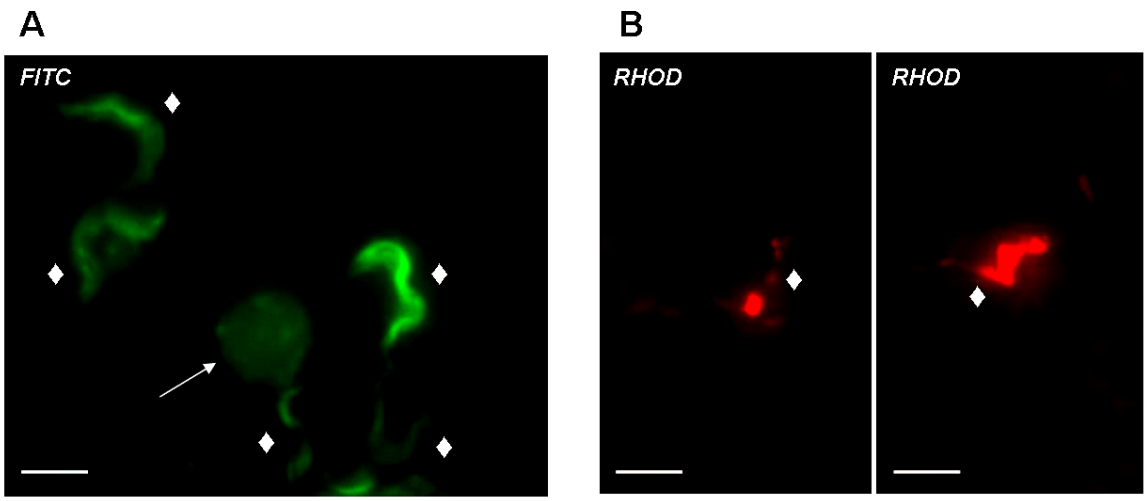

Figure 4.24 – Thick blood smears stained with acridine orange or propidium iodide before air-drying.
To prepare the specimens, a drop of *T. b. brucei*-infected blood (20 µl) at high parasitaemia was put on a slide and mixed with a drop of dye (20 µM). After spreading, the thick smears were left to air-dry and, then, viewed under the 100× objective of the Zeiss Axioplan microscope without addition of any coverslip. Samples stained with acridine orange (A) were excited under the FITC filer set, while those stained with propidium iodide (B) were excited using the RHOD filer set. Note that the blood samples used for staining with either fluorophore had the same high parasitaemia (1×10^6 cells/ml), but propidium iodide could stain only few, probably damaged, trypanosomes in the specimens.
FITC 68 ms exposure; RHOD 30 ms exposure; 100× objective. →: white blood cell; ♦: trypanosome. Bar: 10 µM.

with 30 µl of 5 µM acridine orange or propidium iodide and a coverslip was applied. Despite the additional processing steps, however, these samples did not show any improvement compared to those directly stained without the treatment in distilled water and methanol (data not shown).

The thickness of this kind of blood preparation evidently did not allow the solution of the fluorophore to distribute evenly among the layers of dried blood cells and, therefore, reach all parasites at a sufficient concentration for brilliant staining. It might be possible to obtain better specimens by exposing them to the fluorophore solution for longer times, but this would cause a further delay for the diagnostic result. An easier and faster method could be the direct addition of the dye solution to the drop of blood just after its collection and before the preparation of the thick film. To verify the efficacy of this procedure, solutions of acridine orange or propidium iodide (20 µM) were mixed with the drop of blood on the microscope slide before spreading the sample in a circle with the corner of another slide and leave it to air-dry at room temperature. Using this method, samples stained with the cell-permeable acridine orange resulted in a better quality than those stained after the thick film had already been dried (Figure 4.24 A): trypanosomes showed a higher fluorescence, while the white blood cell nuclei emission was less bright. The general background was

also lower and the image more focused. Propidum iodide, however, did not stain trypanosomes or other nucleated cells in these specimens, leading to a general red background. It is probable that the time needed for the smear to dry (several minutes) was not sufficient for this dye to permeate the cells and only trypanosomes with damaged membranes internalised the fluorophore becoming highly fluorescent (Figure 4.24 B).

Of all the protocols used, direct application of acridine orange to the drop of blood before preparation of the thick film appeared to be the best technique, both for its straightforward procedure and the quality of the fluorescence. To allow even higher levels of trypanosome staining, it could also be possible to collect the blood in a small tube, in which incubation with the fluorophore could proceed for longer times, followed by preparation of the thick smear (this was the protocol most used to stain infected blood samples during this project, see Section 2.5.3.2).

When considering the use of fluorescently stained thick blood smears for diagnosis, another important aspect to consider is the necessity of having a microscope equipped with a high magnification, oil-immersion objective to examine the samples. Even though fluorescent parasites could also be detected in the thick specimen using the 40× objective, in the field high magnification objectives (100×) are used in order to identify, with confidence, trypanosomes in thick smears, where they usually appear deformed. The current LED Cytoscience microscope, however, has only a single, fixed 40× objective fitted, not suited to view thick smears. Future prototypes will have to take into account this issue and include higher magnification objectives in their design.

4.2.7 Double stain with Giemsa and fluorophores

The introduction of LED fluorescence microscopes in health care facilities of HAT endemic countries would be intended not only as a substitute to traditional parasitological techniques, but also as a complementary tool. The combination of both light and fluorescence microscopy could offer a simple way of improving accuracy of parasitological examination, by offering the possibility to re-check dubious specimens for diagnostic confirmation. This would be particularly useful for fixed samples, whether thin or thick Giemsa-stained blood films. For this reason, it would be ideal that each specimen could be easily examined using both techniques. Therefore, the possibility of double staining Giemsa-treated thin blood samples with acridine orange or propidium iodide, a procedure shown to be feasible for some fluorescent dyes (Guy *et al*., 2007), was assessed.

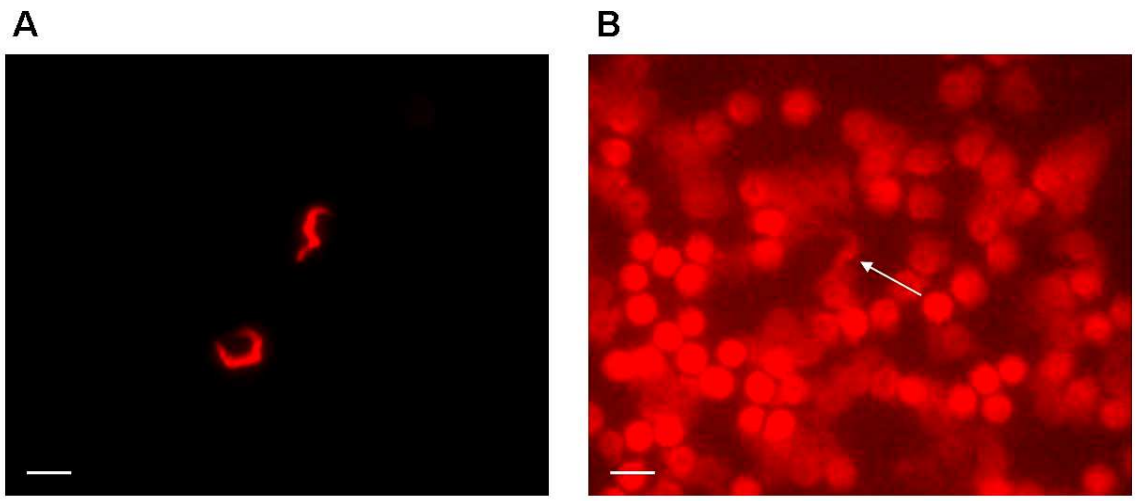

Figure 4.25 – Thin blood smears stained with propidum iodide alone or double-stained with Giemsa and the fluorophore.
(A) Blood smear labelled with 50 µl of 5 µM propidium iodide.
(B) Giemsa-stained blood smear (5% Giemsa solution) subsequently stained with 5 µM of propidium iodide. Murine blood infected with *T. b. brucei* w.t. (1×10^6 cells/ml) was used to prepare the thin films, which were left to air-dry and kept in a slide box for several weeks before staining. Both specimens were viewed under the same experimental conditions, using the RHOD filter of the Zeiss Axioplan microscope.
RHOD 68 ms exposure; 40× objective. The arrow in panel B indicates a trypanosome. Bar: 10 µM.

Thin infected blood smears, stained with a 5% Giemsa solution (Section 2.5.3.3), were subsequently treated with 5 µM of either fluorophore and viewed under the fluorescence microscope. In these specimens, however, neither trypanosomes nor white blood cells acquired fluorescence (Figure 4.25 B for the specimen stained with propidium), a result probably due to the fact that the binding sites targeted by the fluorophores (i.e. nucleic acids) were already occupied by the Giemsa stain.

An alternative protocol could involve sequential staining of the same specimen, by introducing a destaining step of the Giemsa solution before the addition of the fluorophore. To destain Giemsa-labeled specimens we soaked thin films in a solution of 90% ethanol and 1.5% HCl for 30 minutes (Suzuki *et al*., 1991). The samples were, then, stained with 5 µM of acridine orange or propidium iodide and immediately examined under fluorescence microscopy. The destaining procedure proved capable of eliminating enough Giemsa dye in order to allow both fluorophores to label parasites, but the emission was not as brilliant as in samples directly stained for florescence microscopy. Moreover, the background was relatively high and this hampered quick detection of parasites.

Simultaneous labelling of the same specimen with a fluorophore and the histological Giemsa stain would offer the advantage of complementing bright field and fluorescence microscopy. However, the incompatibility of the dyes used usually hampers this approach,

as observed for association of propidium iodide and acridine orange with Giemsa. In the future, it will be important to verify other combinations of staining agents or, eventually, to define a straightforward and efficient destaining protocol, in order to improve the overall diagnostic performance and accuracy of microscopy.

4.3 Discussion

4.3.1 New fluorophores for the arsenical drug resistance test

The arsenical drug resistance test was developed as a quick, simple assay to identify trypanosome strains resistant to diamidines and arsenical drugs (Stewart *et al*., 2005). As for other diagnostic techniques, its introduction in poor-income endemic countries is mainly hampered by the need for expensive, sophisticated fluorescence microscopes, but the use of cheaper LED-driven instruments could make this technique more easily affordable. We showed the feasibility of performing the test in association with a prototypical UV LED-illuminated microscope (Chapter 3), although the detailed conditions of the test still need optimisation.

The original assay developed by Stewart and collaborators used UV fluorescent diamidines as substrates (Stewart *et al*., 2005). However, UV LED light sources for fluorescence microscopy are not yet widely available as compared to LEDs for excitation of green-emitting fluorophores. The LED Cytoscience SMR microscope, for example, works in this spectral region (λ_{EX}=472 nm, λ_{EM}>500 nm). We were, therefore, interested in identifying new compounds to use as substrates for the test but with longer excitation wavelengths than those of the originally used UV fluorescent compounds. The series of five green fluorescent pentamidine analogues synthesised in Prof. D. W. Boykin's laboratory appeared to be interesting for this purpose, since they carried the P2/*Tb*AT1 recognition motif and had longer excitation wavelengths than that of their parental compound DB75 (Table 4.1). The Alamar blue data confirmed a dependence on this transporter for uptake into trypanosomes (Table 4.4). DB1680 appeared to rely less on this mechanism of uptake, but we failed to prove a possible involvement of an endocytic mechanism of internalisation. Passive diffusion through the membrane could represent another route of entry for DB1680: the polar nature given by the dicationic structure of the DB compounds is thought to hamper the interaction with the lipid layer, but the presence of multiple aromatic rings in the molecule linker could increase its lipophilicity and allow a faster diffusion. Although the other four compounds of the series lost some trypanocidal activity in the absence of an active P2 transporter, we were not able to identify clear differences in fluorescence development in treated trypanosome strains expressing, or not expressing, the P2 amino-purine transporter (Figure 4.11). The main problem with these diamidines, however, was their low fluorescence, which did not allow detection of green signal within

short incubation times (within 15 minutes). The low emission was probably caused by the intrinsic low yields of the compounds, but also by the use of an inappropriate detection system, since the standard FITC filter only partially matched the spectral region in which the green diamidines fluoresced. Due to their excitation maxima being too short, the five dyes were also incompatible with the LED Cytoscience SMR microscope. The use of another LED source with a shorter excitation wavelength (~420 nm) fitted into this instrument, however, could allow the detection of the diamidines' green fluorescence.

The five green fluorescent molecules were capable of specifically staining trypanosomes in blood samples (Figure 4.9), a characteristic that could make them possible fluorescent markers for trypanosomes, if appropriate filter sets and LED sources could lead to higher yields from the compounds.

4.3.2 Intracellular distribution of the five pentamidine analogues

The study of the fluorescent properties of the pentamidine analogues revealed interesting staining features which raised new questions about their intracellular targets and mechanism of trypanotoxicity. As with other diamidines (Mathis *et al*., 2007) these compounds were good DNA binders: melting temperatures measured for DB1464, DB1680 and DB1692 bound to a poly(dA)·poly(dT) oligomer were 9.4, 15.0 and 17.0 °C respectively (these data were kindly provided by Prof. D. W. Boykin). However, during our experiments none of the five compounds apparently labelled the nucleus of trypanosomes, while all of them brightly stained the kinetoplast DNA (kDNA). This result was unexpected, since nuclear DNA, which is surrounded by a porous membrane, should be more accessible to fluorophores than the kinetoplast, which is enclosed inside the mitochondrial membrane. It is probable that most diamidines reach the kDNA before other intracellular targets because the mitochondrial membrane potential acts as a potent driving force (de Koning, 2008). However, during our experiments, visible fluorescence inside the nucleus did not develop even after long incubation times (up to 8 h) (Figure 4.4). A possible explanation for the lack of signal development from inside the nucleus is that the pentamidine analogues did enter the organelle to reach the chromosomal DNA, but an unknown phenomenon caused quenching of their emission. Another possibility could be a shift in fluorescence of the compounds bound to nuclear DNA that could not be detected using our standard filter sets. Further investigations will be needed to understand these results.

Another interesting feature concerning the staining pattern of the green fluorescent compounds was their accumulation in a series of cytoplasmic corpuscles, as already observed for other diamidines (Mathis *et al*., 2006). As previously discussed with regard to DB75 fluorescent pattern (Chapter 3), the identity of these corpuscles is still unclear and needs to be investigated in more details, especially to understand if they localise within the mitochondrion or correspond to cytoplasmic vesicles. The causes of the red fluorescence shift observed under the RHOD filter (Figure 4.8) are also unknown: it could be caused by peculiar environmental conditions inside organelles or by binding to cytoplasmic macromolecules. Mathis and colleagues were of the opinion that it was acidocalcisomes that accumulated diamidines, an identification based on the similarity to the fluorescent pattern of acridine orange in trypanosomes and its abolition following pre-treatment with compounds which inhibit acidification of intracellular organelles (Mathis *et al*., 2006 and 2007). Some observations made during our experiments with the green fluorescent diamidines were consistent with this theory, although a definitive identification could not be made. The posterior fluorescent spots observed after DB1680 treatment (Figure 4.8), and initially believed to be endosomes, for example, overlapped the area occupied by the acidocalcisomes labelled, during another experiment, with acridine orange (Figure 4.20). The identification of these cytoplasmic vesicles, stained by the fluorophores, as acidocalcisomes would offer an explanation for the fluorescence bathochromic shift (i.e. red emission) observed for all the compounds of the series: these organelles have an acidic pH and contain phosphates, both of which can interact with the compounds and influence their fluorescence spectra. Similarly, the brighter fluorescent spot labelled by DB1692 and visible under the RHOD filter after 1 hour of incubation (Figure 4.8) could be identified with the lysosome, another acidic organelle located at the posterior of the cell. The corpuscles observed following *T. b. brucei* treatment with the green fluorescent diamidines, using the FITC channel, generally appeared more similar to those visualised during our experiments with DB75 (Section 3.2.7) than to the acidocalcisomes evidenced by Mathis and collaborators (Mathis *et al*., 2006 and 2007). Unlike the myriad of vesicles that became visible in 2 or 4 hours incubation (depending on the diamidine used) described by these authors, the green fluorescent pentamidine analogues we tested were observed in only a limited number of corpuscles, which were stained within 1 hour of incubation. The use of different fluorophores and experimental conditions (in particular, different filter sets) could explain the discrepancies between our results and those published by Mathis and collaborators, but future studies will be necessary to clarify the intracellular distribution of these compounds.

4.3.3 Phenanthridines and acridine orange as fluorescent probes for trypanosomes

By being both fluorescent in the range of the available LED Cytoscience SMR microscope and trypanocidal (which may imply specific internalisation into parasites), phenanthridines appeared to be promising compounds for our project. Fluorescence of isometamidium inside trypanosomes, however, was found to be too low to be considered of any utility for fluorescence diagnostics (Figure 4.13). Moreover, this phenanthridine preferentially accumulated inside the kinetoplast and did not allow determination of parasites shape in the sample. The staining properties of ethidium bromide and its analogue propidium iodide proved more interesting. Both compounds could stain viable trypanosomes in blood samples, revealing the whole cells shape (Figures 4.12 and 4.15). Propidium iodide, in particular, produced a brilliant and stable emission once bound to trypanosomes' nucleic acids. This compound is supposed to be a membrane-impermeant molecule, which is generally considered unable to enter intact cells (Foglieni *et al*., 2001). However, propidium was clearly able to permeate trypanosomes in blood samples at a relatively fast rate, which depended on the concentration of the compound and on the temperature of incubation (Figure 4.17). Internalisation of this phenanthridine appeared to be enhanced when cells were treated at 37°C rather than at room temperature, indicating a probable transport-mediated uptake. This hypothesis was supported by indications, obtained in our laboratory, of transporter involvement in the internalisation of the propidium structural analogue ethidium bromide (Chris Ward, personal communication). Future studies on this subject could reveal how these trypanocidal drugs enter the parasites. In fixed specimens, where the integrity of the membranes was lost, the staining properties of propidium iodide and ethidium bromide were excellent (Figures 4.14 and 4.18), although staining of other nucleated cells in the specimens was evident.

Acridine orange, an analogue of phenanthridine, was the fluorophore with the best characteristics among those tested. As propidium iodide, it was able to stain trypanosomes instantaneously in fixed blood samples at very low concentrations (Figure 4.22). This fluorophore could also enter viable parasites quickly, probably due to its lipophilic nature (Figure 4.21). Acridine orange has the advantage of being less expensive than propidium iodide (~£80 for 1 g for acridine, ~£90 for 100 mg for propidium from Molecular Probes, Invitrogen) and very low concentrations are needed for microscopy. Since phenanthridines are intercalating agents and, therefore, potential mutagens and carcinogens, the fact that very low concentrations can be used not only reduces the costs, but also the risks

associated with the handling of the fluorophore. The fluorescent properties of acridine orange have already been exploited for the diagnosis of HAT in the quantitative buffy coat test (Bailey and Smith, 1992), which is very sensitive but also too expensive and sophisticated to be widely applied in poor rural settings. The use of this fluorophore to label trypanosomes in microscopy specimens is relatively straightforward and definitively faster than the currently used Giemsa stain. We showed how the dye could be directly applied to dry but also wet thin blood smear, further decreasing the time needed for specimen preparation (since there was no need to dry or fix the sample). This also facilitated the identification of labelled trypanosomes by their fast movement among blood cells. Acridine orange stained live parasites in medium with a bright, stable fluorescence (Figure 4.19), and we would expect it to stain parasites in human fluids other than blood, such as lymph node aspirate or cerebrospinal fluid, equally well. The simple addition of a drop of dye to a wet film prepared with these human samples could enable a faster detection of trypanosomes, normally identified only by their active wriggling in unstained samples (Chappuis *et al*., 2005). However, the application of aspecific, membrane-permeant fluorophores, such as acridine orange, might be problematic for CSF samples, where the high white blood cell count, usually associated with HAT infection, could interefere with parasite visualisation. Moreover, other co-infecting microorganisms present in the sample (in particular blood) may be stained aswell, thus complicating diagnosis. These aspects will need to be verified by future experiments. Direct application of acridine orange during the preparation of thick smears (Section 4.2.6) proved to be a fast and simple procedure to label trypanosomes in these specimens. Since the entire parasite cell was stained, trypanosomes could be identified even if their shape was slightly deformed in these preparations.

Due to its ideal fluorescent characteristics, acridine orange has been independently chosen by FIND (Foundation for Innovative New Diagnostics) to develop new fluorescence-based diagnostics for trypanosomiasis (http://www.finddiagnostics.org/).

4.3.4 Practical considerations on the use of the LED Cytoscience SMR microscope

The LED Cytoscience SMR microscope (Figure 1.8) excited acridine orange and propidium iodide yielding bright fluorescence. The instrument proved easy to use and could be positioned in a dim dark room. However, when utilising the instrument we noticed some defects, which will need to be considered when developing new prototypes

for field use. First, the presence of a single eyepiece could result in eye fatigue after hours of microscopy, as already pointed out (Hänscheid, 2008). A fake, blind eyepiece positioned in the place of the one missing could easily solve this issue, by allowing the microscopist to keep the unused eye open during slide observation. A second problem was represented by the fact that the stage could not be moved. This obliged the microscopist to manually move the slide horizontally, with consequent loss of time and difficulties in homogeneously screening the specimen. The introduction of a cross-table to clamp slides and move them on the stage would make the microscope more practical, with only a minor loss in compactness. A third aspect to be mentioned was the presence on the instrument of a single, low magnification, 40× objective. This was ideal to quickly screen thin film, but not to view thick smears, for which a high magnification 100× objective is commonly used. In the field, thick specimens are usually preferred to thin ones because of their higher sensitivity (Chappuis *et al*., 2005). Fitting an appropriate, high magnification objective (100× or 60×) in microscopes designed for the field will, therefore, have to be considered in future prototypes.

5

Synthesis of UV fluorescent amino acid derivatives

5.1 Introduction

One aspect of this research project involved the direct synthesis of potential fluorescent probes for African trypanosomes. In designing the new molecules, it was decided to couple fluorescent moieties to a parasite surface transporter's substrate, in order to ensure fast and specific internalisation into parasites. This strategy had already been attempted by previous work by Azema and collaborators (Azema *et al*., 2004), who designed fluorescent substrates of the glucose transporter family by linking a dansyl chloride group (which is fluorescent) to hexoses. These fluorophores, however, seemed to enter into trypanosomes without interacting with the transporters, probably due to their lipophilic nature, which allowed them to diffuse through the plasma membrane.

Nutrient uptake routes represent useful pathways to carry toxins and other compounds into parasites. Internalisation of the fluorescent diamidines described in Chapters 3 and 4 was assured by the activity of other classes of trypanosome transporters, including the amino-purine transporter P2/*Tb*AT1, and the high and low affinity pentamidine transporters (HAPT and LAPT). To deliver fluorescent groups into trypanosomes, we chose to exploit a different class of parasite carriers: the amino acid transporters. Trypanosomatids possess a large family of specific and generic amino acids transporters (Barrett and Gilbert, 2006; Jackson, 2007), since these parasites are auxotrophic for the essential amino acids of humans (Berriman *et al*., 2005). The high affinity of these carriers could assure the concentration of the designed substrates against their concentration gradient. Moreover, addition of hydrophobic aromatic substituents, typical of fluorogenic groups, to polar amino acids was expected to lead to products still hydrophilic enough to preclude passive diffusion through the membrane, as happened for the hexose analogues mentioned above (Azema *et al*., 2004). Obviously, amino acid transporters, as glucose transporters, are not exclusive to trypanosomes. However, differences in affinity and rate of activity between parasite and human carriers might ensure specific internalisation into parasites (a phenomenon difficult to predict in advance), as observed for the sugar derivatives designed by Azema and colleagues (Azema *et al*., 2004).

To generate fluorescent amino acid conjugates, different aromatic substituents were linked to the side-chain of various amino acids. Fluorophores included UV fluorescent groups such as dansyl chloride (λ_{EX}=337 nm, λ_{EM}=492 nm) and 2-(bromomethyl)naphthalene (λ_{EX}=274 nm, λ_{EM}=334 nm). Among them, dansyl chloride was considered of particular interest. This compound [5-(dimethylamino)naphthalene-1-sulfonyl chloride], is a

naphthalene-based, lipophilic fluorophore, nonfluorescent until it reacts with amines. It is generally used for amino acid and protein covalent labelling (Chersi *et al*., 1997; Gonçalves, 2009), but sugars too are often fluorescently tagged with this organic probe (Hermetter *et al*., 2001; Azema *et al*., 2004).

The work was carried out under the supervision of Dr. A. Sutherland in the Chemistry Department of the University of Glasgow. Purity and characterisation of the compounds generated were verified by IR, ^{1}H NMR/^{13}C NMR spectroscopy and mass spectrometry analyses. Optical activity was also determined. Full chemical characterisation and detailed synthetic procedures are presented in Section 5.2.4, while general experimental details are in Section 2.8. The biological and fluorescent properties of the amino acid derivatives obtained were, successively, assessed on *in vitro*, wild type trypanosomes.

5.2 Results

5.2.1 Synthesis of a dichlorobenzyl tyrosine derivative

The first compound synthesised was a tyrosine analogue (Tyr(Cl_2-Bzl)-OH, named FG10) (Figure 5.1). This compound was chosen for the presence in its molecular structure of two aromatic rings (one from the lateral chain of the amino acid, the other from a condensed dichlorobenzyl alcohol moiety), and, therefore, likely to have fluorescent properties. Another reason for this choice was the possibility of obtaining the product from a commercially available starting material ([Boc-*O*-(2,6-dichlorobenzyl)-L-tyrosine], or Boc-Tyr(Cl_2-Bzl)-OH, from Sigma-Aldrich) through a single, standard reaction. This offered an opportunity to gain some initial experience in the chemistry laboratory.

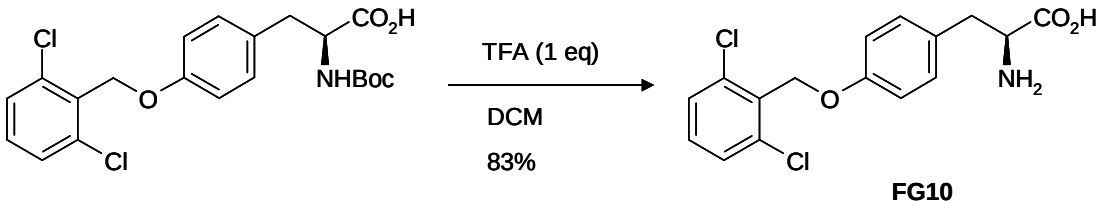

Figure 5.1 – Synthesis of Tyr(Cl_2-Bzl)-OH (FG10) from Boc-Tyr(Cl_2-Bzl)-OH. The single reaction involved the deprotection of the amino group of the commercially available tyrosine analogue.

The tyrosine derivative FG10 was produced with good yield (83%) by removing the protective *t*-Boc residue from the amino group of tyrosine, following a standard procedure.

5.2.2 Synthesis of a 2-methylnaphthalene serine derivative

A second compound was obtained by linking a 2-methylnaphthalene substituent (the fluorophore) to the side-chain of the amino acid L-serine, following a two step procedure (Figure 5.2). Alkylation of 2-(bromomethyl)naphthalene to the hydroxyl group of *N*-Boc-serine (Sigma-Aldrich) gave the desired intermediate product (FG60, 46% yield). A previous attempt to perform this reaction using the methyl ester of serine as starting material, instead, did not give the expected product. In this case, the addition of the aromatic electrophile 2-(bromomethyl)naphthalene generated a mixture of two unknown compounds, one of which contained a methyl ester. This mixture was treated with 6 M HCl under reflux conditions in an effort to hydrolyse the ester. However, this proved unsuccessful, completely decomposing the molecules.

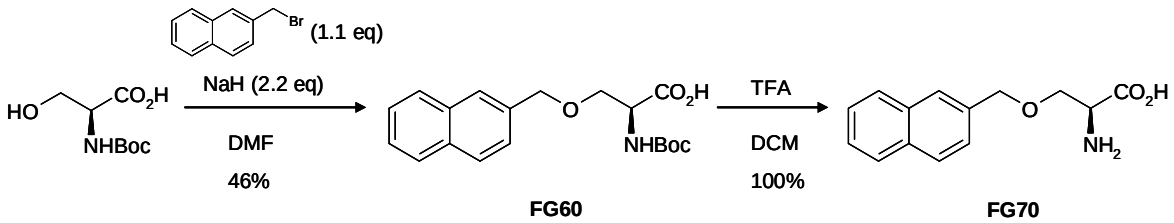

Figure 5.2 – Synthesis of the 2-methylnaphthalene serine derivative FG70. Synthesis involved alkylation of an analogue of the amino acid serine (amino group protected by a *t*-Boc residue) with 2-(bromomethyl)naphthalene, to give the intermediate compound FG60, and subsequent deprotection of the amino group of the amino acid to generate the final product.

The second reaction of the synthetic pathway involved treatment with TFA to release the protecting *t*-Boc group from the amino group of serine, generating the final product (FG70) with 100% yield.

5.2.3 Synthesis of a dansyl chloride lysine derivative

The synthesis of a dansyl chloride derivative was then attempted. This molecule was considered quite promising since the addition of a dansyl substituent to primary amino groups is known to give a stable blue or blue-green fluorescence to the product. A first attempt to obtain a serine derivative through condensation of dansyl chloride with the side-chain of this amino acid failed, probably due to an intramolecular rearrangement that led to the unprotected carboxyl group of serine to attack the S-O bond, resulting in the elimination of the adduct (data not shown).

We then decided to change starting material, using the amino acid lysine, and to protect its carboxyl group at the outset. The long side-chain of this amino acid represented a steric barrier to possible intramolecular rearrangement and its nitrogen was expected to form a stronger chemical bond with the sulfur of the dansyl chloride than the oxygen of serine. Following this approach we were able to obtain the final product (FG400) in five steps (Figure 5.3). Each reaction was carried out at first on a small scale and, if it proved successful, a larger scale reaction was set up. A modified lysine (Boc-Lys(Cbz)-OH, Sigma-Aldrich), with the amino group protected by a *t*-Boc residue and the lateral chain blocked by a carbobenzyloxy (Cbz) group, was used as starting material. Synthesis started by blocking the free carboxylic acid of lysine by addition of an ethyl group, following a standard procedure (the compound obtained was named FG90). Successively, the side-chain of the amino acid was deprotected using a hydrogenation reaction, to expose the amino group for the subsequent condensation with the fluorophore. Conditions applied for this reaction were the same as those published by Bergeron and collaborators (Bergeron *et.*

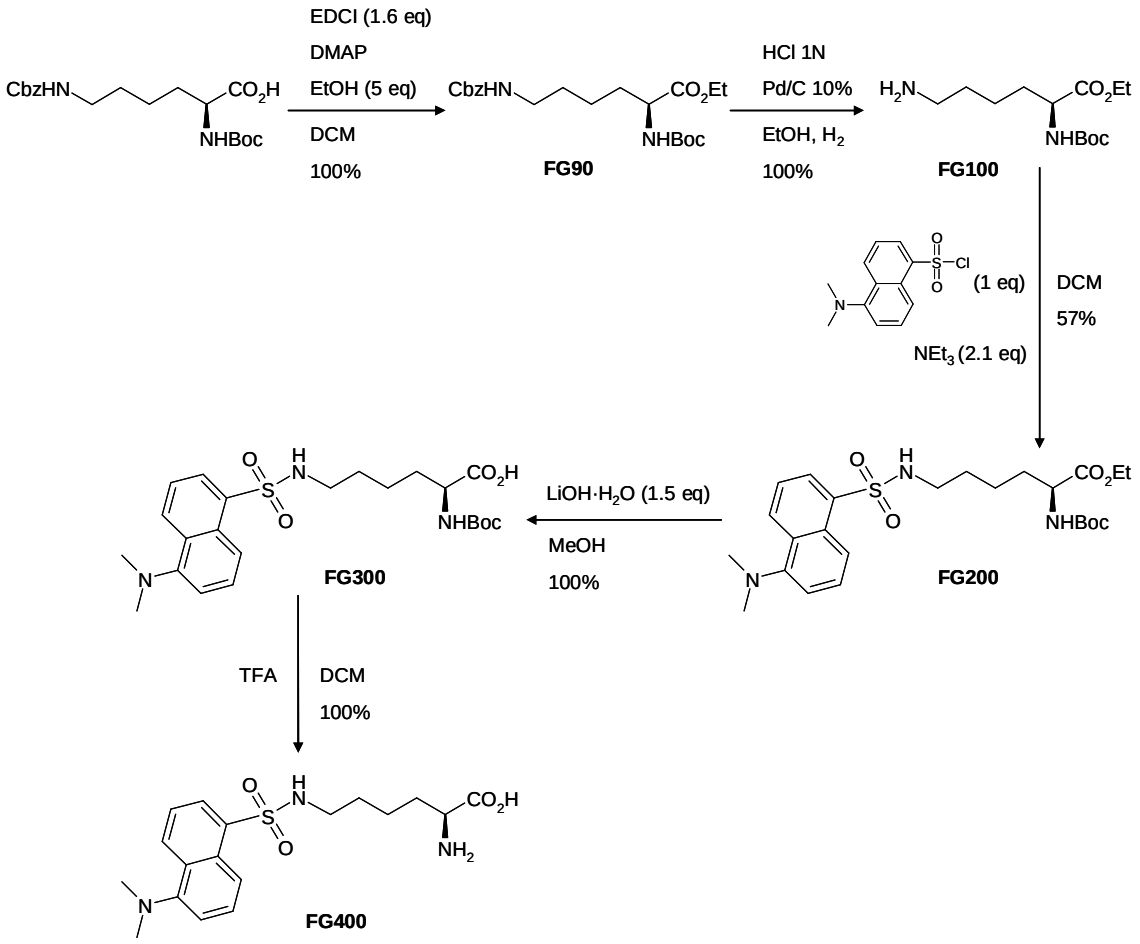

Figure 5.3 – Synthesis of the dansyl chloride lysine derivative FG400.
The carboxyl group of the starting material (a lysine molecule with both amino groups blocked) was initially protected by an ethyl residue to generate FG90. The amine of the side-chain of lysine was, then, exposed (in the compound FG100) for the subsequent fusion with the dansyl chloride group (the joined product was named FG200). Both the carboxyl and amino group of the amino acid were, successively, deprotected to give the final product FG400.

al., 1997). The product (FG100) was obtained using an acid environment and Pd/C as catalyst and it was purified by filtration through Celite® as a $Cl^-NH_3^+$ salt. Interestingly, the use of the acid reagent (HCl 1 N) helped the removal of the Cbz-protecting group without taking the *t*-Boc group off. The next step was the condensation of the lysine derivative with dansyl chloride. For this reaction, a procedure published by Ceroni and collaborators was followed with some modifications (Ceroni *et al*., 2002). Two equivalents of NEt_3 were needed to first eliminate the $Cl^-NH_3^+$ salt and then to act as a reagent. The product FG200 was obtained with a 57% yield after purification by flash silica gel chromatography. Standard procedures were followed in the last two reactions to deprotect the amino and carboxylic groups of lysine, to generate the final product FG400. ^{1}H NMR spectroscopy (Figure 5.4), mass spectrometry (Figure 5.5) and IR spectra (Figure 5.6) of the dansyl chloride derivative are shown below.

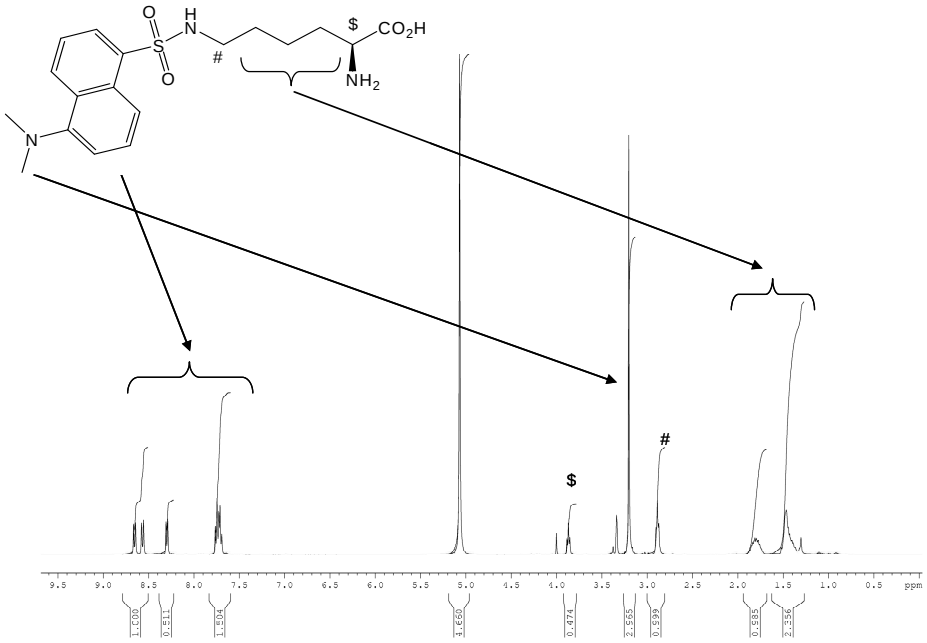

Figure 5.4 – 400 MHz ^{1}H-NMR spectrum of the dansyl chloride lysine derivative FG400 (sample dissolved in CD_3OD).
Peaks generated by the different hydrogens of the molecule are indicated by arrows and symbols.

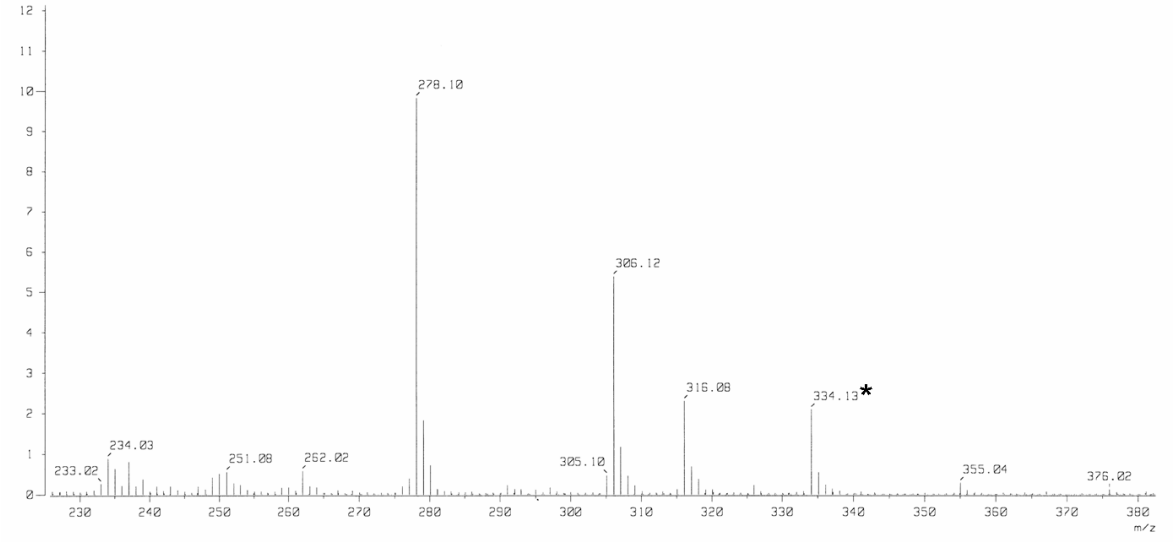

Figure 5.5 – Electron impact positive (EI^{+}) mass spectrum of FG400.
The peak identifying the compound is indicated by an asterisk. The mass shown in the spectrum (MW 334.1) corresponds to the mass of the molecule (MW 379.5) after elimination of its carboxylic group (occurred during the application of this mass spectrometry technique).

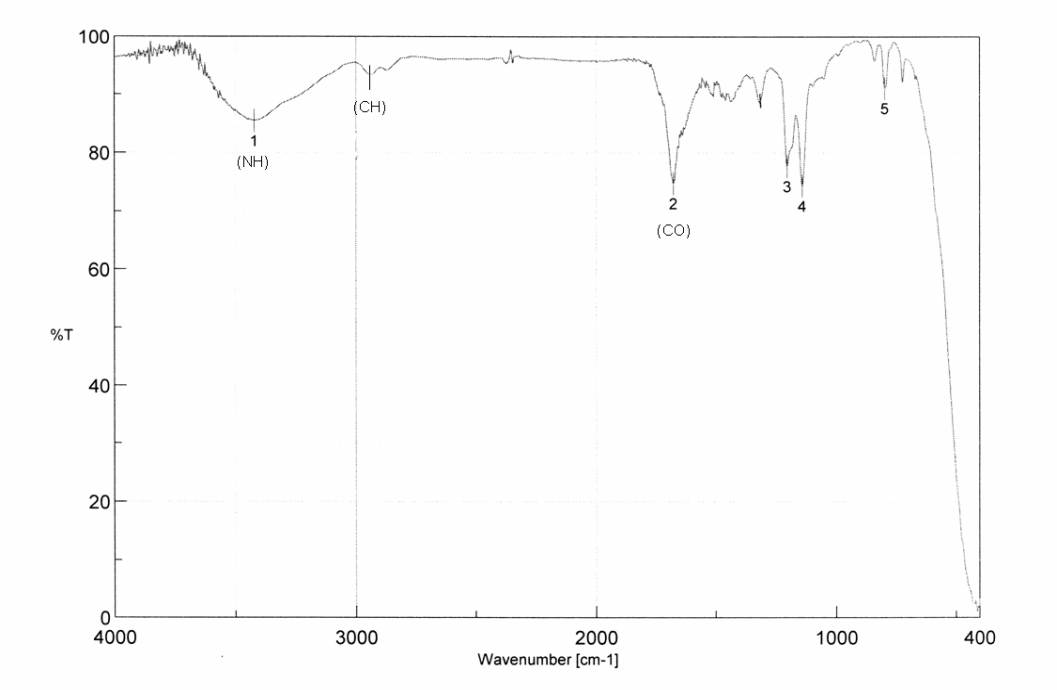

Figure 5.6 – IR spectrum of FG400.
The main functional groups are indicated underneath the corresponding absorption peaks.

5.2.4 Experimental details

(2*S*)-2-Amino-3-[4-(2,6-dichlorobenzyloxy)phenyl]propionic acid (FG10)

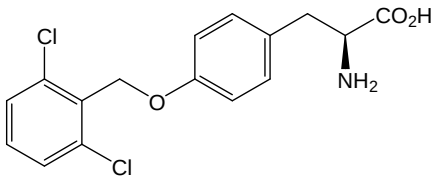

Trifluoroacetic acid (3 ml) was added to a solution of Boc-Tyr(Cl_2-Bzl)-OH (1.00 g, 2.27 mmol) in DCM (10 ml). The solution was left stirring overnight at room temperature and then the solvent was evaporated *in vacuo*. Starting material, TFA salt and impurities were eliminated by extraction with EtOAc and H_2O (4 × 50 ml) and the combined aqueous phases were finally dried to give the product (FG10) as a white powder (0.64 g, 83%). mp: 204-206°C (lit. 200-203°C; Yamashiro and Li, 1973); $[\alpha]_D^{23}$ –18.2 (*c* 1.0, MeOH); ν_{max}(KBr)/cm^{-1}: 3442 (NH), 2990 (CH), 1665 (CO), 1521, 1243, 1023; δ_H (400 MHz, CD_3OD): 3.01 (1H, dd, *J* 14.6, 8.5 Hz, 3-*H*H), 3.26-3.28 (1H, m, 3-H*H*), 3.86 (1H, dd, *J* 8.5, 4.5 Hz, 2-H), 5.28 (2H, s, CH_2O), 7.03 (2H, d, *J* 8.8 Hz, 2 × Ar-H), 7.26 (2H, d, *J* 8.8 Hz, 2 × Ar-H), 7.34-7.38 (1H, m, 1 × Ar-H), 7.44-7.46 (2H, m, 2 × Ar-H); δ_C (100 MHz, CD_3OD): 37.3 (CH_2), 57.1 (CH), 66.2 (CH_2), 116.3 (CH), 129.3 (ArC), 129.8 (2 × ArCH), 131.7 (2 × ArCH), 132.1 (2 × ArCH), 133.6 (ArC), 138.1 (2 × ArC), 159.8 (ArC), 173.2

(CO); LRMS (FAB^+): 340.2 ($[MH]^+$, 99%), 294.2 (24), 265.1 (17), 176.8 (15), 159.9 (60); HRMS calcd for $C_{16}H_{16}{}^{35}Cl_2NO_3$ 340.0507, found 340.0510.

(*2S*)-2-(*tert*-Butoxycarbonylamino)-3-(naphthalen-2-ylmethoxy)propionic acid (FG60)

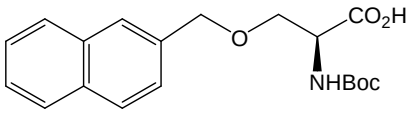

A solution of *N*-(*tert*-butoxycarbonyl)-L-serine (0.50 g, 2.44 mmol) in DMF (10 ml) was prepared at 4°C under argon conditions. After slow addition of 60% NaH powder (0.23 g, 5.37 mmol), the solution was left stirring for 0.5 h and then 2-(bromomethyl)naphthalene (0.59 g, 2.68 mmol) was added. The mixture was left stirring for another hour at 4°C and, finally, overnight at room temperature. The addition of a saturated aqueous solution of NaCl (30 ml) gave a precipitate that was filtered and the filtrate was extracted with diethyl ether (3 × 25 ml). HCl was added to the aqueous layer until pH 2 was reached and the solution was immediately extracted with EtOAc (3 × 25 ml). The collected organic phases were dried over $MgSO_4$ and the solvent was evaporated *in vacuo*. The obtained residue was purified by flash column chromatography on silica gel, using a gradient of petroleum ether/ethyl acetate as eluent to give the product as a brown oil (0.39 g, 46%). $[\alpha]_D{}^{25}$ +20.7 (*c* 1.0, $CHCl_3$); ν_{max}(neat)/cm^{-1}: 3439 (NH), 2979 (CH), 1685 (CO), 1508, 1163, 818, 754; δ_H (400 MHz, $CDCl_3$): 1.37 (9H, s, 3 × CH_3), 3.67 (1H, dd, *J* 9.2, 3.2 Hz, 3-*H*H), 3.90 (1H, dd, *J* 9.2, 3.2 Hz, 3-H*H*), 4.42-4.44 (1H, m, 2-H), 4.61 (2H, s, CH_2O), 5.37 (1H, d, *J* 8.4 Hz, NH), 7.32-7.34 (1H, m, Ar-H), 7.37-7.42 (2H, m, 2 × Ar-H), 7.65 (1H, br s, Ar-H), 7.73-7.74 (3H, m, 3 × Ar-H); δ_C (100 MHz, $CDCl_3$): 28.3 (3 × CH_3), 53.8 (CH), 69.7 (CH_2), 73.6 (CH_2), 80.4 (C), 125.6 (ArCH), 126.1 (ArCH), 126.2 (ArCH), 126.7 (ArCH), 127.7 (ArCH), 127.9 (ArCH), 128.4 (ArCH), 133.1 (ArC), 133.2 (ArC), 134.7 (ArC), 155.8 (C), 175.2 (C); LRMS (CI^+): 346.3 ($[MH]^+$, 5%), 290.2 (56), 272.2 (10), 141.2 (99), 132.1 (10); HRMS calcd for $C_{19}H_{24}NO_5$ 346.1654, found 346.1658.

(2*S*)-2-Amino-3-(naphthalen-2-ylmethoxy)propionic acid (FG70)

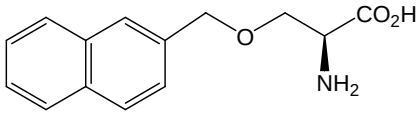

To a solution of FG60 (0.35 g, 1.02 mmol) in DCM (10 ml), the reagent trifluoroacetic acid (4 ml) was added and the solution was left stirring overnight at room temperature. Evaporation of the solvent gave the TFA salt product as an oil (0.32 g, 100%). ν_{max}(neat)/cm^{-1}: 3420 (NH), 2925 (CH), 1675 (CO), 1509, 1203, 817; δ_H (400 MHz, DMSO-d6): 3.76-3.91 (2H, m, 3-H_2), 3.96-3.97 (1H, m, 2-H), 4.61-4.76 (2H, m, CH_2O), 7.42-7.59 (4H, m, Ar-H), 7.82-8.02 (3H, m, Ar-H); δ_C (100 MHz, DMSO-d6): 54.2 (CH), 59.4 (CH_2), 72.5 (CH_2), 25.4 (ArCH), 125.8 (ArCH), 126.0 (ArCH), 126.2 (ArCH), 127.6 (ArCH), 127.7 (ArCH), 127.9 (ArCH), 133.5 (ArC), 134.5 (ArC), 140.0 (ArC), 169.5 (CO); LRMS (FAB^+): 246.2 ($[MH]^+$, 9%), 142.2 (54), 102.7 (20), 81.0 (100), 59.4 (35); HRMS calcd for $C_{14}H_{16}NO_3$ 246.1130, found 246.1114.

Ethyl (2*S*)-6-(Benzyloxycarbonylamino)-2-(*tert*-butoxycarbonylamino)hexanoate (FG90)

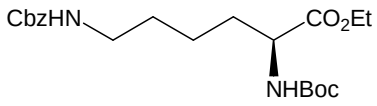

A stirred solution of Boc-Lys(Cbz)-OH (0.50 g, 1.32 mmol) in dry DCM (15 ml) was prepared under argon atmosphere. The reagent EDCI (0.40 g, 2.11 mmol), the catalyst DMAP (0.10 g) and dry ethanol (0.40 ml, 6.60 mmol) were sequentially added to the solution, which was allowed to stir at room temperature for 48 h. The mixture was, then, extracted with H_2O (2 × 30 ml) and the collected organic phases were dried over $MgSO_4$ and, finally, concentrated *in vacuo* to give FG90 as an oil (0.54 g, 100%). $[\alpha]_D^{25}$ +2.0 (*c* 1.0, $CHCl_3$); ν_{max}(neat)/cm^{-1}: 3339 (NH), 2936 (CH), 1712 (CO), 1525, 1251, 1167, 1026; δ_H (400 MHz, $CDCl_3$): 1.29 (3H, t, *J* 7.2 Hz, C*H*$_3$-CH_2), 1.38-1.45 (11H, m, 3 × CH_3, 4-H_2), 1.50-1.57 (2H, m, 3-H_2), 1.60-1.69 (1H, m, 5-*H*H), 1.79-1.81 (1H, m, 5-H*H*), 3.17-3.22 (2H, q, *J* 6.8 Hz, 6-H_2), 4.17-4.22 (2H, m, OC*H*$_2$-CH_3), 4.24-4.29 (1H, m, 2-H), 5.03 (½H, br m, NH), 5.10 (2H, s, CH_2), 5.18-5.20 (½H, m, NH), 6.49-6.50 (½H, m, NH), 7.31-7.37 (5H, m, Ar-H), 8.22-8.24 (½H, m, NH); δ_C (100 MHz, $CDCl_3$): 14.2 (CH_3), 22.4 (CH_2), 28.3 (3 × CH_3), 29.4 (CH_2), 32.4 (CH_2), 40.6 (CH_2), 53.3 (CH), 61.3 (CH_2), 66.6 (CH_2), 79.8 (C), 128.1 (ArCH), 128.2 (3 × ArCH), 128.5 (ArCH), 136.6 (C), 155.6 (C), 156.5 (C) 172.8 (C); LRMS (CI^+): 409.5 ($[MH]^+$, 12%), 353.5 (37), 309.5 (73), 245.3 (55), 123.2 (98); HRMS calcd for $C_{21}H_{33}N_2O_6$ 409.2339, found 409.2340.

Ethyl (2*S*)-6-Amino-2-(*tert*-butoxycarbonylamino)hexanoate (FG100)

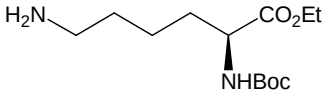

1 N HCl (1.30 ml) was added to a stirred solution of FG90 (0.51 g, 1.25 mmol) in EtOH (20 ml). After addition of 0.05 g of Pd/C 10%, H_2 at atmospheric pressure was introduced and the mixture was left stirring for 3 h before further catalyst (0.02 g) was added. The solution was stirred at room temperature under H_2 atmosphere overnight. The black suspension was then filtered through Celite® and washed with EtOH (3 × 25 ml). The filtrate was, finally, dried *in vacuo* to give FG100 as an oil (0.38 g, 100%). $[\alpha]_D^{24}$ +2.3 (*c* 1.0, $CHCl_3$); ν_{max}(neat)/cm^{-1}: 3413 (NH), 2979 (CH), 1701 (CO), 1523, 1369, 1166, 1025; δ_H (400 MHz, $CDCl_3$): 1.21 (3H, t, *J* 7.0 Hz, C*H*$_3$-CH_2); 1.37 (10H, br s, 9 × CH_3, 1 × 4-*H*H), 1.51-1.74 (5H, m, 3-H_2, 4-H*H*, 5-H_2), 2.87-2.96 (2H, m, 6-H_2), 4.09-4.19 (3H, m, OC*H*$_2$-CH_3, 2-H), 5.22 (½H, br d, *J* 7.2 Hz, NH), 6.52 (½H, d, *J* 7.2 Hz, NH), 7.52 (2H, br s, NH_2); δ_C (100 MHz, $CDCl_3$): 14.2 (CH_3), 22.6 (CH_2), 27.6 (CH_2), 28.4 (3 × CH_3), 32.1 (CH_2), 39.8 (CH_2), 53.4 (CH), 61.4 (CH_2), 79.8 (C), 155.6 (C), 172.7 (C); LRMS (CI^+): 275.3 ($[MH]^+$, 100%), 219.2 (77), 175.2 (33), 156.2 (12), 123.2 (23); HRMS calcd for $C_{13}H_{27}N_2O_4$ 275.1971, found 275.1974.

Ethyl (2*S*)-2-(*tert*-Butoxycarbonylamino)-6-(5-dimethylaminonaphthalene-1-sulfonylamino)hexanoate (FG200)

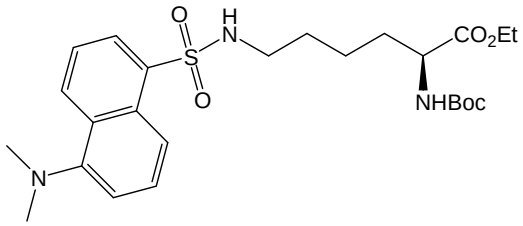

NEt_3 (0.40 ml, 2.84 mmol) was added to a stirred solution of FG100 (0.37 g, 1.35 mmol) in DCM anhydrous (10 ml) under argon atmosphere. Dansyl chloride (0.36 g, 1.35 mmol), previously suspended in dry DCM (10 ml), was added dropwise to the solution, which was left stirring overnight at room temperature. After removal of the solvent under reduced pressure, the yellow-brown residue was resuspended in DCM and washed with H_2O (30 ml), saturated aqueous Na_2CO_3 solution (30 ml) and again with H_2O (3 × 30 ml). The organic layer was, then, dried over Na_2SO_4 and concentrated *in vacuo*. The yellow-brown oil was resuspended in a small amount of DCM, purified by silica gel column

chromatography using a gradient of DCM : MeOH (from 100% : 0% to 95% : 5%) and finally dried *in vacuo* to give the product as a yellow oil (0.39 g, 57%). $[\alpha]_D^{25}$ +9.6 (*c* 1.0, $CHCl_3$); ν_{max}(neat)/cm^{-1}: 3362 (NH), 2939 (CH), 1710 (CO), 1458, 1367, 1321, 1145, 1092, 791; δ_H (400 MHz, $CDCl_3$): 1.17-1.24 (5H, m, 4-H_2, CH_3-CH_2), 1.28-1.45 (12H, m, 3-H_2, 3 × CH_3), 1.50-1.59 (1H, m, 5-H_2), 2.81 (8H, br s, 6-H_2, 2 × N-CH_3), 4.06-4.11 (3H, m, OCH_2-CH_3, 2-H), 5.17 (1H, d, *J* 8.4 Hz, N*H*Boc), 5.73 (1H, br t, *J* 5.8 Hz, SO_2-NH), 7.11 (1H, d, *J* 7.4 Hz, Ar-H), 7.43-7.49 (2H, m, 2 × Ar-H), 8.18 (1H, d, *J* 7.4 Hz, Ar-H), 8.31 (1H, d, *J* 8.8 Hz, Ar-H), 8.47 (1H, d, *J* 8.8 Hz, Ar-H); δ_C (100 MHz, $CDCl_3$): 14.2 (CH_3), 22.2 (CH_2), 28.4 (3 × CH_3), 29.0 (CH_2), 32.3 (CH_2), 43.0 (CH_2), 45.5 (2 × CH_3), 53.1 (CH), 61.4 (CH_2), 80.0 (C), 115.2 (ArCH), 118.7 (ArCH), 123.2 (ArCH), 128.4 (ArCH), 129.6 (ArC), 129.7 (ArCH), 129.9 (ArC), 130.5 (ArCH), 134.6 (ArC), 152.1 (ArC), 155.5 (C), 172.7 (C); LRMS (FAB^+): 530.2 ($[MNa]^+$, 100%), 507.2 (100), 452.2 (53), 408.2 (39), 317.2 (13), 170.8 (99), 59.4 (38); HRMS calcd for $C_{25}H_{37}N_3O_6NaS$ 530.2301, found 530.2317.

(2*S*)-2-(*tert*-Butoxycarbonylamino)-6-(5-dimethylaminonaphthalene-1-sulfonylamino)hexanoic acid (FG300)

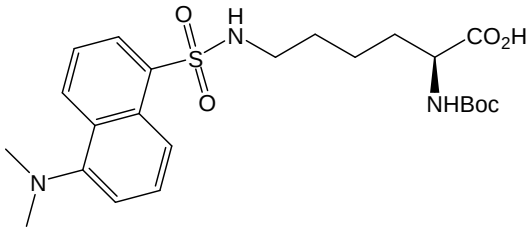

FG200 (0.20 g, 0.39 mmol) was dissolved in MeOH (10 ml) and the solution was cooled to 4ºC. LiOH·H_2O (0.03 g, 0.59 mmol) dissolved in H_2O (5 ml) was added dropwise to the mixture and the reaction was, then, warmed to room temperature and allowed to stir overnight. The reaction mixture was dried under reduced pressure and the resulting residue was resuspended in H_2O. After acidification to pH 2 by addition of 2 M HCl, the mixture was extracted with EtOAc (3 × 25 ml) and the organic layer was dried over $MgSO_4$ and concentrated *in vacuo* to give FG300 as a yellow viscous oil (0.20 g, 100%). $[\alpha]_D^{25}$ +4.7 (*c* 1.0, $CHCl_3$); ν_{max}(neat)/cm^{-1}: 3370 (NH), 2937 (CH), 1695 (CO), 1509, 1316, 1161, 1062; δ_H (400 MHz, $CDCl_3$): 1.18-1.34 (13H, m, 3-H_2, 4-H_2, 3 × CH_3), 1.40-1.58 (2H, m, 5-CH_2), 2.80 (8H, br s, 6-H_2, 2 × N-CH_3), 4.11-4.12 (1H, m, 2-H), 5.17-5.19 (1H, br d, *J* 6 Hz, NHBoc), 5.39 (1H, br s, SO_2-NH), 7.10 (1H, d, *J* 7.2 Hz, Ar-H), 7.40-7.46 (2H, m, 2 × Ar-H), 8.13-8.14 (1H, m, Ar-H), 8.22-8.24 (1H, m, Ar-H), 8.43 (1H, d, *J* 8.8 Hz, Ar-H); δ_C

(100 MHz, $CDCl_3$): 22.2 (CH_2), 28.4 (3 × CH_3), 28.9 (CH_2), 31.8 (CH_2), 42.8 (CH_2), 45.5 (2 × CH_3), 53.1 (CH), 80.2 (C), 115.4 (ArCH), 119.2 (ArCH), 123.4 (ArCH), 128.4 (ArCH), 129.5 (ArCH), 129.6 (ArC), 129.7 (ArC), 130.2 (ArCH), 134.8 (ArC), 151.5 (ArC), 155.8 (C), 176.5 (C); LRMS (FAB^+): 502.2 ($[MNa]^+$, 49%), 479.2 (39), 424.2 (35), 170.9 (100), 168.9 (37), 86.0 (17); HRMS calcd for $C_{23}H_{33}N_3O_6NaS$ 502.1988, found 502.1973.

(S)-2-Amino-6-(5-dimethylamino-naphthalene-1-sulfonylamino)-hexanoic acid (FG400)

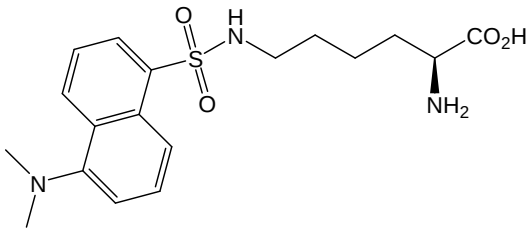

FG300 (0.08 g, 0.16 mmol) was dissolved in DCM (10 ml) at room temperature. After addition of TFA (1 ml) the solution was allowed to stir overnight. The reaction mixture was then concentrated *in vacuo* to give FG400 as a yellow viscous oil (0.08 g, 100%). $[\alpha]_D^{26}$ +6.8 (*c* 1.0, MeOH); ν_{max}(neat)/cm^{-1}: 3422 (NH), 2940 (CH), 1677 (CO), 1202, 1141, 796; δ_H (400 MHz, CD_3OD): 1.39-1.52 (4H, m, 3-H_2, 4-H_2), 1.76-1.89 (2H, m, 5-H_2), 2.89 (2H, t, *J* 5.8, 6-H_2), 3.20 (6H, s, 2 × N-CH_3), 3.87 (1H, br t, *J* 6.4 Hz, 2-H), 7.69-7.76 (3H, m, Ar-H), 8.30 (1H, d, *J* 7.2 Hz, Ar-H), 8.57 (1H, d, *J* 8.4 Hz, Ar-H), 8.65 (1H, d, *J* 8.4 Hz, Ar-H); δ_C (100 MHz, CD_3OD): 23.0 (CH_2), 30.3 (CH_2), 31.0 (CH_2), 43.4 (CH_2), 46.5 (2 × CH_3), 53.8 (CH), 117.9 (ArCH), 123.2 (ArCH), 125.6 (ArCH), 129.0 (ArCH), 129.7 (ArCH), 129.9 (C), 130.5 (ArCH), 130.9 (C), 137.6 (C), 149.0 (C), 171.8 (CO); LRMS (EI^+): 334.1 ($[M\text{-}COOH]^+$, 2%), 306.1 (6), 278.1 (10), 171.1 (64), 154.0 (9), 95.0 (12), 69 (100), 45 (68); HRMS calcd for $C_{17}H_{24}N_3O_2S$ 334.1589, found 334.1583.

5.2.5 Biological evaluation

5.2.5.1 Fluorescence spectra

Once the synthesis was completed, the biological properties of the three amino acid derivatives were evaluated. The fluorescence excitation and emission spectra of the compounds were measured using solutions of the molecules in distilled water (Section 2.6). Pre-scan of FG10 and FG70 (0.5 to 10 μM) revealed that both molecules absorbed

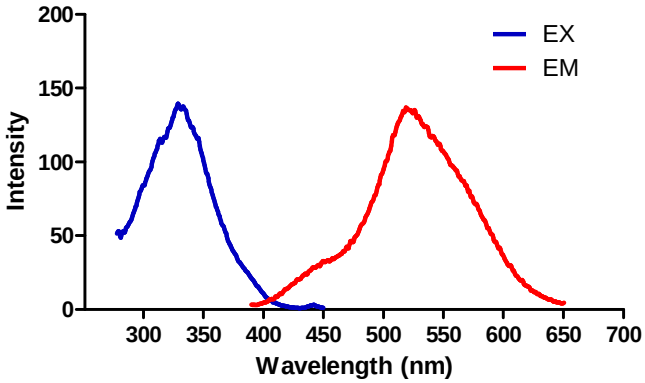

Figure 5.7 – Fluorescence spectra of FG400.
The spectra were measured using a 10 µM solution of the compound in dH_2O.
EX; excitation spectrum; EM: emission spectrum.

UV radiation, but no relevant emission peaks could be identified in the visible region of the spectrum, thus preventing more accurate spectra measurements (data not shown). For the lysine derivative FG400, instead, we could measure an excitation wavelength maximum of 333 nm and emission of 520 nm (Figure 5.7). Another absorption peak in the UV region, with maximum at 247 nm was identified. Fluorescence intensity in aqueous solution was weak (see, for comparison, the spectra of DB75 shown in Figure 4.6). Both the large Stokes shift (i.e. distance between excitation and emission maxima) and the low yield found for our dansyl chloride conjugate were in agreement with the data reported for this class of fluorophores (the Molecular Probes Handbook, available online at the website http://probes.invitrogen.com/handbook/, indicates for dansyl sulfonamides an absorptivity as weak as ε ~4,000 $cm^{-1}M^{-1}$ at 330-340 nm and a low quantum yield).

5.2.5.2 Trypanotoxicity

The Alamar Blue assay (Section 2.4) was performed to obtain some indication concerning interaction of the synthesised molecules with trypanosomes: trypanotoxicity could be expressed after entry of the compounds into the cell, a requirement for their use as fluorescent probes. The results, however, did not give any information on this subject, showing that none of the amino acid derivatives had any trypanocidal activity up to 100 µM (Figure 5.8). Treatment with the three compounds did not appear to alter the normal cell motility and morphology.

5.2.5.3 Fluorescence microscopy

To directly visualise the ability of the amino acid derivatives to stain live cells, treated *in vitro* wild type trypanosomes were viewed under the standard filter sets of the Zeiss

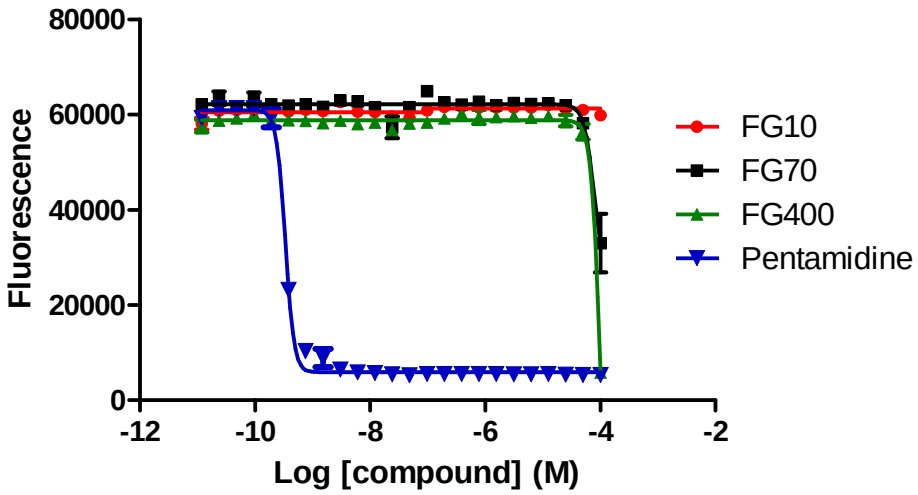

Figure 5.8 – Sensitivity of *T. b. brucei* w.t. S427 to the three amino acid derivatives. The data shown are from a representative Alamar Blue experiment. Pentamidine was used as positive control. For each curve, the lowest concentration data point is the "no drug" negative control. Error bars represent the standard deviation of the two replicates. Fluorescence is in arbitrary units.

Axioplan fluorescence microscope. Parasites incubated for up to 2 hours with 100 μM FG10 and FG70 did not show any fluorescence emission when excited using DAPI or FITC channels. This confirmed the findings obtained with the spectra measurements, which showed no emission in the visible region for these conjugates.

The dansyl chloride lysine derivative FG400, instead, appeared to accumulate into trypanosomes and labelled the cells after only 15 minutes of incubation, when given at 100 μM (Figure 5.9). A blue, faint emission could be detected using the DAPI filter set: the entire cell was stained and some more intense spots were visible in its posterior region. A slightly better signal was obtained with the FITC channel. The use of this filter to excite the fluorophore allowed evidence of the entire shape of the parasites, including the flagellum, and various bright corpuscles spread throughout the whole cell body. The use of 50 μM FG400 gave similar results, but a further decrease to 10 μM proved insufficient for trypanosome labelling. Dye emission (especially upon DAPI excitation) seemed to diminish at long incubation times (from 1 hour). The cause of this phenomenon is still unknown; it is possible that the activity of intracellular enzymes determined the release of the nonfluorescent dansyl residue from the amino acid. As already mentioned, FG400 had a large Stokes shift (λ_{EX}=333 nm, λ_{EM}=520 nm), which did not match any of the standard filter sets fitted on the Zeiss microscope (DAPI: λ_{EX}=365 nm, λ_{EM}=445 nm; FITC: λ_{EX}=470 nm, λ_{EM}=519 nm). This factor could have contributed to the low emission observed during qualitative fluorescence microscopy, along with the intrinsic low yield of the dansyl conjugate. Following incubation of trypanosomes in blood samples (100 μM for

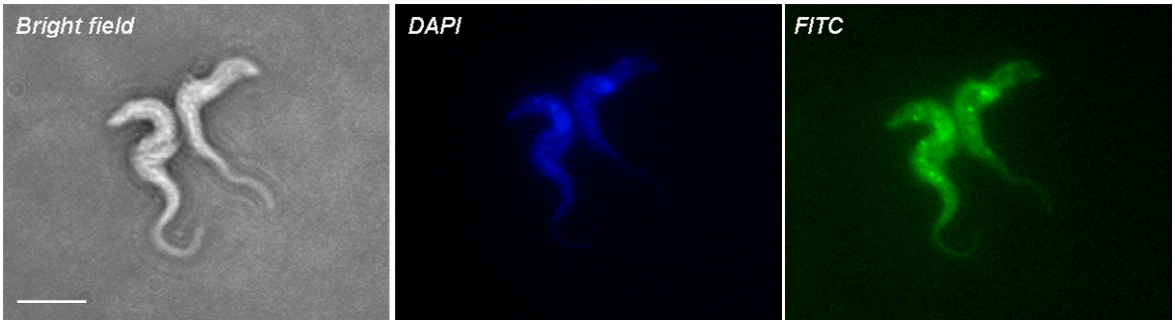

Figure 5.9 – Fluorescence imges of trypanosomes stained with FG400.
Aliquots of *T. b. brucei* w.t parasites from culture were incubated with 100 μM FG400 at 37℃ for 15 minutes. Trypanosomes were, then, immobilised in 1% agarose and viewed under DAPI and FITC filters of the Zeiss Axioplan microscope.
DAPI 33 ms exposure, FITC 60 ms exposure; 100× objective. Bar: 10 μM.

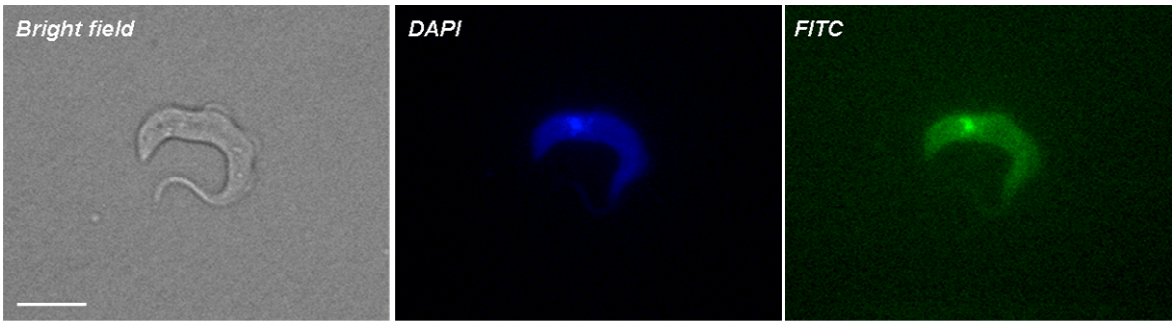

Figure 5.10 – Fluorescence images of trypanosomes stained with DB1919.
The compound DB1919 was kindly provided by Prof. D. W. Boykin (Georgia State University, Atlanta). Aliquots of *T. b. brucei* w.t parasites from culture were incubated with 10 μM of the compound at 37℃ for 1 hour. Trypanosomes were, the n, immobilised in 1% agarose and viewed under DAPI and FITC filter of the Zeiss Axioplan microscope.
DAPI 33 ms exposure, FITC 60 ms exposure; 100× objective. Bar: 10 μM.

up to 2 h) no fluorescent parasites were observed, possibly due to some quenching phenomenon happening inside this complex matrix.

The fluorescence pattern of FG400 was similar to that of another dansyl chloride derivative (DB1919) synthesised in Prof. D. W. Boykin's laboratory and kindly provided us to test for our project. In this compound, the dansyl chloride group was linked to an amidino moiety (the recognition motif of the P2 amino-purine transporter), instead of the lateral chain of an amino acid, as in FG400. Treatment of *in vitro* wild type cells with 10 μM of this compound also yielded a faint fluorescence under both DAPI and FITC filter sets (Figure 5.10). At this dose, the emission started to be detectable after 15 minutes of incubation. The use of lower concentrations (1 or 5 μM) of the fluorophore or shorter times of incubation were not sufficient to obtain a recordable signal. A bright fluorescent spot positioned in the posterior of the cell (similar to that observed inside trypanosomes stained with the dansyl lysine derivative) was clearly evident under DAPI and FITC filter, but for this molecule we were not able to see other cytoplasmic corpuscles. The brighter spot labelled by both dansyl conjugates could be generated by compound internalised by

endocytosis and accumulated inside endosomes. Further studies will be needed to verify this hypothesis. As observed for FG400, also DB1919 fluorescence in infected blood samples was extremely low, close to background levels (data not shown).

5.3 Discussion

In this chapter, the synthesis and biological evaluation of three amino acid derivatives, designed as possible fluorescent probes for trypanosomes, is described. This phase of the project offered me the opportunity to learn the work carried out in an organic chemistry laboratory and to participate directly in the initial development (from its creation to its testing) of new chemical agents.

The synthetic strategy adopted involved the fusion of fluorogenic groups to the side-chain of amino acids. The intention was to exploit these biomolecules as "haptophore" (anchorer) moieties, able to rapidly convey the fluorophores into trypanosomes by means of surface amino acid transporters activity. This approach was similar to that used in the field of drug development to introduce toxins into parasites by linking them to substrates of specific trypanosome membrane transporters (Baliani *et al*., 2005; Barrett and Gilbert, 2006; Chollet *et al*., 2009). Although the complexity of the synthetic pathway increased from the first to the last of the three compounds synthesised (a single reaction to generate FG10, two for FG70, five for FG400), a basic strategy was followed for all of them: (1) potentially reactive groups of the amino acid were protected or deprotected in preparation for the reaction of alkylation; (2) the fluorogenic moiety was fused with the side-chain of the amino acid; (3) the groups still blocked were deprotected, to release the final amino acid derivative.

Of the three amino acid conjugates synthesised, the dansyl chloride lysine derivative FG400 was the only one that showed a detectable signal in the visible region of the spectrum (λ_{EM}=520 nm). The blue-green fluorescence of this compound was visible in *in vitro* trypanosomes treated with the fluorophore (Figure 5.9). However, fluorescence was generally low, even when the compound was used at a relatively high dose (100 μM). The emission of dansyl chloride derivates is known to be weak in aqueous solution and environment-sensitive. Both of these factors could have contributed to the low and unstable emission observed. Moreover the compound would need specific filters to be optimally excited and detected (λ_{EX}~340 nm, λ_{EM}>520 nm), while standard DAPI and FITC channels only partially overlapped the spectra of this conjugate. No fluorescent signal could be detected in treated infected blood samples, possibly due to some quenching event which occurred in these specimens. The lack of fluorescence in *ex-vivo* samples did not allow a check for specific labelling of trypanosomes as compared to other mammalian cells present in the blood film.

No indication regarding the mechanism of entry of FG400 into trypanosomes was obtained. We expected the molecule to be internalised through the activity of specific amino acid transporters, but other routes could not be excluded. Addition of substituents to the core amino acid structure could affect the function and stereochemistry of the "haptophore", thus preventing recognition by binding sites of specific transporters. Among other routes, endocytosis could have contributed to the uptake of FG400. The presence of fluorescent corpuscles in the region where endosomes are normally localised (Figure 5.9) suggested this hypothesis, but these corpuscles and the other smaller bright spots (spread throughout the whole cell length), observed in treated parasites, could equally represent secondary sites of accumulation following transporter uptake.

The synthesised tyrosine (FG10) and serine (FG70) conjugates did not show any interesting fluorescent properties. Although we could measure excitation peaks in the UV region of the spectrum for both compounds, no visible emission was evidenced by spectrometry or qualitative fluorescence microscopy for any of them. No increase of autofluorescence in cells treated with the tyrosine derivative FG10 was observed. Tyrosine is a fluorescent amino acid (λ_{EM}=300 nm), responsible for the intrinsic fluorescence of cells and tissues together with the other aromatic amino acids tryptophan and phenylalanine and molecules such as NADH and FAD (Petty, 2007). Evidently, the experimental conditions adopted and the low yields of this amino acid (ε ~1,405 $cm^{-1}M^{-1}$ at 274 nm) did not allow detection of increased emission in treated cells.

To conclude, the overall fluorescence of the three amino acid derivatives proved too low to be considered of real interest for use in field fluorescence diagnostics of trypanosomiasis, but in the future new, more effective fluorogenic derivatives for parasite labelling could be synthesised following the same approach adopted here.

6

Construction of a *TbAT1*-RFP reporter system to study the sub-cellular localisation of the P2 transporter

6.1 Introduction

6.1.1 The P2 amino-purine transporter and its substrates

The P2 amino-purine transporter is a membrane carrier found only in *Trypanosoma brucei* (Carter and Fairlamb, 1993; Mäser *et al.*, 1999). The protein is encoded by a single copy gene named *TbAT1*, which is located in the subtelomeric region of chromosome V (Lanteri *et al*., 2006; Stewart *et al*., 2010). The physiological substrates of this carrier are adenosine and adenine, which the parasite needs to scavenge from the human host, since it lacks the pathway for purine synthesis *de novo* (Geiser *et al*., 2005). The importance of this transporter lies in its primary role in the uptake of various toxic compounds, including diamidine and melaminophenyl arsenical trypanocidal drugs, which share the same recognition motif that the P2 transporter uses to interact with its physiological ligands (Carter and Fairlamb, 1993; Barrett and Fairlamb, 1999; de Koning, 2008). Loss of activity of this transporter can cause the development of drug resistance, especially for those drugs (diminazene, DB75) that rely nearly exclusively on its activity for their uptake into trypanosomes (de Koning *et al*., 2004; Lanteri *et al*., 2006). On the other hand, the presence in *T. brucei* of other related low affinity transporters partially compensate for loss of P2 activity in *tbat1*$^{-/-}$ cells (which lacks both alleles of the *TbAT1* gene) and derived lines, allowing lower but significant internalisation of drugs such as pentamidine and melarsoprol into parasites (de Koning, 2001b; Matovu *et al*., 2003).

All of the fluorescent diamidines tested during this project were substrates of the P2 amino-purine transporter. As already mentioned, DB75 is internalised mainly through this route (Lanteri *et al*., 2006) and this substrate specificity has been exploited to develop the arsenical drug resistance fluorescence test (Stewart *et al*., 2005; Chapter 3). Similarly, DAPI relies on the P2 transporter for uptake into trypanosomes, but this compound has also significant affinity for the high affinity pentamidine transporter (HAPT) (Bridges *et al*., 2007). Not surprisingly, the Alamar Blue data on drug sensitivity indicated that the five green fluorescent diamidines synthesised in Prof. D. W. Boykin's laboratory was mediated by P2 activity, although other transporters appeared to play a role in their accumulation, as shown by fluorescence images of the *tbat1*$^{-/-}$ cell line incubated with these compounds (Chapter 4).

Since a significant part of this project had focused on studying the ability of different compounds to enter via the P2 carrier, either alone or as one of several transporters, it was

of interest to investigate important aspects of the activity of this carrier under different conditions.

6.1.2 Regulation of the P2 transporter expression

Extensive study has elucidated the substrate specificity and kinetics of the P2 transporter (Carter and Fairlamb, 1993; Barrett and Fairlamb, 1999; Mäser *et al*., 1999; de Koning, 2001a; de Koning *et al*., 2004; Lanteri *et al*., 2006; Collar *et al*., 2009) and various efforts have been made in order to exploit this knowledge to target toxic compounds into trypanosomes through this route (Tye *et al*., 1998; Stewart *et al*., 2004; Baliani *et al*., 2005; Barrett and Gilbert, 2006; Chollet *et al*., 2009; Landfear, 2009). However, very little is known about the localisation of this carrier within the parasite or about the regulatory mechanisms of its expression under different environmental conditions. It is known that P2 activity is dependent on the life cycle stage of *T. b. brucei*, being expressed in bloodstream forms but not in procyclics (de Koning, 2001a). Moreover, several strands of evidence obtained in our laboratory indicate that P2 activity is down-regulated in bloodstream cells grown in culture compared to its expression levels in parasites from *in vivo* models. Uptake of radiolabelled adenosine into *T. b. brucei* cells through this transporter route was found to be much lower in cells from culture than in cells from rat (Pui Ee Wong, University of Glasgow, unpublished; Figure 6.1).

Other uptake assays showed that trypanosomes grown *in vivo* and subsequently transferred to broth culture gradually down-regulated the adenosine P2-mediated transport activity; levels similar to continuously *in vitro*-grown parasites were reached after 8 hours (Pui Ee Wong, unpublished). This phenomenon could be a response of parasites to the rich *in vitro* environment, where nutrients are easily available in the medium and high transporter expression would be energetically unfavourable. Other data obtained by Pui Ee Wong in our laboratory demonstrated that the expression of the P2 transporter was higher in trypanosomes which had reached high parasitaemia levels compared to those that had reached only low blood parasitaemia (Pui Ee Wong, unpublished). This observation could be another indication that high levels of P2 expression help protozoan parasites to better compete for nutrients (in this case, purines) inside their host.

Understanding how trypanosomes regulate the expression of this transporter in response to changes in their environment and life cycle stage is important, especially when considering the crucial role of P2 in the internalisation of various trypanocidal compounds. The

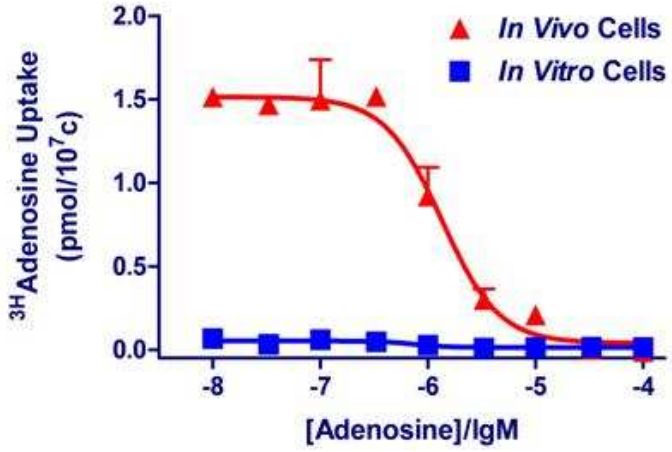

Figure 6.1 – Adenosine uptake in trypanosomes grown either in tissue culture or harvested from rat blood.
***T. b. brucei* S427 w.t. cells from culture (*in vitro* cells, blue ■) were directly used for the assay after washing in CBSS, while parasites grown in rats (*in vivo* cells, red ▲) were separated from blood cells by elution over a DE52 column and washed in CBSS before use. Uptake of [^{3}H]adenosine (10 nM) was measured in the presence of increasing concentrations of unlabeled adenosine after 30 sec incubation. Data were fitted to a sigmoid curve using the nonlinear regression equation of GraphPad Prism 5.0 software package. Data and graph were kindly provided by Pui Ee Wong (University of Glasgow, unpublished), and are included here to provide context for work conducted as part of this thesis.**

observation that P2 expression is linked to the level of parasitaemia could have pharmacokinetic implications for drug development, considering that in humans *T. b. gambiense* usually gives rise to very low parasitaemia levels while concentration of *T. b. rhodesiense* in human hosts is normally quite high. Furthermore, investigations with compounds whose entry into trypanosomes has some dependency on P2 may be influenced by the expression levels of this carrier. For example, during this project, it emerged that various fluorophores (especially DB75 and propidium iodide) yielded a brighter fluorescence emission in *ex-vivo* stained trypanosomes (blood films) than cells derived from *in vitro* culture, treated under the same experimental conditions (Chapters 3 and 4). This difference may be due to the *in vitro* down-regulation of the P2 transporter in the case of DB75, but a similar mechanism, involving other transporters, could also be valid for propidium iodide. The use of trypanosomes grown in rodent blood for testing of fluorophores was, thus, not only justified by the fact that these blood samples better mimic the human specimens used for diagnosis than cultured parasites, but also by the observation that the staining properties of *ex-vivo* trypanosomes could prove different than those of cells cultivated *in vitro*.

The biological mechanisms that trypanosomes use to regulate the levels of the P2 transporter are not known. Various phenomena could be involved in this process, including different levels of transcription of the *TbAT1* gene, instability of the mRNA, post-transcriptional modifications or compartmentalisation of the protein. Here, the

construction, by genetic engineering, of a fluorescently tagged P2 transporter, aimed to localise the carrier in trypanosomes under various environmental conditions, is described.

6.1.3 TbAT1 *fluorescent tagging*

Previous attempts to generate antibodies against the P2 transporter protein to assess its intracellular localisation failed (Richard Burchmore, personal communication). We, therefore, decided to study P2 expression and cell distribution by constructing a reporter system, in which the *TbAT1* gene was expressed together with a fluorescent protein. For tagging, we chose the monomeric red fluorescent protein mCherry (λ_{EX}=587 nm, λ_{EM}=610 nm). This fluorophore was derived, by sequential mutations, from mRFP1 (Campbell, *et al*., 2002), the monomeric mutant of the *Discosoma* sp. reef coral tetrameric DsRed protein (Shaner *et al*., 2004). The mCherry protein is reported to have high photostability, high pH-stability and a good maturation rate (measured as the time needed to reach its full fluorescence) (Shaner *et al*., 2004 and 2005) and it has already been successfully expressed in various organisms (Snaith *et al*., 2005; Pisharath *et al*., 2007; Pradel *et al*., 2007). To ensure that the fluorescent tag itself did not interfere with the biological function of the target transporter, two constructs were prepared: one with the gene encoding for the red fluorescent protein linked to the C-terminus of *TbAT1* (*TbAT1::mCherry*, C-t construct) and one with the *mCherry* gene linked to its N-terminus (*mCherry::TbAT1*, N-t construct).

The tetracycline-responsive expression vector pHD676 (Biebinger *et al*., 1997) was chosen for cloning. The decision to use an inducible system was made in order to obtain a tight control on transcription, minimising the risk of over-expression of the exogenous genes, which could lead to mislocalization of the encoded protein. The two fusion constructs (*TbAT1::mCherry* and *mCherry::TbAT1*) were designed to be inserted within pHD676 as *Hin*dIII-*Bam*HI fragments, with insert downstream of a procyclic acidic repetitive protein (PARP) promoter, containing tetracycline operator sequences (Wirtz and Clayton, 1995; Figure 6.3 A). When transfected into a cell line genetically modified to express a tetracycline repressor (bloodstream form strain 449), the transcription of the exogenous genes was expected to be repressed until addition to the medium of the inducer tetracycline. This antibiotic, by binding the repressor, released it from the operator. A separate constitutive promoter drove transcription of the hygromycin selectable marker (Biebinger *et al*., 1997). pHD676 was designed to integrate, once linearised, into the trypanosome's genome within the non-transcribed intergenic spacers of the rRNA repeat region, with an orientation opposite to that of rRNA gene transcription (Wirtz and Clayton,

1995). Both constructs (N-t and C-t) were also transfected into the *tbat1*$^{-/-}$ line lacking the endogenous P2 transporter (Matovu *et al*., 2003), where they were expected to work in a constitutive way.

6.2 Results

6.2.1 Preparation of the TbAT1-mCherry *recombinant constructs*

6.2.1.1 Amplification of *TbAT1* and *mCherry* ORF

The *TbAT1* ORF was amplified from gDNA extracted from *T. b. brucei* S427 wild type by using the high proofreading enzyme KOD Hot Start DNA polymerase (Novagen) (Section 2.7.2.1). Two different sets of primers, containing the appropriate restriction sites for subsequent cloning, were designed for its amplification (Table 2.2): MB407 and MB408 for the N-t sequence (*mCherry* ORF upstream *TbAT1*), MB411 and MB412 for the C-t (*mCherry* downstream the *TbAT1* sequence). The gene for the mCherry fluorescent protein was amplified, using the same high fidelity enzyme, from vector p2664 (Kelly *et al*., 2007), developed in Dr. M. Carrington's laboratory (University of Cambridge). Another two sets of primers flanking the *mCherry* ORF were designed for its amplification (Table 2.2): MB405 and 406 for the N-t construct, MB409 and MB410 for the C-t. A pair of glycine residues was introduced as a linker between the *TbAT1* and *mCherry* sequences in order to provide flexibility to the fused protein.

6.2.1.2 Sequence analysis

Sequencing of the PCR products showed that both of the *TbAT1* amplicons (for N-t and C-t constructs) had the correct sequence (data not shown). The *mCherry* N-t product sequence also proved correct. The *mCherry* amplicon for C-t tagging, however, possessed a single point mutation at base 64 of its ORF, where the change from a cytosine to an adenine corresponded to an amino acid change from a histidine to an asparagine (Figure 6.2). Another discrepancy between our mCherry protein sequence (for both N-t and C-t tagging) and that published by Shaner and collaborators (Shaner *et al*., 2004) was the presence in our products of an asparagine instead of an aspartic acid at position 8. This Asp^{8} residue was encoded by the gene sequence in p2664 used as template for *mCherry* amplification, and therefore was not the product of a mutation event. Restriction sites introduced for cloning proved correct for all of the amplicons.

```
mCherry C-t    (1) GGPMATSGMVSKGEENNMAIIKEFMRFKVNMEGSVNGHEFEIEGEGEGRP
mCherry N-t    (1) HKLMATSGMVSKGEENNMAIIKEFMRFKVHMEGSVNGHEFEIEGEGEGRP

mCherry C-t   (51) YEGTQTAKLKVTKGGPLPFAWDILSPQFMYGSKAYVKHPADIPDYLKLSF
mCherry N-t   (51) YEGTQTAKLKVTKGGPLPFAWDILSPQFMYGSKAYVKHPADIPDYLKLSF

mCherry C-t  (101) PEGFKWERVMNFEDGGVVTVTQDSSLQDGEFIYKVKLRGTNFPSDGPVMQ
mCherry N-t  (101) PEGFKWERVMNFEDGGVVTVTQDSSLQDGEFIYKVKLRGTNFPSDGPVMQ

mCherry C-t  (151) KKTMGWEASSERMYPEDGALKGEIKQRLKLKDGGHYDAEVKTTYKAKKPV
mCherry N-t  (151) KKTMGWEASSERMYPEDGALKGEIKQRLKLKDGGHYDAEVKTTYKAKKPV

mCherry C-t  (201) QLPGAYNVNIKLDITSHNEDYTIVEQYERAEGRHSTGGMDELYKGSGTA-
mCherry N-t  (201) QLPGAYNVNIKLDITSHNEDYTIVEQYERAEGRHSTGGMDELYKGSGTAG

mCherry C-t  (250) GS-
mCherry N-t  (251) GGP
```

Figure 6.2 –Amino acid sequence alignment of mCherry PCR products for N-t and C-t tagging.
***mCherry* ORF was amplified from vector p2664 (Kelly *et al*., 2007). Discrepancies between our products and the published mCherry sequence (Shaner *et al*., 2004) are shaded in red. The first amino acid change (Asp^{8}→Asn) is at position 8 of both N-t and C-t products; the second mutation (His^{22}→Asn) is at position 22 of the C-t product. Additional residues introduced by PCR amplification upstream and downstream the *mCherry* ORF, containing the restriction sites and the stop codon (-), are shaded in grey.**

6.2.1.3 Cloning into the expression vector pHD676

The *TbAT1* and *mCherry* genes were first linked together in a pGEM-T Easy plasmid (Promega) and, then, the whole *Hin*dIII-*Bam*HI fragment containing the fused ORF (*TbAT1::mCherry* or *mCherry::TbAT1*) was excised and inserted into the expression vector pHD676 (Biebinger *et al*., 1997) to generate either the N-t (pMB-G94) or C-t (pMB-G95) final expression constructs (see Figure 2.1 for a schematic representation of the preparation of the constructs and Figure 6.3 A for the vectors maps). Interestingly, the bacterial pellet transformed with the C-t vector was pink, while the N-t transformants had a normal yellowish colour. Insertion of the *TbAT1* and *mCherry* genes inside pHD676 was assessed by restriction digest analysis (Figure 6.3 B). The use of *Hin*dIII-*Bam*HI enzymes released the correct 2148 bp fragment containing the fused *TbAT1* and *mCherry* sequences. Double *Hin*dIII-*Apa*I digest released the expected 754 bp fragment (containing *mCherry*) from pMB-G94 and a 1405 bp fragment (containing *TbAT1*) from pMB-G95. Digest with *Apa*I-*Bam*HI gave the correct 1394 bp band (*TbAT1*) in pMB-G94 and 743 bp band (*mCherry*) in pMB-G95. Sequencing of the vectors confirmed the correctness of the insertion for both N-t and C-t *Hin*dIII-*Bam*HI fragments.

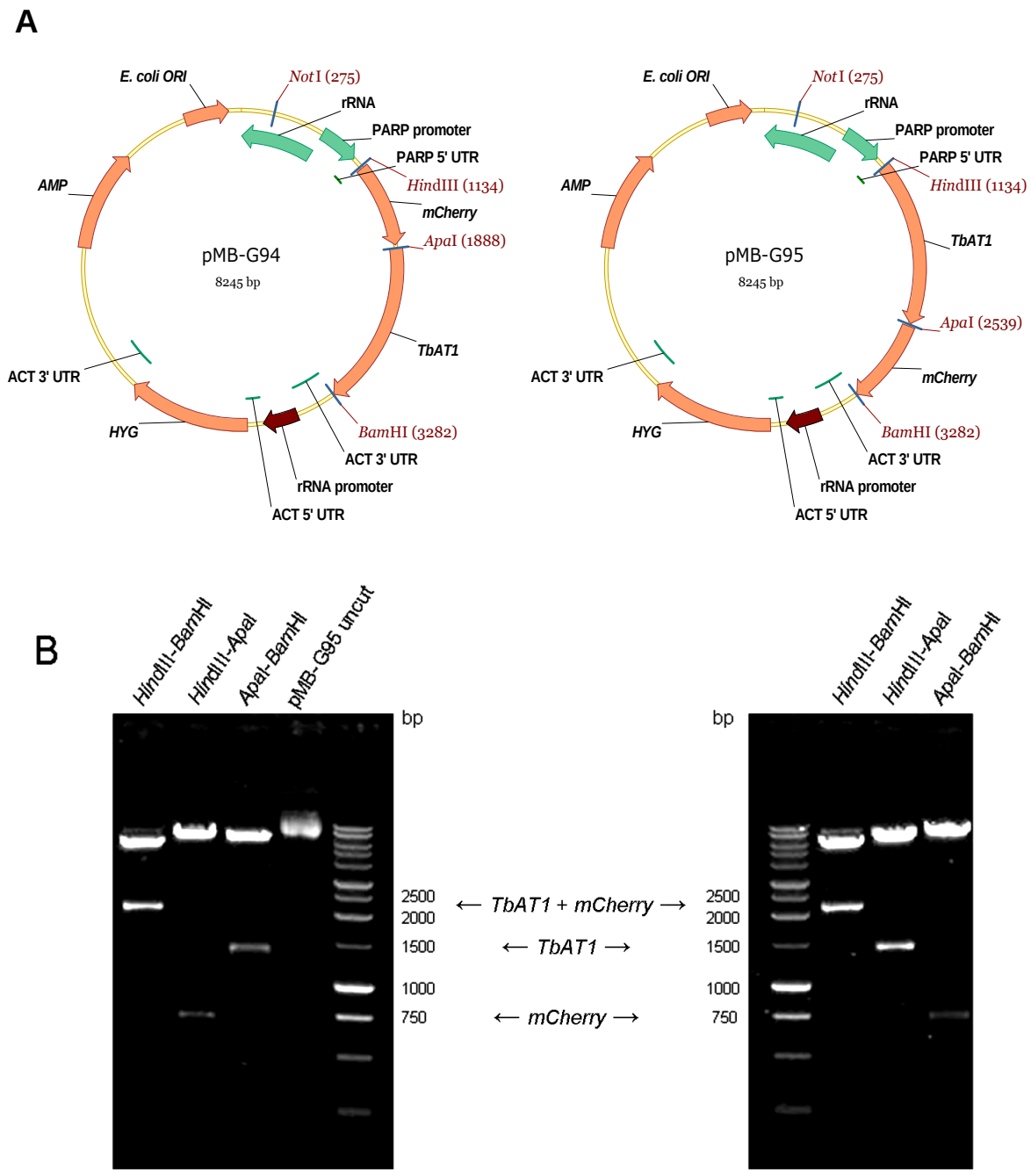

Figure 6.3 – Maps of pMB-G94 and pMB-G95 and their restriction profiles.
(A) The two constructs pMB-G94 and pMB-G95 were derived from pDH676 by insertion of *TbAT1-mCherry* fused ORFs (*TbAT1::mCherry* or *mCherry::TbAT1*) as *Hin*dIII-*Bam*HI fragment downstream of a tetracycline-inducible PARP promoter, containing the tetracycline operator sequence. The hygromycin phosphotransferase gene (*HYG*) for hygromycin resistance was under control of a different constitutive rRNA promoter. Regulatory 5' and 3' actin (*ACT*) and PARP untranslated regions (5' or 3' UTR) are indicated. Stable integration in the rRNA intergenic region was obtained after linearization at the unique *Not*I site.
(B) Restriction digest products of the two vectors, run on a 1% agarose gel (1 kb ladder, Promega). The uncut vector pMB-G95 was loaded as positive control.

6.2.2 Transfection and PCR screening of clones

Bloodstream form *T. brucei* strain 449 (Biebinger *et al*., 1997) and the *tbat1*$^{-/-}$ strain (Matovu *et al*., 2003) were transfected with 10 μg of either linearised vector pMB-G94 or pMB-G95 (Section 2.7.5). Clones were obtained for both cell lines after selection with 5 μg/ml hygromycin. All transfectant lines grew well in culture in the presence of the selective drug, duplicating at a similar rate as the parental lines.

To check for the presence of the vectors inside transfectants a PCR analysis was performed. A fragment spanning *TbAT1* and *mCherry* domains was amplified from gDNA extracted from the clones (Section 2.7.2.2). Primers MB363 (annealing inside the *mCherry* ORF) and MB182 (annealing inside the *TbAT1* ORF) were used for amplification of the N-t construct (expected product size of 1302 bp), and MB181 (annealing inside the *TbAT1* ORF) and MB410 (annealing at the 3' of the *mCherry* ORF) were used for the C-t construct (expected product size of 1455 bp) (Table 2.3 for primer sequences). Various transfectants, derived from both 449 and *tbat1*$^{-/-}$ cell lines, showed the expected band following PCR amplification (Figure 6.4). Four of them were chosen for subsequent molecular and biological assays (these clones are indicated with asterisks in Figure 6.4): two 449-derived lines transfected with pMB-G94 or pMB-G95 (449 Cl.4 N-t, 449 Cl.7 C-t, respectively) and two *tbat1*$^{-/-}$-derived lines transfected with either vector (*tbat1*$^{-/-}$ Cl.6 N-t, *tbat1*$^{-/-}$ Cl.9 C-t). Some clones did not yield any product. Nevertheless, absence of an amplified fragment for these lines could be due to limiting quantities of gDNA template rather than to unsuccessful transfection, since all of the clones grew well under drug pressure. Amplification of the endogenous actin gene, however, gave clear bands for all clones, indicating the presence of DNA template in all samples.

Although PCR analysis confirmed the presence of the constructs inside some of the transfectants, these results could not distinguish between their presence as stable gDNA integrated copies or as transient episomes. Bloodstream form trypanosomes, however, generally fail to maintain episomal plasmids, especially when compared to procyclic form (Patnaik *et al*., 1993; Burkard *et al*., 2007); hence, it was assumed DNA was integrated.

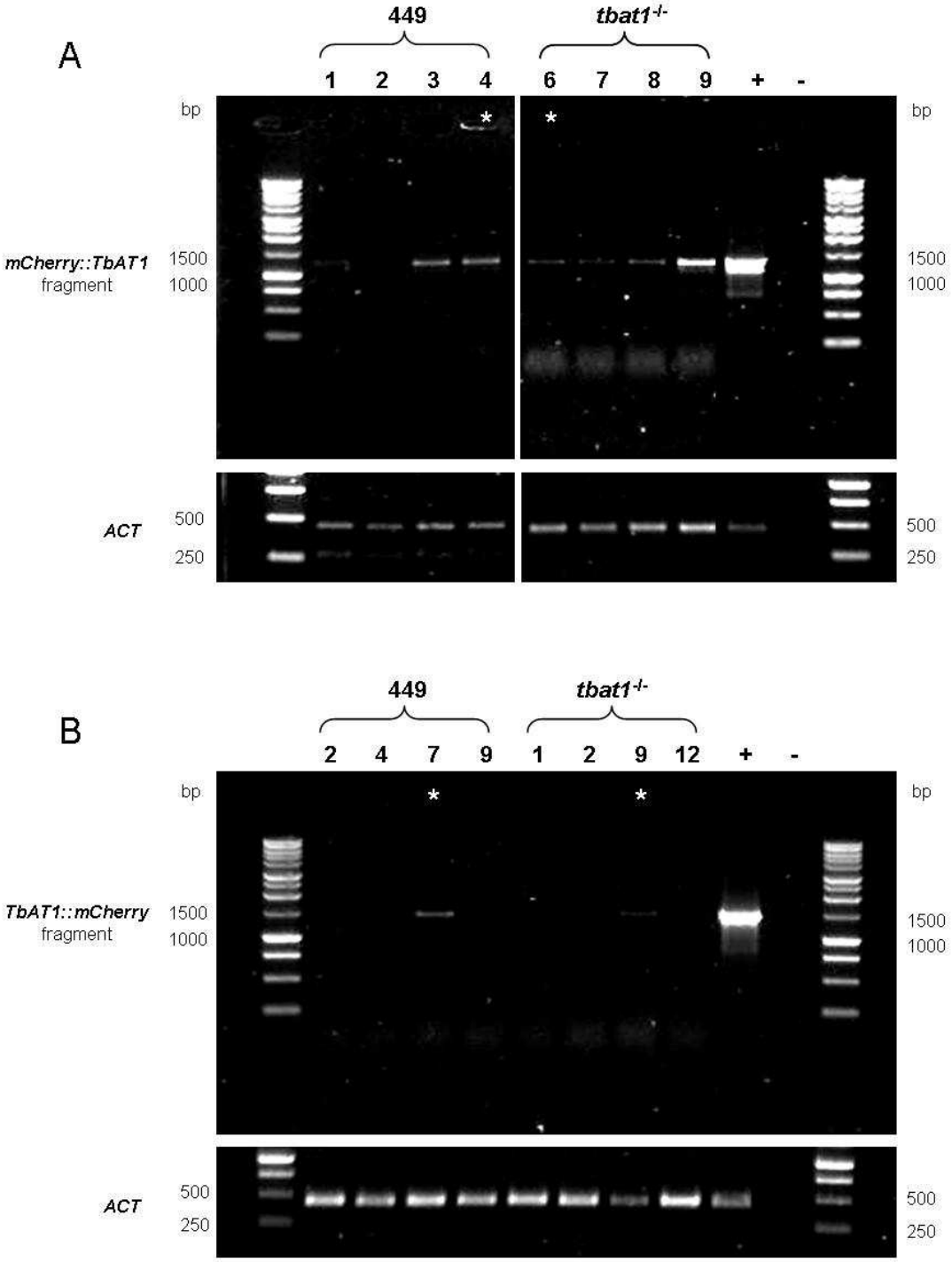

Figure 6.4 – PCR screening of transgenic bloodstream form cell lines.
Genomic DNA from clones obtained after transfection of the 449 and *tbat1*$^{-/-}$ lines with either pMB-G94 (N-t clones, panel A) or pMB-G95 (C-t clones, panel B) was extracted using the DNeasy® Blood and Tissue Kit (Qiagen). A fragment spanning the fused *TbAT1* and *mCherry* sequences was amplified using specific primers (Table 2.3). The expected band size for the N-t fragment was 1302 bp, for the C-t 1455 bp. Amplicons were run on a 1% agarose gel (1 kb ladder, Promega). Numbers at the top of the gel indicate different clones: (A) 449 clones 1,2,3,4 were obtained after transfection of 449 line with pMB-G94; *tbat1*$^{-/-}$ clones 6,7,8,9 were obtained after transfection of *tbat1*$^{-/-}$ line with pMB-G94. (B) 449 clones 2,4,7,9 were obtained after transfection of 449 line with pMB-G95; *tbat1*$^{-/-}$ clones 1,2,9,12 were obtained after transfection of *tbat1*$^{-/-}$ line with pMB-G95. Actin (*ACT*, expected band size 455 bp) amplification was used to verify presence of gDNA template in the PCR samples. Clones chosen for successive biological assays are indicated with an asterisk.
+: positive control (purified plasmid); -: negative control (no gDNA).

6.2.3 Southern blot

Southern blot hybridization (Section 2.7.6) was used to determine correct and stable integration of the constructs within the non-transcribed rRNA spacer of the trypanosome's genome, in the reverse orientation relative to endogenous rRNA genes transcription. The ORFs of both *TbAT1* and *mCherry* were used as probes. Two clones (449 Cl.7 C-t and 449 Cl.4 N-t) were selected for study. At the same time, the gDNA of the parental line 449 was also analysed to determine the restriction pattern of the endogenous copy of the *TbAT1* gene.

6.2.3.1 Clone 449 Cl.7 C-t

The gDNA of clone 449 Cl.7 C-t and its parental line 449 were digested with seven different restriction enzymes and probed with the *TbAT1* ORF. Southern analysis of the 449 line identified the position of the endogenous copy of the *TbAT1* gene (Figure 6.5). All band sizes corresponded to the expected restriction pattern of the *TbAT1* genomic region (24 kb total length) annotated for *T. brucei* in GeneDB (http://www.genedb.org/Homepage), except for *Stu*I. The expected band for this enzyme was 6.7 kb, while the fragment in our blot had a size of ~3.7 kb, possibly due to heterogeneity between the published 927 strain genome and that of 427 strain used during our experiments. The sizes of the bands for the other enzymes were: *Pst*I: 6.8 kb; *Hin*dIII: 13.9 kb; *Bgl*II: no bands; *Nco*I: 3.5 and 3.9 kb; *Xho*I: 2.7 kb; *Spe*I: 8.7 kb.

In the derived clone 449 Cl.7 C-t, insertion of the vector pMB-G95 (containing the exogenous *TbAT1* copy) yielded additional bands (Figure 6.5). To determine the correctness of integration, the size of these bands was compared to the published restriction maps of the rRNA locus (Biebinger *et al*., 1996 and 1997), schematically reproduced in Figure 6.6 together with the restriction pattern of the two transfected vectors. In addition to the endogenous 6.8 kb band, *Pst*I digestion yielded an extra-band of the expected size (8 kb). Digestion with *Hin*dIII, *Stu*I and *Bgl*II yielded two additional bands instead of the single one expected. An explanation for this result is the possible insertion of two copies of the vector in two separated rRNA spacers with different restriction polymorphisms, a known characteristic of this genomic region that complicates analysis (Biebinger *et al*., 1996). Nevertheless, insertion in other regions of the genome for one or both constructs can not be excluded. If this hypothesis was right we would expect a similar double band pattern also for *Pst*I, *Nco*I and *Xho*I, but this was not observed. *Hin*dIII digestion produced

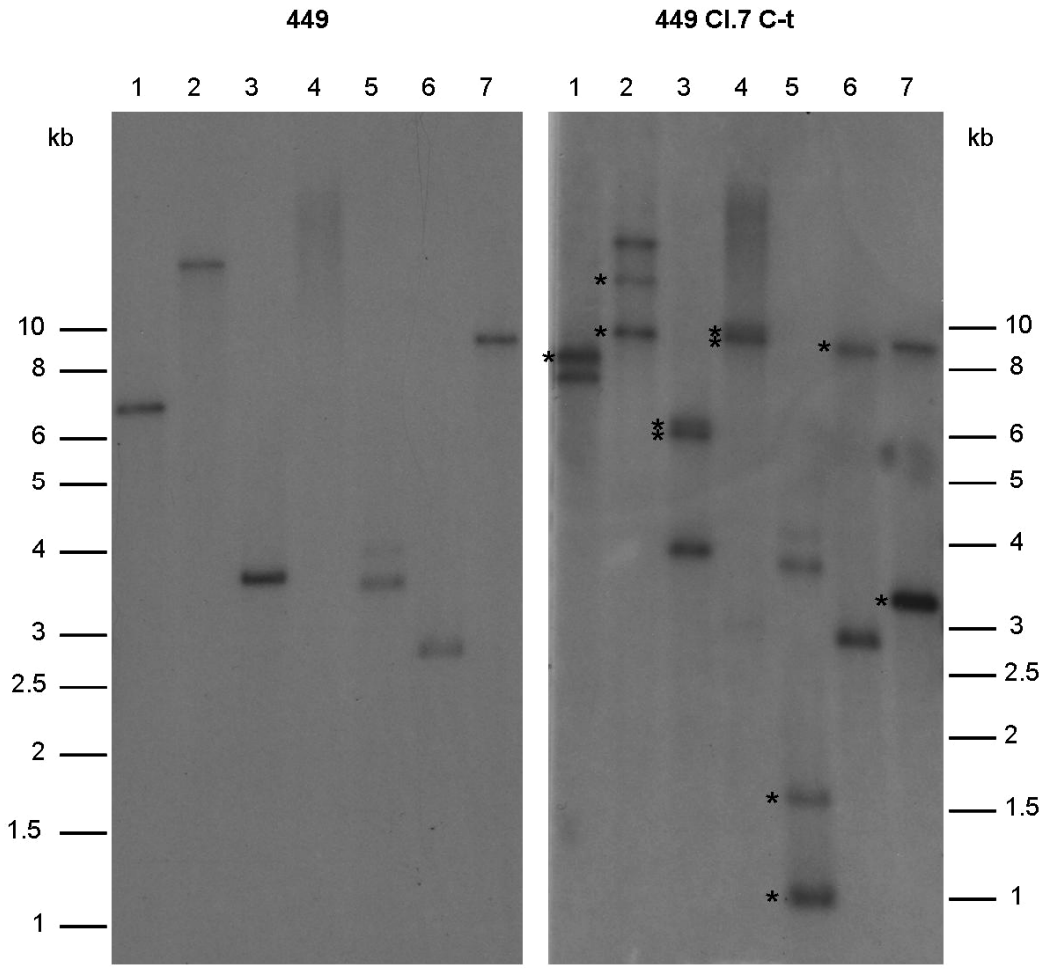

Figure 6.5 – Southern blot analysis of line 449 and derived clone 449 Cl. 7 C-t, hybridized with *TbAT1* probe.
gDNA of both cell lines was digested with seven different enzymes and hybridized with a probe constituted by the whole *TbAT1* ORF to verify integration in the rRNA non-transcribed spacer. Asterisks denote the extra bands hybridized in the derived clone compared to the parental line.
1: *Pst*I; 2: *Hin*dIII; 3: *Stu*I; 4: *Bgl*II; 5: *Nco*I; 6: *Xho*I; 7: *Spe*I.

a band of ~9 kb and another that could correspond to the expected 12.3 kb, but the exact size of this band was difficult to determine, being beyond the range of the molecular weight ladder used. The expected band size after *Stu*I digestion was of 5.7 kb, as found, while the slightly bigger band (~5.9 kb) could derive from a polymorphic restriction site in another rRNA spacer. The size of the bands yielded following *Bgl*II digestion (~8.8 and 9.7 kb) could not be explained using the mapped sites, and other polymorphic *Bgl*II restriction sequences must be present in our line, if the vector targeted the rRNA spacer. *Nco*I digestion generated an expected band of 0.9 kb and another one of ~1.6 kb expanding outside the vector length, as the band (~8.5 kb) generated by *Xho*I digestion (no restriction map of the rRNA locus was available for these two enzyme). *TbAT1* probing following *Spe*I digestion yielded the correct vector-internal 3.2 kb fragment. Overall we can conclude that the vector had integrated into the *T. brucei* genome, but that this integration had not been targeted to the precise location anticipated, or else polymorphisms between the

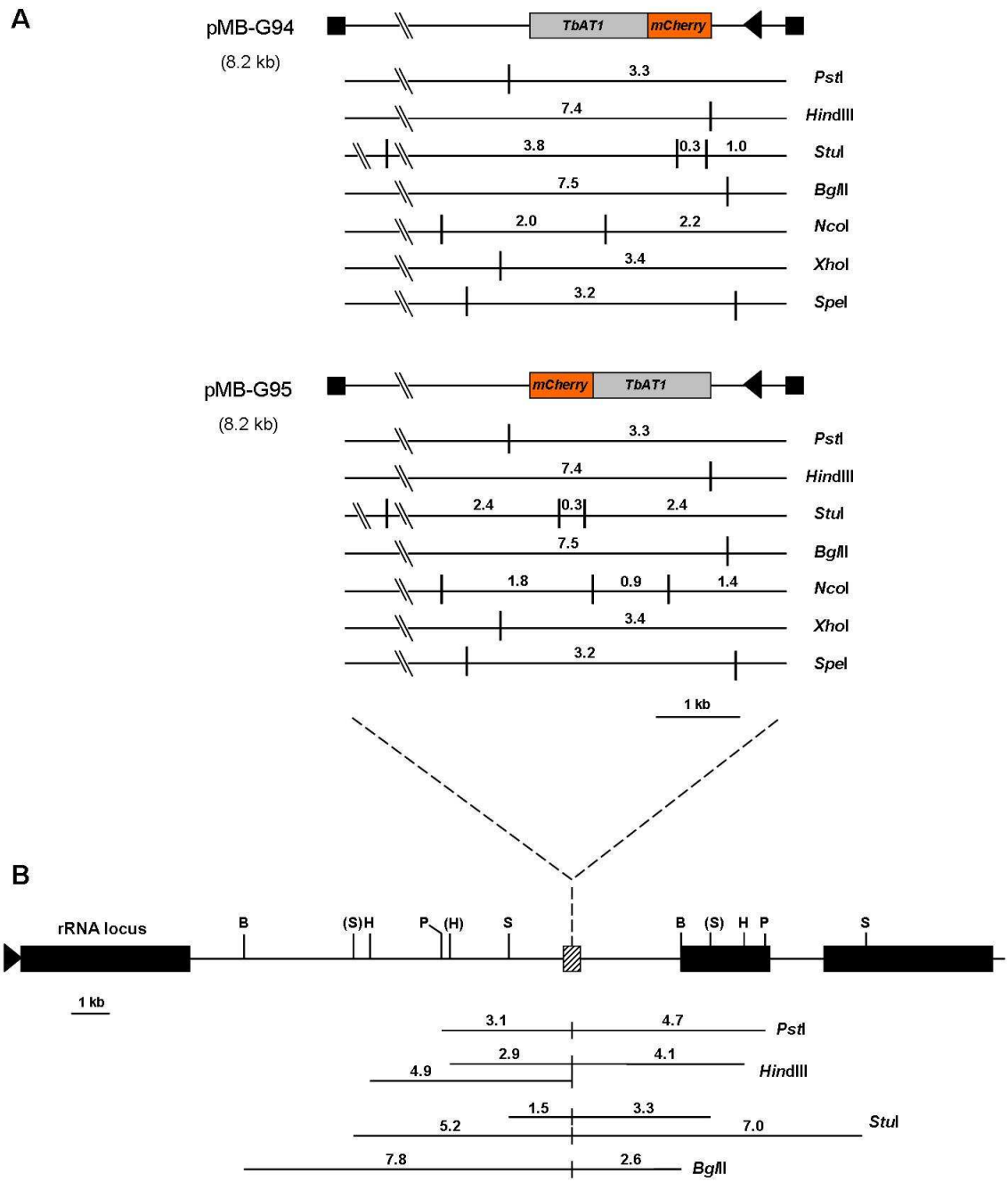

Figure 6.6 – Restriction digest map of vectors pMB-G94 and pMB-G95 and of the rRNA locus of *T. b. brucei*.
(A) Schematic representation of the two vectors used for transfection (pMB-G94 and pMB-G95) linearised at the unique *Not*I site. Underneath each construct are illustrated the restriction fragments resulting from their digestion with the seven enzymes used for Southern blotting (*Pst*I, *Hin*dIII, *Stu*I, *Bgl*II, *Nco*I, *Xho*I, *Spe*I).
(B) Restriction map of the the rRNA locus of *T. b. brucei* S427 (adapted from Biebinger *et al.*, 1996 and 1997), with the size of the fragments expected by digest of this locus with *Pst*I, *Hin*dIII, *Stu*I and *Bgl*II indicated underneath (restriction map of this locus for *Nco*I, *Xho*I, *Spe*I was not available).
Restriction sites that vary between loci are in brackets. Black boxes represent the rRNA genes. The striped box indicates the site of vector integration. Arrows indicate the direction of transcription. B: *Bgl*II; H: *Hin*dIII; P: *Pst*I; S: *Stu*I.

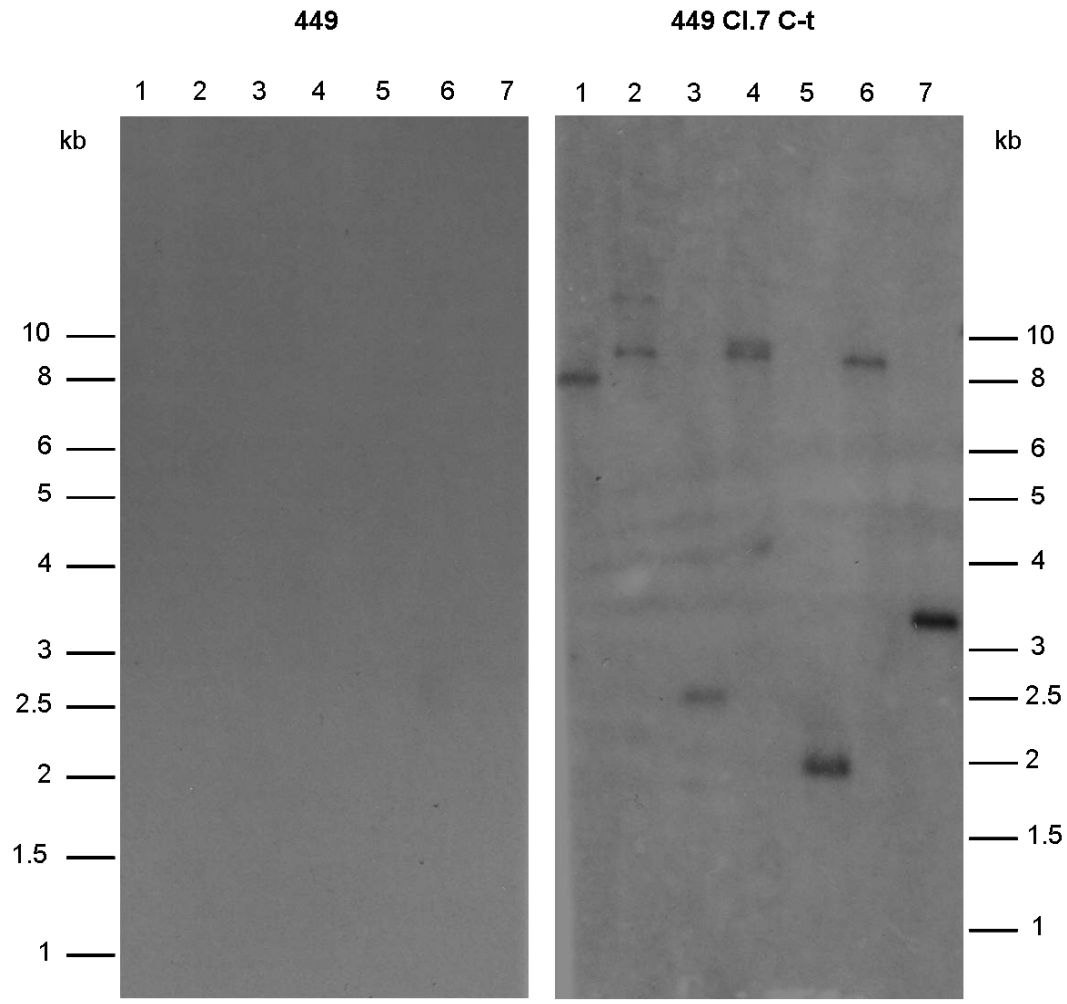

Figure 6.7 – Southern blot analysis of line 449 and derived clone 449 Cl.7 C-t, hybridized with *mCherry* probe.
gDNA of both cell lines was digested with seven different enzymes and hybridized with a probe constituted by the *mCherry* ORF to verify integration in the rRNA non-transcribed spacer.
1: *Pst*I; 2: *Hin*dIII; 3: *Stu*I; 4: *Bgl*II; 5: *Nco*I; 6: *Xho*I; 7: *Spe*I.

non-transcribed intergenic spacers in the ribosomal locus of 427 genome (the strain from which b.f. 449 derives) affected restriction patterns.

After probing with *TbAT1*, the two membranes were stripped (Section 2.7.6.4) and re-probed with the *mCherry* ORF. As expected, hybridization of the gDNA from the parental line (449) yielded no bands (Figure 6.7). In the derived clone 449 Cl.7 C-t, *Pst*I, *Hin*dIII, *Bgl*II, *Xho*I and *Spe*I digestion yielded the same bands detected using the *TbAT1* probe (8 kb for *Pst*I, 9.0 and 12.3 kb for *Hin*dIII, 8.8 kb and 9.7 for *Bgl*II, 8.5 kb for *Xho*I and 3.2 kb for *Spe*I) (Figure 6.7). *Stu*I digestion showed the correct 2.4 kb band. The other very small band expected after digestion with this enzyme (0.3 kb) had gone off the end of the gel and does not appear in the blot shown in Figure 6.7. *Nco*I digestion yielded the expected 1.8 kb band.

6.2.3.2 Clone 449 Cl.4 N-t

As for the C-t clone, the Southern blot of the N-t clone (449 Cl.4 N-t) showed additional bands compared to the parental 449 line (Figure 6.8), indicative of integration of the vector into the parasite genome (the digestion pattern for the parental line has already been shown in Figure 6.5). For this clone each enzyme yielded a single extra band pattern compared to the 449 line, suggesting a single insertion event. The size of some of the bands expanding beyond the length of the vector, and expected to be identical to the bands obtained for the C-t clone (Figure 6.6), actually differed from these. Hence, integration of the constructs inside the genome of the two clones appeared to be at two different sites. In 449 Cl.4 N-t *Pst*I digestion should have yielded an additional band of 8 kb identical to that of the C-t clone, but in the N-t clone a band with a slightly bigger size (~8.5 kb) was observed. *Hin*dIII yielded an extra band, slightly smaller than that generated by the endogenous *TbAT1* copy (13.9 kb), but bigger than the band of 12.3 kb found in the C-t clone. *Xho*I digestion, instead, yielded a band of 8.5 kb identical to the C-t clone. Digestion with either *Stu*I, *Nco*I or *Spe*I were expected to generate bands contained within the length of the vector and all of these enzymes yielded correct band sizes:the *Stu*I band was 3.8 kb,the *Nco*I band was 2.0 kb and the *Spe*I band was 3.2 kb. The second band yielded by *Nco*I digestion (a faintly detectable 2.4 kb band) must be due to a site just downstream the site of integration, as inferred also for the C-t clone. Finally, *Bgl*II digestion generated a high molecular weight band of ~14 kb.

The use of the *mCherry* probe confirmed the presence of the sequence of the fluorescent protein within the clone 449 Cl.4 N-t, although the bands appeared faint in this particular blot (Figure 6.8). Bands obtained after digestion with *Pst*I, *Hin*dIII, *Bgl*II, *Xho*I and *Spe*I were identical, as expected, to the bands obtained after hybridization with the *TbAT1* probe (*Pst*I and *Xho*I 8.5 kb, *Hin*dIII 13.5 kb, *Bgl*II 14 kb, *Spe*I 3.2 kb). *Stu*I digestion generated an expected 4.3 kb band, but the small 0.3 kb band and the other expected 3.8 kb band were not detectable on the blot (the first one had probably run out of the gel and the second could have resulted too faint to be detectable). *Nco*I digestion yielded the expected 2.4 kb band.

Summarising, Southern blot hybridization confirmed the presence of the exogenous *TbAT1* and *mCherry* fused ORF in the genome of both analysed clones. Integration of pMB-G94 and pMB-G95 in the genome of the two clones seemed to have occurred at two different loci, none of which could be unequivocally identified with the rRNA spacers.

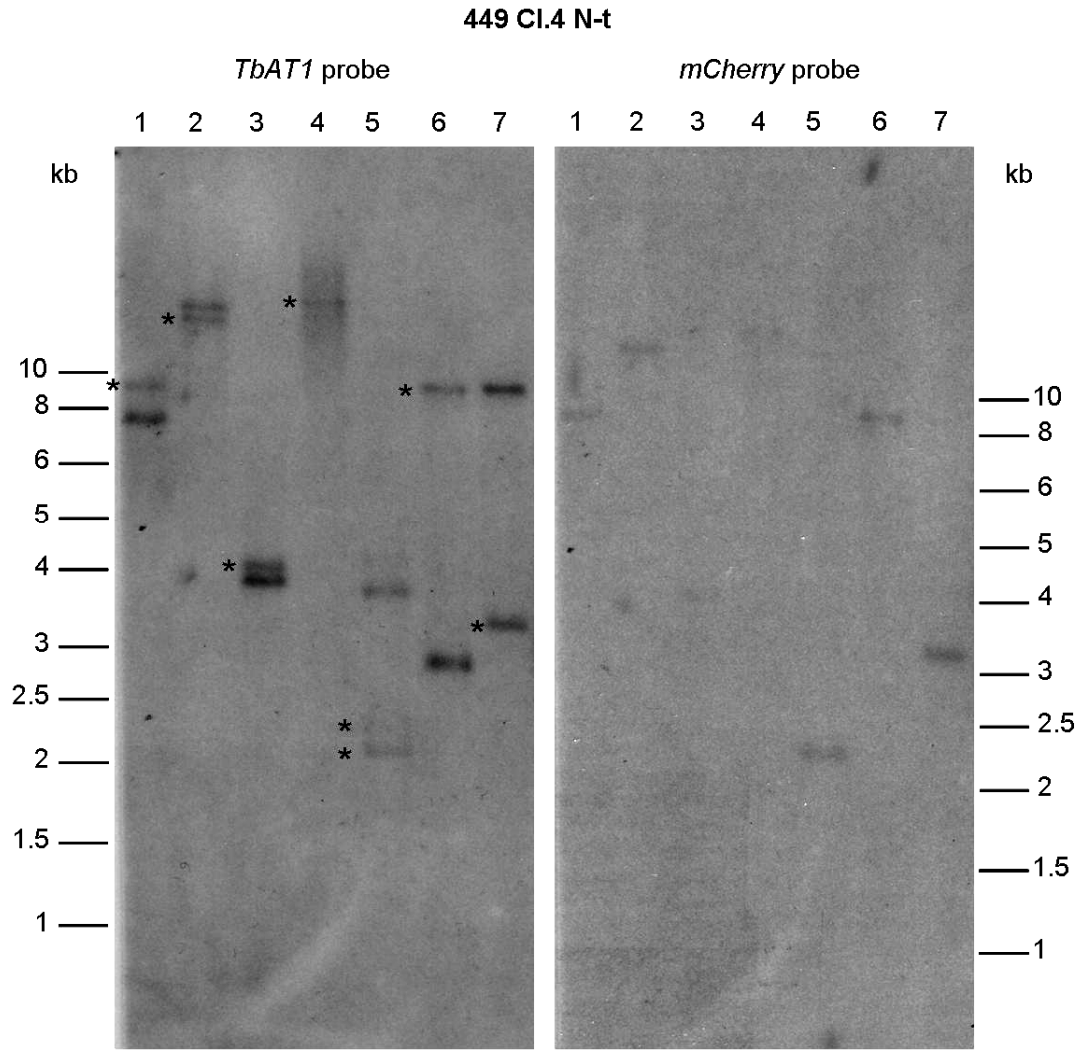

Figure 6.8 – Southern blot analysis of clone 449 Cl.4 N-t, hybridized with *TbAT1* and *mCherry* probes.
gDNA of both cell lines was digested with seven different enzymes and hybridized with a probe constituted by the *TbAT1* (left) or *mCherry* (right) ORF to verify integration in the rRNA non-transcribed spacer. Asterisks denote the extra bands hybridized in the derived clone compared to the parental line.
1: *Pst*I; 2: *Hin*dIII; 3: *Stu*I; 4: *Bgl*II; 5: *Nco*I; 6: *Xho*I; 7: *Spe*I.

6.2.4 Western blot

Southern analysis confirmed the presence of the fused *TbAT1-mCherry* reporter constructs inside the genome of the clones, but we had no indication concerning their correct transcription and translation. Integration in a silent region of the genome or rearrangements of the vectors during transfection were not ruled out by DNA analysis. Therefore, to study the expression of the constructs, a Western blot was performed (Section 2.7.10).

To detect the protein formed by the fusion of *Tb*AT1-mCherry sequences a DsRed monoclonal antibody (Clontech Laboratories), which also recognised the mCherry protein, was used. This was confirmed by the positive control, represented by a cytosolic fusion

protein containing the *mCherry* sequence and expressed in *Leishmania mexicana* (kindly provided by Elmarie Myburgh, University of Glasgow) (Figure 6.9). Unfortunately, our experiments failed to detect the *Tb*AT1-mCherry fusion protein (predicted protein size was 78 kDa: 27 kDa for the mCherry protein and 51 kDa for the P2 transporter). Instead, the mCherry antibody always bound to a 175 kDa protein, particularly abundant in the aqueous fraction but also detectable in the total protein extract of the clones analysed (Figure 6.9). This high molecular weight protein was not specific for our transfectants, since it was also detected in the parental line 449 (and in the other parental line *tbat1*$^{-/-}$, data not shown).

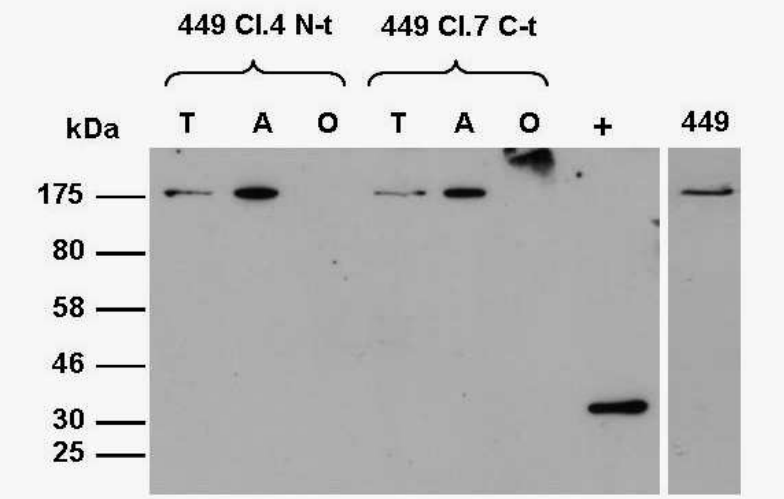

Figure 6.9 – Western blot analysis of cell extracts from clone 449 Cl.4 N-t and 449 Cl.7 C-t. After growth in the presence of the inducer tetracycline, cells were lysed for differential extraction of proteins (Section 2.7.7). Total protein extract (T), enriched aqueous (A) and organic (O) protein fractions were prepared for both clones and probed with the DsRed monoclonal antibody (1:250) and the goat anti-mouse secondary antibody (1:2,000). The positive control (+) is represented by the total cell lysate from a *Leishmania mexicana* line expressing a cytosolic fusion protein containing mCherry (kindly provided by Elmarie Myburgh, University of Glasgow). Total cell lysate from the parental line 449, probed with the same antibody, is shown on the right.

There are a number of potential reasons for the inability to detect our fusion protein. First, low levels of expression of the construct in the clones could have yielded only low amounts of protein (too low to generate a signal in the blot). The unknown mechanism involved in P2 down-regulation *in vitro* could have played a role in this phenomenon. For this reason, total cell lysate from clones grown *in vivo* (where P2 is not down-regulated) was analysed following the same procedure as for *in vitro* cells, but these samples also failed to show the expected protein (data not shown). Extraction of membrane proteins can be difficult; hence the organic fractions (where the fusion protein was expected to be present) were extracted using the non-ionic detergent Triton X-114, resulting in very viscous samples: this hampered both loading and running of the fractions; a smeared signal, stuck inside the well of the polyacrylamide gel of 449 Cl.7 C-t clone (Figure 6.9,

449 Cl.7 C-t clone, lane O) could derive from a protein sample that did not run properly inside the gel.

Western blot analysis, therefore, was inconclusive and failed to demonstrate successful expression of the fusion protein in *T. brucei*, although a low abundant membrane protein might escape detection using these procedures.

6.2.5 Drug sensitivity

Since Western blot analysis failed to demonstrate the successful expression of the *Tb*AT1-mCherry reporter protein, we performed some biological assays as another means to assess functional expression. To determine whether the exogenous *TbAT1* copy was functionally expressed inside the cells, the Alamar Blue assay was performed (Section 2.4). The test allows determination of bloodstream form trypanosome drug sensitivity, which reveals differences depending on the expression of the *Tb*AT1 transporter in the cells. Four drugs were tested: DB75 and diminazene, two diamidines principally dependent on the P2 transporter for their uptake into parasites (Lanteri *et al*., 2006; de Koning *et al*., 2004), pentamidine, another diamidine only partially dependent on P2 activity (de Koning, 2001a), and suramin, a molecule thought to enter the cells by receptor-mediated endocytosis without any interaction with the P2 transporter (Fairlamb, 2003). IC_{50} (half maximal inhibitory concentration) values for the 449-derived lines were measured in the absence of tetracycline, or after addition of the inducer at 1 μg/ml, 48 h before performing the test, in order to obtain complete induction of reporter expression (Wirtz and Clayton, 1995). All transfectant lines were cultivated in the presence or absence (removal was carried out 48 h before the test) of hygromycin, before and during the assay, to monitor possible interaction of this antibiotic with the other drugs or eventual effects on cell growth.

IC_{50} values showed that addition of hygromycin to the medium did not interfere with the activity of the four drugs (Table 6.1), but slightly decreased the cell growth rate of the transfectants compared to the parental line (which was grown in absence of antibiotics). Therefore, to compare the effects of the various drugs on the tested cell lines, only data obtained with clones grown in medium without hygromycin were considered in this discussion.

For all of the transformants it was evident that a significant increase in sensitivity to P2-transported drugs (DB75 and diminazene) was induced compared to the parental line (Table 6.1 and Figure 6.10), suggesting active expression of the exogenous copy (or

copies) of *TbAT1*. For clone 449 Cl.4 N-t (Figure 6.10 A), the IC_{50} value following DB75 treatment was 11.6-fold lower than the value measured for the parental line 449 in the presence of tetracycline, and 2.6-fold lower in case of diminazene treatment. Both differences were statistically significant (P <0.01) by the Student's *t*-test. Increase of sensitivity of the clone compared to the 449 line was much smaller following pentamidine (1.2-fold) and suramin (1.4-fold) incubation. Although the data measured for clone 449 Cl.4 N-t incubated with suramin was found significantly lower (P <0.01) than that of line 449, in the presence of tetracycline, this result was not confirmed by any of the other transformants analysed. The causes of the slightly higher sensitivity to suramin of clone 449 Cl.4 N-t compared to its parental line could be ascribed to a slightly lower growth rate of the clone, or to some other mutational event which could have increased its sensitivity to the drug (especially in the presence of tetracycline). An absence of the inducer tetracycline in the medium resulted in IC_{50} values being very similar between the clone and its parental line, indicating a successful regulation of the system.

Clone 449 Cl.7 C-t (Figure 6.10 C) was also significantly more sensitive to DB75 (6.7-fold lower IC_{50}, P <0.01 by the *t*-test) and diminazene (5.7-fold lower IC_{50}, P <0.001) compared to line 449, in the presence of tetracycline. The clone was only 1.3-fold more sensitive to pentamidine than 449 and did not show any significant difference with the parental line after suramin treatment. This clone transfected with the C-t construct appeared to have a worse regulation compared to clone 449 Cl.4 N-t and, even in the absence of tetracycline, it still maintained higher sensitivity towards DB75 (P <0.01), diminazene (P <0.001) and pentamidine (P <0.05) than 449 line. This result could be explained by lessened control at the tetracycline-responsive site, or by different levels of transcription between rRNA spacers or other possible integration sites. Variability between phenotypes of different clones is a common phenomenon and it has already been observed in bloodstream transfectants (Biebinger *et al*., 1996).

For *tbat1*$^{-/-}$-derived lines (Figure 6.10 B and D), the absence of the endogenous P2 background resulted in more significant differences between transfectant and parental IC_{50} values. *tbat1*$^{-/-}$ Cl.6 N-t was 85.2-fold more sensitive to DB75 treatment than *tbat1*$^{-/-}$ cell line (P <0.001) and 14.5-fold to diminazene (P <0.01). Clone *tbat1*$^{-/-}$ Cl.9 C-t showed a similar trend, resulting in its being 117.1-fold more sensitive to DB75 and 27.2 to diminazene than *tbat1*$^{-/-}$ (P <0.001 in both cases). Differences between transfectants and parental line drastically diminished following pentamidine treatment and disappeared following suramin incubation for both *tbat1*$^{-/-}$-derived clones.

Compound	IC_{50} (nM)							
	449	**449 Cl.4 N-t**				***tbat1*$^{-/-}$**	***tbat1*$^{-/-}$ Cl.6 N-t**	
		+Hyg +Tet	+Hyg -Tet	-Hyg +Tet	-Hyg -Tet		+Hyg	-Hyg
DB75	0.81 ± 0.49	0.04 ± 0.03**	0.92 ± 0.74	0.07 ± 0.06**	0.49 ± 0.17	35.79 ± 6.20	0.70 ± 0.45***	0.42 ± 0.34***
Diminazene	21.18 ± 5.36	3.72 ± 0.60***	19.08 ± 5.39	8.16 ± 7.79**	19.10 ± 2.73	139.93 ± 31.10	12.36 ± 3.01**	9.62 ± 0.78**
Pentamidine	0.19 ± 0.08	0.07 ± 0.03**	0.13 ± 0.12	0.16 ± 0.15	0.16 ± 0.12	0.25 ± 0.03	1.08 ± 0.72*	0.29 ± 0.08
Suramin	9.19 ± 0.80	7.65 ± 1.95*	7.88 ± 3.06	6.78 ± 1.22**	7.82 ± 3.14	7.74 ± 1.43	7.66 ± 2.16	7.30 ± 1.05

Compound	IC_{50} (nM)							
	449	**449 Cl.7 C-t**				***tbat1*$^{-/-}$**	***tbat1*$^{-/-}$ Cl.9 C-t**	
		+Hyg +Tet	+Hyg -Tet	-Hyg +Tet	-Hyg -Tet		+Hyg	-Hyg
DB75	2.29 ± 1.17	0.59 ± 0.72**	0.27 ± 0.10**	0.34 ± 0.17**	0.50 ± 0.35**	49.20 ± 11.22	0.87 ± 0.31***	0.42 ± 0.32***
Diminazene	25.47 ± 7.87	4.57 ± 2.07***	8.01 ± 2.31***	4.49 ± 1.71***	7.35 ± 2.22***	244.90 ± 61.08	13.24 ± 2.38***	9.02 ± 2.72***
Pentamidine	0.32 ± 0.15	0.19 ± 0.10	0.17 ± 0.10*	0.24 ± 0.15	0.16 ± 0.09*	0.73 ± 0.12	0.16 ± 0.05***	0.54 ± 0.37
Suramin	10.69 ± 2.10	11.03 ± 0.68	10.94 ± 4.64	11.25 ± 1.00	9.83 ± 3.48	11.42 ± 3.92	8.82 ± 1.67	11.37 ± 1.86

Table 6.1 – Drug sensitivity of four transfectant lines to different trypanocidal drugs.
Half maximal inhibitory concentration (IC_{50} value) was measured for the four clones under analysis and their parental lines (449 and *tbat1*$^{-/-}$) by the Alamar Blue assay (Section 2.4) following 72 h exposure to four trypanocidal drugs (DB75, diminazene, pentamidine and suramin).
Sensitivity of the 449-derived clones (449 Cl.4 N-t and 449 Cl.7 C-t) was assessed in the presence or absence of the inducer tetracycline (Tet, 1 μg/ml) added to the cell culture 48 h before performing the test. Effects on IC_{50} values of the presence of the selective antibiotic hygromycin (Hyg, 10 μg/ml) were also evaluated for 449-derived clones and *tbat1*$^{-/-}$-derived clones (*tbat1*$^{-/-}$ Cl.6 N-t and *tbat1*$^{-/-}$ Cl.9 C-t): Hyg was normally present in the culture medium used for clones growth and it was eventually eliminated 48 h before the test.
Data are reported ± the standard deviation and represent the mean of at least three independent experiments. Statistical differences between the IC_{50} values found for each clone (in every condition tested) and those of the corresponding parental line were calculated by the unpaired, one-tailed Student's *t*-test. The levels of significance were: * *P* <0.05; ** *P* <0.01; * *P* <0.001.**

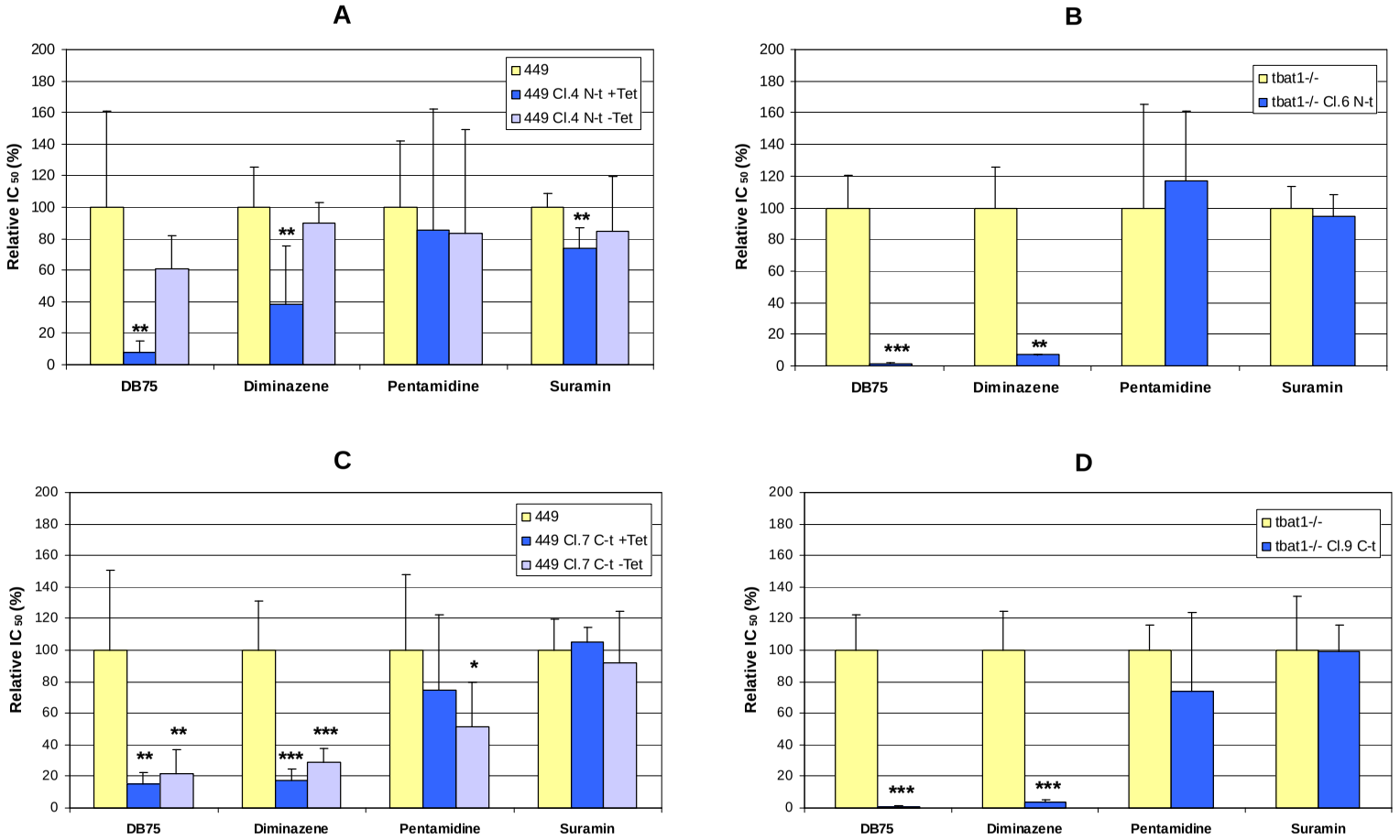

Figure 6.10 – Sensitivity of four clones and their parental lines to four different trypanocidal drugs.
Sensitivity of clones 449 Cl.4 N-t (A), *tbat1*$^{-/-}$ Cl.6 N-t (B), 449 Cl.7 C-t (C) and *tbat1*$^{-/-}$ Cl.9 C-t (D) is expressed as IC_{50} values relative to the corresponding parental line (449 or *tbat1*$^{-/-}$), considered as 100%. 449-derived clones were grown in the presence or absence of the inducer tetracycline (Tet, 1 µg/ml). Transfectants were grown in absence of hygromycin in the medium from 48 h before the test. Data are shown ± the standard deviation and represent the mean of three independent experiments. Statistical differences between the IC_{50} values of each clone and those of the corresponding parental line were calculated by the unpaired one-tailed Student's *t*-test and are indicated by asterisks. The levels of significance were: * *P* <0.05; ** *P* <0.01; * *P* <0.001.**

In conclusion, the drug sensitivity data were consistent with successful and inducible expression of the reporter gene. Furthermore, it appeared that both N-terminal and C-terminal fusions were functional, which indicated neither terminus played a role in the transport process of the P2 permease.

6.2.6 Fluorescence microscopy

The Alamar Blue results indicated that the exogenous copy of the *TbAT1* gene was actively expressed and functional, but these data did not give any indications concerning the expression of the fused mCherry protein. To assess expression of the genetically encoded fluorescent protein inside trypanosomes all of the clones were analysed by fluorescence microscopy. The microscopy study was also expected to reveal the subcellular distribution of the fused protein and, therefore, of the P2 amino-purine transporter, which represented the final aim of this work.

6.2.6.1 Fluorescence of clones grown *in vitro*

In vitro transfectants were viewed under the Zeiss Axioplan fluorescence microscope using the DsRed filter (λ_{EX}=545 nm, λ_{EM}=605 nm), which matched the recommended wavelengths for the mCherry protein (Shaner *et al*., 2005). For 449-derived clones, construct expression was induced with tetracycline (1 μg/ml) 48 h before viewing. Initial screening of live *in vitro* parasites revealed a very low and hardly detectable fluorescence for all of the clones. Nevertheless, fluorescence levels of the transfectants appeared higher compared to the autofluorescence shown by parental 449 and *tbat1*$^{-/-}$ lines (no images were acquired, since fast cell movement hampered the exposure to the camera for prolonged times).

Due to this low fluorescence of the clones, long times of exposure were necessary in order to acquire images and, therefore, cells needed to be fixed. Various fixatives were tested. Immersion in MeOH overnight did not give clear samples for microscopy and the use of 2.5% glutaraldehyde was found responsible to induce a high autofluorescence in both clones and parental lines upon DsRed filter excitation (see Sections 2.5.2.3 and 2.5.2.4 for fixation procedures). The induction of autofluorescence by glutaraldehyde is a problem known in the literature and, apparently, is due to formation of cross-links of the fixative with the ε-amino groups of lysine residues on proteins (Collins and Goldsmith, 1981; Choromanski, 1984). The fact that glutaraldehyde had been successfully used in our laboratory for fixation of *T. b. gambiense* cells (stib 386 and Eliane) for fluorescence

microscopy studies (Paul Capewell, University of Glasgow, personal communication) could be due to their different composition in the external protein coat compared to the 427-derived strains used here (for example, different VSGs might be expressed). For our experiments, fixation in 3% formaldehyde (Section 2.5.2.5) provided the best samples for microscopy, without inducing cell autofluorescence, and was, therefore, used to fix the clones and parental lines under study for image acquisition. Fixed trypanosomes were viewed immediately or the day after fixation, since a deterioration of the samples was observed within a week after their preparation.

Images acquired using long exposure times for the camera (1.8 s) allowed capture of the low fluorescence from trypanosomes (Figure 6.11). All transfectants examined had a relative higher emission compared to their parental lines, for which only a very low autofluorescence could be detected. Quantitative measurement of the percentage of fluorescence intensity for one of the clones analysed (449 Cl.4 N-t) revealed that its emission was just double the autofluorescence of the 449 line (Figure 6.12). However, it is also noteworthy that the threshold used for quantification of cells fluorescence had to be changed for the parental 449 line in order to exclude its high background. Due to the even lower emission of *tbat1*$^{-/-}$-derived clones, it was not possible to obtain fluorescence measurements for these lines.

Comparison of the fluorescence micrographs of transfectants and their parental lines (Figure 6.11) showed that, in general, *tbat1*$^{-/-}$-derived clones had a lower fluorescence than 449-derived cells and clones expressing the C-t construct yielded a lower emission than the corresponding parasites transfected with the N-t vector. Nevertheless, each transfectant line had internal variability and fluorescence levels varied among cells from the same clone. The difference in fluorescence emission of the various transfectants compared to their parental lines suggested expression of the fluorescent mCherry protein, albeit at very low levels. Moreover, each clone's fluorescence appeared to be associated with the plasma membrane, as expected for the transmembrane transporter protein P2. The signal showed a patchy distribution throughout the whole cell body, but was not present in the flagellum. The clones transfected with the C-t construct (derived from both 449 and *tbat1*$^{-/-}$ lines) often demonstrated one (or more) large and bright fluorescent spot(s), in a region between the nucleus and the flagellar pocket. Since the endomembrane system is located in this area of the cell (Field *et al*., 2007), it could be possible that these fluorescent dots identified with mature or intermediate forms of the fusion protein accumulated inside vesicles, before their transport to the plasma membrane. The P2 transporter might, then, be redistributed to

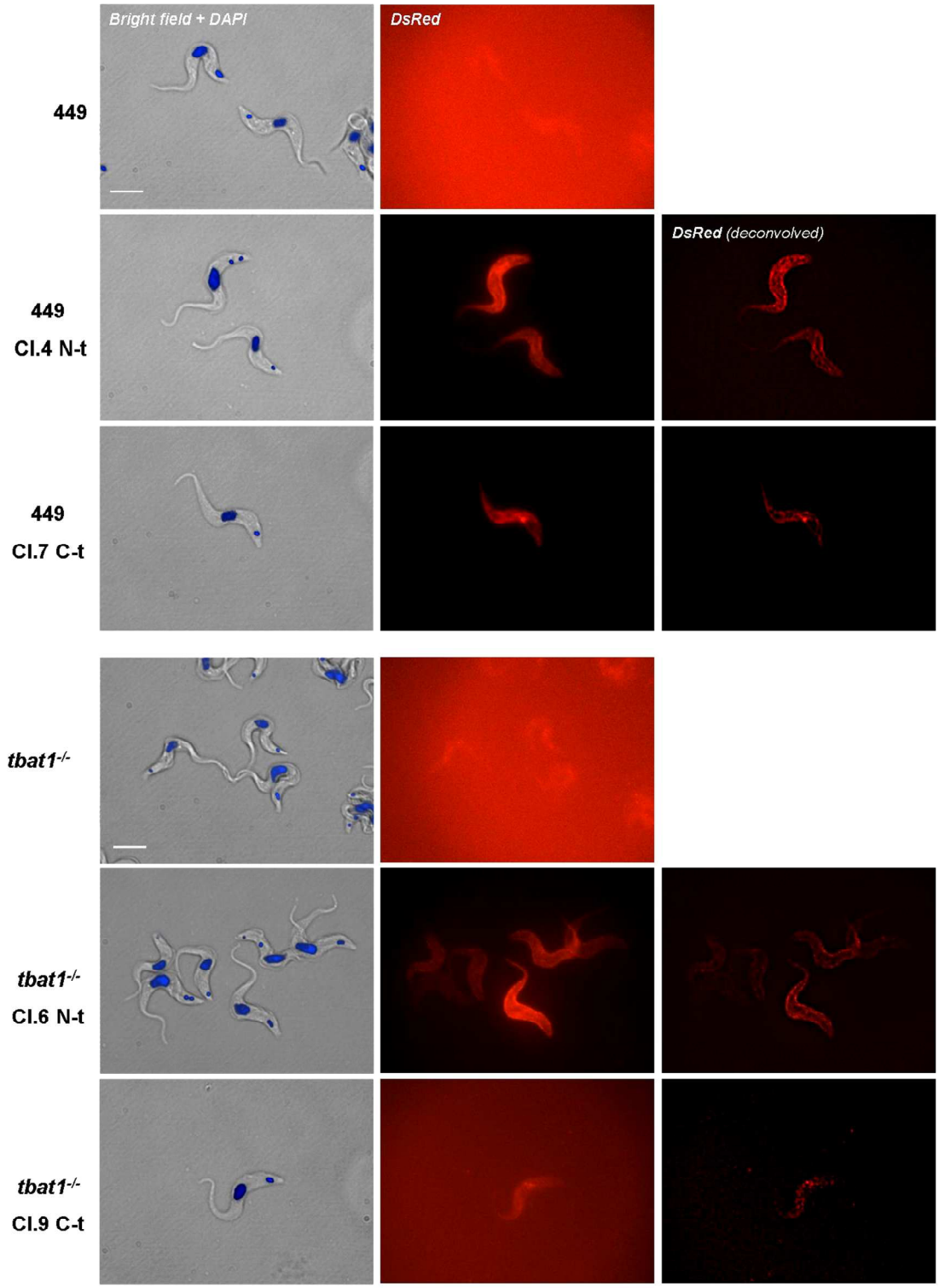

Figure 6.11 – Fluorescence images of four *in vitro*-grown clones expressing the P2 transporter fused with the mCherry fluorescent protein.
Strain 449-derived clones were induced with 1 μg/ml tetracycline 48 h before microscopy examination. After fixation in formaldehyde all cells were excited under the DsRed filter of the Zeiss Axioplan microscope. Parental cell lines (449 and *tbat1*$^{-/-}$) were processed as their derived clones in order to compare their autofluorescence level. Acquired fluorescent images (centre) were deconvolved (right) using the iterative restoration program of Volocity Imaging software (Improvision). Bright field images counterstained with DAPI, to identify the position of the nucleus and the kinetoplast, are shown on the left.
DsRed 1.8 s exposure; 100× objective. Bar: 10 μm.

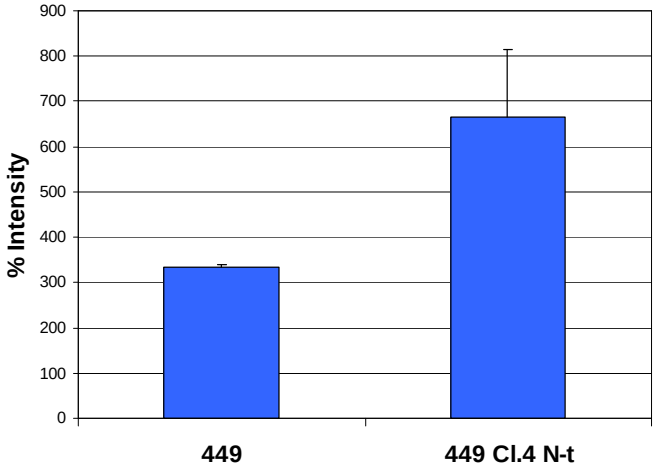

Figure 6.12 – Percentage of fluorescence intensity measured for clone 449 Cl.4 N-t. Emission of the clone is compared to the autofluorescence measured for its parental 449 line under the same experimental conditions. Samples of both cell lines were fixed in formaldehyde. Clone 449 Cl.4 N-t was incubated with 1 µg/ml tetracycline, 48 h before microscopy, to induce expression of the fusion protein mCherry::*Tb*AT1. Fluorescence intensity of 100 cells for each line was measured using the Volocity software quantitation package (Improvision) upon DsRed filter excitation of the Zeiss Axioplan microscope.

the cell surface from these cytosolic stocks, following specific external stimuli, a phenomenon already observed for other protozoan membrane proteins such as the proteins associated with differentiation of *T. brucei* (Dean *et al*., 2009) and the polyamine transporter TcPOT1.1 of *T. cruzi* (Hasne *et al*., 2010). Nevertheless, the fact that this pattern was much less frequent inside N-t clones supported the hypothesis that the C-t tagging of the P2 transporter interfered with its distribution to the targeted cell membrane, leading to the accumulation of the fusion protein inside an intermediate vesicle.

6.2.6.2 Fluorescence of clones grown *in vivo*

The low fluorescence of *in vitro* transfectants could have been caused by unsuccessful transcription of the constructs containing the fused *TbAT1-mCherry* sequence. Trypanosomes, however, are known to regulate gene expression mainly at the post-transcriptional level, rather than by modulating transcriptional activity (Berberof *et al*., 1995). Other downstream regulatory mechanisms (such as mRNA stability or protein folding and distribution), could have contributed to the low levels of fluorescence. Various uptake assays carried out in our laboratory demonstrated a significant down-regulation of the P2 transporter activity in *in vitro* cells compared to parasites grown in rodents (Section 6.1.2). Therefore, the fluorescence of *in vivo*-grown transfectants was studied, in order to exclude possible endogenous down-regulation mechanisms interfering with our construct expression.

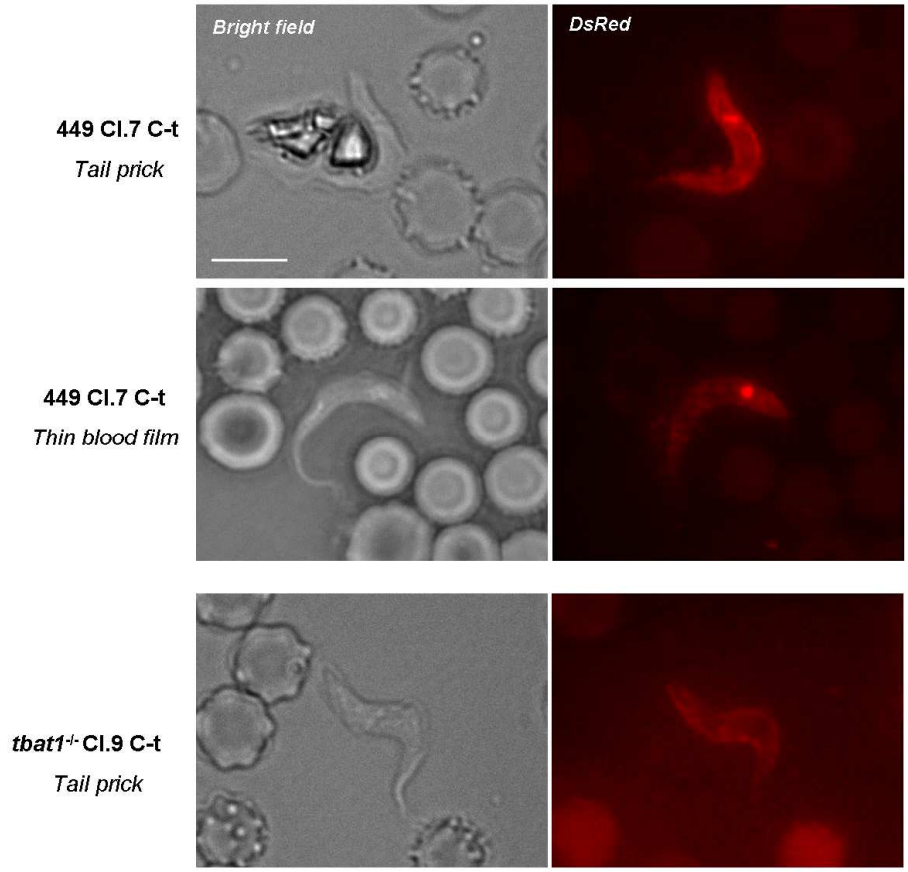

Figure 6.13 – Fluorescence images of two C-t clones expressing the *Tb*AT1::mCherry fusion protein and grown in mice.
Water containing doxycycline (200 μg/ml) in a 5% sucrose solution was given to mice infected with 449-derived clone in order to induce the transcription of the transfected C-t construct (Wirtz *et al*., 1998). Tail prick samples were obtained 3 days post-infection, while the blood smears were prepared 4 days post-infection (Section 2.3 for procedures). All samples were viewed under the DsRed filter of the Zeiss Axioplan microscope.
DsRed 1.0 s exposure; 100× objective. Bar: 10 μm.

Two clones transfected with the C-t construct (449 Cl.7 C-t and *tbat1*$^{-/-}$ Cl.9 C-t) were injected into ICR mice by Dr. P.E. Wong. To induce the expression of the system in the 449-derived clone, 200 μg/ml doxycycline (a water soluble form of tetracycline) were added to the drinking water of the mouse infected with this transfectant line (Wirtz *et al*., 1998; Krieger *et al*., 2000). Both clones were able to infect mice, but while the *tbat1*$^{-/-}$-derived line reached a very high parasitaemia four days post-infection, the 449-derived clone remained at a low concentration. Fluorescence intensity of parasites in blood samples (Figure 6.13) was, however, very similar to their fluorescence observed in *in vitro*-grown trypanosomes (Figure 6.11). The *tbat1*$^{-/-}$- derived clone, especially, had an extremely faint emission, which hampered image acquisition. In the 449 Cl.7 C-t line, the fluorescent dot already observed in formaldehyde-fixed cells, was clearly visible in the posterior part of the cell. The low levels of fluorescence obtained for both *in vitro* and *in vivo* transfectants indicated that they could be more likely ascribed to the chosen expression system rather than to other parasitic regulatory mechanisms.

6.3 Discussion

The main aim of this molecular biology project was to tag the P2 amino-purine transporter with a fluorescent protein, in order to localise it inside trypanosomes by fluorescence microscopy. Two tetracycline-inducible constructs were built by linking the red fluorescent protein mCherry either at the N-terminus or C-terminus of the *TbAT1* gene, which encodes the transporter. Constructs were transfected into bloodstream form 449 (a transgenic line expressing the tetracycline repressor) (Biebinger *et al*., 1997) and into the *tbat1*$^{-/-}$ line, which lacks both alleles of the *TbAT1* gene (Matovu *et al*., 2003) and in which we expected to have a constitutive expression of the constructs. Unfortunately, microscopy experiments showed very low fluorescence intensity yields for all of the transfectant lines, thus making them unsuitable for more thorough localisation studies.

The lack of bright fluorescence emission of the mCherry protein could be ascribed to various factors. First of all, the change of the amino acid at position 22 (His^{22}→Asn) of the mCherry protein for C-t tagging (Figure 6.2) could have altered the phenotype of the mature protein, since this residue was one of the mutations introduced during its generation (Shaner *et al*., 2004). This hypothesis, though, was not supported by fluorescence microscopy (Figure 6.11), which showed equally low levels of emission for the C-t and the N-t construct (which did not have this mutation). Despite being indicated as another critical residue (Shaner *et al*., 2004), the other amino acid change at position 8 (Asp^{8}→Asn) of both N-t and C-t mCherry products, was not expected to affect the phenotype of the mature fluorescent protein, since this particular mutation was also present in the sequence of other mCherry proteins successfully used to build fusion constructs (Elmarie Myburgh, University of Glasgow, personal communication).

Another possible explanation for our result could be the use of an unsuitable expression system. Vector pHD676 was chosen in order to control the transcription of the fused *Tb*AT1-mCherry protein, avoiding the problems of mislocalisation and assembly into non-physiological complexes often encountered with over-expressed tagged proteins (Shen *et al*., 2001; Shahi *et al*., 2002). The use of this vector, however, could have been responsible for low levels of fused protein, affecting the overall fluorescence signal. The PARP promoter, which drives the expression of the exogenous constructs in pHD676, is known to be down-regulated in bloodstream forms once integrated within the rRNA spacer or in other genomic sites, and this could have contributed to low expression (Biebinger *et al*., 1996). Nevertheless, in trypanosomes gene expression is mostly regulated at the post-

transcriptional level, rather than by modulation of transcription (Berberof *et al*., 1995). The choice of another vector containing different untranslated regulatory regions (UTR) encoding for trans-splicing and polyadenylation signals (such as VSG 3'UTR), could have a significant impact on the levels and stability of the transcribed mRNA and therefore, on the overall expression of the exogenous genes. Instability of the two fused proteins could be another possible cause for the low fluorescence shown by our clones. The presence of the tagged P2 transporter could have prevented correct folding of the mCherry protein to its mature form, disrupting its fluorescent properties.

Despite unsatisfactory fluorescence intensity emission shown by the clones, various data indicated that the phenotype of transfectants differed from that of the parental lines. The additional copy(ies) of the *TbAT1* gene introduced by transfection appeared to be actively expressed, as shown by the Alamar Blue data (Table 6.1). Hence, it was reasonable to expect that the whole construct (*mCherry*::*TbAT1* or *TbAT1*::*mCherry*) was correctly transcribed and translated, although the precise targeted genomic region remained unclear for the clones analysed (Section 6.2.3). However, we could not detect the mCherry protein inside cell lysates (Figure 6.9), indicating that the protein was not produced or that its levels inside parasites were under detection limits of the Western analysis performed. The fused mCherry protein yielded very low fluorescence emission, but direct comparison by fluorescence microscopy with the parental lines revealed, for all of the clones, a higher signal than the autofluorescence of cell lines 449 and *tbat1*$^{-/-}$ (Figure 6.11). The emission observed in fixed transfectants, moreover, showed a staining pattern at the cell periphery, consistent with a membrane distribution. If this signal was indeed derived from the mCherry-tagged transporter, we can conclude that the P2 carrier localises all along the trypanosome cell body, in a patchy pattern, and it is not present in the flagellum of the cells. In various clones (especially transfectants containing the C-t construct) one, or more, large, fluorescent spots were detected in the posterior part of the cell, in an area between nucleus and kinetoplast. These fluorescent dots could correspond to immature forms of the protein contained inside cell compartments, such as vesicles of the Golgi apparatus or the endoplasmic reticulum; alternatively, they could represent unprocessed proteins not correctly expressed. Another option would be that these spots represent stocks of the mature form of the P2 transporter, accumulated inside vesicles, ready to be redistributed to the cell surface, in response to changes in the parasite's external environment. This mechanism had already been observed for other parasitic membrane proteins, whose distribution was found to shift from an area corresponding to (or adjacent to) the flagellar pocket, to the cell surface, as a result of thermal (Dean *et al*., 2009) or metabolic (Hasne *et*

al., 2010) stimuli. The presence of sequestered stocks of P2 in the clones analysed during this work would be in agreement with the fact that these cells were *in vitro*-grown parasites, which, as mentioned above (Section 6.1.2), show a relatively low P2 activity. Nevertheless, three observations contrasted with this model: (1) the spots evidenced by fluorescence microscopy were mainly observed in parasites transfected with the C-t construct, suggesting a defective expression of this vector (for example, an eventual signal associated to the C-terminus of *TbAT1* and directing the transporter to the membrane could have been disturbed by the tag protein); (2) the fluorescent inclusions appeared not only in *in vitro* parasites but also in *in vivo* cells, in which the P2 transporter is expected to be highly expressed on the cell surface; (3) the spots appeared generally closer to the nucleus than to the flagellar pocket, therefore strengthening the hypothesis of an immature form of the protein stuck in some early vesicle of the endosomal system. A series of studies carried out on *Leishmania* species demonstrated that these parasitic protozoa cope with purine starvation by upregulating nucleoside transporter proteins at a post-transcriptional level, primarily by enhancing translation, without modifying protein turnover (Carter *et al*., 2010; Ortiz *et al*., 2010). A similar control mechanism of expression can not be ruled out for the P2 transporter of *T. brucei*, but further study will be required to verify this hypothesis.

The fluorescent tagging approach used during this project to build a fluorescent P2 amino-purine transporter, has left a series of questions, making it difficult to draw solid conclusions. It would be interesting to study the expression of the *Tb*AT1-mCherry fused protein in a different over-expression vector, to try and enhance levels of expression, or to tag the transporter with a different fluorescent protein (such as the Green Fluorescent Protein) to rule out possible problems related to the specific tagging gene. Different approaches for protein detection could also be pursued. Previous work carried out in our laboratory already attempted, unsuccessfully, to generate and express a fusion construct containing a Myc-tagged *TbAT1* sequence (Bridges, 2006). A more interesting approach would be to epitope-tag the *TbAT1* gene at its endogenous chromosomal locus, in order to mimic more closely its expression regulation under physiological conditions (Shen *et al*., 2001).

7

General discussion

Accurate and early diagnosis of human African trypanosomiasis is paramount both for interrupting the progression of this deadly disease in the patient and for stopping the transmission cycle of the parasite. Nevertheless, the diagnostic tools available for use in HAT endemic countries remain inaccurate and inadequate, leading to misdiagnosis and under-detection. Despite the enormous progress made by the academic world in the field of molecular parasitology, this knowledge has only had a minor impact on the work of health personnel in rural areas of Africa (Brun and Balmer, 2006). Nowadays, the identification of *T. b. gambiense* infected individuals still relies on the activity of mobile teams, whose equipment consists in a thirty-year-old serological test (the CATT test), used to rapidly screen the population at risk, and on basic light microscopes, used to confirm the infection (Chappuis *et al*., 2005). The urgent need for better diagnostics which are cheap and robust, but also rapid and user-friendly is hindered both at the development stage, due to the perspective of low return on investment for commercial companies, but also during the phase of field application, because of the lack of resources and of trained personnel, the underdeveloped health care system and the remoteness of many endemic foci. The recent institution of public-private partnerships (above all the Foundation for Innovative New Diagnostics, FIND) aims at the identification and implementation of diagnostics for neglected diseases and is hopefully destined to change this state of affairs (Steverding, 2006).

Parasitological examination represents the weak point in the *T. b. gambiense* HAT diagnostic algorithm (Lutumba *et al*., 2005). Conventional light microscopy techniques are insensitive, time-consuming and inadequate for use in screening programmes. A series of new, highly sensitive and specific molecular diagnostic approaches are currently under study and, in the future, might replace the inefficient methods utilised today (Radwanska, 2010). Although the introduction in the field of relatively sophisticated technologies (in particular PCR techniques) has been slow, their evolution into practical solutions offers concrete potential. The loop-mediated isotermal amplification (LAMP) reaction (Njiru *et al*., 2008b) and the lateral flow test (dipstick) (Deborggraeve *et al*., 2006) are two examples of these attempts to simplify diagnostics.

The introduction of fluorescence technologies in HAT endemic countries is another option to improve the efficiency of the parasitological confirmation step. The advantages offered by fluorescence microscopy over conventional light microscopy in terms of increased sensitivity and gain in reading time have been reported in many studies on other tropical infectious diseases (Keiser *et al*., 2002; Steingart *et al*., 2006) and have been confirmed in

fields trials (Torrea *et al*., 2008). The use of fluorescence for diagnosis of trypanosomiasis is not new, as it has already been applied in the sensitive, but expensive, quantitative buffy coat assay (Bailey and Smith, 1992). The real innovation is represented by the development of new LED light sources suitable for fluorescence imaging, which allow the design of instruments that are more compact, energetically efficient and cheaper than conventional ones (Jones *et al*., 2005 and 2007). All of these characteristics make LED-illuminated instruments ideal for use by mobile teams, and not exclusively of reference health centres.

A preliminary evaluation of diverse fluorophores and staining protocols to use with LED fluorescence microscopes for trypanosomiasis diagnosis was the main aim of this project. Fluorescent staining of parasites with acridine orange proved to be a very straightforward and fast procedure for labelling trypanosomes in both fresh and fixed specimens. The emission of this fluorophore could be easily detected using the SMR LED microscope manifactured by Cytoscience, making their use immediately available for field testing. Also the diamidine DB75 appeared to be a very interesting probe for trypanosome diagnosis. Its utilisation as a vital dye or to stain fixed specimens proved particularly effective in blood samples and its excitation under a UV LED light source was excellent. Of note, the procedures followed for preparation of fluorescent specimens were extremely easy to perform and did not require specialist skills. Furthermore, the LED microsocopes used during this project proved to be user-friendly and efficient. Future work will have to validate the use of LED fluorescence microscopy on human samples and under field conditions, where researchers will have to pay particular attention on how to preserve reagent stability and how to create a dark/dim environment in which to perform microscopy (in case of outdoor use).

The exploitation of surface transporters peculiar to trypanosomes appeared an useful and straightforward way to specifically target fluorophores to these parasites and improved compounds may be developed following this approach. In the future, then, the synthesis of more efficient and specific fluorescent molecular markers for trypanosomes may allow not just parasite detection, but also speciation (Radwanska *et al*., 2002c). Moreover, the use of fluorescent probes could be extremely useful for other aspects of disease management, as demonstrated by the arsenical drug resistance test developed in our laboratory (Stewart *et al*., 2005). Finally, the potential positive impact that fluorescence microscopy applications could have in the management of African animal trypanosomiasis, for which the diagnostic problems are very similar to those encountered for HAT, should not be underestimated.

Although the introduction of fluorescence microscopy in the field would bring significant advantages, potentially reducing the workload of microscopists and making HAT diagnosis more reliable, it will not be sufficient to detect all cases. This technique will not increase the theoretical detection limit of conventional light microscopy (Radwanska, 2010) and, due to the low parasite loads typical of this disease, a sample concentration step will still be required. Efforts have already been made to improve the format and the efficacy of the most sensitive concentration technique available, the mAECT (Büscher *et al*., 2009; Camara *et al*., 2010). In the future, microfluidics technologies might help in the separation and concentration of parasites from blood (Huang *et al*., 2004), making this procedure faster and more efficient.

The crucial importance of the parasitological examination step originates from the necessity to confirm the result of serological tests (mainly the CATT test), which are ideal for mass screening, but not specific or sensitive enough to allow decisions for treatment (Chappuis *et al*., 2005). Various laboratories are, today, very active in the search for new serodiagnostic markers for HAT, with the aim of designing a more specific alternative to the CATT test, but an antigen detection test for trypanosomes, despite being highly advocated, has not been developed yet (Radwanska, 2010). Recent advances in genomics, proteomics and metabolomics may enable the identification of new trypanosome markers to exploit in serodiagnosis. Another very interesting application of these last two technologies is their use in the identification of specific host fingerprints, to utilise as indicators of disease (Agranoff *et al*., 2005; Wang *et al*., 2008). Surrogate biomarkers of infection are also under evaluation for trypanosomiasis staging, a very problematic step in HAT diagnosis, for which the only specific diagnostic test is currently represented by the detection of trypanosomes in the CSF (Lejon and Büscher, 2005). The design of a non-invasive serological test, that does not require a dangerous and painful lumbar puncture to stage the disease, would be a great improvement in HAT field diagnostics (Lejon *et al*., 2006). Moreover, this increasing number of informations will hopefully bring to the development of a serological test for *T. b. rhodesiense*, which is still lacking.

During the last decade a coordinated and efficacious use of the, although limited, tools available (both diagnostic and therapeutic) has determined a decline in the number of HAT cases (Barrett, 2006). The introduction of new diagnostics and the amelioration of the tests already in use would certainly accelerate this process. The validation of better tools will also provide HAT health personnel of adequate instruments to face future challenges. In particular, the perspective of a decrease of HAT prevalence will require the use of always

more specific assays, while the foreseen overlap of *T. b. gambiense* and *T. b. rhodesiense* infections in Uganda will require tests able to differentiate between the two subspecies, in order to decide for appropriate treatment regimen. Together with significant improvements in patient management and disease control, availability of better diagnostics will also have positive effects on other aspects of HAT research and surveillance, such as patients recruitment for drug trials, epidemiological studies, evaluation of interventions and monitoring of drug resistance onset. Finally, simplification of diagnostic tests and procedures might help to move from expensive, active case-finding programs, carried out by specialised teams, towards a more incisive participation of the local health care system, improving the overall sustainability of HAT intervention policies (Checchi *et al*., 2006).

Appendices

Appendix A: HMI-9 medium (pH 7.4)

Components (mg/L)		
Salts, etc	$CaCl_2$	165
	KCl	330
	KNO_3	0.076
	$MgSO_4$	98
	NaCl	4,500
	$NaHCO_3$	3,020
	$NaH_2PO_4 \cdot H_2O$	125
	$Na_2SeO_3 \cdot 5\ H_2O$	0.017
	Glucose	4,500
	Phenol Red	15
	HEPES	5,960
	Bathocuproine sulfonate	28
	Mercaptoethanol	15
L-amino acids	Alanine	25
	Arginine·HCl	84
	Asparagine	25
	Aspartic acid	30
	Cysteine	182
	Cystine	91
	Glutamic acid	75
	Glutamine	584
	Glycine	30
	Histidine·HCl·H_2O	42
	Isoleucine	105
	Leucine	105
	Lysine·HCl	146
	Methionine	30
	Phenylalanine	66
	Proline	40
	Serine	42
	Threonine	95
	Tryptophan	16
	Tyrosine	104
	Valine	94
Vitamins, etc	B12	0.013
	Biotin	0.013
	D-Ca pantothenate	4
	Choline chloride	4
	Folic Acid	4
	i-Inositol	7.2
	Nicotinamide	4
	Pyridoxal·HCl	4
	Riboflavin	0.4
	Thiamine·HCl	4
Organic acids	Pyruvate·Na	114
Purines, etc	Hypoxanthine	136
	Thymidine (deoxy)	39
Lipids & serum	Serum	10%

Appendix B: general buffers and solutions

CBSS buffer (pH 7.4)

Hepes	25 mM
NaCl	120 mM
KCl	5.4 mM
$CaCl_2$	0.6 mM
$MgSO_4 \cdot 7\ H_2O$	0.4 mM
Na_2HPO_4	5.6 mM
D-glucose	11.1 mM

LB medium -Luria Bertani broth- (pH 7)

LB powder (Sigma-Aldrich)	25 g
dH_2O	1 L

LB agar

Luria Agar (Sigma-Aldrich)	35 g
dH_2O	1 L

PBS

NaCl	137 mM
KCl	2.7 mM
Na_2HPO_4	10 mM
KH_2PO_4	2 mM

Phosphate buffer *for Giemsa stain* (pH 7.2)

Na_2HPO_4	20 mM
KH_2PO_4	4.4 mM

PSG buffer (pH 8)

Na_2HPO_4	56.9 mM
NaH_2PO_4	3.9 mM
NaCl	43.5 mM
Glucose	60 mM

TAE buffer (50×) (pH 8.5)

Tris-acetate	2 M
EDTA (pH 8.0)	50 mM

TE buffer

Tris-HCl (pH 8)	10 mM
EDTA (pH 8)	1 mM

Appendix C: buffers and solutions for Southern blot

Denaturation solution

NaCl	1.5 M
NaOH	0.5 M

Denhardt's reagent (50×)

Ficoll 400 (w/v)	1%
Polyvinylpyrrolidone (w/v)	1%
Bovine serum albumin (w/v)	1%

Depurination solution

HCl	0.25 M

Lysis buffer *for gDNA extraction*

Tris-HCl (pH 8)	10 mM
EDTA	100 mM
N-Lauroylsarcosine (w/v)	1%
Proteinase K (added fresh)	100 μg

Neutralising solution

Tris-HCl (pH 7.4)	1 M
NaCl	1.5 M

Prehybridisation/hybridisation solution

Formamide (v/v)	50%
SSC	5×
Denhardt's reagent	10×
SDS (w/v)	0.1%
NaH_2PO_4 (pH 6.5)	20 mM
EDTA (pH 8)	5 mM
Herring sperm DNA (Promega)	200 μg/ml

SSC (20×) (pH 7)

NaCl	3 M
Tri-sodium citrate	0.3 M

Washing solution *for membrane stripping*

SSC	0.1×
SDS (w/v)	0.1%
Tris-HCl (pH 7.6)	0.2 M

Appendix D: buffers and solutions for protein extraction, SDS-PAGE and Western blot

Coomassie Brilliant Blue stain

Coomassie Brilliant Blue (w/v)	0.1%
Methanol (v/v)	45%
Glacial acetic acid (v/v)	10%

Laemmli buffer (2×)

Tris-HCl (pH 6.8)	0.125 M
Glycerol (v/v)	20%
SDS (w/v)	4%
β-mercaptoethanol (v/v)	10%
Bromophenol blue (w/v)	0.003%

Running buffer (5×)

Tris-Base (pH 8.3)	0.125 M
Glycine	0.96 M
SDS (w/v)	0.5%

Running gel (10%)

Tris-HCl (pH 8.8)	0.38 M
SDS (w/v)	0.1%
Acryl/bis 30% (Amresco) (v/v)	10%
Ammonium persulfate (w/v)	0.05%
TEMED (v/v)	0.1%

Stacking gel (3%)

Tris-HCl (pH 6.8)	0.25 M
SDS (w/v)	0.1%
Acryl/bis 30% (Amresco) (v/v)	3%
Ammonium persulfate (w/v)	0.05%
TEMED (v/v)	0.1%

STEN buffer

Sucrose	250 mM
Tris-HCl (pH 7.5)	25 mM
EDTA	1 mM
NaCl	150 mM

Transfer buffer

Tris-base (pH 8.3)	25 mM
Glycine	0.7 M

References

Abel P.M., Kiala G., Lôa V., Behrend M., Musolf J., Fleishmann H., Théophile J., Krishna S. and Stich A. (2004). Retaking sleeping sickness control in Angola. *Trop. Med. Int. Health* **9** (1):141-148.

Adeoye G.O. and Nga I.C. (2007). Comparison of quantitative buffy coat technique (QBC) with Giemsa-stained thick film (GTF) for diagnosis of malaria. *Parasitol. Int.* **56** (4):308-312.

Afewerk Y., Clausen P.H., Abebe G., Tilahun G. and Mehlitz D. (2000). Multiple-drug resistant *Trypanosoma congolense* populations in village cattle of Metekel district, north-west Ethiopia. *Acta Trop.***76** (3):231-238.

Agbe A. and Yielding K.L. (1995). Kinetoplasts play an important role in the drug responses of *Trypanosoma brucei*. *J. Parasitol.* **81** (6):968-973.

Agranoff D., Stich A., Abel P. and Krishna S. (2005). Proteomic fingerprinting for the diagnosis of human African trypanosomiasis. *Trends Parasitol.* **21** (4):154-157.

Akobeng A.K. (2007). Understanding diagnostic tests 1: sensitivity, specificity and predictive values. *Acta Paediatr.* **96** (3):338-341.

Alibu V.P., Richter C., Voncken F., Marti G., Shahi S., Renggli C.K., Seebeck T., Brun R. and Clayton C. (2006). The role of *Trypanosoma brucei* MRPA in melarsoprol susceptibility. *Mol. Biochem. Parasitol.* **146** (1):38-44.

Altman D.G. and Bland J.M. (1994a). Diagnostic tests 1: sensitivity and specificity. *BMJ* **308** (6943):1552.

Altman D.G. and Bland J.M. (1994b). Diagnostic tests 2: predictive values. *BMJ* **309** (6947):102.

Anonymous (2007). Neglected diagnostics. *Nat. Methods* **4** (11):877-878.

Anthony R.M., Kolk A.H.J., Kuijper S. and Klatser P.R. (2006). Light emitting diodes for auramine O fluorescence microscopic screening of *Mycobacterium tuberculosis*. *Int. J. Tuberc. Lung Dis.* **10** (9):1060-1062.

Azema L., Claustre S., Alric I., Blonski C., Willson M., Perie J., Baltz T., Tetaud E., Bringaud F., Cottem D., Opperdoes F.R. and Barrett M.P. (2004). Interaction of substituted hexose analogues with the *Trypanosoma brucei* hexose transporter. *Biochem. Pharmacol.* **67** (3):459-467.

Bailey J.W. and Smith D.H. (1992). The use of the acridine orange QBC® technique in the diagnosis of African trypanosomiasis. *Trans. R. Soc. Trop. Med. Hyg.* **86** (6):630.

Baird J.K., Purnomo and Jones T.R. (1992). Diagnosis of malaria in the field by fluorescence microscopy of QBC® capillary tubes. *Trans. R. Soc. Trop. Med. Hyg.* **86** (1):3-5.

Balasegaram M., Young H., Chappuis F., Priotto G., Raguenaud M.E., Checchi F. (2009). Effectiveness of melarsoprol and eflornithine as first-line regimens for gambiense sleeping sickness in nine Médecins Sans Frontières programmes. *Trans. R. Soc. Trop. Med. Hyg.* **103** (3):280-290.

Baliani A., Bueno G.J., Stewart M.L., Yardley V., Brun R., Barrett M.P and Gilbert I.H. (2005). Design and synthesis of a series of melamine-based nitroheterocycles with activity against trypanosomatid parasites. *J. Med. Chem.* **48** (17):5570-5579.

Banerjee D. and Pal S.K. (2008). Dynamics in the DNA recognition by DAPI: exploration of the various binding modes. *J. Phys. Chem. B.* **112** (3):1016-1021.

Bank H.L. (1988). Rapid assessment of islet viability with acridine orange and propidium iodide. *In Vitro Cell. Dev. Biol.* **24** (4):266-273.

Banoo S., Bell D., Bossuyt P., Herring A., Mabey D., Poole F., Smith P.G., Sriram N., Wongsrichanalai C., Linke R., O'Brien R., Perkins M., Cunningham J., Matsoso P., Nathanson C.M., Olliaro P., Peeling R.W. and Ramsay A., TDR Diagnostics Evaluation Expert Panel (2007). Evaluation of diagnostic tests for infectious diseases: general principles. *Nat. Rev. Microbiol.* **5** (Supp. 11):S17-29.

Barrett M.P. (2006). The rise and fall of sleeping sickness. *Lancet* **367** (9520):1377-1378.

Barrett M.P. and Fairlamb. A.H. (1999). The biochemical basis of arsenical-diamidine crossresistance in African trypanosomes. *Parasitol. Today* **15** (4):136-140.

Barrett M.P. and Gilbert I.H. (2006). Targeting of toxic compounds to the trypanosome's interior. *Adv. Parasitol.* **63**:125-183.

Barrett M.P., Boykin D.W., Brun R. and Tidwell R.R. (2007). Human African trypanosomiasis: pharmacological re-engagement with a neglected disease. *Br. J. Pharmacol*. **152** (8):1155-1171.

Barrett M.P., Burchmore R.J.S., Stich A., Lazzari J.O., Frasch A.C., Cazzulo J.J., Krishna S. (2003). The trypanosomiases. *Lancet* **362** (9394):1469-1480.

Becker S., Franco J.R., Simarro P.P., Stich A., Abel P.M. and Steverding D. (2004). Real-time PCR for detection of *Trypanosoma brucei* in human blood samples. *Diagn. Microbiol. Infect. Dis.* **50** (3):193-199.

Bengaly Z., Kasbari M., Desquesnes M. and Sidibé I. (2001). Validation of a polymerase chain reaction assay for monitoring the therapeutic efficacy of diminazene aceturate in trypanosome-infected sheep. *Vet. Parasitol.* **96** (2):101-113.

Berberof M., Pérez-Morga D. and Pays E. (2001). A receptor-like flagellar pocket glycoprotein specific to *Trypanosoma brucei gambiense*. *Mol. Biochem. Parasitol.* **113** (1):127-138.

Berberof M., Vanhamme L., Tebabi P., Pays A., Jefferies D., Welburn S. and Pays E. (1995). The 3'-terminal region of the mRNAs for VSG and procyclin can confer stage specificity to gene-expression in *Trypanosoma brucei*. *EMBO J.* **14** (12):2925-2934.

Bergeron R.J., Ludin C., Muller R., Smith R.E. and Phanstiel O. (1997). Development of a hypusine reagent for peptide synthesis. *J. Org. Chem.* **62** (10):3285-3290.

Berriman M., Ghedin E., Hertz-Fowler C., Blandin G., Renauld H., Bartholomeu D.C., Lennard N.J., Caler E., Hamlin N.E., Haas B., Böhme W., Hannick L., Aslett M.A., Shallom J., Marcello L., Hou L.H., Wickstead B., Alsmark U.C.M., Arrowsmith C., Atkin R.J., Barron A.J., Bringaud F., Brooks K., Carrington M., Cherevach I., Chillingworth T.J., Churcher C., Clark L.N., Corton C.H., Cronin A., Davies R.M., Doggett J., Djikeng A., Feldblyum T., Field M.C., Fraser A., Goodhead I., Hance Z., Harper D., Harris B.R., Hauser H., Hostetler J., Ivens A., Jagels K., Johnson D., Johnson J., Jones K., Kerhornou A.X., Koo H., Larke N., Landfear S., Larkin C., Leech V., Line A., Lord A., MacLeod A., Mooney P.J., Moule S., Martin D.M.A., Morgan G.W., Mungall K., Norbertczak H., Ormond D., Pai G., Peacock C.S., Peterson J., Quail M.A., Rabbinowitsch E., Rajandream, M.A., Reitter C., Salzberg S.L., Sanders M., Schobel S., Sharp S., Simmonds M., Simpson A.J., Tallon L., Turner C.M.R., Tait A., Tivey A.R., Van Aken S., Walker D., Wanless D., Wang S.L., White B., White O., Whitehead S., Woodward J., Wortman J., Adams M.D., Embley T.M., Gull K., Ullu E.,

Barry J.D., Fairlamb A.H., Opperdoes F., Barrell B.G., Donelson J.E., Hall N., Fraser C.M., Melville S.E. and El Sayed N.M. (2005). The genome of the African trypanosome *Trypanosoma brucei*. *Science* **309** (5733):416–422.

Biebinger S., Rettenmaier S., Flaspohler J., Hartmann C., Peña-Diaz J., Wirtz L.E., Hotz H.R., Barry J.D. and Clayton C. (1996). The PARP promoter of *Trypanosoma brucei* is developmentally regulated in a chromosomal context. *Nucleic Acids Res.* **24** (7):1202-1211.

Biebinger S., Wirtz L.E., Lorenz P. and Clayton C. (1997). Vectors for inducible expression of toxic gene products in bloodstream and procyclic *Trypanosoma brucei*. *Mol. Biochem. Parasitol.* **85** (1):99-112.

Bisser S., Lejon V., Preux P.M., Bouteille B., Stanghellini A., Jauberteau M.O., Büscher P. and Dumas M. (2002). Blood-cerebrospinal fluid barrier and intrathecal immunoglobulins compared to field diagnosis of central nervous system involvement in sleeping sickness. *J. Neurol. Sci.* **193** (2):127-135.

Bisser S., N'Siesi F.X., Lejon V., Preux P.M., Van Nieuwenhove S., Bilenge C.M.M. and Buscher P. (2007). Equivalence trial of melarsoprol and nifurtimox monotherapy and combination therapy for the treatment of second-stage *Trypanosoma brucei gambiense* sleeping sickness. *J. Infect. Dis.* **195** (3):322-329.

Bitonti A.J., McCann P.P. and Sjoerdsma A. (1986). Necessity of antibody response in the treatment of African trypanosomiasis with α-Difluoromethylornithine. *Biochem. Pharmacol.* **35** (2):331-334.

Blum J.A., Zellweger M.J., Burri C. and Hatz C. (2008). Cardiac involvement in African and American trypanosomiasis. *Lancet Infect. Dis.* **8** (10):631-641.

Boibessot I., Turner C.M.R., Watson D.G., Goldie E., Connel G., McIntosh A., Grant M.H. and Skellern G.G. (2002). Metabolism and distribution of phenanthridine trypanocides in *Trypanosoma brucei*. *Acta Trop*. **84** (3):219-228.

Borowy N. K., Fink E. and Hirumi H. (1985). *In vitro* activity of the trypanocidal diamidine DAPI on animal-infective *Trypanosoma brucei brucei*. *Acta Trop.* **42** (4):287-298.

Borst P. and Ouellette M. (1995). New mechanisms of drug resistance in parasitic protozoa. *Annu. Rev. Microbiol.* **49**:427-60.

Bouteille B., Mpandzou G., Cespuglio R., Ngampo S., Peeling R.W., Vincendau P. and Buguet A. (2009). Cerebrospinal fluid B lymphocyte identification for diagnosis and follow-up in human African trypanosomiasis in the field. *Trop. Med Int. Health* **14** (12):1-8.

Boykin D.W. (2002). Antimicrobial activity of the DNA minor groove binders furamidine and analogs. *J. Braz. Chem. Soc.* **13** (6):736-771.

Brickman M.J., Cook J.M. and Balber A.E. (1995). Low temperature reversibly inhibits transport from tubular endosomes to a perinuclear, acidic compartment in African trypanosomes. *J. Cell Sci.* **108** (Pt 11):3611-3621.

Bridges D. (2006). Mechanisms of drug resistance in *T. brucei*; beyond the P2 transporter... PhD Thesis, University of Glasgow.

Bridges D.J., Gould M.K., Nerima B., Maser P., Burchmore R.J.S. and de Koning H.P. (2007). Loss of the high-affinity pentamidine transporter is responsible for high levels of cross-resistance between arsenical and diamidine drugs in African trypanosomes. *Mol. Pharmacol.* **71** (4):1098-1108.

Bromidge T., Gibson W., Hudson K. and Dukes P. (1993). Identification of *Trypanosoma brucei gambiense* by PCR amplification of variant surface glycoprotein genes. *Acta Trop.* **53** (2):107-119.

Brun R. and Balmer O. (2006). New developments in human African trypanosomiasis. *Curr. Opin. Infect. Dis.* **19** (5):415-420.

Brun R., Blum J., Chappuis F. and Burri C. (2009). Human African trypanosomiasis. *Lancet*. **375** (9709):148-159.

Brun R., Schumacher R., Schmid C., Kunz C., Burri C. (2001). The phenomenon of treatment failures in human African trypanosomiasis. *Trop. Med. Int. Health* **6** (11):906-914.

Brunk U.T., Neuzil J. and Eaton J.W. (2001). Lysosomal involvement in apoptosis. *Redox Rep*. **6** (2):91-97.

Buguet A., Bisser S., Josenando T., Chapotot F. and Cespuglio R. (2005). Sleep structure: a new diagnostic tool for stage determination in sleeping sickness. *Acta Trop.* **93** (1):107-117.

Bukachi S.A., Wandibba S. and Nyamongo I.K. (2009). The treatment pathways followed by cases of human African trypanosomiasis in western Kenya and eastern Uganda. *Ann. Trop. Med. Parasitol.* **103** (3):211-220.

Burkard G., Fragoso C.M. and Roditi I. (2007). Highly efficient stable transformation of bloodstream forms of *Trypanosoma brucei*. *Mol. Biochem. Parasitol.* **153** (2):220-223.

Burri C. and Brun R. (2003). Eflornithine for the treatment of human African trypanosomiasis. *Parasitol. Res.* **90** (Supp. 1):S49-52.

Büscher P. and Lejon V. (2004). Diagnosis of human African trypanosomiasis. In: *The Trypanosomiasis* (eds I. Maudlin, P.H. Holmes and M.A. Miles), CABI, Wallingford, pp. 203-218.

Büscher P., Draelants E., Magnus E., Vervoort T. and Van Meirvenne N. (1991). An experimental latex agglutination test for antibody detection in human African trypanosomiasis. *Ann. Soc. Belg. Med. Trop*. **71** (4):267-273.

Büscher P., Mumba Ngoyi D., Kaboré J., Lejon V., Robays J., Jamonneau V., Bebronne N., Van der Veken W. and Biéler S. (2009). Improved models of mini anion exchange centrifugation technique (mAECT) and modified single centrifugation (MSC) for sleeping sickness diagnosis and staging. *PLoS Negl. Trop. Dis.* **3** (11):e471.

Büscher P., Shamamba S.K.B., Mumba Ngoyi D., Pyana P., Baelmans R., Magnus E. and Overmeir C.V. (2005). Susceptibility of *Grammomys surdaster* thicket rats to *Trypanosoma brucei gambiense* infection. *Trop. Med. Int. Health* **10** (9):850-855.

Camara M., Camara O., Ilboudo H., Sakande H., Kaboré J., N'Dri L., Jamonneau V. and Bucheton B. (2010). Sleeping sickness diagnosis: use of buffy coats improves the sensitivity of the mini anion exchange centrifugation test. *Trop. Med. Int. Health* **15** (7):796-799.

Campbell R.E., Tour O., Palmer A.E., Steinbach P.A., Baird G.S., Zacharias D.A. and Tsien R.Y. (2002). A monomeric red fluorescent protein. *Proc. Natl. Acad. Sci. USA* **99** (12):7877-7882, 2002.

Caramello P., Lucchini A., Savoia D. and Gioannini P. (1993). Rapid diagnosis of malaria by use of fluorescent probes. *Diagn. Microbiol. Infect. Dis.* **17** (4):293-297.

Carter N.S. and Fairlamb A.H. (1993). Arsenical-resistant trypanosomes lack an unusual adenosine transporter. *Nature* **361** (6408):173-176.

Carter N.S., Yates P.A., Gessford S.K., Galagan S.R., Landfear S.M. and Ullman B. (2010). Adaptive responses to purine starvation in *Leishmania donovani*. *Mol. Microbiol*. **78**(1):92-107.

Cattand P. (2001). L'epidémiologie de la trypanosomiase humaine africaine: une histoire multifactorielle complexe. *Med. Trop*. **61** (4-5):313-322.

Cattand P., Jannin J. and Lucas P. (2001). Sleeping sickness surveillance: an essential step towards elimination. *Trop. Med. Int. Health* **6** (5):348-361.

Cattand P., Miézan B.T. and de Raadt P. (1988). Human African trypanosomiasis: use of double centrifugation of cerebrospinal fluid to detect trypanosomes. *Bull. World Health Organ.* **66** (1):83-86.

Ceroni P., Laghi I., Maestri M., Balzani V., Gestermann S., Gorka M. and Vogtle F. (2002). Photochemical, photophysical and electrochemical properties of six dansyl-based dyads. *New J. Chem.* **26** (1):66-75.

Chalfie M., Tu Y., Euskirchen G., Ward W.W. and Prasher D.C. (1994). Green fluorescent protein as a marker for gene-expression. *Science* **263** (5148):802-805.

Chappuis F., Loutan L., Simarro P., Lejon V. and Büscher P. (2005). Options for field diagnosis of human African trypanosomiasis. *Clin. Microbiol. Rev.* **18** (1):133-146.

Chappuis F., Stivanello E., Adams K., Kidane S., Pittet A. and Bovier P.A. (2004). Card agglutination test for trypanosomiasis (CATT) end-dilution titer and cerebrospinal fluid cell count as predictors of human African trypanosomiasis (*Trypanosoma brucei gambiense*) among serologically suspected individuals in southern Sudan. *Am. J. Trop. Med. Hyg.* **71** (3):313-317.

Checchi F., Diap G. and Karunakara U. Human African trypanosomiasis. Facing the challenges caused by neglect: the need for new treatment and diagnostics. Médecins Sans Frontières, Campaign for Access to Essential Medicines, Geneva, 2006.

Checchi F., Filipe J.A., Haydon D.T., Chandramohan D. and Chappuis F. (2008a). Estimates of the duration of the early and late stage of gambiense sleeping sickness. *BMC Infect. Dis.* **8**:16.

Checchi F., Filipe J.A.N., Barrett M.P. and Chandramohan D. (2008b). The natural progression of Gambiense sleeping sickness: What is the evidence? *PLoS Negl. Trop. Dis.* **2** (12):e303.

Chen J., Rauch C.A., White J.H., Englund P.T. and Cozzarelli N.R. (1995). The topology of the kinetoplast DNA network. *Cell* **80** (1):61-69.

Chersi A., di Modugno F. and Rosanò L. (1997). Selective "in synthesis" labelling of peptides by fluorochromes. *Biochim. Biophys. Acta* **1336** (1):83-88.

Chollet C., Baliani A., Wong P.E., Barrett M.P. and Gilbert I.H. (2009). Targeted delivery of compounds to *Trypanosoma brucei* using the melamine motif. *Bioorg. Med. Chem.* **17** (6):2512-2523.

Choromanski L. (1984). Comparison of the levels of autofluorescence caused by fixatives in fluorescence assay on trypanosomes. *J. Parasitol.* **70** (6):979-980.

Clausen P.H., Wiemann A., Patzelt R., Kakaire D., Poetzsch C., Peregrine A. and Mehlitz D. (1998). Use of a PCR assay for the specific and sensitive detection of *Trypanosoma* spp. in naturally infected dairy cattle in peri-urban Kampala, Uganda. *Ann. N. Y. Acad. Sci.* **849**:21-31.

Clayton C.E., Estévez A.M., Hartmann C., Alibu V.P., Field M. and Horn D. (2005). Down-regulating gene expression by RNA interference in *Trypanosoma brucei*. *Methods Mol. Biol.* **309**:39-60.

Codjia V., Mulatu W., Majiwa P.A.O., Leak S.G.A., Rowlands G.J., Authié E., d'Ieteren G.D.M. and Peregrine A.S. (1993). Epidemiology of bovine trypanosomiasis in the Ghibe valley, southwest Ethiopia. 3. Occurrence of populations of *Trypanosoma congolense* resistant to diminazene, isometamidium and homidium. *Acta Trop.* **53** (2):151-163.

Cole R.W. and Turner J.N. (2008). Light-emitting diodes are better illumination sources for biological microscopy than conventional sources. *Microsc. Microanal*. **14** (3):243-250.

Collar C.J., Al Salabi M.I., Stewart M.L., Barrett M.P., Wilson W.D. and de Koning H.P. (2009). Predictive computational models of substrate binding by a nucleoside transporter. *J. Biol. Chem.* **284** (49):34028-34035.

Collins J.S. and Goldsmith T.H. (1981). Spectral properties of fluorescence induced by glutaraldehyde fixation. *J. Histochem. Cytochem.* **29** (3):411-414.

Connor R.J. (1992). The diagnosis, treatment and prevention of animal trypanosomiasis under field conditions. In: *Programme for the control of African animal trypanosomiasis and related development: ecological and technical aspects.* Proceedings FAO Animal Production and Health Paper **100**, pp.1-38.

Coppens I., Baudhuin P., Opperdoes F.R. and Courtoy P.J. (1993). Role of acidic compartments in *Trypanosoma brucei*, with special reference to low-density lipoprotein processing. *Mol. Biochem. Parasitol.* **58** (2):223-232.

Coppens I., Levade T. and Courtoy P.J. (1995). Host plasma low density lipoprotein particles as an essential source of lipids for the bloodstream forms of *Trypanosoma brucei*. *J. Biol. Chem.* **270** (11):5736-5741.

Courtin D., Jamonneau V., Mathieu J.F., Koffi M., Milet J., Yeminanga C.S., Kumeso V.K.B., Cuny G., Bilengue C.M.M. and Garcia A. (2006). Comparison of cytokine plasma levels in human African trypanosomiasis. *Trop. Med. Int. Health* **11** (5):647-653.

Courtioux B., Boda C., Vatunga G., Pervieux L., Josenando T., M'Eyi P.M., Bouteille B., Jauberteau-Marchan M.O. and Bisser S. (2006). A link between chemokine levels and disease severity in human African trypanosomiasis. *Int. J. Parasitol.* **36** (9):1057-1065.

Cox A., Tilley A., McOdimba F., Fyfe J., Eisler M., Hide G. and Welburn S. (2005). A PCR based assay for detection and differentiation of African trypanosome species in blood. *Exp. Parasitol.* **111** (1):24-29.

Cox B.A., Yielding L.W. and Yielding K.L. (1984). Subcellular localisation of photoreactive ethidium analogs in *Trypanosoma brucei* by fluorescence microscopy. *J. Parasitol*. **70** (5):694-702.

Cox F.E.G. (2004). History of sleeping sickness (African trypanosomiasis). *Infect. Dis. Clin. North. Am*. **18** (2):231-245.

Croft S.L., Barrett M.P. and Urbina J.A. (2005). Chemotherapy of trypanosomiases and leishmaniasis. *Trends Parasitol.* **21** (11):508-512.

de Koning H.P. (2001a). Uptake of pentamidine in *Trypanosoma brucei brucei* is mediated by three distinct transporters: implications for cross-resistance with arsenicals. *Mol. Pharmacol*. **59** (3):586-592.

de Koning H.P. (2008). Ever-increasing complexities of diamidine and arsenical crossresistance in African trypanosomes. *Trends Parasitol.* **24** (8):345-349.

de Koning H.P.(2001b). Transporters in African trypanosomes: role in drug action and resistance. *Int. J. Parasitol.* **31** (5-6):512-522.

de Koning H.P., Anderson L.F., Stewart M., Burchmore R.J.S., Wallace L.J.M. and Barrett M.P. (2004). The trypanocide diminazene aceturate is accumulated predominantly through the TbAT1 purine transporter: additional insights on diamidine resistance in African trypanosomes. *Antimicrob. Agents Chemother.* **48** (5):1515-1519.

Dean S., Marchetti R., Kirk K. and Matthews K.R. (2009). A surface transporter family conveys the trypanosome differentiation signal. *Nature* **459** (7244):213-217.

Deborggraeve S., Claes F., Laurent T., Mertens P., Leclipteux T., Dujardin J.C., Herdewijn P. and Büscher P. (2006). Molecular dipstick test for diagnosis of sleeping sickness. *J. Clin. Microbiol.* **44** (8):2884-2889.

Deiman B., van Aarle P. and Sillekens P. (2002). Characteristics and applications of nucleic acid sequence-based amplification (NASBA). *Mol. Biotechnol*. **20** (2):163-179.

Delacollette C. and Van der Stuyft P. (1994). Direct acridine orange staining is not a "miracle" solution to the problem of malaria diagnosis in the field. *Trans. R. Soc. Trop. Med. Hyg.* **88** (2):187-188.

Delespaux V. and de Koning H.P. (2007). Drugs and drug resistance in African trypanosomiasis. *Drug Resist. Updat.* **10** (1-2):30-50.

Delespaux V., Geysen D., Van den Bossche P. and Geerts S. (2008). Molecular tools for the rapid detection of drug resistance in animal trypanosomes. *Trends Parasitol.* **24** (5):236-242.

Denise H. and Barrett M.P. (2001). Uptake and mode of action of drugs used against sleeping sickness. *Biochem. Pharmacol.* **61** (1):1-5.

Docampo R. and Moreno S.N.J. (1999). Acidocalcisome: a novel Ca^{2+} storage compartment in trypanosomatids and apicomplexan parasites. *Parasitol. Today* **15** (11):443-448.

Doua F., Miézan T.W., Singaro J.R.S., Yapo F.B. and Baltz T. (1996). The efficacy of pentamidine in the treatment of early-late stage *Trypanosoma brucei gambiense* trypanosomiasis. *Am. J. Trop. Med. Hyg.* **55** (6):586-588.

Dukes P., Gibson W.C., Gashumba J.K., Hudson K.M., Bromidge T.J., Kaukus A., Asonganyi T. and Magnus E. (1992). Absence of the LiTat 1.3 (CATT antigen) gene in *Trypanosoma brucei gambiense* stocks from Cameroon. *Acta Trop.* **51** (2):123-134.

Eisler M.C., Lessard P., Masake R.A., Moloo S.K. and Peregrine A.S. (1998). Sensitivity and specificity of antigen-capture ELISAs for diagnosis of *Trypanosoma congolense* and *Trypanosoma vivax* infections in cattle. *Vet. Parasitol.* **79** (3):187-201.

Ekwanzala M., Pepin J., Khonde N., Molisho S., Bruneel H. and De Wals P. (1996). In the heart of darkness: sleeping sickness in Zaire. *Lancet* **348** (9039):1427-1430.

Empson M.B. (2001). Statistic in the pathology laboratory: characteristics of diagnostic tests. *Pathology* **33** (1):93-95.

Enanga B., Burchmore R.J.S., Stewart M.L. and Barrett M.P. (2002). Sleeping sickness and the brain. *Cell. Mol. Life Sci*. **59** (5):845-858.

Etchegorry M.G., Helenport J.P., Pecoul B., Jannin J. and Legros D. (2001). Availability and affordability of treatment for human African trypanosomiasis. *Trop. Med. Int. Health* **6** (11):957-959.

Ezeani M.C., Okoro H., Anosa V.O., Onyenekwe C.C., Meludu S.C., Dioka C.E. and Azikiwe C.C. (2008). Immunodiagnosis of bovine trypanosomiasis in Anambra and Imo states, Nigeria, using enzyme-linked immunosorbent assay: zoonotic implications to human health. *J. Vector Borne Dis.* **45** (4):292-300.

Fairlamb A.H. (2003). Chemotherapy of human African trypanosomiasis: current and future prospects. *Trends Parasitol.* **19** (11):488-494.

Fèvre E.M., Picozzi K., Jannin J., Welburn S.C. and Maudlin I. (2006). Human African trypanosomiasis: epidemiology and control. *Adv. Parasitol.* **61**:167-221.

Fèvre E.M., Wissmann B.V., Welburn S.C. and Lutumba P. (2008). The burden of human African trypanosomiasis. *PLoS Negl. Trop. Dis.* **2**(12):e333.

Field M.C. and Carrington M. (2009). The trypanosome flagellar pocket. *Nat. Rev. Microbiol.* **7** (11):775-786.

Field M.C., Allen C.L., Dhir V., Goulding D., Hall B.S., Morgan G.W., Veazey P. and Engstler M. (2004). New approaches to the microscopic imaging of *Trypanosoma brucei*. *Microsc. Microanal.* **10** (5):621-636.

Field M.C., Natesan S.K.A., Gabernet-Castello C. and Koumandou V.L. (2007). Intracellular trafficking in the trypanosomatids. *Traffic* **8** (6):629-639.

Florijn R.J., Slats J., Tanke H.J. and Raap A.K. (1995). Analysis of antifading reagents for fluorescence microscopy. *Cytometry* **19** (2):177-182.

Foglieni C., Meoni C. and Davalli A.M. (2001). Fluorescent dyes for cell viability: an application on prefixed conditions. *Histochem. Cell Biol.* **115** (3):223-229.

Frommel T.O. and Balber A.E. (1987). Flow cytofluorometric analysis of drug accumulation by multidrug-resistant *Trypanosoma brucei brucei* and *T. b. rhodesiense*. *Mol. Biochem. Parasitol.* **26** (1-2):183-191.

Gallardo-Escárate C., Alvarez-Borrego J., Von Brand E., Dupré E., Del Río-Portilla M.A. (2007). Relationship between DAPI-fluorescence fading and nuclear DNA content: an alternative method to DNA quantification? *Biol. Res.* **40** (1):29-40.

Garcia A., Courtin D., Solano P., Koffi M. and Jamonneau V. (2006). Human African trypanosomiasis: connecting parasite and host genetics. *Trends Parasitol.* **22** (9):405-409.

Garcia A., Jamonneau V., Magnus E., Laveissière C., Lejon V., N'Guessan P., N'Dri L., Van Meirvenne N. and Büscher P. (2000). Follow-up of Card Agglutination Trypanosomiasis Test (CATT) positive but apparently aparasitaemic individuals in Côte d'Ivoire: evidence for a complex and heterogeneous population. *Trop. Med. Int. Health* **5** (11):786-793.

García-Salcedo J.A., Pérez-Morga D., Gijón P., Dilbeck V., Pays E. and Nolan D.P. (2004). A differential role for actin during the life cycle of *Trypanosoma brucei*. *EMBO J.* **23** (4):780-789.

Gardner B.J. and Mason S.F. (1967). Structure and optical activity of DNA-aminoacridine complex. *Biopolymers* **5** (1):79-94.

Gay F., Traoré B., Zanoni J., Danis M. and Fribourg-Blanc A. (1996). Direct acridine orange fluorescence examination of blood slides compared to current techniques for malaria diagnosis. *Trans. R. Soc. Trop. Med. Hyg.* **90** (5):516-518.

Geiser F., Lüscher A., de Koning H.P., Seebeck T. and Mäser P. (2005). Molecular pharmacology of adenosine transport in *Trypanosoma brucei*: P1/P2 revisited. *Mol. Pharmacol.* **68** (3):589-595.

Gibson W. (2001). Molecular characterization of field isolates of human pathogenic trypanosomes. *Trop. Med. Int. Health* **6** (5):401-406.

Gibson W. (2002a). Epidemiology and diagnosis of African trypanosomiasis using DNA probes. *Trans. R. Soc. Trop. Med. Hyg*. **96** (Supp. l.1):S141-143.

Gibson W., Backhouse T. and Griffiths A. (2002b). The human serum resistance associated gene is ubiquitous and conserved in *Trypanosoma brucei rhodesiense* throughout East Africa. *Infect. Genet. Evol.* **1** (3):207-214.

Gillingwater K., Kumar A., Anbazhagan M., Boykin D.W., Tidwell R.R. and Brun R. (2009). *In vivo* investigations of selected diamidine compounds against *Trypanosoma evansi* using a mouse model. *Antimicrob. Agents Chemother*. **53** (12):5074-5079.

Giroud C., Ottones F., Coustou V., Dacheux D., Biteau N., Miezan B., Van Reet N., Carrington M., Doua F. and Baltz T. (2009). Murine models for *Trypanosoma brucei gambiense* disease progression – From silent to chronic infections and early brain tropism. *PLoS Neg. Trop. Dis.* **3** (9):e509.

Gonçalves M.S. (2009). Fluorescent labeling of biomolecules with organic probes. *Chem. Rev*. **109** (1):190-212.

Gould M.K., Vu X.L., Seebeck T. and de Koning H.P. (2008). Propidium iodide-based methods for monitoring drug action in the kinetoplastidae: comparison with the Alamar Blue assay. *Anal. Biochem.* **382** (2):87-93.

Guy R., Liu P., Pennefather P. and Crandall I. (2007). The use of fluorescence enhancement to improve the microscopic diagnosis of falciparum malaria. *Malar. J.* **6**:89.

Hainard A., Tiberti N., Robin X., Lejon V., Mumba Ngoyi D., Matovu E., Enyaru J.C., Fouda C., Ndung'u J.M., Lisacek F., Müller M., Turck N. and Sanchez J.C. (2009). A combined CXCL10, CXCL8 and H-FABP panel for the staging of human African trypanosomiasis patients. *PLoS Neg. Trop. Dis.* **3** (6):e459.

Hänscheid T. (2008). The future looks bright: low-cost fluorescent microscopes for detection of *Mycobacterium tuberculosis* and *Coccidiae*. *Trans. R. Soc. Trop. Med. Hyg*. **102** (6):520-521.

Hasker E., Mitashi P., Baelmans R., Lutumba P., Jacquet D., Lejon V., Kande V., Declercq J., Van der Veken W. and Boelaert M. (2010). A new format of the CATT test for the detection of human African trypanosomiasis, designed for use in peripheral health facilities. *Trop. Med. Int. Health* **15** (2):263-267.

Hasne M.P., Coppens I., Soysa R. and Ullman B. (2010). A high-affinity putrescine-cadaverine transporter from *Trypanosoma cruzi*. *Mol. Microbiol.* **76** (1):78-91.

Hawking F. and Sen A.B. (1960). The trypanocidal action of homidium, quinapyramine and suramin. *Br. J. Pharmacol. Chemother.* **15** (4):567-570.

Hendry C., Dionne K., Hedgepeth A., Carroll K. and Parrish N. (2009). Evaluation of a rapid fluorescent staining method for detection of mycobacteria in clinical specimens. *J. Clin. Microbiol.* **47** (4):1206-1208.

Hermetter A., Scholze H., Stütz A.E., Withers S.G. and Wrodnigg T.M. (2001). Powerful probes for glycosidases: novel, fluorescently tagged glycosidase inhibitors. *Bioorg. Med. Chem. Lett.* **11** (10):1339-1342.

Hirumi H. and Hirumi K. (1994). Axenic culture of African trypanosome bloodstream forms. *Parasitol. Today* **10** (2):80-84.

Hong M. and Simpson L. (2003). Genomic organization of *Trypanosoma brucei* kinetoplast DNA minicircles. *Protist* **154** (2):265-279.

Houwen B. (2000). Blood film preparation and staining procedures. *Lab. Hematol*. **6**:1-7.

Huang L.R., Cox E.C., Austin R.H. and Sturm J.C. (2004). Continuous particle separation through deterministic lateral displacement. *Science* **304** (5673):987-990.

Hung N.V., Sy D.N., Anthony R.M., Cobelens F.G. and van Soolingen D. (2007). Fluorescence microscopy for tuberculosis diagnosis. *Lancet Infect. Dis.* **7** (4):238-239.

Husain O.A.N., Millett J.A. and Grainger J.M. (1980). Use of polylysine-coated slides in preparation of cell samples for diagnostic cytology, with special reference to urine sample. *J. Clin. Pathol.* **33** (3):309-311.

Hutchinson O.C., Fèvre E.M., Carrington M. and Welburn S.C. (2003). Lessons learned from the emergence of a new *Trypanosoma brucei rhodesiense* sleeping sickness focus in Uganda. *Lancet Infect. Dis.* **3** (1):42-45.

Hutchinson O.C., Webb H., Picozzi K., Welburn S. and Carrington M. (2004). Candidate protein selection for diagnostic markers of African trypanosomiasis. *Trends Parasitol.* **20** (11):519-523.

Inojosa W.O., Augusto I., Bisoffi Z., Josenado T., Abel P.M., Stich A. and Whitty C.J.M. (2006). Diagnosing human African trypanosomiasis in Angola using a card agglutination test: observational study of active and passive case finding strategies. *B. M. J.* **332** (7556):1479-1481.

Jackson A.P. (2007). Origins of amino acid transporter loci in trypanosomatid parasites. *BMC Evol. Biol.* **7**:26.

Jamonneau V., Solano P. and Cuny G. (2001). Utilisation de la biologie moleculaire dans le diagnostic de la trypanosomose humaine africaine. *Med. Trop*. **61** (4-5):347-354.

Jamonneau V., Solano P., Koffi M., Denizot M. and Cuny R. (2004). Apports et limites du diagnostic de la trypanosomiase humaine africaine. *Med. Sci. (Paris)* **20** (10):871-875.

Jamonneau V., Truc P., Garcia A., Magnus E. and Buscher P. (2000). Preliminary evaluation of LATEX/*T. b. gambiense* and alternative versions of CATT/*T. b. gambiense* for the serodiagnosis of Human African Trypanosomiasis of a population at risk in Côte d'Ivoire: considerations for mass-screening. *Acta Trop.* **76** (2):175-183.

Jannin J. and Cattand P. (2004). Treatment and control of human African trypanosomiasis. *Curr. Opin. Infect. Dis.* **17** (6):565-570.

Johnson G.D., Davidson R.S., McNamee K.C., Russell G., Goodwin D. and Holborow E.J. (1982). Fading of immunofluorescence during microscopy: a study of phenomenon and its remedy. *J. Immunol. Methods* **55** (2):231-242.

Jones D., Broeckman E., Derschum H., Mandy F. and Ries H. (2005). LED fluorescence microscopy made for space for use on earth. *Proc. Roy. Microsc. Soc*. **40** (2):91-96.

Jones D., Nyalwidhe J., Tetley L. and Barrett M.P. (2007). McArthur revisited: fluorescence microscopes for field diagnostics. *Trends Parasitol.* **23** (10):468-469.

Joshi P.P., Shegokar V.R., Powar R.M., Herder S., Katti R., Salkar H.R., Dani V.S., Bhargava A., Jannin J. and Truc P. (2005). Human trypanosomiasis caused by *Trypanosoma evansi* in India: the first case report. *Am. J. Trop. Med. Hyg.* **73** (3):491-495.

Kapuscinski J. (1990). Interactions of nucleic acids with fluorescent dyes: spectral properties of condensed complexes. *J. Histochem. Cytochem.* **38** (9):1323-1329.

Kapuscinski J. (1995). DAPI: a DNA-specific fluorescent probe. *Biotech. Histochem.* **70** (5):220-233.

Kawamoto F. (1991). Rapid diagnosis of malaria by fluorescence microscopy with light microscope and interference filter. *Lancet* **337** (8735):200-202.

Kazibwe A.J. (2008). Factors influencing the spread and selection of drug resistance in Human African Trypanosomiasis. PhD Thesis, University of Glasgow.

Kazibwe A.J.N., Nerima B., de Koning H.P., Maser P., Barrett M.P. and Matovu E. (2009). Genotypic status of the TbAT1/P2 adenosine transporter of *Trypanosoma brucei gambiense* isolates from northwestern Uganda following melarsoprol withdrawal. *PLoS Negl. Trop. Dis.* **3** (9):e523.

Keiser J., Utzinger J., Premji Z., Yamagata Y. and Singer B.H. (2002). Acridine orange for malaria diagnosis: its diagnostic performance, its promotion and implementation in Tanzania, and the implications for malaria control. *Ann. Trop. Med. Parasitol.* **96** (7):643-654.

Kelly S., Reed J., Kramer S., Ellis L., Webb H., Sunter J., Salje J., Marinsek N., Gull K., Wickstead B. and Carrington M. (2007). Functional genomics in *Trypanosoma brucei*: a collection of vectors for the expression of tagged proteins from endogenous and ectopic gene loci. *Mol. Biochem. Parasitol.* **154** (1):103-109.

Kennedy P.G. (2006a). Diagnostic and neuropathogenesis issues in human African trypanosomiasis. *Int. J. Parasitol.* **36** (5):505-512.

Kennedy P.G. (2006b). Human African trypanosomiasis–neurological aspects. *J. Neurol.* **253** (4):411-416.

Kennedy P.G. (2008). The continuing problem of human African trypanosomiasis (sleeping sickness). *Ann. Neurol*. **64** (2):116-127.

Kim S.K., Eriksson S., Kubista M. and Nordén B. (1993). Interaction of 4',6-Diamidino-2-Phenylindole (DAPI) with Poly[D(G-C)$_2$] and Poly[d(G-m^{5}C)$_2$]: evidence for major groove binding of a DNA probe. *J. Am. Chem. Soc.* **115** (9):3441-3447.

Kimber C.D. (1984). Further improvements in the miniature anion/exchange centrifugation technique (mAECT) for field work. *Trans. R. Soc. Trop. Med. Hyg.* **78** (5):702-703.

Kinabo L.D.B. and Bogan J.A. (1988). The pharmacology of isometamidium. *J. Vet. Pharmacol. Ther.* **11** (3):233-245.

Koffi M., Solano P., Denizot M., Courtin D., Garcia A., Lejon V., Büscher P., Cuny G. and Jamonneau V. (2006). Aparasitemic serological suspects in *Trypanosoma brucei gambiense* human African trypanosomiasis: a potential human reservoir of parasites? *Acta Trop.* **98** (2):183-188.

Kong H.H., and Chung D.I. (1995). Comparison of acridine orange and Giemsa stains for malaria diagnosis. *Korean J. Parasitol.* **33** (4):391-394.

Krieger S., Schwarz W., Ariyanayagam M.R., Fairlamb A.H., Krauth-Siegel R.L. and Clayton C. (2000). Trypanosomes lacking trypanothione reductase are avirulent and show increased sensitivity to oxidative stress. *Mol. Microbiol.* **35** (3):542-552.

Kristjanson P.M., Swallow B.M., Rowlands G.J., Kruska R.L. and de Leeuw P.N. (1999). Measuring the costs of African animal trypanosomosis, the potential benefits of control and returns to research. *Agric. Syst.* **59** (1):79-98.

Landfear S.M. (2009). Transporters for drug delivery and as drug targets in parasitic protozoa. *Clin. Pharmacol. Ther.* **87** (1): 122-125.

Lang D.S., Zeiser T., Schultz H., Stellmacher F., Vollmer E., Zabel P. and Goldmann T. (2008). LED-FISH: Fluorescence microscopy based on light emitting diodes for the molecular analysis of Her-2/neu oncogene amplification. *Diagn. Pathol.* **3**:49.

Lanteri C.A., Stewart M.L., Brock J.M., Alibu V.P., Meshnick S.R., Tidwell R.R. and Barrett M.P. (2006). Roles for the *Trypanosoma brucei* P2 transporter in DB75 uptake and resistance. *Mol. Pharmacol.* **70** (5):1585-1592.

Lanteri C.A., Tidwell R.R. and Meshnick S.R. (2008). The mitochondrion is a site of trypanocidal action of the aromatic diamidine DB75 in bloodstream forms of *Trypanosoma brucei*. *Antimicrob. Agents Chemother.* **52** (3):875-882.

Lanteri C.A., Trumpower B.L., Tidwell R.R. and Meshnick S.R. (2004). DB75, a novel trypanocidal agent, disrupts mitochondrial function in *Saccharomyces cerevisiae*. *Antimicrob. Agents Chemother.* **48** (10):3968-3974.

Leach T.M. and Roberts C.J. (1981). Present status of chemotherapy and chemoprophylaxis of animal trypanosomiasis in the Eastern hemisphere. *Pharmacol. Ther.* **13** (1):91-147.

Legros D., Evans S., Maiso F., Enyaru J.C.K. and Mbulamberi D. (1999). Risk factors for treatment failure after melarsoprol for *Trypanosoma brucei gambiense* trypanosomiasis in Uganda. *Trans. R. Soc. Trop. Med. Hyg.* **93** (4):439-442.

Legros D., Ollivier G., Gastellu-Etchegorry M., Paquet C., Burri C., Jannin J. and Büscher P. (2002). Treatment of human African trypanosomiasis - present situation and needs for research and development. *Lancet Infect. Dis.* **2** (7):437-440.

Lejon V. and Büscher P. (2001). Stage determination and follow-up in sleeping sickness. *Med. Trop.* **61** (4-5):355-360.

Lejon V. and Büscher P. (2002). Le diagnostic du stade dans la maladie du sommeil: vers une nouvelle approche. *Bull. Soc. Pathol. Exot.* **95** (5):338-340.

Lejon V. and Büscher P. (2005). Cerebrospinal fluid in human African trypanosomiasis: a key to diagnosis, therapeutic decision and post-treatment follow-up. *Trop. Med. Int. Health* **10** (5):395-403.

Lejon V., Boelaert M., Jannin J., Moore A. and Buscher P. (2003a). The challenge of *Trypanosoma brucei gambiense* sleeping sickness diagnosis outside Africa. *Lancet Infect. Dis.* **3** (12):804-808.

Lejon V., Büscher P., Magnus E., Moons A., Wouters I. and Van Meirvenne N. (1998). A semi-quantitative ELISA for detection of *Trypanosoma brucei gambiense* specific antibodies in serum and cerebrospinal fluid of sleeping sickness patients. *Acta Trop.* **69** (2):151-164.

Lejon V., Jamonneau V., Solano P., Atchade P., Mumba D., Nkoy N., Bébronne N., Kibonja T., Balharbi F., Wierckx A., Boelaert M. and Büscher P. (2006). Detection of trypanosome-specific antibodies in saliva, towards non-invasive serological diagnosis of sleeping sickness. *Trop. Med. Int. Health* **11** (5):620-627.

Lejon V., Lardon J., Kenis G., Pinoges L., Legros D., Bisser S., N'Siesi X., Bosmans E. and Büscher P. (2002a). Interleukin (IL)-6, IL-8 and IL-10 in serum and CSF of *Trypanosoma brucei gambiense* sleeping sickness patients before and after treatment. *Trans. R. Soc. Trop. Med. Hyg.* **96** (3):329-333.

Lejon V., Legros D., Richer M., Ruiz J.A., Jamonneau V., Truc P., Doua F., Djé N., N'Siesi F.X., Bisser S., Magnus E., Wouters I., Konings J., Vervoort T., Sultan F. and Büscher P. (2002b). IgM quantification in the cerebrospinal fluid of sleeping sickness patients by a latex card agglutination test. *Trop. Med. Int. Health* **7** (8):685-692.

Lejon V., Mumba Ngoyi D., Boelaert M. and Büscher P. (2010). A CATT negative result after treatment for human African trypanosomiasis is no indication for cure. *PLoS Negl. Trop. Dis.* **4** (1):e590.

Lejon V., Reiber H., Legros D., Dje N., Magnus E., Wouters I., Sindic C.J.M. and Büscher P. (2003b). Intrathecal immune response pattern for improved diagnosis of central nervous system involvement in trypanosomiasis. *J. Infect. Dis.* **187** (9):1475-1483.

Lejon V., Roger I., Mumba Ngoyi D., Menten J., Robays J., N'Siesi F.X., Bisser S., Boelaert M. and Büscher P. (2008). Novel markers for treatment outcome in late-stage *Trypanosoma brucei gambiense* trypanosomiasis. *Clin. Infect. Dis.* **47** (1):15-22.

Lichtman J.W. and Conchello J.A. (2005). Fluorescence microscopy. *Nat. Methods* **2** (12):910-919.

Lindh J.M., Torr S.J., Vale G.A. and Lehane M.J. (2009). Improving the cost-effectiveness of artificial visual baits for controlling the tsetse fly *Glossina fucipes fucipes*. *PLoS Neg. Trop. Dis.* **3** (7):e474.

Liu B., Liu Y., Motyka S.A., Agbo E.E.C. and Englund P.T. (2005). Fellowship of the rings: the replication of kinetoplast DNA. *Trends Parasitol.* **21** (8):363-369.

Liu J.Y., Qiao X.G., Du D.Y. and Lee M.G.S. (2000). Receptor-mediated endocytosis in the procyclic form of *Trypanosoma brucei*. *J. Biol. Chem.* **275** (16):12032-12040.

Liu M.K., Cattand P., Gardiner I.C. and Pearson T.W. (1989). Immunodiagnosis of sleeping sickness due to *Trypanosoma brucei gambiense* by detection of anti-procyclic antibodies and trypanosome antigens in patients' sera. *Acta Trop.* **46** (4):257-266.

Liu Y., Kumar A., Boykin D.W. and Wilson W.D. (2007). Sequence and length dependent thermodynamic differences in heterocyclic diamidine interactions at AT base pairs in the DNA minor groove. *Biophys. Chem.* **131** (1-3):1-14.

Longin A., Souchier C., Ffrench M. and Bryon P.A. (1993). Comparison of anti-fading agents used in fluorescence microscopy: image analysis and laser confocal microscopy study. *J. Histochem. Cytochem.* **41** (12):1833-1840.

Louis F.J., Büscher P. and Lejon V. (2001). Le diagnostic de la trypanosomiase humaine africaine en 2001. *Med. Trop.* **61** (4-5):340-346.

Lumsden W.H.R., Kimber C.D., Evans D.A. and Doig S.J. (1979). *Trypanosoma brucei*: miniature anion-exchange centrifugation technique for detection of low parasitaemias: adaptation for field use. *Trans. R. Soc. Trop. Med. Hyg.* **73** (3):312-317.

Lun Z.R., Reid S.A., Lai D.H., Li F.J. (2009). Atypical human trypanosomiasis: a neglected disease or just an unlucky accident? *Trends Parasitol*. **25** (3):107-108.

Lutumba P., Meheus F., Robays J., Miaka C., Kande V., Büscher P., Dujardin B. and Boelaert M. (2007). Cost-effectiveness of algorithms for confirmation test of human African trypanosomiasis. *Emerg. Infect. Dis*. **13** (10):1484-1490.

Lutumba P., Robays J., Miaka C., Kande V., Mumba D., Büscher P., Dujardin B. and Boelaert M. (2006). Validité, coût et faisabilité de la mAECT et CTC comme tests de confirmation dans la détection de la Trypanosomiase Humaine Africaine. *Trop. Med. Int. Health* **11** (4):470-478.

Lutumba P., Robays J., Miaka C., Kande V., Simarro P.P., Shaw A.P.M., Dujardin B. and Boelaert M. (2005). Efficience de différentes stratégies de détection de la Trypanosomiase Humaine Africaine à *T. b. gambiense*. *Trop. Med. Int. Health* **10** (4):347-356.

Machado C.R., Augusto-Pinto L., McCulloch R. and Teixeira S.M. (2006). DNA metabolism and genetic diversity in Trypanosomes. *Mutat. Res.* **612** (1):40-57.

MacInnes J.W. and McClintock. M (1970). Differences in fluorescence spectra of acridine orange-DNA complexes related to DNA base composition. *Biopolymers* **9** (11):1407-1411.

Magnus E., Lejon V., Bayon D., Buyse D., Simarro P., Verloo D., Vervoort T., Pansaerts R., Buscher P. and Van Meirvenne N. (2002). Evaluation of an EDTA version of CATT/*Trypanosoma brucei gambiense* for serological screening of human blood samples. *Acta Trop.* **81** (1):7-12.

Maina N.W.N., Maina K.J., Mäser P. and Brun R. (2007a). Genotypic and phenotypic characterization of *Trypanosoma brucei gambiense* isolates from Ibba, South Sudan, an area of high melarsoprol treatment failure rate. *Acta Trop.* **104** (2-3):84-90.

Maina N.W.N., Oberle M., Otieno C., Kunz C., Maeser P., Ndung'u J.M. and Brun R. (2007b). Isolation and propagation of *Trypanosoma brucei gambiense* from sleeping sickness patients in south Sudan. *Trans. R. Soc. Trop. Med. Hyg.* **101** (6):540-546.

Marais B.J., Brittle W., Painczyk K., Hesseling A.C., Beyers N., Wasserman E., van Soolingen D. and Warren R.M. (2008). Use of light-emitted diode fluorescence microscopy to detect acid-fast bacilli in sputum. *Clin. Infect. Dis.* **47** (2):203-207.

Mäser P., Lüscher A. and Kaminsky R. (2003). Drug transport and drug resistance in African trypanosomes. *Drug Resist. Updat.* **6** (5):281-290.

Mäser P., Sütterlin C., Kralli A. and Kaminsky R. (1999). A nucleoside transporter from *Trypanosoma brucei* involved in drug resistance. *Science* **285** (5425):242-244.

Mathis A.M., Bridges A.S., Ismail M.A., Kumar A., Francesconi I., Anbazhagan M., Hu Q., Tanious F.A., Wenzler T., Saulter J., Wilson W.D., Brun R., Boykin D.W., Tidwell R.R. and Hall J.E. (2007). Diphenyl furans and aza analogs: effects of structural modification on *in vitro* activity, DNA binding, and accumulation and distribution in trypanosomes. *Antimicrob. Agents Chemother.* **51** (8):2801-2810.

Mathis A.M., Holman J.L.,. Sturk L.M, Ismail M.A., Boykin D.W., Tidwell R.R. and Hall J.E. (2006). Accumulation and intracellular distribution of antitrypanosomal diamidine compounds DB75 and DB820 in African trypanosomes. *Antimicrob. Agents Chemother.* **50** (6):2185-2191.

Matovu E., Enyaru J.C.K., Legros D., Schmid C., Seebeck T. and Kaminsky R. (2001a). Melarsoprol refractory *T. b. gambiense* from Omugo, north-western Uganda. *Trop. Med. Int. Health* **6** (5):407-411.

Matovu E., Geiser F., Schneider V., Mäser P., Enyaru J.C.K., Kaminsky R., Gallati S. and Seebeck T. (2001b). Genetic variants of the *TbAT1* adenosine transporter from African trypanosomes in relapse infections following melarsoprol therapy. *Mol. Biochem. Parasitol.* **117** (1):73-81.

Matovu E., Stewart M.L., Geiser F., Brun R., Mäser P., Wallace L.J.M., Burchmore R.J., Enyaru J.C.K., Barrett M.P., Kaminsky R., Seebeck T. and de Koning H.P. (2003). Mechanisms of arsenical and diamidine uptake and resistance in *Trypanosoma brucei*. *Eukaryot. Cell* **2** (5):1003-1008.

Maudlin I. (2006). African trypanosomiasis. *Ann. Trop. Med. Parasitol.* **100** (8):679-701.

Mendoza M., Mijares A., Rojas H., Rodríguez J. P., Urbina J. A. and DiPolo R. (2002). Physiological and morphological evidences for the presence acidocalcisomes in *Trypanosoma evansi* - Single cell fluorescence and ^{31}P NMR studies. *Mol. Biochem. Parasitol.* **125** (1-2):23-33.

Metzger W.G. and Nkeyi M. (1995). Immediate detection of malaria parasites by acridine orange staining. *Trans. R. Soc. Trop. Med. Hyg.* **89** (5):577.

Miézan T.W., Doua F., Cattand P. and de Raadt P. (1991). Evaluation du Testryp CATT appliqué au sang prélevé sur papier filtre et au sang dilué, dans le foyer de trypanosomiase à *Trypanosoma brucei gambiense* en Côte d'Ivoire. *Bull. World Health Organ.* **69** (5):603-606.

Miézan T.W., Meda A.H., Doua F. and Cattand P. (1994). Évaluation des techniques parasitologiques utilisées dans le diagnostic de la trypanosomose humaine à *Trypanosoma gambiense* en Côte d'Ivoire. *Bull. Soc. Pathol. Exot.* **87** (2):101-104.

Miézan T.W., Meda H.A., Doua F., Djè N.N., Lejon V. and Büscher P. (2000). Single centrifugation of cerebrospinal fluid in a sealed Pasteur pipette for simple, rapid and sensitive detection of trypanosomes. *Trans. R. Soc. Trop. Med. Hyg*. **94** (3):293.

Minion J., Sohn H. and Pai M. (2009). Light-emitting diode technologies for TB diagnosis: what is on the market? *Expert Rev. Med. Devices* **6**(4):341-345.

Molyneux D.H. (1975). Diagnostic methods in animal trypanosomiasis. *Vet. Parasitol*. **1** (1):5-17.

Morgan G.W., Hall B.S., Denny P.W., Carrington M. and Field M.C. (2002). The kinetoplastida endocytic apparatus. Part I: a dynamic system for nutrition and evasion of host defences. *Trends Parasitol.* **18** (11):491-496.

Mori Y. and Notomi T. (2009). Loop-mediated isothermal amplification (LAMP): a rapid, accurate, and cost-effective diagnostic method for infectious diseases. *J. Infect. Chemother.* **15** (2):62-69.

Morrison L.J., Marcello L., McCulloch R. (2009). Antigenic variation in the African trypanosome: molecular mechanisms and phenotypic complexity. *Cell. Microbiol.* **11** (12):1724-1734.

Mugasa C.M., Laurent T., Schoone G.J., Kager P.A., Lubega G.W. and Schallig H.D.F.H. (2009). Nucleic acid sequence-based amplification with oligochromatography for detection of *Trypanosoma brucei* in clinical samples. *J. Clin. Microbiol.* **47** (3):630-635.

Mugasa M., Schoone G.J., Ekangu R.A., Lubega G.W., Kager P.A. and. Schallig H.D.F.H. (2008). Detection of *Trypanosoma brucei* parasites in blood samples using real-time nucleic acid sequence-based amplification. *Diagn. Microbiol. Infect. Dis.* **61** (4):440-445.

Mumba Ngoyi D., Lejon V., N'Siesi F.X., Boelaert M. and Büscher P. (2009). Comparison of operational criteria for treatment outcome in *gambiense* human African trypanosomiasis. *Trop. Med. Int. Health* **14** (4):438-444.

Mumba Ngoyi D., Lejon V., Pyana P., Boelaert M., Ilunga M., Menten J., Mulunda J.P., Van Nieuwenhove S., Muyembe Tamfum J.J. and Büscher P. (2010). How to shorten patient follow-up after treatment for *Trypanosoma brucei gambiense* sleeping sickness. *J. Infect. Dis.* **201** (3):453-463.

Murray M., Murray P.K. and McIntyre W.I.M. (1977). Improved parasitological technique for diagnosis of African trypanosomiasis. *Trans. R. Soc. Trop. Med. Hyg.* **71** (4):325-326.

Naessens J. (2006). Bovine trypanotolerance: a natural ability to prevent severe anaemia and haemophagocytic syndrome? *Int. J. Parasitol.* **36** (5):521-528.

Nendaz M.R. and Perrier A. (2004). Sensibilité, spécificité, valeur prédictive positive et valeur prédictive négative d'un test diagnostique. *Rev. Mal. Respir.* **21** (2 Pt 1):390-393.

Njiokou F., Laveissière C., Simo G., Nkinin S., Grébaut P., Cuny G. and Herder S. (2006). Wild fauna as a probable animal reservoir for *Trypanosoma brucei gambiense* in Cameroon. *Infect. Genet. Evol.* **6** (2):147-153.

Njiru Z. K., Mikosza A.S.J., Armstrong T., Enyaru J.C., Ndung'u J.M. and Thompson A.R.C. (2008a). Loop-mediated isothermal amplification (LAMP) method for rapid detection of *Trypanosoma brucei rhodesiense*. *PLoS Negl. Trop. Dis.* **2** (1):e147.

Njiru Z.K., Mikosza A.S. J., Matovu E., Enyaru J.C.K., Ouma J.O., Kibona S.N., Thompson R.C.A. and Ndung'u J.M. (2008b). African trypanosomiasis: sensitive and rapid detection of the sub-genus *Trypanozoon* by loop-mediated isothermal amplification (LAMP) of parasite DNA. *Int. J. Parasitol.* **38** (5):589-599.

Njiru Z.K., Ndung'u K., Matete G., Ndung'u J.M. and Gibson W.C. (2004). Detection of *Trypanosoma brucei rhodesiense* in animals from sleeping sickness foci in East Africa using the serum resistance associated (*SRA*) gene. *Acta Trop.* **90** (3):249-254.

Noireau F., Lemesre J.L., Nzoukoudi M.Y., Louembet M.T., Gouteux J.P. and Frezil J.L. (1988). Serodiagnosis of sleeping sickness in the Republic of the Congo: comparison of indirect immunofluorescent antibody test and card agglutination test. *Trans. R. Soc. Trop. Med. Hyg*. **82** (2):237-240.

Notomi T., Okayama H., Masubuchi H., Yonekawa T., Watanabe K., Amino N. and Hase T. (2000). Loop-mediated isothermal amplification of DNA. *Nucleic Acids Res*. **28** (12):e63.

Odiit M., Coleman P.G., McDermott J.J., Fèvre E.M., Welburn S.C. and Woolhouse M.E.J. (2004). Spatial and temporal risk factors for the early detection of *Trypanosoma brucei rhodesiense* sleeping sickness patients in Tororo and Busia districts, Uganda. *Trans. R. Soc. Trop. Med. Hyg*. **98** (10):569-576.

Ollivier G. and Legros D. (2001). Trypanosomiase humaine africaine: historique de la thérapeutique et de ses échecs. *Trop. Med. Int. Health* **6** (11):855-863.

Ono M., Murakami T., Kudo A., Isshiki M., Sawada H. and Segawa A. (2001). Quantitative comparison of anti-fading mounting media for confocal laser scanning microscopy. *J. Histochem. Cytochem.* **49** (3):305-311.

Opperdoes F.R. (1987). Compartmentation of carbohydrate metabolism in trypanosomes. *Annu. Rev. Microbiol.* **41**:127-151.

Ormerod W.E. (1951). A study of basophilic inclusion bodies produced by chemotherapeutic agents in trypanosomes. *Br. J. Pharmacol. Chemother.* **6** (2):334-341.

Ortiz D., Sanchez M.A., Quecke P. and Landfear S.M. (2009). Two novel nucleobase/pentamidine transporters from *Trypanosoma brucei*. *Mol. Biochem. Parasitol.* **163** (2):67-76.

Ortiz D., Valdés R., Sanchez M.A., Hayenga J., Elya C., Detke S. and Landfear S.M. (2010). Purine restriction induces pronounced translational upregulation of the NT1 adenosine/pyrimidine nucleoside transporter in *Leishmania major*. *Mol. Microbiol*. **78** (1):108-118.

Ortiz-Ordóñez J.C., Sechelski J.B. and Seed J.R. (1994). Mechanism of lysis of *Trypanosoma brucei gambiense* by human serum. *J. Parasitol.* **80** (6):924-930.

Pansaerts R., Van Meirvenne N., Magnus E. and Verhelst L. (1998). Increased sensitivity of the card agglutination test CATT/*Trypanosoma brucei gambiense* by inhibition of complement. *Acta Trop.* **70** (3):349-354.

Papadopoulos M.C., Abel P.M., Agranoff D., Stich A., Tarelli E., Bell B.A., Planche T., Loosemore A., Saadoun S., Wilkins P. and Krishna S. (2004). A novel and accurate diagnostic test for human African trypanosomiasis. *Lancet* **363** (9418):1358-1363.

Paquet C., Ancelle T., Gastellu-Etchegorry M., Castilla J. and Harndt I. (1992). Persistence of antibodies to *Trypanosoma brucei gambiense* after treatment of human trypanosomiasis in Uganda. *Lancet* **340** (8813):250.

Patnaik P.K., Kulkarni S.K. and Cross G.A. (1993). Autonomously replicating single-copy episomes in *Trypanosoma brucei* show unusual stability. *EMBO J.* **12** (6):2529-2538.

Pays E. and Vanhollebeke B. (2008). Mutual self-defence: the trypanolytic factor story. *Microbes Infect.* **10** (9):985-989.

Penchenier L., Grebaut P., Njokou F., Eyenga V.E. and Buscher P. (2003). Evaluation of LATEX/*T .b. gambiense* for mass screening of *Trypanosoma brucei gambiense* sleeping sickness in Central Africa. *Acta Trop.* **85** (1):31-37.

Penchenier L., Simo G., Grébaut P., Nkinin S., Laveissière C. and Herder S. (2000). Diagnosis of human trypanosomiasis, due to *Trypanosoma brucei gambiense* in central Africa, by the polymerase chain reaction. *Trans. R. Soc. Trop. Med. Hyg.***94** (4):392-394.

Pépin J. and Méda H.A. (2001). The epidemiology and control of human African trypanosomiasis. *Adv. Parasitol.* **49**:71-132.

Peregrine A.S., Gray M.A. and Moloo S.K. (1997). Cross-resistance associated with development of resistance to isometamidium in a clone of *Trypanosoma congolense*. *Antimicrob. Agents Chemother.* **41** (7):1604-1606.

Perkins M.D. and Small P.M. (2006). Partnering for better microbial diagnostics. *Nat. Biotechnol.* **24** (8):919-921.

Petty H.R. (2007). Fluorescence microscopy: established and emerging methods, experimental strategies, and applications in immunology. *Microsc. Res. Tech.* **70** (8):687-709.

Picozzi K., Carrington M. and Welburn S.C. (2008). A multiplex PCR that discriminates between *Trypanosoma brucei brucei* and zoonotic *T. b. rhodesiense*. *Exp. Parasitol.* **118** (1):41-46.

Picozzi K., Fèvre E.M., Odiit M., Carrington M., Eisler M.C., Maudlin I., Welburn S.C. (2005). Sleeping sickness in Uganda: a thin line between two fatal diseases. *BMJ* **331** (7527):1238-1242.

Picozzi K., Tilley A., Fèvre E.M., Coleman P.G., Magona J.W., Odiit M., Eisler M.C. and Welburn S.C. (2002). The diagnosis of trypanosome infections: applications of novel technology for reducing disease risk. *Afr. J. Biotechnol.* **1** (2):39-45.

Pisharath H., Rhee J.M., Swanson M.A., Leach S.D. and Parsons M. J. (2007). Targeted ablation of beta cells in the embryonic zebrafish pancreas using *E. coli* nitroreductase. *Mech. Dev.* **124** (3):218-229.

Pradel N., Santini C.L., Bernadac A., Shih Y.L., Goldberg M.B. and Wu L.F. (2007). Polar positional information in *Escherichia coli* spherical cells. *Biochem. Biophys. Res. Commun.* **353** (2):493-500.

Priotto G., Fogg C., Balasegaram M., Erphas O., Louga A., Checchi F., Ghabri S. and Piola P. (2006). Three drug combinations for late-stage *Trypanosoma brucei gambiense* sleeping sickness: a randomized clinical trial in Uganda. *PLoS Clin. Trials* **1** (8):e39.

Priotto G., Kasparian S., Mutombo W., Ngouama D., Ghorashian S., Arnold U., Ghabri S. Baudin E., Buard V., Kazadi-Kyanza S., Ilunga M., Mutangala W., Pohlig G., Schmid C., Karunakara U., Torreele E. and Kande V. (2009). Nifurtimox-eflornithine combination therapy for second-stage African *Trypanosoma brucei gambiense* trypanosomiasis: a multicentre, randomised, phase III, non-inferiority trial. *Lancet* **374** (9683):56-64.

Radwanska M. (2010). Emerging trends in the diagnosis of human African trypanosomiasis. *Parasitology*. Epub ahead of print.

Radwanska M., Chamekh M., Vanhamme L., Claes F., Magez S., Magnus E., De Baetselier P., Buscher P. and Pays E. (2002a). The serum resistance-associated gene as a diagnostic tool for the detection of *Trypanosoma brucei rhodesiense*. *Am. J. Trop. Med. Hyg.* **67** (6):684-690.

Radwanska M., Claes F., Magez S., Magnus E., Perez-Morga D., Pays E. and Buscher P. (2002b). Novel primer sequences for polymerase chain reaction-based detection of *Trypanosoma brucei gambiense*. *Am. J. Trop. Med. Hyg.* **67** (3):289-295.

Radwanska M., Magez S., Perry-O'Keefe H., Stender H., Coull J., Sternberg J.M., Büscher P. and Hyldig-Nielsen J.J. (2002c). Direct detection and identification of African trypanosomes by fluorescence *in situ* hybridization with peptide nucleic acid probes. *J. Clin. Microbiol.* **40** (11):4295-4297.

Rasnik I., McKinney S.A. and Ha T. (2006). Nonblinking and longlasting single-molecule fluorescence imaging. *Nat. Methods* **3** (11):891-893.

Raz B., Iten M., GretherBuhler Y., Kaminsky R. and Brun R. (1997). The Alamar Blue® assay to determine drug sensitivity of African trypanosomes (*T. b. rhodesiense* and *T. b. gambiense*) *in vitro*. *Acta Trop.* **68** (2):139-147.

Rebeski D.E., Winger E.M., Van Rooij E.M.A., Schöchl R., Schuller W., Dwinger R.H., Crowther J.R. and Wright P. (1999). Pitfalls in the application of enzyme-linked immunoassays for the detection of circulating trypanosomal antigens in serum samples. *Parasitol. Res.* **85** (7):550-556.

Remme J.H.F., Blas E., Chitsulo L., Desjeux P.M.P., Engers H.D., Kanyok T.P., Kayondo J.F.K., Kioy D.W., Kumaraswami V., Lazdins J.K., Nunn P.P., Oduola A., Ridley R.G., Toure Y.T., Zicker F. and Morel C.M. (2002). Strategic emphases for tropical diseases research: a TDR perspective. *Trends Microbiol*. **10** (10):435-440.

Reyna-Bello A., García F.A., Rivera M., Sansó B. and Aso P.M. (1998). Enzyme-linked immunosorbent assay (ELISA) for detection of anti-*Trypanosoma evansi* equine antibodies. *Vet. Parasitol.* **80** (2):149-157.

Riccardi C. and Nicoletti I. (2006). Analysis of apoptosis by propidium iodide staining and flow cytometry. *Nat. Protoc.* **1** (3):1458-1461.

Rickman L.R. and Robson J. (1970). The testing of proven *Trypanosoma brucei* and *T. rhodesiense* strains by the blood incubation infectivity test. *Bull. World Health Organ*. **42** (6):911-916.

Rifkin M.R. (1983). Interaction of high-density lipoprotein with *Trypanosoma brucei*: effect of membrane stabilizers. *J. Cell. Biochem.* **23** (1-4):57-70.

Ripamonti D., Massari M., Arici C., Gabbi E., Farina C., Brini M., Capatti C. and Suter F. (2002). African sleeping sickness in tourists returning from Tanzania: the first 2 Italian cases from a small outbreak among European travelers. *Clin. Infect. Dis.* **34** (1):E18-E22.

Robays J., Bilengue M.M.C., Van der Stuyft P. and Boelaert M. (2004). The effectiveness of active population screening and treatment for sleeping sickness control in the Democratic Republic of Congo. *Trop. Med. Int. Health* **9** (5):542-550.

Robertson J.B., Zhang Y. and Johnson C.H. (2009). Light-emitting diode flashlights as effective and inexpensive light sources for fluorescence microscopy. *J. Microsc.* **236** (1):1-4.

Rodgers J. (2009). Human African trypanosomiasis, chemotherapy and CNS disease. *J. Neuroimmunol.* **211** (1-2):16-22.

Rodrigues C.O., Scott D.A. and Docampo R. (1999). Characterization of a vacuolar pyrophosphatase in *Trypanosoma brucei* and its localization to acidocalcisomes. *Mol. Cell. Biol.* **19** (11):7712-7723.

Rosenblatt J.E. (2009). Laboratory diagnosis of infections due to blood and tissue parasites. *Clin. Infect. Dis.* **49** (7):1103-1108.

Ruiz J.A., Simarro P.P. and Josenando T. (2002). Control of human African trypanosomiasis in the Quiçama focus, Angola. *Bull. World Health Organ.* **80** (9):738-745.

Sachs R. (1984). The superiority of the miniature anion-exchange centrifugation technique for detecting low grade trypanosome parasitaemias. *Trans. R. Soc. Trop. Med. Hyg.***78** (5):694-696.

Sambrook J. and Russell D.W. (2001). *Molecular cloning: a laboratory manual*, 3rd edition, Cold Spring Harbor Laboratory Press, New York, prot. 6.33-6.64.

Sanborn W.R., Heuck C.C., El Aouad R. and Storch W.B. Fluorescence microscopy for disease diagnosis and environmental monitoring. WHO Publications, Eastern Mediterranean Series **28**, Cairo, 2005.

Schmid C., Richer M., Bilenge C.M.M., Josenando T., Chappuis F., Manthelot C.R., Nangouma A., Doua F., Asumu P.N., Simarro P.P. and Burri C. (2005). Effectiveness of a 10-day melarsoprol schedule for the treatment of late-stage human African trypanosomiasis: confirmation from a multinational study (IMPAMEL II). *J. Infect. Dis.* **191** (11):1922-1931.

Schnaufer A., Domingo G.J. and Stuart K. (2002). Natural and induced dyskinetoplastic trypanosomatids: how to live without mitochondrial DNA. *Int. J. Parasitol.* **32** (9):1071-1084.

Scott A.G., Tait A. and Turner C.M.R. (1996). Characterisation of cloned lines of *Trypanosoma brucei* expressing stable resistance to MelCy and suramin. *Acta Trop.* **60** (4):251-262.

Shahi S.K., Krauth-Siegel R.L. and Clayton C.E. (2002). Overexpression of the putative thiol conjugate transporter *Tb*MRPA causes melarsoprol resistance in *Trypanosoma brucei*. *Mol. Microbiol.* **43** (5):1129-1138.

Shaner N.C., Campbell R.E., Steinbach P.A., Giepmans B.N.G., Palmer A.E. and Tsien R.Y. (2004). Improved monomeric red, orange and yellow fluorescent proteins derived from *Discosoma* sp. red fluorescent protein. *Nat. Biotechnol.* **22** (12):1567-1572.

Shaner N.C., Steinbach P.A. and Tsien R.Y. (2005). A guide to choosing fluorescent proteins. *Nat. Methods* **2** (12):905-909.

Shapiro H.M. and Perlmutter N.G. (2008). Killer applications: toward affordable rapid cell-based diagnostics for malaria and tuberculosis. *Cytometry B Clin. Cytom.* **74** (Supp. l.1):S152-164.

Shapiro T.A. and Englund P.T. (1990). Selective cleavage of kinetoplast DNA minicircles promoted by antitrypanosomal drugs. *Proc. Nat. Acad. Sci. USA* **87** (3):950-954.

Shen S.Y., Arhin G.K., Ullu E. and Tschudi C. (2001). In vivo epitope tagging of *Trypanosoma brucei* genes using a one step PCR-based strategy. *Mol. Biochem. Parasitol.* **113** (1):171-173.

Shimamura M., Hager K.M. and Hajduk S.L. (2001). The lysosomal targeting and intracellular metabolism of trypanosome lytic factor by *Trypanosoma brucei brucei*. *Mol. Biochem. Parasitol.* **115** (2):227-237.

Simarro P.P., Franco J.R., Ndongo P., Nguema E., Louis F.J. and Jannin J. (2006). The elimination of *Trypanosoma brucei gambiense* sleeping sickness in the focus of Luba, Bioko Island, Equatorial Guinea. *Trop. Med. Int. Health* **11** (5):636-646.

Simarro P.P., Jannin J. and Cattand P. (2008). Eliminating human African trypanosomiasis: Where do we stand and what comes next? *PLoS Med.* **5** (2):174-180.

Simarro P.P., Ruiz J.A., Franco J.R. and Josenando T. (1999). Attitude towards CATT-positive individuals without parasitological confirmation in the African Trypanosomiasis (*T. b. gambiense*) focus of Quiçama (Angola). *Trop. Med. Int. Health* **4** (12):858-861.

Simpson L. and Shaw J. (1989). RNA editing and the mitochondrial cryptogenes of kinetoplastid protozoa. *Cell* **57** (3):355-366.

Sinha A., Grace C., Alston W.K., Westenfeld F. and Maguire J.H. (1999). African trypanosomiasis in two travelers from the United States. *Clin. Infect. Dis.* **29** (4):840-844.

Small G.M., Imanaka T. and Lazarow P.B. (1988). Immunoblotting of hydrophobic integral membrane proteins. *Anal. Biochem.* **169** (2):405-409.

Smith D.H., Pepin J. and Stich A.H.R. (1998). Human African trypanosomiasis: an emerging public health crisis. *Br. Med. Bull.* **54** (2):341-355.

Snaith H. A., Samejima I. and Sawin K.E. (2005). Multistep and multimode cortical anchoring of tea1p at cell tips in fission yeast. *EMBO J.* **24** (21):3690-3699.

Sodeman T.M. (1970). Use of fluorochromes for detection of malaria parasites. *Am. J. Trop. Med. Hyg.* **19** (1):40-42.

Solano P., Jamonneau V., N'Guessan P., N'Dri L., Dje N.N., Miezan T.W., Lejon V., Buscher P. and Garcia A. (2002). Comparison of different DNA preparation protocols for PCR diagnosis of Human African Trypanosomosis in Côte d'Ivoire. *Acta Trop.* **82** (3):349-356.

Steingart K.R., Henry M., Ng V., Hopewell P.C., Ramsay A., Cunningham J., Urbanczik R., Perkins M., Aziz M.A. and Pai M. (2006). Fluorescence versus conventional sputum smear microscopy for tuberculosis: a systematic review. *Lancet Infect. Dis.* **6** (9):570-581.

Steverding D. (2006). A new initiative for the development of new diagnostic tests for human African trypanosomiasis. *Kinetoplastid Biol. Dis.* **5**:1.

Stewart M.L., Bueno G.J., Baliani A., Klenke B., Brun R., Brock J.M., Gilbert I.H. and Barrett M.P. (2004). Trypanocidal activity of melamine-based nitroheterocycles. *Antimicrob. Agents Chemother.* **48** (5):1733-1738.

Stewart M.L., Burchmore R.J., Clucas C., Hertz-Fowler C., Brook K., Tait A., MacLeod A., Turner C.M., de Koning H.P., Wong P.E. and Barrett M.P. (2010). Multiple genetic mechanisms lead to the loss of functional TbAT1 expression in drug resistant trypanosomes. *Eukaryot. Cell* **9** (2):336-343.

Stewart M.L., Krishna S., Burchmore R.J.S., Brun R., de Koning H.P., Boykin D.W., Tidwell R.R., Hall J.E. and Barrett M.P. (2005). Detection of arsenical drug resistance in *Trypanosoma brucei* with a simple fluorescence test. *Lancet* **366** (9484):486-487.

Stich A., Abel P.M. and Krishna S. (2002). Human African trypanosomiasis. *BMJ* **325** (7357):203-206.

Stich A., Barrett M.P. and Krishna S. (2003). Waking up to sleeping sickness. *Trends Parasitol*. **19** (5):195-197.

Sturk L.M., Brock J.L., Bagnell C.R., Hall J.E. and Tidwell R.R. (2004). Distribution and quantitation of the anti-trypanosomal diamidine 2,5-bis(4-amidinophenyl)furan (DB75) and its *N*-methoxy prodrug DB289 in murine brain tissue. *Acta Trop*. **91** (2):131-143.

Suzuki H., Futsuhara Y., Takaiwa F. and Kurata N. (1991). Localization of glutelin gene in rice chromosome by *in situ* hybridization. *Jpn. J. Genet.* **66** (3):305-312.

Suzuki T., Fujikura K., Higashiyama T. and Takata K. (1997). DNA staining for fluorescence and laser confocal microscopy. *J. Histochem. Cytochem.* **45** (1):49-53.

Suzuki T., Matsuzaki T., Hagiwara H., Aoki T and Takara K. (2007). Recent advances in fluorescent labeling techniques for fluorescence microscopy. *Acta Histochem. Cytochem.* **40** (5):131-137.

Tanious F.A., Veal J.M., Buczak H., Ratmeyer L.S., Wilson W.D. (1992). DAPI (4',6-Diamidino-2-phenylindole) binds differently to DNA and RNA: minor-groove binding at AT sites and intercalation at AU sites. *Biochemistry* **31** (12):3103-3112.

Taylor A.E.R. (1960). Absorption of prothidium by *Trypanosoma rhodesiense*. *Br. J. Pharmacol. Chemother.* **15** (2):230-234.

Thekisoe O.M.M., Bazie R.S.B., Coronel-Servian A.M., Sugimoto C., Kawazu S. and Inoue N. (2009). Stability of loop-mediated isothermal amplification (LAMP) reagents and its amplification efficiency on crude trypanosome DNA templates. *J. Vet. Med. Sci.* **71** (4):471-475.

Thekisoe O.M.M., Kuboki N., Nambota A., Fujisaki K., Sugimoto C., Igarashi I., Yasuda J. and Inoue N. (2007). Species-specific loop-mediated isothermal amplification (LAMP) for diagnosis of trypanosomosis. *Acta Trop.* **102** (3):182-189.

Thuita J.K., Karanja S.M., Wenzler T., Mdachi R.E., Kagira J.M., Tidwell R. and Brun R. (2008). Efficacy of the diamidine DB75 and its prodrug DB289, against murine models of human African trypanosomiasis. *Acta Trop.* **108** (1):6-10.

Tomita G. (1967). Fluorescence-excitation spectra of acridine orange-DNA and -RNA systems. *Biophysik* **4** (1):23-29.

Torr S.J., Hargrove J.W. and Vale G.A. (2005). Towards a rational policy for dealing with tsetse. *Trends Parasitol.* **21** (11):537-541.

Torrea G., Chakaya J., Mayabi M. and Van Deun A. (2008). Evaluation of the FluoreslenS^{TM} and fluorescence microscopy blinded rechecking trial, Nairobi, Kenya. *Int. J. Tuberc. Lung Dis.* **12** (6):658-663.

Torreele E., Bourdin B., Bray M., Tweats D., Mazué D., Dormeyer M., Colombo P., Kaiser M., Brun R. and Pécoul B. (2009). Fexinidazole: a new drug candidate for

human African trypanosomiasis. Abstr. S52. BSP Spring & Malaria meeting, Edinburgh.

Trouiller P., Olliaro P., Torreele E., Orbinski J., Laing R. and Ford N. (2002). Drug development for neglected diseases: a deficient market and a public-health policy failure. *Lancet* **359** (9324):2188-2194.

Truc P., Aerts D., McNamara J.J., Claes Y., Allingham R., Le Ray D. and Godfrey D.G. (1992). Direct isolation *in vitro* of *Trypanosoma brucei* from man and other animals, and its potential value for the diagnosis of gambian trypanosomiasis. *Trans. R. Soc. Trop. Med. Hyg*. **86** (6):627-629.

Truc P., Jamonneau V., Cuny G., and Frézil J.L. (1999). Use of polymerase chain reaction in human African trypanosomiasis stage detection and follow-up. *Bull. World Health Organ.* **77** (9):745-748.

Truc P., Jamonneau V., N'Guessan P., Diallo P.B. and Garcia A. (1998a). Parasitological diagnosis of human African trypanosomiasis: a comparison of the QBC® and miniature anion-exchange centrifugation techniques. *Trans. R. Soc. Trop. Med. Hyg.* **92** (3):288-289.

Truc P., Jamonneau V., N'Guessan P., N'Dri L., Diallo P.B. and Butigieg X. (1998b). Simplification of the miniature anion-exchange centrifugation technique for the parasitological diagnosis of human African trypanosomiasis. *Trans. R. Soc. Trop. Med. Hyg.* **92** (5):512.

Truc P., Jamonneau V., N'Guessan P., N'Dri L., Diallo P.B. and Cuny G. (1998c). *Trypanosoma brucei* ssp. and *T. congolense*: mixed human infection in Cote d'Ivoire. *Trans. R. Soc. Trop. Med. Hyg.* **92** (5):537-538.

Truc P., Lejon V., Magnus E., Jamonneau V., Nangouma A., Verloo D., Penchenier L. and Büscher P. (2002). Evaluation of the micro-CATT/*Trypanosoma brucei gambiense*, and LATEX/*T. b. gambiense* methods for serodiagnosis and surveillance of human African trypanosomiasis in West and Central Africa. *Bull. World Health Organ.* **80** (11):882-886.

Tye C.K., Kasinathan G., Barrett M.P., Brun R., Doyle V.E., Fairlamb A.H., Weaver R. and Gilbert I.H. (1998). An approach to use an unusual adenosine transporter to selectively deliver polyamine analogues to trypanosomes. *Bioorg. Med. Chem. Lett.* **8** (7):811-816.

Uilenberg G. (adapted from the original edition by W.P. Boyt). A field guide for the diagnosis, treatment and prevention of African animal trypanosomosis. FAO, Rome, 1998.

Valnes K. and Brandtzaeg P. (1985). Retardation of immunofluorescence fading during microscopy. *J. Histochem. Cytochem.* **33** (8):755-761.

Van Meirvenne N., Magnus E., Büscher P. (1995). Evaluation of variant specific trypanolysis tests for serodiagnosis of human infections with *Trypanosoma brucei gambiense*. *Acta Trop*. **60** (3):189-199.

Vanhecke C., Guevart E., Ezzedine K., Receveur M.C., Jamonneau V., Bucheton B., Camara M., Vincendau P. and Malvy D. (2010). La trypanosomose humaine africaine en faciès épidémiologique de mangrove. Présentation, déterminants et prise en charge dans le contexte de la Guinée (2005 à 2007). *Pathol. Biol.(Paris)* **58** (1):110-116.

Vercesi A.E., Moreno S.N.J. and Docampo R. (1994). Ca^{2+}/H^{+} exchange in acidic vacuoles of *Trypanosoma brucei*. *Biochem. J.* **304** (Pt 1):227-233.

Vickerman K. (1977). The dyskinetoplasty mutation in *Trypanosoma evansi* and other flagellates. *Protozoology* **3**:57-69.

Vincendeau P. and Bouteille B. (2006). Immunology and immunopathology of African trypanosomiasis. *An. Acad. Bras. Cienc.* **78** (4):645-665.

Vogelsang J., Kasper R., Steinhauer C., Person B., Heilemann M., Sauer M. and Tinnefeld P. (2008). A reducing and oxidizing system minimizes photobleaching and blinking of fluorescent dyes. *Angew. Chem. Int. Ed. Engl.* **47** (29):5465-5469.

Vreysen M.J. (2001). Principles of area-wide integrated tsetse fly control using the sterile insect technique. *Med. Trop*. **61** (4-5):397-411.

Wang Y.L., Utzinger J., Saric J., Li J.V., Burckhardt J., Dirnhofer S., Nicholson J.K., Singer B.H., Brun R. and Holmes E. (2008). Global metabolic responses of mice to *Trypanosoma brucei brucei* infection. *Proc. Natl. Acad. Sci. U S A* **105** (16):6127-6132.

Waring M.J. (1965). Complex formation between ethidium bromide and nucleic acids. *J. Mol. Biol.* **13** (1):269-282.

Watson J.V. and Chambers S.H. (1977). Fluorescence discrimination between diploid cells on their RNA content: possible distinction between clonogenic and non-clonogenic cells. *Br. J. Cancer* **36** (5):592-600.

Welburn S.C., Fèvre E.M., Coleman P.G., Odiit M. and Maudlin I. (2001a). Sleeping sickness: a tale of two diseases. *Trends Parasitol*. **17** (1):19-24.

Welburn S.C., Maudlin I. and Simarro P.P. (2009). Controlling sleeping sickness-a review. *Parasitology* **136** (14):1943-1949.

Welburn S.C., Picozzi K., Fevre E.M., Coleman P.G., Odiit M., Carrington M. and Maudlin I. (2001b). Identification of human-infective trypanosomes in animal reservoir of sleeping sickness in Uganda by means of serum-resistance-associated (SRA) gene. *Lancet* **358** (9298):2017-2019.

Wenzler T., Boykin D.W., Ismail M.A., Hall J.E., Tidwell R.R. and Brun R. (2009). New treatment option for second-stage African sleeping sickness: *in vitro* and *in vivo* efficacy of aza analogs of DB289. *Antimicrob. Agents Chemother*. **53** (10): 4185-4192.

WHO (1998). Control and surveillance of African trypanosomiasis. *WHO Technical Report Series*. **881**:1-113.

WHO (2006a). Development and evaluation of new diagnostic tests for human African trypanosomiasis. *Wkly. Epidemiol. Rec*. **81** (6):59-60.

WHO (2006b). Human African trypanosomiasis (sleeping sickness): epidemiological update. *Wkly. Epidemiol. Rec*. **81** (8):71-80.

WHO. Report of the scientific working group on African trypanosomiasis, Geneva, 4-8 June, 2001.

Widener J., Nielsen M. J., Shiflett A., Moestrup S. K. and Hajduk S. (2007). Hemoglobin is a co-factor of human trypanosome lytic factor. *PLoS Pathog.* **3** (9):1250-1261.

Widengren J., Chmyrov A., Eggeling C., Löfdahl P.A. and Seidel C.A.M. (2007). Strategies to improve photostabilities in ultrasensitive fluorescence spectroscopy. *J. Phys. Chem. A.* **111** (3):429-440.

Wilkes J.M., Peregrine A.S. and Zilberstein D. (1995). The accumulation and compartmentalization of isometamidium chloride in *Trypanosoma congolense*, monitored by its intrinsic fluorescence. *Biochem. J.* **312** (Pt 1):319-327.

Wilson W.D., Nguyen B., Tanious F.A., Mathis A., Hall J.E., Stephens C.E. and Boykin D.W. (2005). Dications that target the DNA minor groove: compound design and preparation, DNA interactions, cellular distribution and biological activity. *Curr. Med. Chem. Anticancer Agents* **5** (4):389-408.

Wirtz E. and Clayton C. (1995). Inducible gene expression in trypanosomes mediated by a prokaryotic repressor. *Science* **268** (5214):1179-1183.

Wirtz E., Hoek M. and Cross G.A.M. (1998). Regulated processive transcription of chromatin by T7 RNA polymerase in *Trypanosoma brucei*. *Nucleic Acids Res.* **26** (20):4626-4634.

Wongsrichanalai C., Pornsilapatip J., Namsiripongpun V., Webster H.K., Luccini A., Pansamdang P., Wilde H. and Prasittisuk M. (1991). Acridine orange fluorescent microscopy and the detection of malaria in populations with low-density parasitemia. *Am. J. Trop. Med. Hyg.* **44** (1):17-20.

Woo P.T. (1970). The haematocrit centrifuge technique for the diagnosis of African trypanosomiasis. *Acta Trop.* **27** (4): 384-386.

Yamashiro D. and Li C.H. (1973). Adrenocorticotropins. 44. Total synthesis of the human hormone by the solid-phase method. *J. Am. Chem. Soc.* **95** (4):1310-1315.

Yeramian P., Meshnick S.R., Krudsood S., Chalermrut K., Silachamroon U., Tangpukdee N., Allen J., Brun R., Kwiek J.J., Tidwell R. and Looareesuwan S. (2005). Efficacy of DB289 in Thai patients with *Plasmodium vivax* or acute, uncomplicated *Plasmodium falciparum* infections. *J. Infect. Dis.* **192** (2):319-322.

Yuste R. (2005). Fluorescence microscopy today. *Nat. Methods* **2** (12):902-904.

Zelenin A.V. (1966). Fluorescence microscopy of lysosomes and related structures in living cells. *Nature* **212** (5060):425-426.

Zelenin A.V. (1999). Acridine orange as probe for cell and molecular biology. In: *Fluorescent and luminescent probes for biological activity*, 2nd edition (ed.: W.T. Mason), Academic Press, London, pp 117-135.

Zilberstein D., Wilkes J., Hirumi H. and Peregrine A.S. (1993). Fluorescence analysis of the interaction of isometamidium with *Trypanosoma congolense*. *Biochem. J.* **292** (Pt 1):31-35.

Zillmann U., Konstantinov S.M., Berger M.R. and Braun R. (1996). Improved performance of the anion-exchange centrifugation technique for studies with human infective African trypanosomes. *Acta Trop.* **62** (3):183-187.